

# **Environmental and physiological control of dynamic photosynthesis**

**Elias Kaiser**

## **Thesis committee**

### **Promotor**

Prof. Dr Leo F.M. Marcelis  
Professor of Horticulture and Product Physiology  
Wageningen University

### **Co-promotors**

Dr Jeremy Harbinson  
Assistant professor, Horticulture and Product Physiology  
Wageningen University

Dr Ep Heuvelink  
Associate professor, Horticulture and Product Physiology  
Wageningen University

### **Other members**

Prof. Dr Herbert van Amerongen, Wageningen University  
Prof. Dr Lourens Poorter, Wageningen University  
Dr Tracy Lawson, University of Essex, Colchester, UK  
Dr Steven M. Driever, Wageningen University

This research was conducted under the auspices of the Graduate School of  
Production Ecology and Research Conservation



# **Environmental and physiological control of dynamic photosynthesis**

**Elias Kaiser**

## **Thesis**

submitted in fulfilment of the requirements of the degree of doctor  
at Wageningen University

by the authority of the Rector Magnificus

Prof. Dr A.P.J. Mol,

in the presence of the

Thesis committee appointed by the Academic Board

to be defended in public

on Monday 15 February 2016

at 4 p.m. in the Aula.

Elias Kaiser  
Environmental and physiological control of dynamic photosynthesis  
248 pages.

PhD thesis, Wageningen University, Wageningen, NL (2016)  
With references, with summary in English

ISBN 978-94-6257-634-6

# CONTENTS

<b>Chapter 1</b>	General introduction	1
<b>Chapter 2</b>	Dynamic photosynthesis in different environmental conditions	13
<b>Chapter 3</b>	Photosynthetic induction in tomato ( <i>Solanum lycopersicum</i> ) leaves and its diffusional, carboxylation and electron transport processes as affected by CO <sub>2</sub> concentration, temperature, air humidity and blue light	33
<b>Chapter 4</b>	Elevated CO <sub>2</sub> increases photosynthesis in fluctuating irradiance irrespective of photosynthetic induction state	65
<b>Chapter 5</b>	Strongly increased stomatal conductance in tomato does not speed up photosynthetic induction in ambient CO <sub>2</sub> concentration	99
<b>Chapter 6</b>	Metabolic and diffusional limitations of photosynthesis in fluctuating irradiance in <i>Arabidopsis thaliana</i>	119
<b>Chapter 7</b>	Modelling the effects of non-photochemical quenching and metabolic regulation on dynamic leaf photosynthesis	153
<b>Chapter 8</b>	General discussion	195
	References	215
	Summary	231
	Samenvatting	235
	Acknowledgements	239
	About the author	243



# **CHAPTER 1**

## General introduction

Elias Kaiser

*“It is therefore evident that photosynthesis is a process which shows a gradual acceleration until a steady state is reached. A question of great interest now presents itself: what is the cause of the initial acceleration and why is a steady state attained after a certain length of time?”*

*Osterhout and Haas, 1918*

Scientists tend to they keep as many variables constant as possible, in order to identify effects of the factor(s) they are investigating – following the well-known *ceteris paribus* principle. In photosynthesis research, this necessity for highly uniform growth and measurement conditions has formed a ‘*culture of the steady state*’. Within this culture, the assumption is that photosynthesis in natural conditions obeys the laws and limitations of relationships identified under steady-state conditions, which are found when the intensity and spectrum of irradiance, humidity and temperature are constant. However, in nature those environmental factors fluctuate constantly. This is especially true for irradiance. Fluctuations in irradiance cause photosynthesis rates to react dynamically and decrease average photosynthesis rates compared to those in the steady state, due to limitations introduced by lags in the irradiance-dependent regulation of processes like electron transport, carbon fixation, sucrose metabolism and gas diffusion within the leaf. If not accounted for, these limitations lead to overestimations of photosynthesis when steady-state models of photosynthesis are used. Environmental factors such as CO<sub>2</sub> concentration, temperature and humidity modulate the rates of change of photosynthesis in fluctuating irradiance (i.e. dynamic photosynthesis). Reducing the limitations imposed on dynamic photosynthesis may be a useful avenue for improving overall crop photosynthesis. This thesis explores the environmental and physiological control of dynamic photosynthesis.

### **Fluctuating irradiance in nature: sunflecks**

Wind frequently causes leaf angles to vary, and it moves canopies above a given leaf. Thereby, the irradiance incident on a leaf fluctuates, at least in direct sunlight. Cloud formation and movement, diurnal movement of the sun and natural leaf movement add to this variability. Natural fluctuations in irradiance above a given threshold are called sunflecks (Pearcy *et al.*, 1990; Way & Pearcy, 2012). Because the threshold irradiance is defined differently for different sites and/or canopies, the term ‘sunfleck’ has no quantitative definition that is generally applicable (Way & Pearcy, 2012; Smith & Berry, 2013). However, sunflecks can be classified according to properties like duration, intensity, frequency, total fraction of daily irradiance (Pearcy *et al.*, 1990), direct/diffuse fraction and area (Smith & Berry, 2013). Sunfleck properties are highly dependent on canopy structural

characteristics such as canopy height, shape, size and the number, orientation and clumping of leaves (Naumburg & Ellsworth, 2002; Way & Pearcy, 2012). The probability of sunflecks decreases exponentially with increasing leaf area index (LAI), and is further affected by the dispersion of leaves (Pearcy *et al.*, 1990). Thus, in canopies where leaf clumping at the end of branches is common (as in many trees), the probability of sunflecks is higher than in canopies with a more homogeneous dispersion of leaves (Pearcy, 1990).

From the top to the bottom of a canopy, transient irradiance regimes range from sunlight that is sometimes interspersed with shade, to shade interrupted by sunlight (Pearcy, 1990). In forest understories, sunflecks contribute 20-80% of the total irradiance, and a similar percentage of daily carbon gain is attributable to sunflecks (Pearcy, 1990). Thus, plants at the bottom of forests rely heavily on sunflecks for growth. Since sunflecks have been studied in more detail in forests than in crop canopies (Pearcy, 1990), it is unclear how strongly overall photosynthesis in crop canopies depends on sunflecks. However, measurements in a soybean canopy showed that sunflecks were shorter (most sunflecks were 0.4-0.8 s long) and brighter ( $1000-1500 \mu\text{mol m}^{-2} \text{s}^{-1}$ ) than those in forests (Pearcy *et al.*, 1990). In maize and sunflower canopies, sunflecks tended to be more heterogeneous than in structurally more homogeneous wheat canopies (Peressotti *et al.*, 2001).

### **Dynamic photosynthesis: physiological limitations in fluctuating irradiance**

Since irradiance is the principal driver of photosynthesis, fluctuations in irradiance lead to rapidly changing rates of photosynthesis (dynamic photosynthesis). The regulation of light interception, electron and proton transport, carbon fixation, sugar synthesis and CO<sub>2</sub> diffusion is geared towards the use of, but also protection from, sunflecks (Pearcy *et al.*, 1996; Foyer *et al.*, 2012; Tikkanen *et al.*, 2012; Kono & Terashima, 2014). For example, several enzymes in the Calvin cycle are activated in an irradiance-dependent manner; this means that their activation state increases when a shade-adapted leaf is exposed to higher irradiance and decreases when a leaf adapted to high irradiance is exposed to shade (Sassenrath-Cole *et al.*, 1994). Also stomata, balancing CO<sub>2</sub> diffusion into the leaf against leaf water loss, open and close in an irradiance-dependent manner (e.g. Knapp, 1992; Vico *et al.*, 2011). However, the activation of these processes takes time, which introduces limitations on overall photosynthesis rates. These transient limitations are additional to the limitations imposed upon steady-state photosynthesis (e.g. Chen *et al.*, 2014).

When a leaf adapted to darkness or shade is exposed to a higher irradiance, its photosynthesis rate gradually increases towards a stable, steady-state value. This process was discovered almost a century ago (Osterhout & Haas, 1918), has been termed photosynthetic induction and typically takes 10-30 minutes (Pearcy *et al.*, 1996). Often, the

time course of photosynthetic induction resembles a negative-exponential transient, however in some species it may be sigmoidal due to very low initial stomatal conductance ( $g_s$ ) and slow stomatal opening. During this time course, its rate is assumed to be limited mainly by three processes (Percy *et al.*, 1996; 1997). Within the first minute of photosynthetic induction, the main limitation is typically due to the incomplete activation state of several enzymes in the Calvin cycle which together regenerate ribulose-1,5-bisphosphate (RuBP), the substrate used for CO<sub>2</sub> fixation (Sassenrath-Cole & Percy, 1992; Sassenrath-Cole *et al.*, 1994). The second phase is due to the slow activation of ribulose-1,5-bisphosphatase caboxylase oxygenase (Rubisco), the Calvin cycle enzyme central to photosynthesis, which fixes CO<sub>2</sub> (and O<sub>2</sub>) using RuBP. Time constants (defined as the time to reach ~63% of a total change) of Rubisco activation are typically in the range of 4-5 minutes (Woodrow & Mott, 1989). The third phase is due to limitation by stomata, which are partially closed in darkness (to limit leaf water loss) and open slowly by swelling of the stomatal guard cells. This means that, until final stomatal conductance ( $g_s$ ) is reached, leaf photosynthesis operates under a stronger limitation due to low leaf internal CO<sub>2</sub> concentration ( $C_i$ ) than in the steady state (Allen & Percy, 2000b). Since time constants of stomatal opening are in the range of 4-30 minutes (Vico *et al.*, 2011), this phase typically takes most time of the overall induction response. Additionally, in darkness or very low irradiance ( $<5 \mu\text{mol m}^{-2} \text{s}^{-1}$ ), the quantum yield of photosynthesis is transiently reduced (Kirschbaum *et al.*, 2004), most likely due to a transient mismatch between the activation states of enzymes active in the Calvin cycle and sucrose synthesis (Kirschbaum *et al.*, 2005). Next to the 'classical' limitations imposed by RuBP regeneration, Rubisco activation state and  $g_s$ , further limitations on photosynthetic induction may be imposed by slow activation of enzymes in the pathway of sucrose metabolism (Stitt & Grosse, 1988), downregulation of electron transport rates (ETR) by non-photochemical quenching (NPQ; Zhu *et al.*, 2004), or dynamic changes in leaf mesophyll conductance ( $g_m$ ).

After a stepwise decrease in irradiance to shade or darkness, net photosynthesis rates decrease rapidly, however for a few seconds they are higher than steady-state photosynthesis in low irradiance. This process is called post-illumination CO<sub>2</sub> fixation (or assimilatory charge, Laisk *et al.*, 1984). It is driven by pools of RuBP and its precursors in the Calvin cycle, and by ATP formation due to residual electron and proton transport along the electron transport chain (Sharkey *et al.*, 1986). Thereafter, photosynthesis rates often exhibit a transient decrease below final, steady-state levels. This decrease is called post-illumination CO<sub>2</sub> burst and is caused by a number of processes, among which the transient rise in photorespiratory CO<sub>2</sub> production is most pronounced (at least in C<sub>3</sub> plants; Vines *et al.*, 1983; Prinsley *et al.*, 1986). Furthermore, upon a return to low



irradiance, the enzymes limiting RuBP regeneration are slowly deactivated, with time constants of 2-3 minutes. Rubisco deactivation typically takes longer, with time constants of 20-28 minutes (Pearcy *et al.*, 1996). Furthermore,  $g_s$  also decreases, with time constants of 6-18 minutes (Vico *et al.*, 2011).

### **Measuring photosynthesis transients**

Measuring the time course of photosynthesis in response to changes in irradiance is mostly done by acclimating the leaf to a stable irradiance, imposing a stepwise change in irradiance, and rapidly logging the leaf's  $CO_2$  or  $O_2$  exchange until a new steady state is reached. Changes in  $g_s$  are often monitored simultaneously by logging leaf water vapour exchange. Together with transient  $CO_2$  data, these can then be used to calculate the time course of  $C_i$ . Furthermore, chlorophyll fluorescence time courses are sometimes used to monitor the leaf's change in photosynthetic activity (e.g. Alter *et al.*, 2012; Hubbart *et al.*, 2012; Yamori *et al.*, 2012). Leaf enzymatic activity can be assessed by rapidly freezing leaf material at several time points after stepwise changes in irradiance and measuring metabolite pool sizes and/or enzyme activation state changes (e.g. Sharkey *et al.*, 1986; Sassenrath-Cole & Pearcy, 1992; 1994); such studies are, however, costly due to large requirements for leaf material, chemicals, equipment and time. Studies of photosynthetic induction of leaves either adapted to darkness or shade (i.e. background irradiance) and then exposed to high irradiance are the most frequently used. Gas exchange or chlorophyll fluorescence studies of the loss of photosynthetic induction of leaves adapted to high irradiance are more scarce. This is because, in order to measure the leaf's decline in photosynthetic induction state, the leaf needs to be re-exposed to high irradiance at several previously chosen time points. Therefore, loss-of-induction studies are ~4 times more time consuming than photosynthetic induction studies. Another useful type of experiment for assessing dynamic photosynthesis is the application of lightflecks, i.e. artificial sunflecks with defined timing, intensity and spectrum. Continuously changing irradiance, e.g. in the form of sine waves, has also been used to retrieve multiple time constants of processes involved in dynamic photosynthesis (Dau & Hansen, 1989).

### **The language of dynamic photosynthesis: how can transients be characterised?**

Because of the time-dependency of dynamic photosynthesis, characterising and analysing its transients is not straightforward. During photosynthetic induction, for example, several time points can be chosen to give a 'snapshot' of the process at that time, e.g. photosynthetic induction state at 60 seconds after a stepwise change in irradiance. The

time to reach a pre-defined induction state, e.g. time to reach 50 or 90% of full photosynthetic induction, is also an often-used index. These indices are useful for analysing the effects of treatments on transient photosynthesis rates, but by themselves they provide little mechanistic insight. A better understanding of the underlying physiology of dynamic photosynthesis can be reached by the help of a) limitation analysis, b) mutants or transformants of sub-processes of dynamic photosynthesis and/or c) (semi-) mechanistic models (see below). Limitation analysis is the attempt to separate the effects of stomatal and biochemical limitations that are apparent during photosynthetic induction (i.e. they disappear in the steady state; Allen & Pearcy, 2000). There are several methods to assess stomatal limitation during transients, none of which are perfect. A part of this thesis will be devoted to analysing the usefulness of the methods used to analyse transient stomatal limitation.

### **Environmental modulation of dynamic photosynthesis**

Photosynthesis is strongly dependent on a leaf's micro-environment: besides irradiance, for example, CO<sub>2</sub> concentration [CO<sub>2</sub>], temperature, humidity and the spectral composition of irradiance affect it. The effects of those factors on steady-state photosynthesis have been measured countless times, and (in most cases) there is a solid mechanistic framework to explain them (e.g. Farquhar *et al.*, 1980; Bernacchi *et al.*, 2001; Sharkey *et al.*, 2007; Yamori *et al.*, 2014). These factors also affect the rate with which transient photosynthesis reacts to a change in irradiance. However, their effects on non-steady-state photosynthesis are less well characterised and the mechanistic framework to explain them is weaker (Way & Pearcy, 2012). Leaf temperature and leaf-to-air vapour pressure deficit (VPD<sub>leaf-air</sub>) can change rapidly throughout the day. In fact, they co-vary with irradiance, and are therefore a function of sunfleck frequency and intensity (Schymanski *et al.*, 2013).

Natural [CO<sub>2</sub>], on the other hand, changes more slowly, but currently rises by ~2 ppm year<sup>-1</sup> due to human fossil fuel consumption and changes in land use (IPCC, 2013). The effects of rising [CO<sub>2</sub>] are therefore highly relevant for photosynthesis research to assess future ecosystem functioning (Naumburg *et al.*, 2001; Leakey *et al.*, 2002). Apart from affecting photosynthesis on its own, rising [CO<sub>2</sub>] (and other greenhouse gases) may also affect future temperature and humidity (IPCC, 2013). The first part of this thesis is dedicated to the characterization of the environmental control of dynamic photosynthesis, and possible applications of this knowledge are presented below.

## **Targets for improvement of dynamic photosynthesis**

In 2050, the number of people on earth is projected to reach 9 billion (Godfray *et al.*, 2010). At the same time, the expected partial transition from fossil fuel use to energy crops increases the competition for arable land (Zhu *et al.*, 2010; Ort *et al.*, 2015). Furthermore, climate change and the associated increase in climate uncertainty are threatening future crop production (IPCC, 2013). For those reasons, it is expected that productivity per unit area will have to double, while input of fertilizers, energy, water etc. should decrease (Tilman *et al.*, 2011). Past yield improvements during the 'green revolution' that took place in the 2<sup>nd</sup> half of the twentieth century have mainly been brought about by breeding for a higher harvest index and a more intensive use of fertilizers and plant protection chemicals (Zhu *et al.*, 2010). It is often argued that a future increase in crop productivity can be brought about by increasing the efficiency of photosynthesis (Long *et al.*, 2006; Zhu *et al.*, 2010; Ort *et al.*, 2015). One possible avenue of achieving this is to decrease the limitations imposed on dynamic photosynthesis. Examples for this are a) Rubisco whose activation state is less irradiance-dependent (Carmo-Silva & Salvucci, 2013; Carmo-Silva *et al.*, 2014), b) lower NPQ or faster NPQ regulation (Zhu *et al.*, 2004; Murchie & Niyogi, 2011; Hubbart *et al.*, 2012; Armbruster *et al.*, 2014) and c) increased  $g_s$  or faster  $g_s$  regulation (Lawson & Blatt, 2014). The second part of this thesis is dedicated to exploring potential limitations of dynamic photosynthesis by physiological mechanisms, and to the identification of targets for crop improvement.

## **The need for dynamic models of photosynthesis**

Models of photosynthesis are often used as submodels for crop growth, forest growth or even global carbon cycle models (von Caemmerer, 2013). Especially the steady-state photosynthesis model developed by Farquhar, von Caemmerer and Berry (1980) has been used in numerous applications and is of great importance as a research and predictive tool. However, predictions from steady-state models tend to overestimate average photosynthesis rates, because they do not account for the dynamics of photosynthetic induction and its inherent time lags (Percy *et al.*, 1997; Naumburg & Ellsworth, 2002; Küppers & Pfiz, 2009).

Temporal fluctuations of irradiance within canopies are still poorly characterized (see above), making a general statement about the superiority of dynamic over steady-state photosynthesis models impossible. The overestimation of integrated photosynthesis rates by steady-state models depends on the average irradiance, the frequency and intensity of sunflecks, and species-specific responses to fluctuating irradiance, at a given spot (Percy *et al.*, 1997; Naumburg *et al.*, 2001); it has been estimated to be anywhere between 0 and 35%

of total photosynthesis rates per day (Naumburg & Ellsworth, 2002). Within the shaded understory, application of a steady-state model to estimate plant growth resulted in an annual overestimation of 325%, while the overestimation was only 15% in open spaces compared to a dynamic photosynthesis model (Küppers & Pfiz, 2009). Thus, including the dynamics of key photosynthetic components does increase the accuracy of model simulations, but the usefulness of such time-consuming parameterisations strongly depends on the irradiance environment the model is used for. Several (versions of) dynamic photosynthesis models have been published in the last three decades, and the number of parameters used has been between six (Stegemann *et al.*, 1999) and >200 (Zhu *et al.*, 2013), depending on their intended use and level of detail.

Several models of dynamic photosynthesis (Pearcy *et al.*, 1997; Kirschbaum *et al.*, 1998; Naumburg *et al.*, 2001) that are inspired by the model of Farquhar *et al.* (1980) simulate the activation state of Rubisco based on steady-state irradiance- response curves for a given situation. This limits their application (i.e. parameterisation is necessary for every CO<sub>2</sub> concentration and growth condition) and increases the number of parameters. Furthermore, no model of dynamic photosynthesis published to this day simulates leaf-level NPQ, including the effects of regulated heat dissipation in the antennae of photosystem II (PSII), reductions in absorbance due to irradiance avoidance movement of chloroplasts and photoinhibition of PSII reaction centres. However, these processes have frequently been suggested to play a substantial role in downregulating ETR in natural conditions (Murchie *et al.*, 1999; Zhu *et al.*, 2004; Murchie & Niyogi, 2011). Using a more parsimonious goal-seeking approach, it may be possible to simulate the effects of irradiance and CO<sub>2</sub> concentrations on Rubisco regulation and NPQ, while reducing the number of parameters required. Also, although now commonplace in steady-state models of photosynthesis (von Caemmerer, 2013), no published dynamic photosynthesis model has included the effects of  $g_m$  on CO<sub>2</sub> diffusion towards the site of carboxylation, which affects the maximum rate of carboxylation and (to a lesser extent) maximum ETR (Ethier & Livingston, 2004).

### **Exploring new greenhouse lighting strategies**

In protected cultivation such as in greenhouses or plant factories, lighting for a steady supply of fresh produce is often a necessity (Marcelis *et al.*, 2002; Heuvelink *et al.*, 2006). Not surprisingly, lighting is a large cost factor, e.g. in Dutch greenhouses (Heuvelink *et al.*, 2006). A possible way to increase energy efficiency of supplementary lighting is the use of light emitting diodes (LEDs) instead of the currently used high pressure sodium (HPS) lamps. One property of LEDs is that they can be switched on and off rapidly, whereas HPS

lamps take several minutes to reach their full intensity. Daily electricity prices exhibit large volatility (Huisman & Mahieu, 2003), and these fluctuations are likely to increase with larger inputs from sources of renewable energy, as the inputs to these sources are often weather-dependent (Connolly *et al.*, 2012). Growers using LEDs could therefore use fluctuations in energy prices to determine when to switch their lighting on and off (Kjaer *et al.*, 2011). To properly balance the benefits of a more dynamic irradiance control versus the costs of lower integrated photosynthesis rates, experimentation and model simulation are necessary. Furthermore, because in modern protected cultivation environmental factors can be controlled very accurately, the effects of e.g. CO<sub>2</sub> concentration, temperature, humidity or irradiance spectrum on dynamic photosynthesis are highly relevant, and need a solid experimental and theoretical framework to assess them.

### **Thesis outline**

The thesis addresses two global aspects: *environmental* and *physiological* control of dynamic photosynthesis. Consequently, the thesis consists of two parts (Fig. 1.1), which are, however, strongly connected through the effects of environmental factors on underlying physiological processes. The general approach in this thesis was to elucidate the limitations acting on dynamic photosynthesis, by the use of environmental factors, genetic diversity in the form of mutants, transformants and ecotypes and mathematical modelling. Our aims were to a) closely analyse the effects of the environmental factors CO<sub>2</sub> concentration, air humidity and temperature by detailed measurements of dynamic photosynthesis and its underlying processes, and by building a theoretical framework to elucidate their role, b) assess the extent of limitations by Rubisco activation and  $g_s$  through various mutants/transformants and through environmental factors acting on those components, c) test whether  $g_m$ , NPQ and sucrose metabolism placed limitations on dynamic photosynthesis and d) analyse the usefulness of several methods to assess stomatal limitation after an increase in irradiance.

**Chapter 1** (this chapter) describes the rationale for the research conducted, by introducing the concept of fluctuating irradiance and its effects on photosynthesis rates. The chapter discusses how dynamic photosynthesis is measured and described, and provides a range of possible applications of the insights gained by the research conducted in this dissertation.

**Chapter 2** reviews current literature and builds a mechanistic framework to explore the effects that the environmental factors [CO<sub>2</sub>], temperature and air humidity have on rates of dynamic photosynthesis.

**Chapter 3** is an experimental exploration of the effects of [CO<sub>2</sub>], leaf temperature, VPD<sub>leaf-air</sub> and percentage of blue irradiance on rates of photosynthetic induction in dark-adapted to-

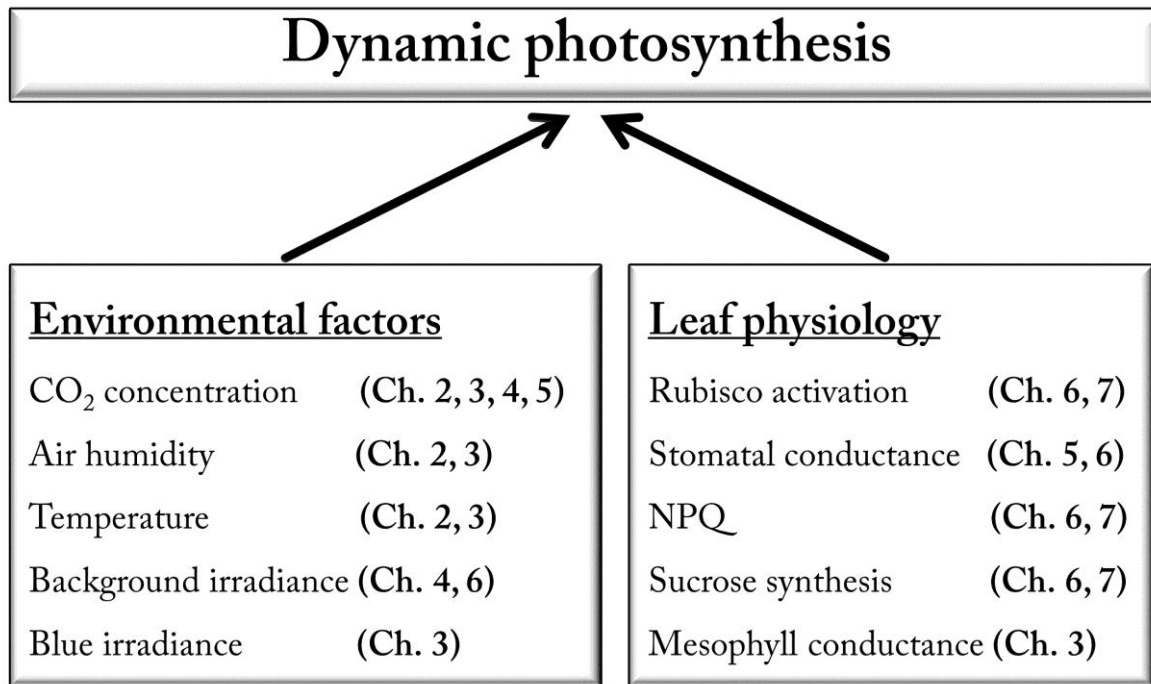


Fig. 1.1. Structure of thesis

tomato leaves. Rubisco activation, stomatal and mesophyll conductance changes, diffusional and biochemical limitations, efficiency of electron transport through photosystem II, NPQ and transient water use efficiency, are highlighted to give a comprehensive overview of the environmental modulation of dynamic photosynthesis.

**Chapter 4** explores whether the effects of [CO<sub>2</sub>] on dynamic photosynthesis are similar across various irradiance environments. Gain and loss of photosynthetic induction in several background irradiance treatments, as well as responses to sinusoidal changes in irradiance, were studied using tomato leaves. From the data, it was estimated how strongly elevated [CO<sub>2</sub>] benefitted dynamic photosynthesis.

**Chapter 5** tests whether stomatal limitation exists during photosynthetic induction in tomato leaves. The abscisic acid-deficient *flacca* mutant and its wildtype were used and exposed to various [CO<sub>2</sub>] levels to change the diffusion gradient. Additionally, using the experimental results, various methods to estimate transient stomatal limitation were tested and compared.

**Chapter 6** identifies and explores some of the physiological limitations underlying dynamic photosynthesis. For this, several mutants, transformants and ecotypes of the model plant *Arabidopsis thaliana*, affecting rates of Rubisco activation, stomatal conductance, non-photochemical quenching and sucrose metabolism, were used. Next to a characterisation of their steady-state responses to [CO<sub>2</sub>] levels and irradiance, leaves were

exposed to stepwise increases and decreases in irradiance (using several intensities) and to lightflecks of several amplitudes and frequencies. In this way, hypotheses about processes limiting dynamic photosynthesis were tested.

Chapter 7 is a modelling exercise of dynamic photosynthesis, based on data obtained from measurements on several mutants of *A. thaliana*. This includes a goal-seeking model that allows reproducing the regulation of Rubisco by irradiance and [CO<sub>2</sub>]. The model also includes a full description of leaf-level NPQ, incorporates  $g_m$  and accounts for the fundamental physics of delays introduced by open gas exchange systems on CO<sub>2</sub> measurements.

Chapter 8 synthesizes the findings in this thesis. It relates the insights gained throughout this dissertation to existing literature to give a comprehensive overview of the state of knowledge about the limitations of dynamic photosynthesis. The methodology of assessing transient stomatal limitations, and some aspects of using chlorophyll fluorescence measurements during photosynthetic induction, are discussed. Finally, possible applications and future perspectives of research on photosynthesis in fluctuating irradiance are presented.





## **CHAPTER 2**

### Dynamic photosynthesis in different environmental conditions

#### **Authors**

Elias Kaiser

Alejandro Morales

Jeremy Harbinson

Johannes Kromdijk

Ep Heuvelink

Leo F.M. Marcelis

Published in:  
Journal of Experimental Botany 2015, 66 (9), pp. 2415-2426

## **Abstract**

Irradiance incident on plant leaves often fluctuates, causing dynamic photosynthesis. Whereas steady-state photosynthetic responses to environmental factors have been extensively studied, knowledge of dynamic modulation of photosynthesis remains scarce and scattered. This review addresses this discrepancy by summarizing available data and by identifying the research questions necessary to advance our understanding of interactions between environmental factors and dynamic behaviour of photosynthesis, using a mechanistic framework. Firstly, dynamic photosynthesis is separated into sub-processes related to proton and electron transport, non-photochemical quenching, control of metabolite flux through the Calvin cycle (activation states of Rubisco and RuBP regeneration, post-illumination metabolite turnover) and control of CO<sub>2</sub> supply to Rubisco (stomatal and mesophyll conductance changes). Secondly, the modulation of dynamic photosynthesis and its sub-processes by environmental factors is described. Increases in ambient CO<sub>2</sub> concentration and temperature (up to approx. 35 °C) enhance rates of photosynthetic induction and decrease its loss, facilitating more efficient dynamic photosynthesis. Depending on the sensitivity of stomatal conductance, dynamic photosynthesis may additionally be modulated by air humidity. Major knowledge gaps exist regarding environmental modulation of loss of photosynthetic induction, dynamic changes in mesophyll conductance, and the extent of limitations imposed by stomatal conductance for different species and environmental conditions. The study of mutants or genetic transformants for specific processes under various environmental conditions could provide significant progress in understanding the control of dynamic photosynthesis.

Keywords: carbon dioxide, CO<sub>2</sub> assimilation, fluctuating irradiance, light transients, lightfleck, sunfleck, temperature, vapour pressure deficit

## Introduction

Photosynthesis is mostly studied using controlled, steady-state conditions. In nature, steady states are rare, and environmental factors, especially irradiance, change rapidly. Assimilation rates in nature result from those factors that limit steady-state photosynthesis as well as those that constrain the speed of response to environmental fluctuations (Naumburg and Ellsworth, 2002; Way and Pearcy, 2012). So, to understand photosynthesis in natural conditions we need to understand photosynthesis in fluctuating irradiance, i.e. dynamic photosynthesis.

Previous research on dynamic photosynthesis has focused on kinetics of underlying processes and interspecific variation in response to fluctuating irradiance (Percy & Way, 2012). In contrast, no clear picture of the effects of ambient CO<sub>2</sub> concentration ([CO<sub>2</sub>]), temperature and leaf-to-air vapour pressure deficit (VPD<sub>leaf-air</sub>) on dynamic photosynthesis exists (Way and Pearcy 2012). These environmental factors influence the rate constants and rates of processes that limit the response of photosynthesis to fluctuating irradiance. As leaf temperature and VPD<sub>leaf-air</sub> often change in parallel with irradiance (Peak and Mott, 2011; Schymanski *et al.*, 2013), transient photosynthesis rates are affected by simultaneous changes in several factors. Atmospheric [CO<sub>2</sub>] changes more slowly, currently rising by approx. 2 μmol mol<sup>-1</sup> year<sup>-1</sup> (IPCC, 2013). Apart from influencing photosynthesis on its own, this increase in [CO<sub>2</sub>] is likely to affect air temperature and humidity (IPCC, 2013). Knowledge of dynamic photosynthesis is solid with respect to responses to changing irradiance, but much less developed regarding the modulation of dynamic photosynthesis by other environmental factors, even when these factors are held constant while irradiance fluctuates. This weakness impacts upon photosynthetic models.

Vegetation and crop science relies heavily on models to predict photosynthesis. Steady-state photosynthesis models are often sophisticated and useful, but tend to overestimate integrated photosynthesis in fluctuating irradiance (Naumburg and Ellsworth, 2002; Timm *et al.*, 2004). The degree of overestimation depends on average irradiance intensity and species-specific responses to fluctuating irradiance (Percy *et al.*, 1997; Naumburg *et al.*, 2001; Naumburg and Ellsworth, 2002), but can be as much as 35% per day (Naumburg and Ellsworth, 2002). Dynamic photosynthesis models, on the other hand, account for the kinetics of photosynthesis as it responds to fluctuating light. Of the dynamic models that exist, none account for all environmental factors mentioned, while some account for the effects of [CO<sub>2</sub>] (Kirschbaum *et al.*, 1998; Naumburg *et al.*, 2001; Vico *et al.*, 2011), leaf temperature (Ozturk *et al.*, 2012; Pepin and Livingston, 1997) and air humidity (Pepin and Livingston, 1997; Vico *et al.*, 2011). To improve dynamic photosynthesis models, we need

better understanding of how environmental factors other than irradiance, even when they are constant, modulate the kinetics of responses to changes in irradiance.

Patterns of fluctuating irradiance can be classified as lightflecks and sunflecks. While lightflecks are artificial increases in irradiance with defined intensity, duration and spectrum (Pearcy *et al.*, 1996), sunflecks are natural increases in irradiance above a threshold intensity, with great temporal, spatial and spectral heterogeneity (Smith and Berry, 2013).

Steady-state responses of photosynthesis to  $[\text{CO}_2]$ , leaf temperature and  $\text{VPD}_{\text{leaf-air}}$  are well understood, which makes analysing gas exchange dynamics in response to fluctuating irradiance easier. In this review, we consider environmental factors besides irradiance to be constant when we look at their role as modulators of dynamic photosynthesis, because a) there are empirical data available on this situation and b) considering two or more factors as changing dynamically would make this already complex process overly complicated. We review the modulation of dynamic photosynthesis by  $[\text{CO}_2]$ , leaf temperature and  $\text{VPD}_{\text{leaf-air}}$ , by a) building a framework of all processes that may affect dynamic photosynthesis on the levels of electron transport, flux of metabolites through the Calvin cycle and leaf  $\text{CO}_2$  diffusion and b) examining the effects of  $[\text{CO}_2]$ , leaf temperature and  $\text{VPD}_{\text{leaf-air}}$  on underlying processes and on dynamic gas exchange parameters. Using this structure, the reader is first introduced to the “machinery” of dynamic photosynthesis in a mechanistic way, making the following analysis of modulation of dynamic photosynthesis by environmental factors much simpler to understand.

### **Dynamic control of photosynthetic gas exchange**

The complex process of dynamic photosynthesis can be deconstructed into three major processes: photosynthetic induction, post-illumination  $\text{CO}_2$  fixation and post-illumination  $\text{CO}_2$  burst (Fig. 2.1). Photosynthetic induction itself is driven by sub-processes such as RuBP regeneration, Rubisco activation and stomatal movement. Changes of mesophyll conductance ( $g_m$ ) and non-photochemical quenching (NPQ) in response to irradiance may further modulate dynamic photosynthesis, and are affected by  $[\text{CO}_2]$  and leaf temperature. All of these processes are described below, in a framework (Fig. 2.2) that will help understand modulation of dynamic photosynthesis by  $[\text{CO}_2]$ , leaf temperature and  $\text{VPD}_{\text{leaf-air}}$ .

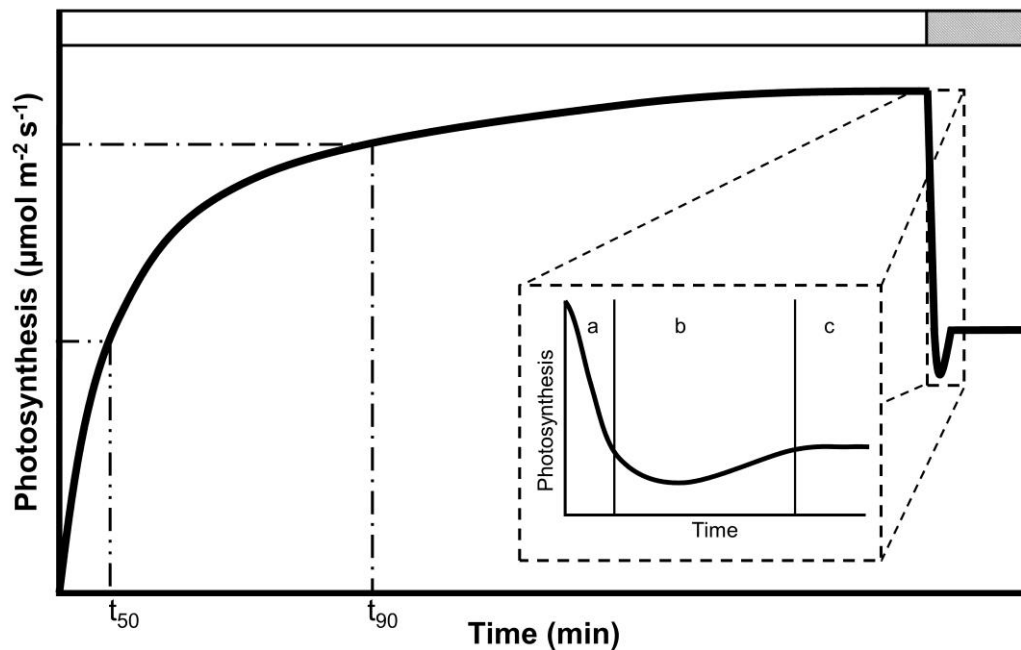


Fig. 2.1. Schematic of transient net photosynthesis phenomena upon increase and decrease in irradiance: Photosynthetic induction in a dark-adapted leaf during lightfleck (high irradiance, e.g.  $1000 \mu\text{mol m}^{-2} \text{s}^{-1}$ , white bar), followed by post-illumination  $\text{CO}_2$  fixation and post-illumination  $\text{CO}_2$  burst after lightfleck (low irradiance, e.g.  $200 \mu\text{mol m}^{-2} \text{s}^{-1}$ , grey bar).  $t_{50}$ ,  $t_{90}$ : time required to reach 50 and 90% of full photosynthetic induction, respectively. Fig. 2.1, inset: a) post-illumination  $\text{CO}_2$  fixation, b) post-illumination  $\text{CO}_2$  burst and c) new steady-state photosynthesis after lightfleck

## Control of electron transport

### *Electron and proton transport*

Light driven charge separation in the reaction centres of photosystems (PS) I and II initiates an electron transport process that results in the oxidation of water on the luminal side and reduction of ferredoxin on the stromal side of the thylakoid, reducing  $\text{NADP}^+$  to NADPH (Cruz *et al.*, 2001; Foyer *et al.*, 2012). Electron transport processes are coupled to proton transport across the thylakoid membrane. Proton transport builds up the proton motive force (pmf), which after dark-light transitions mainly consists of a trans-thylakoid electrical potential ( $\Delta\Psi$ ), but partitions into  $\Delta\Psi$  and a pH gradient across the thylakoid membrane ( $\Delta\text{pH}$ ) after several seconds (Cruz *et al.*, 2001). The pmf affects 1) ATP synthesis, 2) NPQ via  $\Delta\text{pH}$ , 3) maximum electron transport rates (ETR) through the cytochrome  $b_6/f$  complex and 4) movement of  $\text{Mg}^{2+}$ -ions across the thylakoid membrane into the stroma due to  $\Delta\Psi$  (Cruz *et al.*, 2001; Foyer *et al.*, 2012). Regulatory mechanisms of electron and proton transport currently receive much attention due to their pivotal role in protecting the photosynthetic apparatus and in balancing ATP/NADPH ratios in fluctuating light. They are dealt with in great detail in recent reviews (Kramer and Evans, 2011; Foyer *et al.*, 2012; Tikkanen *et al.*, 2012; Kono and Terashima, 2014; Shikanai, 2014).

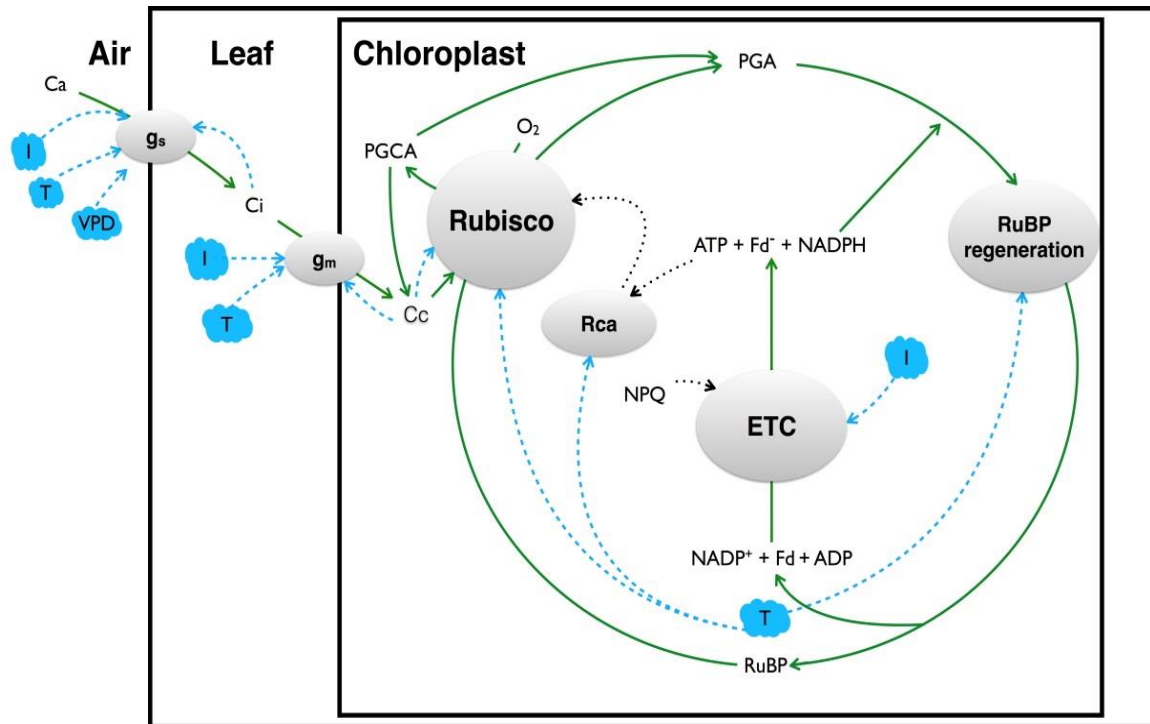


Fig. 2.2. Depiction of major components and processes of dynamic photosynthesis (grey circles), and main effects of environmental factors (blue clouds). Material flows are shown as green solid arrows, information flows between processes as dotted arrows and information flows from environmental factors towards processes as blue, dashed arrows. Depending on its location, CO<sub>2</sub> is named either C<sub>a</sub> (ambient CO<sub>2</sub> concentration), C<sub>i</sub> (substomatal cavity CO<sub>2</sub> concentration) or C<sub>c</sub> (chloroplast CO<sub>2</sub> concentration). Further abbreviations: ADP, adenosine diphosphate; ATP, adenosine triphosphate; ETC, electron transport chain; Fd, ferredoxin; g<sub>m</sub>, mesophyll conductance; g<sub>s</sub>, stomatal conductance; I, irradiance; NADPH, nicotinamide adenine dinucleotide phosphate; NPQ, non-photochemical quenching; O<sub>2</sub>, oxygen; PGA, 3-phosphoglycerate; PGCA, 2-phosphoglycolate; Rca, Rubisco activase; Rubisco, ribulose-1,5-bisphosphate carboxylase oxygenase; RuBP, ribulose-1,5-bisphosphate; T, temperature; VPD, leaf-to-air vapour pressure deficit

In the context of this review, electron and proton transport are mostly important in regulating NPQ and the thioredoxin-ferredoxin system, which in turn activates several of the light-regulated Calvin cycle enzymes.

### *Non-photochemical quenching*

Protecting PSII from damage by absorbed excess energy, NPQ is the result of up to four processes that operate at different time scales. These processes include energy-dependent quenching (qE), state transitions, zeaxanthin-dependent quenching, and photoinhibition (Nilkens *et al.*, 2010; Ruban *et al.*, 2012; Jahns and Holzwarth, 2012). The most important process with regards to fluctuating irradiance is qE, as it responds most quickly to changes in irradiance. Additionally, it normally accounts for the largest fraction of NPQ (Ruban *et al.*, 2012). The formation of qE is strictly dependent on the build-up of ΔpH and its sensing by the PSII protein PsbS (Li *et al.*, 2000; 2004). PsbS is most likely a catalyst of qE (Goral *et al.*, 2012; Hubbart *et al.*, 2012). Furthermore, qE is modulated by the amount of zeaxanthin

and antheraxanthin (Johnson *et al.*, 2011), carotenoids that are formed from violaxanthin in the xanthophyll cycle; the exact role of the xanthophyll cycle in qE is still under debate (Jahns and Holzwarth, 2012).

Half-times for induction and relaxation of qE are between 15 and 60 seconds (Walters and Horton, 1991; Nilkens *et al.*, 2010; Peguero-Pina *et al.*, 2013). Because relaxation kinetics of qE are slower than the rate of change of irradiance, qE transiently competes with ETR after lightflecks and could decrease integrated daily photosynthesis by 13-32%, compared to the hypothetical situation of instant relaxation of qE (Zhu *et al.*, 2004). Relative losses due to downregulated ETR are greater in low irradiance (Tausz *et al.*, 2005). Furthermore, Zhu *et al.* (2004) assumed qE to be strongly affected by leaf temperature, making it a process that could impact on dynamic photosynthesis and be modulated by other environmental factors. In transgenic *Oryza sativa* plants overexpressing PsbS, photosynthetic induction was slower because of decreased ETR (Hubbart *et al.*, 2012). Unfortunately, no data were presented that linked qE relaxation kinetics after decreases in irradiance to photosynthesis rates. Considering the extent of hypothesized effects of slow qE relaxation kinetics on plant productivity (Zhu *et al.*, 2004), it seems worthwhile to underpin those with experimental evidence.

## **Control of metabolite flux through the Calvin cycle**

### *RuBP regeneration activation state*

At low irradiance, pools of RuBP and its precursors are small (Sassenrath-Cole and Pearcy, 1992), but increase in higher irradiance. It is assumed that RuBP concentrations are non-limiting when they are 1.5-2 times the active site concentration of Rubisco (Woodrow and Mott, 1989; Sassenrath-Cole and Pearcy, 1992; Pearcy *et al.*, 1996), a level which is reached or exceeded one minute after illumination (Sassenrath-Cole and Pearcy, 1992). Measured half-times of activation and deactivation of RuBP regeneration are in the range of 2-3 minutes (Kirschbaum and Pearcy, 1988; Sassenrath-Cole and Pearcy, 1994). In dark-adapted leaves, the overall limitation due to inactive RuBP regeneration is small, compared to limitations imposed by inactive Rubisco and closed stomata. However, because RuBP regeneration deactivates more quickly in low irradiance than Rubisco (Sassenrath-Cole and Pearcy, 1992), it can impose large limitations on integrated photosynthesis rates in naturally fluctuating irradiance.

Chloroplast FBPase (fructose-1,6-bisphosphatase) and SBPase (sedoheptulose-1,7-bisphosphatase) activity limit RuBP-regeneration activation (Stitt *et al.*, 1980; Prinsley and Leegood, 1986; Sassenrath-Cole and Pearcy, 1992; 1994; Sassenrath-Cole *et al.*, 1994). Also, PRK (phosphoribulokinase) may limit the activation of RuBP-regeneration (Sassenrath-

Cole and Percy, 1992; Sassenrath-Cole *et al.*, 1994). Activation of PRK saturated at much lower irradiance than FBPase (Sassenrath-Cole and Percy, 1994). Also, PRK activated more quickly than FBPase and SBPase in lightflecks (Champigny and Bismuth, 1976; Laing *et al.*, 1981; Kobza and Edwards, 1987) and deactivated comparably slowly thereafter (Avron and Gibbs, 1974). Altogether, FBPase and SPBase limit the activation of RuBP regeneration more strongly than PRK.

FBPase and SBPase are directly regulated by the thioredoxin-ferredoxin system (Raines *et al.*, 1999; Ruelland and Miginiac-Maslow, 1999). They are oxidized, and therefore inactive, in the dark. Upon illumination, reducing power is transferred from PSI via ferredoxin to thioredoxin, which reduces and thus activates the enzymes (Ruelland and Miginiac-Maslow, 1999). FBPase is further stabilised and positively regulated by its substrate FBP (fructose-1,6-bisphosphate; Scheibe, 2004), stromal pH and  $Mg^{2+}$  (Ishijima *et al.*, 2003), and inhibited by glycerate and its product F6P (fructose-6-phosphate; Gardemann *et al.*, 1986; Schimkat *et al.*, 1990). Also, SBPase activity is positively regulated by  $Mg^{2+}$ , stromal pH and its substrate SBP (sedoheptulose-1,7-bisphosphate; Schimkat *et al.*, 1990), and negatively by inorganic phosphate, glycerate, RuBP and its product S7P (sedoheptulose-7-phosphate; Schimkat *et al.*, 1990; Ishijima *et al.*, 2003).

PRK can form a complex with the enzyme glyceraldehyde-3-phosphate dehydrogenase (GAPDH) and a chloroplast protein, CP12, in darkness (Wedel *et al.*, 1997; Howard *et al.*, 2008). In *Pisum sativum* leaves, the complex dissociated within minutes of illumination; the extent of dissociation increased with irradiance between up to  $300 \mu\text{mol m}^{-2} \text{s}^{-1}$  (Howard *et al.*, 2008), providing flexible regulation of PRK. However, in dark-adapted leaves of other species (*Vicia faba*, *Solanum tuberosum*, *Solanum lycopersicum* and *Spinacia oleracea*), enzymes existed both bound by the PRK/GAPDH/CP12 complex and as free enzymes, while in others (*Phaseolus vulgaris*, *Nicotiana tabacum* and *Arabidopsis thaliana*) the enzymatic complex was almost absent (Howard *et al.*, 2011). Thus, the regulation of PRK and GAPDH activity by CP12 is far from universal among species. It is not clear whether the interspecific differences in PRK regulation impact on RuBP regeneration activation.

### *Rubisco activation state*

To fix carbon, Rubisco must be carbamylated, i.e. Rubisco (E) needs to form a complex (ECM) with  $\text{CO}_2$  and  $Mg^{2+}$  (Woodrow *et al.*, 1996). For carboxylation, RuBP (R) and another  $\text{CO}_2$  molecule need to bind to ECM. Several inhibitory sugar phosphates can bind to Rubisco, preventing ECM formation, or to ECM, preventing carboxylation (Salvucci and Crafts-Brandner, 2004): Firstly, RuBP can bind to uncarbamylated Rubisco and form a



stable but inactive ER complex (Salvucci and Crafts-Brandner, 2004); it may also bind to EC (McNevin *et al.*, 2006). Secondly, by misprotonation of RuBP during carboxylation or oxygenation, inhibitory sugar phosphates such as PDBP (D-glycero-2,3-pentodiulose-1,5-bisphosphate),  $\text{}_3\text{KABP}$  (3-ketoarabinitol bisphosphate) or XuBP (xylulose-1,5-bisphosphate; collectively abbreviated as 'X') are formed, which can bind to carbamylated Rubisco (Salvucci and Crafts-Brandner, 2004; Andralojc *et al.*, 2012). They might also bind to E and EC complexes (McNevin *et al.*, 2006). Thirdly, CA<sub>1</sub>P (2-carboxy-D-arabinitol 1-phosphate) can bind to ECM instead of RuBP in low irradiance or darkness (Parry *et al.*, 2013). CA<sub>1</sub>P is probably present in most species, but not always in concentrations high enough to take effect (Andralojc *et al.*, 2012). In darkness, the activation state of Rubisco can be strongly [CO<sub>2</sub>]-dependent, as long as Rubisco is unaffected by CA<sub>1</sub>P. Namely, the Rubisco activation state can be higher in darkness than in low irradiance, since newly formed RuBP in low irradiance can bind to uncarbamylated Rubisco sites, while in darkness no RuBP is formed and CO<sub>2</sub> binds instead, keeping Rubisco carbamylated (Carmo-Silva and Salvucci, 2013).

To keep ECM catalytically competent and to free inactive ER, EX, ECR and ECX complexes, the chaperone Rubisco activase (Rca) is required (Salvucci *et al.*, 1985; Portis *et al.*, 1986). Rca is inactive in darkness and is activated upon illumination (Portis, 2003). Alternative splicing of the Rca gene results in two isoforms: The  $\alpha$ -isoform in *A. thaliana* is regulated by the thioredoxin-ferredoxin system, while regulation of the smaller  $\beta$ -Rca is unclear and differs across species (Portis, 2003; Carmo-Silva and Salvucci, 2013). When both isoforms are present,  $\alpha$ -Rca controls  $\beta$ -Rca (Zhang and Portis, 1999). Rca requires ATP for catalytic activity and is inhibited by ADP (Zhang and Portis, 1999; Portis, 2003). However, in a recent study using *A. thaliana* mutants, plants containing only  $\beta$ -Rca did not exhibit ADP sensitivity, and kept Rubisco almost fully activated in low irradiance (Carmo-Silva and Salvucci, 2013). Consequently, photosynthetic induction was much faster. In transgenic *N. tabacum* plants with substantially decreased Rca levels, no decreases in steady-state Rubisco activation state were found (Mate *et al.*, 1993). It was inferred that theoretically, a concentration of Rca 200 times lower than Rubisco could suffice to keep Rubisco activated (Mate *et al.*, 1993), although this would slow down the rate of activation significantly. Naturally occurring Rca concentrations are much higher than that, which may help to use fluctuating irradiance more efficiently. The optimal allocation of nitrogen between Rubisco and Rca could therefore depend on a plant's microclimate (Mott and Woodrow, 2000). For more extensive reviews of Rubisco activation, see Parry *et al.*, 2013 and Tcherkez, 2013. For kinetics of Rubisco activation and deactivation, see Pearcy *et al.* (1996).

Generally, the irradiance-dependent regulation of Rubisco is pivotal to dynamic photosynthesis. The activation state of Rubisco is strongly dependent on the functioning of Rca and is further modulated by  $[\text{CO}_2]$  and temperature.

#### *Post-illumination CO<sub>2</sub> fixation*

After decreases in irradiance, it can be observed in rapid gas exchange measurements that assimilation rates do not directly “fall” to a new steady state, but that their decrease lags behind for a few seconds (Fig. 2.1, inset a). This phenomenon, termed post-illumination CO<sub>2</sub> fixation, increases integrated carbon assimilation of a lightfleck and can substantially increase average photosynthesis rates of leaves in sunfleck environments (Pons and Pearcy, 1992; Roden and Pearcy, 1993; Roden, 2003). Post-illumination CO<sub>2</sub> fixation is driven by pools of Calvin cycle intermediates as well as NADPH, ATP and the pmf (Laisk *et al.*, 1984; Sharkey *et al.*, 1986). These pools build up within seconds (Sharkey *et al.*, 1986) and their size increases with irradiance intensity in parallel to photosynthesis rates (Laisk *et al.*, 1984), creating a linear relationship between photosynthesis rates and post-illumination CO<sub>2</sub> fixation (Kirschbaum *et al.*, 2005). Integrated post-illumination CO<sub>2</sub> fixation has been shown to correlate well with RuBP pools over various  $[\text{CO}_2]$  levels (Ruuska *et al.*, 1998), and has been used to estimate RuBP pools (Osmond *et al.*, 1988; Kirschbaum *et al.*, 1998). As metabolite pool sizes are often proportional to photosynthetic capacity, so are rates of post-illumination CO<sub>2</sub> fixation (Sharkey *et al.*, 1986; Osmond *et al.*, 1988; Pearcy *et al.*, 1996). Effects of post-illumination CO<sub>2</sub> fixation on integrated photosynthesis are often negligible (Percy *et al.*, 1994). However, as its fraction of integrated dynamic photosynthesis is inversely related to lightfleck length (Roden and Pearcy, 1993), it could increase photosynthesis in species with strongly fluttering leaves (by 5-15%, as estimated by Roden, 2003), as leaf flutter can facilitate extremely short lightflecks.

#### *Post-illumination CO<sub>2</sub> burst*

After post-illumination CO<sub>2</sub> fixation, a dip in net photosynthesis rates, termed post-illumination CO<sub>2</sub> burst (Decker, 1955) may be visible in gas exchange data (Fig. 2.1, inset b). Post-illumination CO<sub>2</sub> bursts of different kinetics occur in C<sub>3</sub>, CAM and some C<sub>4</sub> plants. Different origins of these bursts related to photorespiration (C<sub>3</sub> and CAM plants; Vines *et al.*, 1983; Crews *et al.*, 1975), overshoots in sucrose synthesis (C<sub>3</sub> plants; Prinsley *et al.*, 1986), phosphoenolpyruvate carboxykinase activity (CAM plants; Crews *et al.*, 1975), and differences in the activity of malate dehydrogenase (C<sub>4</sub> plants; Downton, 1970) have been reported. In this review, only the photorespiratory CO<sub>2</sub> burst will be considered, as it is most pronounced and most strongly modulated by  $[\text{CO}_2]$  and temperature.

The photorespiratory post-illumination CO<sub>2</sub> burst is caused by a transient rise in photorespiratory CO<sub>2</sub> production (Vines *et al.*, 1983; Prinsley *et al.*, 1986). This is usually explained by a lag-time between adjustment of photorespiratory 2-phosphoglycolate (PGCA) recycling relative to Calvin cycle cycling. After lightflecks, PGCA is recycled into 3-phosphoglycerate (PGA) at a rate which is temporarily higher than at steady state; the corresponding consumption of ATP and reductant as well as CO<sub>2</sub> evolution during glycine decarboxylation cause the burst (Rawsthorne and Hylton, 1991). In *Pelargonium x hortorum*, lightflecks of at least 5 minutes duration were required to maximise the burst (Vines *et al.*, 1983). Further, a positive correlation of photosynthesis rates after lightflecks and burst magnitude suggests that this phenomenon requires energy (Vines *et al.*, 1983).

## **Control of CO<sub>2</sub> supply to Rubisco**

### *Stomatal conductance*

Stomatal conductance ( $g_s$ ) often decreases in low irradiance, which, together with slow stomatal opening during lightflecks, may limit dynamic photosynthesis. Stomatal limitation during induction can be calculated by correcting assimilation rates for the change in concentration of CO<sub>2</sub> in the substomatal cavity ( $C_i$ ) (Woodrow and Mott, 1989; Tinoco-Ojanguren and Pearcy, 1993b; Allen and Pearcy, 2000). It is often assumed that  $g_s$  always limits induction, despite reports to the contrary (Ögren and Sundin, 1996; Tausz *et al.*, 2005; Tomimatsu and Tang, 2012). There may be two reasons for this. Firstly, stomatal limitations have often not been analysed, even though the necessary data (dynamic CO<sub>2</sub> exchange and  $g_s$ ) were available (e.g. Chazdon and Pearcy, 1986; Roden and Pearcy, 1993; Pearcy *et al.*, 1997; Pepin and Livingston, 1997; Naumburg and Ellsworth, 2000; Leakey *et al.*, 2002; 2003). Secondly, many studies focus on forest understory species, which may not be representative of other plant functional types. Re-evaluation of published datasets and genotypes with contrasting stomatal behaviour (Tomimatsu and Tang, 2012) may help to quantify stomatal limitations on dynamic photosynthesis.

Rates of stomatal opening and closure after changes in irradiance are highly heterogeneous between species, environmental conditions and plant functional types. In several closely related *Banksia* trees, smaller stomata opened and closed faster in response to lightflecks than larger stomata, possibly due to their larger membrane surface area to volume ratio (Drake *et al.*, 2013). Two meta-analyses found that on average, stomatal opening in lightflecks was faster than stomatal closure after lightflecks (Ooba and Takahashi, 2003; Vico *et al.*, 2011). However, there was large variation in these traits. In fact, several datasets showed faster stomatal closure than opening (Ooba and Takahashi, 2003; Vico *et al.*, 2011), which could be due to different environmental conditions between experiments.

Stomata respond to a myriad of intrinsic and extrinsic factors, among them all environmental factors discussed in this review. For changes in a single factor, the response is often well known. Far less work has been done on the kinetics of the response (Lawson and Blatt, 2014) or simultaneous changes in several factors, which are likely in nature (e.g. increase in irradiance and leaf temperature, decrease in  $C_i$  and  $VPD_{\text{leaf-air}}$ ). Recently, Merilo *et al.* (2014) have shown that effects of different environmental factors on  $g_s$  are non-multiplicative, rarely predictable and strongly species-dependent. This challenges the often-held model assumption that effects of single factors are multiplicative and uniform across species (summarized in Damour *et al.*, 2010).

### *Mesophyll conductance*

Mesophyll conductance ( $g_m$ ), mediating  $CO_2$  diffusion from the substomatal cavity to chloroplast, can be a substantial limitation to photosynthesis. It can vary within minutes, and is affected by changes in irradiance,  $[CO_2]$  and temperature (Flexas *et al.*, 2007; 2008; Tholen *et al.*, 2008, Evans and von Caemmerer, 2013), making it a potentially important process within the framework of this review. The possible components of  $g_m$ , its short-term variability in response to environmental factors and possible artefacts of methods used for its estimation are under ongoing discussion (Tholen *et al.*, 2012; Griffiths and Helliker, 2013). Relevant factors that may potentially contribute to variations in  $g_m$  are carbonic anhydrase, aquaporins, anatomical properties of leaves and cells (Flexas *et al.*, 2012) and the area of chloroplasts facing intercellular spaces (Tholen *et al.*, 2008). Of these, all but the basic anatomical properties of leaves and cells may be affected by short-term changes in environmental factors. Estimating  $g_m$  correctly is difficult, and every method has different drawbacks and underlying assumptions. Therefore, using at least two methods simultaneously is recommended (Flexas *et al.*, 2013). Two methods are currently available for measuring rapidly changing  $g_m$ : the ‘variable J method’, using simultaneous gas exchange and chlorophyll fluorescence (Harley *et al.*, 1992) and online carbon isotope discrimination, using tunable diode laser absorption spectroscopy (e.g. Evans and von Caemmerer, 2013). Combining these methods under various environmental factors should be of great use to determine the dynamics of  $g_m$  in fluctuating irradiance and to underpin theories regarding its regulation.

### **Environmental factors influencing dynamic photosynthesis**

In the remainder of this review, the effects of  $[CO_2]$ , leaf temperature and  $VPD_{\text{leaf-air}}$  on the processes driving dynamic photosynthesis are discussed; they are summarized in Table 2.1. While changes in  $[CO_2]$  are normally gradual, leaf temperature and  $VPD_{\text{leaf-air}}$  fluctuate

almost as rapidly as irradiance itself. Thus, findings with regards to  $[\text{CO}_2]$  effects presented here may be used for future climate change scenarios, while findings regarding the other two factors can be used with regards to current natural conditions.

### *CO<sub>2</sub> concentration*

Increased  $[\text{CO}_2]$  generally stimulates rates of photosynthetic induction, and enhances photosynthesis and growth in fluctuating irradiance (Leakey *et al.*, 2002). In previous work,  $[\text{CO}_2]$  was manipulated either during measurements (Chazdon and Pearcy, 1986) or continuously during plant growth (Naumburg and Ellsworth, 2000; Leakey *et al.*, 2002; Tomimatsu and Tang, 2012; Holišová *et al.*, 2012). In three out of five studies, elevated  $[\text{CO}_2]$  led to faster photosynthetic induction (Chazdon and Pearcy, 1986; Leakey *et al.*, 2002; Tomimatsu and Tang, 2012). Naumburg and Ellsworth (2000) found no differences in induction rates, while Holišová *et al.* (2012) reported faster induction for one of two species in elevated  $[\text{CO}_2]$ . The difference in outcomes between studies may be explained by  $[\text{CO}_2]$  treatment levels (Naumburg and Ellsworth (2000) and Holišová *et al.* (2012) used the narrowest range between  $[\text{CO}_2]$  treatments of the studies mentioned), experimental procedures or species differences.

Combining data from several experiments (Chazdon and Pearcy, 1986; Leakey *et al.*, 2002; Tomimatsu and Tang, 2012) revealed that the time required to reach 90% of full induction

Table 2.1. Effects of environmental factors on processes controlling dynamic photosynthesis after increases or decreases in irradiance. Environmental factors considered are: ambient  $\text{CO}_2$  concentration ( $[\text{CO}_2]$ ), leaf temperature and leaf-to-air vapour pressure deficit ( $\text{VPD}_{\text{leaf-air}}$ )

Change in irradiance	Process	Environmental factor			$\text{VPD}_{\text{leaf-air}}$
		$[\text{CO}_2]$	Temperature		
			Medium <sup>a</sup>	High <sup>b</sup>	
Increase	RuBP-regeneration activation	- <sup>c</sup>	↑	↗	-
	Rubisco activation	~	↑	↓	↘
	Stomatal opening	~	~	~	↓
	qE buildup	↘	↘	↘	-
	Mesophyll conductance increase	?	↑	~	~
Decrease	RuBP-regeneration deactivation	-	?	?	-
	Rubisco deactivation	↓	?	↑	↗
	Stomatal closure	↑	?	?	↑
	Post-illumination $\text{CO}_2$ fixation	↓	↑	↓	?
	Post-illumination $\text{CO}_2$ burst	↓	↑	↑	?

<sup>a</sup> Temperature range: 5 to approx. 30 °C

<sup>b</sup> Temperature range: >30 °C

<sup>c</sup> Symbols: ↑, ↓: increase or decrease in rate of the process when environmental factor increases; ↗, ↘: hypothesized increase and decrease; -: no effect; ~: conflicting relationship throughout literature; ?: unknown relationship

( $t_{90}$ , visualized in Fig. 2.1) decreased with increasing  $[\text{CO}_2]$  (Fig. 2.3;  $R^2=0.51$ ). This effect was more pronounced between 200 and 600  $\mu\text{mol mol}^{-1}$ . Because average  $t_{90}$  was 16 minutes, this indicates positive effects of  $[\text{CO}_2]$  on stomatal limitations. No trend was observed for the time to reach 50% of full induction ( $t_{50}$ ; Fig. 2.3). As average  $t_{50}$  was 3 minutes, a time range in which Rubisco activity is normally most limiting, this suggests that  $[\text{CO}_2]$  did not affect this limitation. The overall effect of  $[\text{CO}_2]$  on  $t_{90}$  was visible for every dataset in Fig. 2.3, suggesting that decreasing  $t_{90}$  with increasing  $[\text{CO}_2]$  is a general response among plants. Induction data from Naumburg and Ellsworth (2000) and Holišová et al. (2012) were not included here, as they were not provided in the original studies.

In *S. oleracea* leaves, after small increases in irradiance, Rubisco activation was highly sensitive to  $[\text{CO}_2]$ . However, after large irradiance increases, it was  $[\text{CO}_2]$ -insensitive ( $[\text{CO}_2]$  range: 100-300  $\mu\text{mol mol}^{-1}$ ; Woodrow *et al.*, 1996). Woodrow and colleagues assumed that  $[\text{CO}_2]$ -sensitive activation reflected a limitation by Rubisco carbamylation,

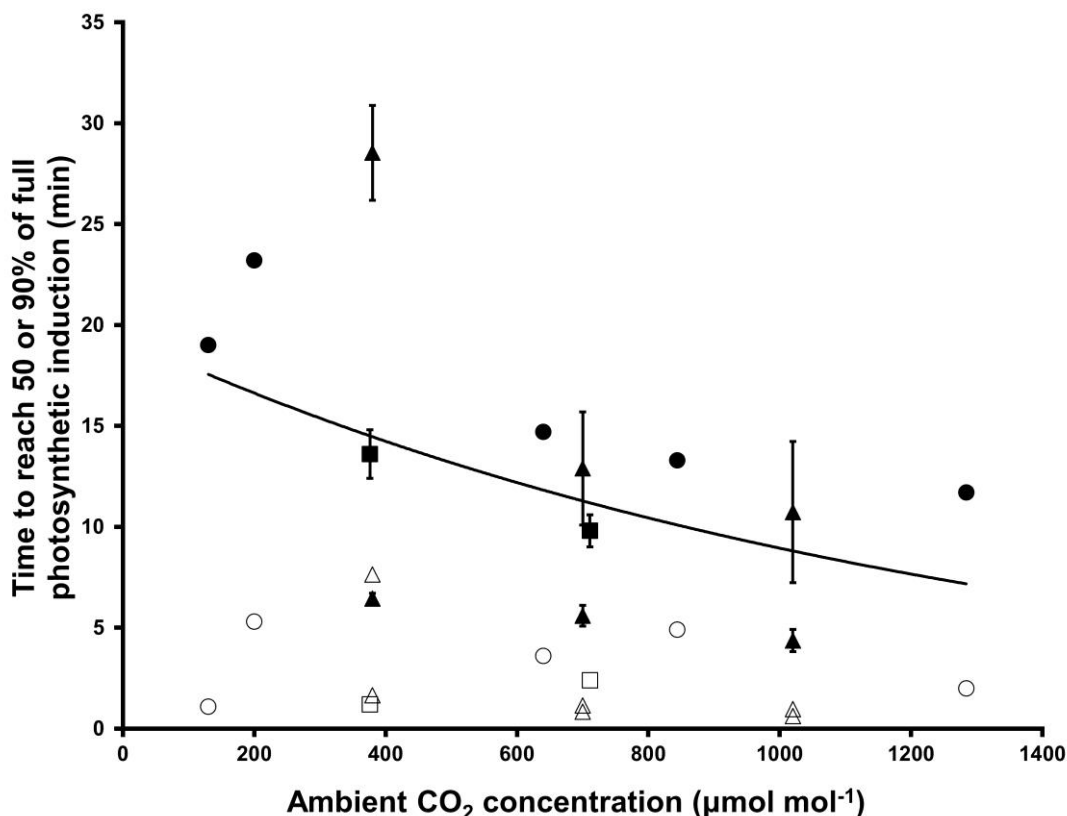


Fig. 2.3. Time (minutes) required to reach 50% ( $t_{50}$ , open symbols) and 90% ( $t_{90}$ , closed symbols) of full photosynthetic induction after a step increase in irradiance, as affected by ambient  $\text{CO}_2$  concentration ( $\mu\text{mol mol}^{-1}$ ). Data by Chazdon and Pearcy, 1986 (circles); Leakey *et al.*, 2002 (squares) and Tomimatsu and Tang, 2012 (triangles). Species included *Alocasia macrorrhiza* (circles), *Shorea leprosula* (squares) and *Populus koreana x trichocarpa* as well as *Populus euramericana* (triangles). Error bars ( $\pm\text{SE}$ ) are shown if supplied in the original publication. The negative exponential relationship ( $R^2 = 0.51$ ) between  $t_{90}$  and  $[\text{CO}_2]$  is described by:  $t_{90} = 22.7e^{-7E-04[\text{CO}_2]}$ . No relationship between  $t_{50}$  and  $[\text{CO}_2]$  was found

while  $[\text{CO}_2]$ -insensitive activation reflected Rca limitation. Elevated  $[\text{CO}_2]$  reduced the loss of induction (i.e. the deactivation of Calvin cycle enzymes and stomatal closure) in low irradiance after 5 (Leakey *et al.*, 2002), 6 and 12 minutes (Naumburg and Ellsworth, 2000), probably slowing down Rubisco deactivation. The relationship between low irradiance and  $[\text{CO}_2]$  affecting the loss of induction needs further exploration, as deactivation of Rubisco can be different between low irradiance and darkness.

High  $[\text{CO}_2]$  generally reduces  $g_s$ . However, effects of  $[\text{CO}_2]$  on  $g_s$  dynamics in fluctuating irradiance are less clear: While stomatal opening rates during lightflecks in elevated  $[\text{CO}_2]$  were increased in Naumburg *et al.* (2001) and Leakey *et al.* (2002), they were decreased in Tomimatsu and Tang (2012). Stomata closed faster after lightflecks in elevated  $[\text{CO}_2]$  (Naumburg *et al.*, 2001). Elevated  $[\text{CO}_2]$  also appears to decrease  $g_m$  in various plant species (Flexas *et al.*, 2007; 2008), however this apparent change may be due to changes in re-assimilation of  $\text{CO}_2$  emitted from the mitochondria (Tholen *et al.*, 2012). Elevated  $[\text{CO}_2]$  decreased steady-state NPQ at various irradiance levels in *Quercus ilex* (Arena *et al.*, 2005), and during long-term exposure in *Betula pendula* (Riikonen *et al.*, 2005). Additionally, elevated  $[\text{CO}_2]$  increased the overall efficiency of electron transport through PSII (Riikonen *et al.*, 2005), which should lead to smaller transient limitations of ETR after decreases in irradiance. Increasing  $[\text{CO}_2]$  decreases post-illumination  $\text{CO}_2$  fixation (Laisk *et al.*, 1984; Ruuska *et al.*, 1998; Sun *et al.*, 1999) and suppresses photorespiration and associated post-illumination  $\text{CO}_2$  burst (Vines *et al.*, 1983; Leakey *et al.*, 2002).

To summarize, elevated  $[\text{CO}_2]$  increases photosynthetic induction rates in  $\text{C}_3$  plants, and leads to slower loss of induction. More work is needed to confirm prior data on  $g_m$  dynamics as affected by both irradiance and  $[\text{CO}_2]$  (Flexas *et al.*, 2007), and to quantify interactions between irradiance and  $[\text{CO}_2]$  during loss of induction.

### *Temperature*

The temperature response of net photosynthesis generally follows a parabolic curve, often with an optimum at the growth temperature (e.g. Yamori *et al.*, 2014). Leaf temperature affects dynamic photosynthesis on many levels, due to temperature sensitivity of Rca and of the enzymes involved (Rubisco, FBPase, SBPase and PRK). Between 5 and 30 °C, net photosynthesis rates (Bernacchi *et al.*, 2013) and enzyme turnover generally increase. Increased turnover possibly reduces limitations due to the activation of RuBP-regeneration and Rubisco.

Combining data from photosynthetic induction experiments with various leaf temperatures during measurements (Küppers and Schneider, 1993; Pepin and Livingston, 1997; Leakey *et al.*, 2003; Yamori *et al.*, 2012; Carmo-Silva and Salvucci, 2013) revealed that

the response of  $t_{90}$  and  $t_{50}$  to leaf temperature was best described by parabolic relationships (Fig. 2.4), albeit with strong scatter. The optimum temperature for rate of photosynthetic induction was approx. 30 °C (Fig. 2.4). However, some datasets did not follow this trend (e.g. increasing  $t_{90}$  between 15 and 25 °C, closed diamonds in Fig. 2.4), leading to a less uniform response of induction rates to temperature than to  $[CO_2]$  (Fig. 2.3). Interestingly though, the parabolic effects of temperature on induction rates found here matched those for rates of Rubisco activation by Rca for *A. thaliana*, *Camelina sativa*, *N. tabacum* and *Gossypium hirsutum* (Carmo-Silva and Salvucci, 2011). At 38 °C compared to 28 °C, *S. leprosula* showed faster loss of photosynthetic induction, and photosynthesis was more strongly reduced in fluctuating (59% reduction) than in constant irradiance (40% reduction; Leakey *et al.*, 2003).

At moderately high temperatures (above 30-35 °C), Rubisco activity decreases (Eckardt and Portis, 1997), due to lowered Rca activity and faster formation of inhibitory sugar phosphates (Feller *et al.*, 1998; Salvucci and Crafts-Brandner, 2004; Yamori *et al.*, 2006). In

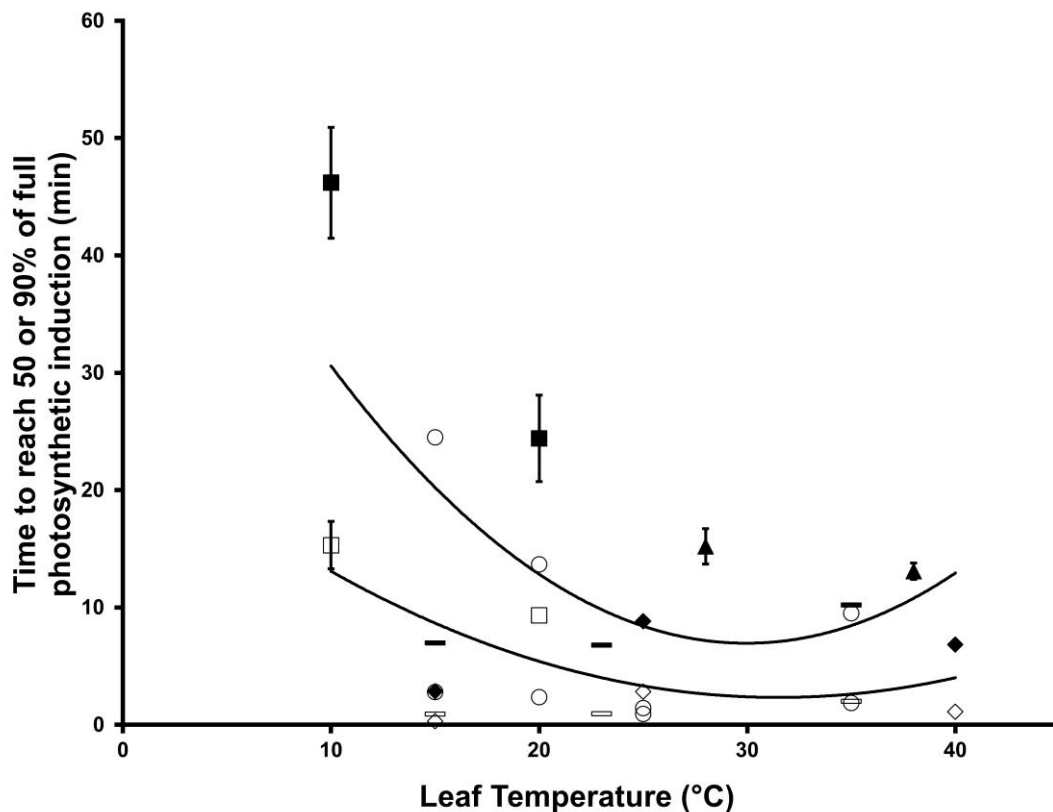


Fig. 2.4. Time (min) required to reach 50% ( $t_{50}$ , open symbols) and 90% ( $t_{90}$ , closed symbols) of full photosynthetic induction after a step increase in irradiance, as affected by leaf temperature ( $T$ , °C). Data by Küppers and Schneider, 1993 (circles); Pepin and Livingston, 1997 (squares); Leakey *et al.*, 2003 (triangles); Yamori *et al.*, 2012 (diamonds) and Carmo-Silva and Salvucci, 2013 (bars). Species included *F. sylvatica* (circles), *Thuja plicata* (squares), *Shorea leprosula* (triangles), *Oryza sativa* (diamonds) and *Arabidopsis thaliana* (bars). Error bars ( $\pm$ SE) are shown if supplied in the original publication. 2<sup>nd</sup> order polynomials were fitted.  $t_{90} = 0.06T^2 - 3.55T + 60.19$ ;  $R^2 = 0.34$  and  $t_{50} = 0.023T^2 - 1.47T + 25.41$ ;  $R^2 = 0.19$



most species, Rca forms high-molecular-weight aggregates that are catalytically incompetent above 30-35 °C (Feller *et al.*, 1998). However, examples of functioning photosynthesis at higher temperatures exist: The desert plant *Rhazya stricta* maintained irradiance- and CO<sub>2</sub>-saturated net photosynthesis rates up to 43 °C, which may be due to differences between the two isoforms of the plant's Rca (Lawson *et al.*, 2014). Transgenic *O. sativa* plants with increased Rca contents showed faster photosynthetic induction at 15, 25 and 40 °C due to higher Rubisco activation state at low irradiance (Yamori *et al.*, 2012). Thus, increased Rca contents or different Rca isoforms can enhance (dynamic) photosynthesis greatly in a large temperature range.

Photorespiration, and hence the post-illumination CO<sub>2</sub> burst, increases with temperature (Peterson, 1983), because the ratio [CO<sub>2</sub>]/[O<sub>2</sub>] in the chloroplast decreases, and because Rubisco specificity for O<sub>2</sub> increases (Foyer *et al.*, 2009). In *O. sativa*, post-illumination CO<sub>2</sub> fixation showed a parabolic response to leaf temperature, increasing in the range 10-30 °C and decreasing at higher leaf temperatures (Sun *et al.*, 1999).

No straightforward relationship exists between  $g_s$  and temperature. While rising temperatures increase net photosynthesis rates and guard cell metabolic activity (stimulating stomatal opening), increased  $C_i$  from higher respiration and photorespiration may have a diminishing effect on stomatal opening (Willmer and Fricker, 1996). Additionally,  $VPD_{\text{leaf-air}}$  increases concomitantly with leaf temperature, which is likely to decrease  $g_s$ . Thus, there is strong variation in optimum temperatures for maximum  $g_s$  (Willmer and Fricker, 1996). Mesophyll conductance, on the other hand, increases in many plant species between 5 and 20 °C and is either constant or decreases at higher temperatures (Flexas *et al.*, 2008). However, in *N. tabacum*,  $g_m$  and temperature were linearly correlated up to 40 °C (Evans and von Caemmerer, 2013).

In irradiance above 1000  $\mu\text{mol m}^{-2} \text{s}^{-1}$ , there was no relationship between NPQ and temperature (Bilger and Björkman, 1991; Clarke and Johnson, 2001), while in lower irradiances, steady-state NPQ decreased with increasing temperature (Clarke and Johnson, 2001). Furthermore, relaxation of NPQ after light-dark transitions was severely slowed down at temperatures below 20 °C (Bilger and Björkman, 1991; Gilmore and Björkman, 1995). Overall, this suggests small initial and quickly relaxing NPQ with increasing temperatures, and therefore reduced limitation of ETR after lightflecks.

Currently, knowledge lacks on how Rubisco deactivation, and decreases in  $g_s$  and  $g_m$  after lightflecks, are influenced by temperature. Furthermore, it is unclear how activation of RuBP regeneration and Rubisco are affected and which of these processes might consequently limit dynamic photosynthesis more strongly at a given temperature. This

knowledge is especially important between 10 and 30 °C, as in this temperature range most global plant productivity takes place.

To summarize, photosynthetic induction rates follow a parabolic response to temperature, with the fastest induction occurring around 30 °C, despite large variation between studies. Above 35 °C, photosynthesis suffers more from high temperature in fluctuating than in constant irradiance. Knowledge is lacking regarding the effects of temperature on the loss of photosynthetic induction and the temperature dependencies of RuBP-regeneration activation and Rubisco activation in fluctuating irradiance.

### *Air Humidity*

Air humidity can affect photosynthesis indirectly through  $C_i$ , as stomata tend to close in dry air. Even though  $g_s$  generally decreases with increasing  $VPD_{air}$ , the extent of stomatal control over transpiration rates differs strongly between species (Monteith, 1995). Whether changes in  $VPD_{air}$  affect rates of dynamic photosynthesis depends on the extent to which  $g_s$ , and consequently  $C_i$ , change in response to  $VPD_{air}$ , which in turn depends on species and leaf water status. The only study on  $VPD_{leaf-air}$  in dynamic photosynthesis (using *Piper aequale* and *Piper auritum*) showed that decreases in  $g_s$  and  $C_i$  in elevated  $VPD_{leaf-air}$  coincided with lowered photosynthetic induction rates, and increased stomatal limitation during induction (Tinoco-Ojanguren and Pearcy, 1993a). Of course, this may not be representative for all plants and growth conditions. Upon illumination, stomata of *P. aequale* and *P. auritum* in elevated  $VPD_{leaf-air}$  exhibited longer lag times in opening, and shorter lag times for closure, thus following a ‘water conservation’ response (Tinoco-Ojanguren and Pearcy, 1993a, b). In *Sambucus nigra* and *Aegopodium podagraria* leaves, stomata both opened and closed faster in elevated  $VPD_{leaf-air}$ ; additionally, stomatal aperture showed stronger oscillations during lightflecks in elevated  $VPD_{leaf-air}$  (Kaiser and Kappen, 2000; Kaiser and Kappen, 2001).

Decreased  $C_i$  between subsequent lightflecks might reduce Rubisco activation state, which would lead to slower Rubisco activation during lightflecks, as well as reduced carboxylation rates due to lower substrate availability. Very little is known about  $VPD_{leaf-air}$  effects on  $g_m$ , and some of the existing data are inconsistent (Flexas *et al.*, 2008). We hypothesize that  $VPD_{leaf-air}$  does not affect the other sub-processes in our framework.

In summary, elevated  $VPD_{leaf-air}$  lowers  $g_s$  to a variable extent, which might decrease  $C_i$ , affecting both carboxylation rates and Rubisco activation in fluctuating irradiance. Knowledge is most strongly lacking on sensitivity of dynamic  $g_s$  changes to  $VPD_{leaf-air}$  between species and its consequences for dynamic photosynthesis.

## Conclusions

The sub-processes of dynamic photosynthesis are differently affected by the climate: the activation state of RuBP-regeneration is only influenced by temperature, while the activation state of Rubisco is directly affected by  $[\text{CO}_2]$  and temperature, and indirectly (via  $C_i$ ) by  $\text{VPD}_{\text{leaf-air}}$ . Steady-state  $g_s$  is affected by all environmental factors. However, reported  $[\text{CO}_2]$  effects on  $g_s$  in fluctuating light are contradictory. In the case of temperature and  $\text{VPD}_{\text{leaf-air}}$  effects on dynamic  $g_s$ , almost no knowledge exists. Additionally, understanding the roles of  $g_m$  and NPQ in dynamic photosynthesis needs more work.

Leaf temperature and  $[\text{CO}_2]$  affect dynamic photosynthesis rates more strongly than  $\text{VPD}_{\text{leaf-air}}$ , however leaf temperature and  $[\text{CO}_2]$  effects have been studied more often, such that this conclusion may shift with more experimental evidence. Data comparison revealed similar directionality for  $[\text{CO}_2]$  effects across studies (Fig. 2.3), while leaf temperature effects were more scattered and non-uniform (Fig. 2.4).  $\text{VPD}_{\text{leaf-air}}$  may affect dynamic photosynthesis indirectly through  $C_i$ . However, its relative impact on photosynthetic gas exchange likely depends on the sensitivity of  $g_s$  to  $\text{VPD}_{\text{leaf-air}}$ . Further, in order to fully understand and quantify dynamic photosynthesis, loss is just as important as gain of photosynthetic induction. Much less literature is available on the former, as loss of induction studies are more time consuming. Loss of induction was diminished in elevated  $[\text{CO}_2]$ , and enhanced in elevated temperatures, while effects of  $\text{VPD}_{\text{leaf-air}}$  have not been reported.

Large leaps in knowledge were recently made by using genetic transformants or mutants of underlying processes of dynamic photosynthesis, e.g. Rubisco activation by Rca (Yamori *et al.*, 2012; Carmo-Silva and Salvucci, 2013) and the regulation of NPQ (Hubbart *et al.*, 2012; Suorsa *et al.*, 2012). Affecting one sub-process of dynamic photosynthesis at a time, as can be done using mutants or genetic transformants, can help understand the regulation of the system and quantify the effects that one sub-process has on dynamic photosynthesis, possibly in various environmental conditions.

## Funding

This work was supported in part by the BioSolar Cells open innovation consortium, supported by the Dutch Ministry of Economic Affairs, and in part by Essent.

## Acknowledgements

Andreas Savvides and Nikolaos Ntagkas are gratefully acknowledged for highly useful discussions and comments on the manuscript.



## CHAPTER 3

Photosynthetic induction in tomato (*Solanum lycopersicum*) leaves and its diffusional, carboxylation and electron transport processes as affected by CO<sub>2</sub> concentration, temperature, air humidity and blue light

**Authors:**

Elias Kaiser

Johannes Kromdijk

Jeremy Harbinson

Ep Heuvelink

Leo F.M. Marcelis

Under review

## Abstract

Plants depend on photosynthesis for growth. In nature, factors like temperature, humidity, CO<sub>2</sub> concentration and spectrum and intensity of irradiance often fluctuate. Whereas irradiance intensity is most influential and has been studied in detail, understanding of interactions with other factors is lacking. It was tested how photosynthetic induction after dark-light transitions was affected by CO<sub>2</sub> concentrations (200, 400, 800 ppm), leaf temperatures (15.5, 22.8, 30.5 °C), leaf-to-air vapour pressure deficit (VPD<sub>leaf-air</sub>; 0.5, 0.8, 1.6, 2.3 kPa) and blue light (0-20%) in tomato leaves (*Solanum lycopersicum*). Rates of photosynthetic induction strongly increased with CO<sub>2</sub> concentrations, due to increased Rubisco activation rates and reduced diffusional limitations. High leaf temperature produced slightly higher induction rates, and increased mesophyll conductance, intrinsic water use efficiency and diffusional limitation. High VPD<sub>leaf-air</sub> slowed down induction rates and Rubisco activation and (at 2.3 kPa) induced damped stomatal oscillations. Blue light had no effect. Slower Rubisco activation in elevated VPD<sub>leaf-air</sub> may be explained by low leaf internal CO<sub>2</sub> concentration in the beginning of induction. The environmental factors CO<sub>2</sub> concentration, temperature and VPD<sub>leaf-air</sub> had significant impacts on rates of photosynthetic induction, as well as on underlying diffusional, carboxylation and electron transport processes. Furthermore, maximising Rubisco activation rates would increase photosynthesis by at most 6-10% in ambient CO<sub>2</sub> concentration (across temperatures and humidities), while maximising rates of stomatal opening would increase photosynthesis by at most 1-2%.

Keywords: Dynamic photosynthesis, CO<sub>2</sub> concentration, temperature, humidity, stomatal conductance, diffusional limitation, Rubisco, *Solanum lycopersicum*

## Introduction

When a dark-adapted leaf is exposed to irradiance, net photosynthesis rates ( $A_n$ ) slowly approach a new steady state. This process, photosynthetic induction, was discovered almost a century ago (Osterhout & Haas, 1918), and its underlying mechanisms have been studied extensively (for review see Pearcy and Way, 2012). The main mechanisms that affect rates of photosynthetic induction, and dynamic responses of photosynthesis to fluctuating irradiance, are activation of Calvin cycle enzymes (including Rubisco) and stomatal opening (Pearcy *et al.*, 1996). However, photosynthetic induction is influenced by many factors: previous irradiance intensity and duration of exposure, plant functional type and environmental conditions modulate its range and kinetics. While previous studies have shown that environmental factors such as  $\text{CO}_2$  concentration ( $C_a$ ), leaf temperature ( $T_{\text{leaf}}$ ), leaf-to-air vapour pressure deficit ( $\text{VPD}_{\text{leaf-air}}$ ) and blue light can modulate the response of photosynthesis as it reacts to fluctuating irradiance (reviewed in Kaiser *et al.*, 2015), no study has systematically compared the effects of all of these factors on the photosynthetic response to dark-light transitions.

Due to the wind-induced movement of leaves, canopies and clouds, irradiance incident on leaves often fluctuates, forcing photosynthesis to respond dynamically, and reducing light use efficiency compared to the steady state. Currently, there is renewed interest in the dynamic components of photosynthesis, as a) faster activation of Rubisco could lead to greater resource use efficiency and productivity (Carmo-Silva *et al.*, 2015), b) stomata that react faster to changes in irradiance could lead to greater intrinsic water use efficiency ( $\text{WUE}_i$ ; Lawson and Blatt, 2014), c) increasing the rate of relaxation of non-photochemical quenching (NPQ) may lead to increased photosynthetic quantum yield when irradiance is limiting (Murchie & Niyogi, 2011) and d) predictions of assimilation that account for the responses to fluctuating irradiances could lead to more accurate forecasts of plant productivity (Kaiser *et al.*, 2015). To address these research questions, behaviour of dynamic photosynthesis in  $\text{C}_3$  crop species must be thoroughly understood. However, most effort in this field has been directed towards understory shrubs and trees, and only few studies have investigated dynamic photosynthesis and its environmental modulation in  $\text{C}_3$  species with high photosynthetic capacity (Carmo-Silva and Salvucci, 2013; Yamori *et al.*, 2012). Such experiments are necessary to quantify limitations to photosynthesis in fluctuating irradiance and to assess how each limiting factor is affected by environmental conditions.

The enzymes that regenerate ribulose-1,5-bisphosphate (RuBP) are activated rapidly during photosynthetic induction (Sassenrath-Cole & Pearcy, 1992). RuBP supply to Rubisco is assumed to be non-limiting after the first minute of induction (Pearcy *et al.*,

1996; Woodrow and Mott, 1989). Rubisco itself typically takes 7-10 minutes to fully activate (Percy *et al.*, 1996), and both the extent of its limitation during photosynthetic induction and the time constant of its activation ( $\tau_R$ ) can be calculated from data obtained by gas exchange measurements (Woodrow & Mott, 1989). The slow increase of stomatal conductance ( $g_s$ ) can impose an additional diffusional limitation on induction. By recalculating the rates of photosynthesis that would have occurred had  $\text{CO}_2$  concentration at the site of carboxylation ( $C_c$ ) been the same as  $C_a$ , the diffusional limitation acting on transient and steady-state  $A_n$  can be quantified. This diffusional limitation may also include a component in the mesophyll, which may be assessed by measuring mesophyll conductance ( $g_m$ ). Mesophyll conductance has often been suggested to vary with irradiance,  $C_a$  and temperature (Flexas *et al.*, 2007; 2008; von Caemmerer and Evans 2015). However, to the best of the authors' knowledge, no study has examined possible changes of  $g_m$  during induction and the additional limitations that these changes could have on dynamic photosynthesis rates.

During photosynthetic induction, electron and proton transport processes undergo rapid changes, affecting the efficiency of electron transport through photosystem II ( $\Phi_{\text{PSII}}$ ) and NPQ. Similar to steady-state photosynthesis,  $\Phi_{\text{PSII}}$  correlates with gross photosynthesis ( $A_{\text{gr}}$ ) during induction (Kořvancová-Zitova *et al.*, 2009; Yamori *et al.*, 2012), and deviations from this relationship can be used to infer the extent of photorespiration, by means of changes in the slope of the  $\Phi_{\text{PSII}}/A_{\text{gr}}$  relationship. NPQ often overshoots at the start of induction (D'Haese *et al.*, 2004), which may be due to the decrease of lumen pH when linear electron transport rate (ETR) is limited by low photosynthetic metabolic activity. Hence, measurement of  $\Phi_{\text{PSII}}$  and NPQ concurrent with gas exchange during photosynthetic induction can provide detailed information about underlying processes of photosynthetic induction.

Dynamic photosynthesis and its modulation by environmental factors other than irradiance intensity must be better understood in order to improve it. We characterized photosynthetic induction in tomato (*Solanum lycopersicum*), a  $C_3$  model species that has a leaf photosynthetic capacity of 20-30  $\mu\text{mol m}^{-2} \text{s}^{-1}$  and is an important crop both in open field and protected cultivation. During photosynthetic induction after a dark-light transition, it is shown how stomatal and mesophyll conductance, intrinsic water use efficiency, Rubisco activation, and electron transport processes are affected by  $C_a$ ,  $T_{\text{leaf}}$ ,  $\text{VPD}_{\text{leaf-air}}$  and blue light. Furthermore, the temporal behaviour of transient diffusional and biochemical limitations is shown. Finally, we discuss how strongly photosynthesis would benefit from higher rates of Rubisco activation or stomatal opening after dark-light transitions.



## Materials and Methods

### *Plant material*

Tomato seeds (*Solanum lycopersicum* 'Cappricia'; Rijk Zwaan, De Lier, NL) were germinated in Rockwool plugs (Grodan, Roermond, NL), which after a week were transferred to Rockwool cubes (10 cm \* 10 cm \* 7 cm; Grodan). Plants were grown in a climate chamber in 16/8 h photoperiod, 22/20 °C (day/night) temperature, 70% relative humidity and 320  $\mu\text{mol m}^{-2} \text{s}^{-1}$  photosynthetically active radiation (PAR), measured at table height. Irradiance was provided by a mixture of white, red and far-red LEDs with emission peaks at 440, 550, 660 and 735 nm. Rockwool cubes were standing in a layer (height: 1-2 cm) of nutrient solution (Yara Benelux B.V., Vlaardingen, the Netherlands), which was replenished every 1-2 days and contained 12.42 mM  $\text{NO}_3$ , 7.2 mM K, 4.1 mM Ca, 3.34 mM  $\text{SO}_4$ , 1.82 mM Mg, 1.2 mM  $\text{NH}_4$ , 1.14 mM P, 30  $\mu\text{M}$  B, 25  $\mu\text{M}$  Fe, 10  $\mu\text{M}$  Mn, 5  $\mu\text{M}$  Zn, 0.75  $\mu\text{M}$  Cu and 0.5  $\mu\text{M}$  Mo (EC 2.1 dS  $\text{m}^{-1}$ , pH 5.5). When plants were between five and six weeks old, leaves 4 and 5, counting from the bottom, were used for measurements. At this stage, growth of these leaves was almost complete (data not shown).

### *Gas exchange and chlorophyll fluorescence measurements*

Measurements of transient and steady-state  $A_n$  were performed using the LI-6400 photosynthesis system (Li-Cor Biosciences, Lincoln, Nebraska, USA) equipped with the leaf chamber fluorometer (Li-Cor Part No. 6400-40, area 2  $\text{cm}^2$ ).

*Photosynthetic induction:* To assess the response of gas exchange to a step increase in irradiance, leaves were first dark-adapted at the treatment levels described below until  $g_s$  was constant (60-120 minutes). Then, irradiance was increased to 1000  $\mu\text{mol m}^{-2} \text{s}^{-1}$  in a step change and gas exchange values were logged every second for 60 minutes. Irradiance of 1000  $\mu\text{mol m}^{-2} \text{s}^{-1}$  was ~5% below saturation, which was a compromise between using a fully saturating irradiance and the desire to avoid photoinhibition of photosynthesis. The flow rate of air was 500  $\mu\text{mol s}^{-1}$ . Other than when adjusted as part of a treatment, the standard conditions in the cuvette were: 397-403 ppm  $C_a$  (range of lowest to highest value), 0.7-1.0 kPa  $\text{VPD}_{\text{leaf-air}}$ , 22.3-23.3 °C  $T_{\text{leaf}}$  and 90 / 10% red / blue light mixture provided by LEDs. Peak intensities of red and blue LEDs were at wavelengths of 635 and 465 nm, respectively. Treatments were applied individually and included: 200, 400 and 800 ppm  $C_a$ , 15.5, 22.8 and 30.5 °C  $T_{\text{leaf}}$ , 0.5, 0.8, 1.6 and 2.3 kPa  $\text{VPD}_{\text{leaf-air}}$  (0.4, 0.9, 1.7 and 2.5  $\text{VPD}_{\text{air}}$ ) and 0, 1, 5, 10 and 20% blue light in a red light background. For each treatment, five biological replicates were used ( $n = 5$ ). All measurements except the 15.5 and 30.5 °C  $T_{\text{leaf}}$  treatments (which were performed in two different climate chambers) were performed in a lab. The values of all cuvette conditions reported here are averages over whole induction

curves. Transient  $A_n$ ,  $g_s$  and  $C_i$  were averaged over 5 data points using a moving average filter to reduce measurement noise. Assimilation was corrected for  $\text{CO}_2$  leaks using dried leaves (Long & Bernacchi, 2003).

To analyse the effect of  $C_a$  and  $T_{\text{leaf}}$  on photosynthetic electron transport processes, another set of induction curves was performed on different leaves, but using the same cuvette conditions as described above. Relative electron transport rate was estimated from measurements of  $\Phi_{\text{PSII}}$ , which was calculated from measurements of  $F_s$  (fluorescence yield under continuous actinic irradiance) and  $F_m'$  (maximum fluorescence yield during a saturating light pulse). The measurements of  $F_m'$  were also used to calculate NPQ according to the Stern-Volmer quenching model and using a measure of  $F_m$  made on dark-adapted leaves. To ensure the accurate measurement of  $F_m'$ , the multi-phase flash (MPF) protocol of the Li-Cor fluorometer was used (Loriaux *et al.*, 2013). Use of MPFs instead of a single saturating pulse prevents underestimation of maximum chlorophyll fluorescence yield in light-adapted leaves of high photosynthetic capacity.  $F_m'$  estimated by the MPF was  $\sim 4\%$  larger than measured  $F_m'$ , and the difference between estimated and measured  $F_m'$  developed within the first ten minutes of light adaptation (Fig. S3.1) Settings of the MPF were determined in preliminary measurements and were  $8500 \mu\text{mol m}^{-2} \text{s}^{-1}$  flash intensity,  $5 \mu\text{mol m}^{-2} \text{s}^{-1}$  measuring beam intensity, 60% decrease of flash intensity during the 2<sup>nd</sup> phase of the MPF and 0.3, 0.7 and 0.4 s duration of the three flash phases. These settings yielded a very good correlation ( $R^2 \approx 0.99$ ) between flash intensity and  $F_m'$  values during flash phase 2, after the first or second minute of induction (data not shown). Preliminary data showed that  $\text{VPD}_{\text{leaf-air}}$  had produced limited effects on  $\Phi_{\text{PSII}}$  or NPQ (data not shown); for that reason, those measurements were not repeated here. Measurements of  $F_m'$  were made once a minute during the first ten minutes of induction, and once every two minutes thereafter.

*$A_n/C_i$  curves:* To estimate the parameters  $V_{\text{Cmax}}$ , ETR, TPU and  $\Gamma^*$ ,  $A_n/C_i$  curves were first performed in photorespiratory and then in non-photorespiratory conditions (21 and 2% oxygen, respectively; Fig. S3.2). Each curve contained 11 points. Leaves were exposed to a range of  $C_a$  between 50 and 1500 ppm. Data were logged every 5 seconds, and averages of 10 values at each  $C_a$  step, after steady-state photosynthesis had visibly been reached, were used. Other cuvette conditions were:  $1000 \mu\text{mol m}^{-2} \text{s}^{-1}$  PAR, 0.8 kPa  $\text{VPD}_{\text{leaf-air}}$  and  $23^\circ\text{C}$   $T_{\text{leaf}}$ .

*$A_n/\text{PAR}$  curves:* To estimate parameters  $R_d$  and  $s$  (lumped parameter scaling  $\Phi_{\text{PSII}}$  to ETR), irradiance-limited curves were performed in non-photorespiratory conditions. The intercept of the linear  $A_n/(\text{PAR} * \Phi_{\text{PSII}} * 0.25)$  relationship (Fig. S3.3) was  $R_d$ , while the slope was  $s$  (Yin *et al.*, 2009). Leaves were adapted to  $200 \mu\text{mol m}^{-2} \text{s}^{-1}$ , until  $A_n$  and  $g_s$  were stable. Then, leaves were exposed to a range of PAR values between 0 and  $200 \mu\text{mol m}^{-2} \text{s}^{-1}$ .

Assimilation was determined as described in  $A_n/C_i$  curves. Additionally,  $\Phi_{PSII}$  was determined as discussed above. Other cuvette conditions were: 400 ppm  $C_a$ , 0.8 kPa  $VPD_{leaf-air}$  and 22 °C  $T_{leaf}$ .

### Calculations

The progress of photosynthetic induction was calculated as the transient rate of photosynthesis ( $A_{n(t)}$ ,  $\mu\text{mol m}^{-2} \text{s}^{-1}$ ) as a percentage of the steady-state rate ( $A_{n(tf)}$ ), corrected for dark respiration ( $A_{n(t_0)}$ ):

$$\text{Photosynthetic induction} = \frac{A_{n(t)} - A_{n(t_0)}}{A_{n(tf)} - A_{n(t_0)}} * 100 \quad (3.1)$$

The relative rates of increase of  $g_s$  ( $\text{mol m}^{-2} \text{s}^{-1}$ ) during induction were calculated similarly. Diffusional limitation was calculated as the percentage by which  $A_n$  would increase if  $\text{CO}_2$  concentration at the site of carboxylation ( $C_c$ ) was equal to  $C_a$ . For this,  $A_n$  was first corrected ( $A_{n(t)_{C_a}}$ ) for changes in transient  $C_i$  ( $C_{i(t)}$ ) using previously determined  $A_n/C_i$  parameters:

$$A_{n(t)_{C_a}} = A_{n(t)} * \frac{\min\{A_{n(c)}(C_a), A_{n(j)}(C_a), A_{n(TPU)}(C_a)\}}{\min\{A_{n(c)}(C_{i(t)}), A_{n(j)}(C_{i(t)}), A_{n(TPU)}(C_{i(t)})\}} \quad (3.2)$$

Rubisco activity-limited  $A_n$  ( $A_{n(c)}$ ), RuBP-limited  $A_n$  ( $A_{n(j)}$ ) and triose phosphate utilization-limited  $A_n$  ( $A_{n(TPU)}$ ) were determined according to Sharkey et al. (2007):

$$A_{n(c)} = V_{Cmax} \left( \frac{C_a - \Gamma^*}{C_a + K_c * \left(1 + \frac{O}{K_o}\right)} \right) - R_d \quad (3.3)$$

$$A_{n(j)} = ETR \left( \frac{C_a - \Gamma^*}{4 * C_a + 8 * \Gamma^*} \right) - R_d \quad (3.4)$$

$$A_{n(TPU)} = 3 * TPU - R_d \quad (3.5)$$

Where  $V_{Cmax}$  ( $\mu\text{mol m}^{-2} \text{s}^{-1}$ ) is maximum velocity of Rubisco for carboxylation,  $\Gamma^*$  is the chloroplast  $\text{CO}_2$  compensation point (ppm) in the absence of day respiration ( $R_d$ ;  $\mu\text{mol m}^{-2} \text{s}^{-1}$ ),  $O$  (ppm) is the chloroplast  $\text{O}_2$  concentration,  $K_c$  (kPa) and  $K_o$  (kPa) are the Michaelis-Menten constants of Rubisco for  $\text{CO}_2$  and for  $\text{O}_2$ , respectively,  $ETR$  ( $\mu\text{mol m}^{-2} \text{s}^{-1}$ ) is the electron transport rate and  $TPU$  ( $\mu\text{mol m}^{-2} \text{s}^{-1}$ ) is the triose phosphate utilization rate. Parameters  $V_{Cmax}$ ,  $ETR$  and  $TPU$  were estimated after Sharkey et al. (2007),  $R_d$  and  $\Gamma^*$  after Yin et al. (2009). Additionally,  $R_d$  was corrected for respiration under the gasket of the gas exchange cuvette (Pons & Welschen, 2002). Parameters  $K_c$  and  $K_o$  were

taken from Sharkey et al. (2007). All parameters were temperature-adjusted (Bernacchi *et al.*, 2001), their values are given in Table 3.1. Diffusional limitation was determined as

$$\text{Diffusional limitation} = \frac{A_{n(t)C_a} - A_{n(t)}}{A_{n(tf)} - A_{n(t_0)}} * 100 \quad (3.6)$$

Biochemical limitation was calculated by using transient  $A_n$  corrected for changes in  $C_i$  ( $A_{n(t)C_i}$ ). Thus, instead of using  $C_a$  in the numerator of Eqn. 3.2, steady-state  $C_i$  ( $C_{i(tf)}$ ) was used. Then, biochemical limitation was calculated as

$$\text{Biochemical limitation} = \frac{A_{n(tf)} - A_{n(t)C_i}}{A_{n(tf)} - A_{n(t_0)}} * 100 \quad (3.7)$$

Time constants of Rubisco activation ( $\tau_R$ ; minutes) were calculated following Woodrow and Mott (1989):

$$\tau_R = \frac{\Delta \text{time}}{\Delta \ln(A_{n(tf)} - A_{n(t)C_i})} \quad (3.8)$$

For the  $C_a$  and  $VPD_{\text{leaf-air}}$  treatments, data from minutes 2-5 during induction were used in Eqn. 3.8, while in the case of  $T_{\text{leaf}}$ , data were taken from minutes 5-8 during induction, to account for a possible slower activation of RuBP regeneration in the beginning of induction in the case of low  $T_{\text{leaf}}$ . Intrinsic water use efficiency ( $WUE_i$ ;  $\mu\text{mol CO}_2 \text{ mmol}^{-1} \text{ H}_2\text{O}$ ) was calculated as:

$$WUE_i = \frac{A_{n(t)}}{g_{s(t)}} \quad (3.9)$$

Table 3.1. Parameters used in the calculations of diffusional limitation (Eqns. 3.3-3.5) and of mesophyll conductance (Eqn. 10). Parameters  $J$ ,  $TPU$  and  $VC_{\text{max}}$  were determined from  $A_n/C_i$  curves after Sharkey et al. (2007),  $K_c$  and  $K_o$  were taken from Sharkey et al. (2007),  $R_d$  and  $\Gamma^*$  were determined from  $A_n/PAR$  and  $A_n/C_i$  curves after Yin et al. (2009). All parameters were temperature-adjusted after Bernacchi et al. (2001)

Parameter	Unit	Temperature		
		15.5 °C	22.8 °C	30.5 °C
$J$	$\mu\text{mol electrons m}^{-2} \text{ s}^{-1}$	94.33	148.16	232.97
$K_c$	Pa	9.29	21.36	49.25
$K_o$	kPa	12.04	15.37	19.63
$R_d$	$\mu\text{mol CO}_2 \text{ m}^{-2} \text{ s}^{-1}$	0.77	1.23	2.00
$TPU$	$\mu\text{mol CO}_2 \text{ m}^{-2} \text{ s}^{-1}$	5.98	10.32	17.84
$VC_{\text{max}}$	$\mu\text{mol CO}_2 \text{ m}^{-2} \text{ s}^{-1}$	43.35	84.86	166.44
$\Gamma^*$	$\mu\text{mol CO}_2 \text{ mol}^{-1} \text{ air}$	36.17	53.37	78.83

Where  $g_{s(t)}$  is transient stomatal conductance.  $\Phi_{PSII}$  and NPQ were calculated after Genty et al. (1989) and Bilger and Björkman (1991), respectively. The coefficient of photochemical quenching (qP) and PSII maximum efficiency ( $F_v'/F_m'$ ) was calculated after Oxborough and Baker (1997). Transient chloroplast  $CO_2$  concentration ( $C_{c(t)}$ ) was calculated as:

$$C_{c(t)} = \frac{\Gamma^*(ETR_{(t)} + 8*(A_{n(t)} + R_d))}{ETR_{(t)} - 4*(A_{n(t)} + R_d)} \quad (3.10)$$

Transient ETR ( $ETR_{(t)}$ ) was calculated as

$$ETR_{(t)} = \Phi_{PSII} * PAR * s \quad (3.11)$$

Where  $s$  is a unitless lumped calibration factor used to scale  $\Phi_{PSII}$  to ETR (Yin *et al.*, 2009). Transient mesophyll conductance ( $g_{m(t)}$ ;  $mo\ m^{-2}\ s^{-1}$ ) was calculated as:

$$g_{m(t)} = \frac{A_{n(t)}}{C_{i(t)} - C_{c(t)}} \quad (3.12)$$

The sensitivity of  $g_m$  to errors in parameter estimations was calculated after Harley et al. (1992), as the slope of  $C_c$  vs.  $A_{gr}$  (gross photosynthesis)

$$\frac{dC_c}{dA_{gr}} = \frac{12*\Gamma^* * ETR_{(t)}}{(ETR_{(t)} - 4*(A_{n(t)} + R_d))^2} \quad (3.13)$$

### *Statistical analysis*

Data were tested for normality (Shapiro-Wilk test; Genstat 16<sup>th</sup> Ed., VSN International, Hemphstead, UK) and homogeneity of variances (Fligner-Killeen test; R, R Core team). Then, one-way analysis of variance (ANOVA; Genstat) was performed, followed by Fisher's protected LSD (Genstat) for determining significant differences between treatments.

## Results

### *Induction of photosynthetic CO<sub>2</sub> fixation*

Overall, the relative rates of photosynthetic induction increased with  $C_a$  (Fig. 3.1A), affecting the time to reach 50 and 90% of full induction ( $t_{A50}$  and  $t_{A90}$ , respectively), but not the induction state at 60 s ( $IS_{60}$ ; Table 3.2). High  $T_{leaf}$  (30.5 °C) increased induction slightly in the first five minutes (Fig. 3.1C), affecting  $IS_{60}$  and  $t_{A50}$ , but not  $t_{A90}$  (Table 3.2). Elevated  $VPD_{leaf-air}$  slowed down induction after ~5 minutes (Fig. 3.1E), increasing  $t_{A90}$  in 1.6 kPa (Table 3.2).  $VPD_{leaf-air}$  of 2.3 kPa induced oscillations of induction rates (Fig. 3.1E), without affecting the various induction parameters. Different percentages of blue light (0-20%) did not affect any of the parameters tested (Table 3.2), nor did they have visible effects on other parameters discussed here (data not shown).

### *Stomatal conductance*

Stomata opened faster in low  $C_a$  (Fig. 3.1B) and reached higher conductance after 60 minutes ( $g_{s(tf)}$ , Table 3.2). However, because  $g_s$  levelled off earlier in intermediate and high  $C_a$ , the time to reach 90% of full stomatal conductance ( $t_{gs90}$ ) was significantly longer in low  $C_a$  (Table 3.2). Both low (15.5 °C) and high  $T_{leaf}$  decreased  $g_s$  in darkness ( $g_{s(to)}$ , Table 3.2) and decreased the extent of stomatal opening during induction (Fig. 3.1D), leading to lower steady-state  $g_{s(to)}$  compared to intermediate  $T_{leaf}$  (22.8 °C). Elevated  $VPD_{leaf-air}$  affected stomata by a) decreasing  $g_{s(to)}$  and  $g_{s(tf)}$ , b) increasing relative opening rates in the first 15 minutes of induction, c) inducing dampening stomatal oscillations at the highest  $VPD_{leaf-air}$  (2.3 kPa) and d) forcing stomata to reach steady-state  $g_s$  more quickly (or quasi steady-state in the case of oscillating  $g_s$ ; Fig. 3.1F, Table 3.2). Despite decreasing  $g_{s(to)}$  by 40-55% compared to low  $VPD_{leaf-air}$ , high  $VPD_{leaf-air}$  did not affect steady-state photosynthesis at 60 minutes ( $A_{n(tf)}$ ; Table 3.2), suggesting that in the steady state, diffusional limitation of  $A_n$  was no longer sensitive to  $VPD_{leaf-air}$ .

### *Intrinsic water use efficiency (WUE<sub>i</sub>)*

$WUE_i$ , a result of dynamic changes in  $A_n$  and  $g_s$ , was strongly affected by  $C_a$ : Not only its steady-state level, but also its rate of change in the first 30 minutes of induction was much higher in high than in low  $C_a$  (Fig. 3.2A). Because of slower  $g_s$  increases with similar increases in  $A_n$  in the beginning of induction, both low and high  $T_{leaf}$  produced higher  $WUE_i$  than intermediate  $T_{leaf}$  (Fig. 3.2B). A similar reasoning applies to  $VPD_{leaf-air}$ : because elevated  $VPD_{leaf-air}$  reduced  $g_s$  more strongly than  $A_n$  during and after induction,  $WUE_i$  was highest in 2.3 kPa, followed by 1.6 kPa (Fig. 3.2C). The 0.8 and 0.5 kPa treatments showed lowest  $WUE_i$  and were no different from each other (Fig. 3.2C).

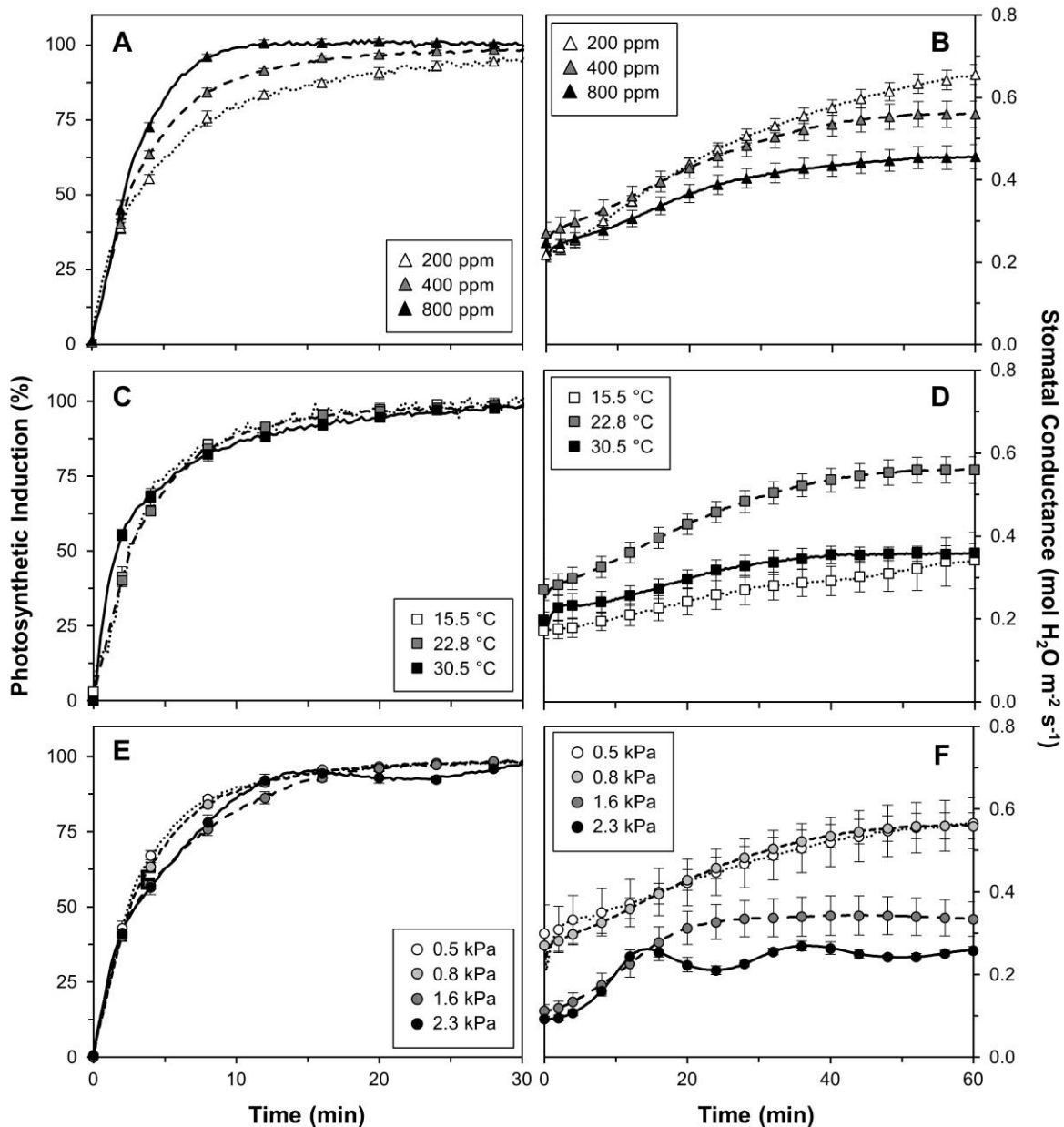


Fig. 3.1. Photosynthetic induction (A, C, E) and stomatal conductance (B, D, F) in dark-adapted tomato leaves, as affected by  $C_a$  (A, B),  $T_{\text{leaf}}$  (C, D) and  $VPD_{\text{leaf-air}}$  (E, F). Irradiance was raised from 0 to  $1000 \mu\text{mol m}^{-2} \text{s}^{-1}$  at time = 0 and kept steady for 60 minutes. In panels A, C and E, the first 30 minutes of induction are shown. Average  $\pm$  SE ( $n = 5$ )

### *Diffusional and biochemical limitations during photosynthetic induction*

Diffusional limitation quantifies the extent to which any resistance to  $\text{CO}_2$  diffusion in the leaf (i.e.  $g_s$  and  $g_m$ ) during and after induction limits photosynthesis. Biochemical limitation quantifies the extent to which biochemical processes that activate during induction limit photosynthesis during induction, but not in the steady state. In all treatments except at high VPD (2.3 kPa), transient diffusional limitation increased to its maximum within the first 15 minutes due to the activation of Rubisco, and then slowly relaxed to its steady-state level as stomata opened. Biochemical limitation was at its maximum in the very beginning

Table 3.2. Dynamic and steady-state parameters of photosynthetic induction in tomato leaves, as affected by  $C_a$ ,  $T_{\text{leaf}}$ ,  $VPD_{\text{leaf-air}}$  and blue light. Dynamic parameters include  $IS_{60}$  (induction 60 seconds after illumination, %),  $t_{A50}$ ,  $t_{A90}$ ,  $t_{g50}$  and  $t_{g90}$  (time (minutes) to reach 50 and 90% of photosynthetic induction and time to reach 50 and 90% of full stomatal opening). Steady-state parameters were calculated by averaging single values over 2 minutes (either in dark-adapted leaves or at the end of induction) and include  $A_{n(t0)}$ ,  $A_{n(tr)}$ ,  $g_{s(t0)}$  and  $g_{s(tr)}$  ( $A_n$  and  $g_s$  in dark and in 1000  $\mu\text{mol m}^{-2} \text{s}^{-1}$ , respectively; units:  $A_n$  expressed in  $\mu\text{mol m}^{-2} \text{s}^{-1}$  and  $g_s$  in  $\text{mol m}^{-2} \text{s}^{-1}$ ). Letters denote significant differences ( $P < 0.05$ ) between treatments, absence of letters denotes absence of significant effects ( $n=5$ ).

Treatment	Dynamic parameters										Averages at start and end of induction				
	$IS_{60}$	$t_{A50}$	$t_{A90}$	$t_{g50}$	$t_{g90}$	$A_D$	$A_L$	$g_{SD}$	$g_{SL}$						
200 $\mu\text{mol mo}$	25.7 ± 3.0	3.2 ± 0.6 b	18.5 ± 4.0 b	19.8 ± 1.2	46.7 ± 1.4 b	-1.1 ± 0.6	11.7 ± 1.3 a	0.22 ± 0.04	0.65 ± 0.05 c						
400 $\mu\text{mol mo}$	21.6 ± 2.7	2.6 ± 0.2 a	10.8 ± 1.4 ab	18.7 ± 3.1	38.2 ± 5.6 a	-1.6 ± 0.3	22.2 ± 1.4 b	0.27 ± 0.06	0.56 ± 0.07 b						
800 $\mu\text{mol mo}$	21.9 ± 4.4	2.2 ± 0.3 a	6.2 ± 0.3 a	18.2 ± 2.2	39.9 ± 4.7 a	-1.3 ± 0.6	27.1 ± 2.3 c	0.25 ± 0.06	0.46 ± 0.07 a						
15.5 °C	15.8 ± 4.5 a	2.7 ± 0.3 b	12.6 ± 1.4	24.4 ± 4.8	42.5 ± 1.4	-1.1 ± 0.3 b	15.6 ± 2.2 a	0.17 ± 0.16 a	0.34 ± 0.14 a						
22.8 °C	21.6 ± 2.7 b	2.6 ± 0.2 b	10.8 ± 1.4	18.7 ± 3.1	38.2 ± 5.6	-1.6 ± 0.3 ab	22.2 ± 1.4 b	0.27 ± 0.06 b	0.56 ± 0.07 b						
30.5 °C	37.8 ± 7.8 c	1.6 ± 0.4 a	13.4 ± 1.6	17.2 ± 1.9	34.5 ± 2.2	-2.3 ± 0.5 a	21.3 ± 3.8 b	0.21 ± 0.03 ab	0.36 ± 0.10 a						
0.5 kPa	22.3 ± 1.1	2.4 ± 0.8	10.7 ± 1.9 a	20.7 ± 0.8 b	45.3 ± 15.6 c	-1.3 ± 0.1	21.5 ± 0.9	0.30 ± 0.01 b	0.57 ± 0.02 b						
0.8 kPa	21.6 ± 3.9	2.6 ± 0.3	10.8 ± 2.6 a	18.7 ± 5.3 b	38.2 ± 13.8 bc	-1.6 ± 0.8	22.2 ± 1.8	0.27 ± 0.04 b	0.56 ± 0.14 b						
1.6 kPa	24.3 ± 2.7	2.8 ± 0.2	13.5 ± 1.4 b	11.7 ± 3.1 a	20.2 ± 5.6 a	-1.5 ± 0.3	20.0 ± 1.4	0.11 ± 0.06 a	0.34 ± 0.07 a						
2.3 kPa	25.5 ± 1.8	3.1 ± 0.1	11.5 ± 5.2 ab	8.7 ± 4.5 a	31.2 ± 7.2 ab	-1.7 ± 0.5	19.4 ± 0.7	0.09 ± 0.05 a	0.26 ± 0.05 a						
0% blue light	24.6 ± 4.4	2.5 ± 0.4	13.8 ± 2.1	17.5 ± 3.1	33.2 ± 6.7	-1.7 ± 0.4	20.5 ± 1.3	0.19 ± 0.07	0.42 ± 0.07						
1% blue light	23.0 ± 4.3	2.7 ± 0.3	13.0 ± 1.4	15.3 ± 3.8	30.8 ± 9.2	-1.9 ± 0.5	20.9 ± 2.1	0.16 ± 0.04	0.46 ± 0.08						
5% blue light	21.5 ± 6.4	2.7 ± 0.3	14.7 ± 3.0	16.8 ± 1.8	35.2 ± 5.5	-2.2 ± 0.4	20.9 ± 1.7	0.17 ± 0.08	0.45 ± 0.09						
10% blue light	21.6 ± 2.7	2.6 ± 0.2	10.8 ± 1.4	18.7 ± 3.1	38.2 ± 5.6	-1.6 ± 0.3	22.2 ± 1.4	0.27 ± 0.06	0.56 ± 0.07						
20% blue light	18.6 ± 5.3	2.7 ± 0.4	12.4 ± 1.2	18.2 ± 1.3	37.6 ± 2.8	-1.4 ± 0.6	22.0 ± 2.5	0.22 ± 0.07	0.51 ± 0.09						



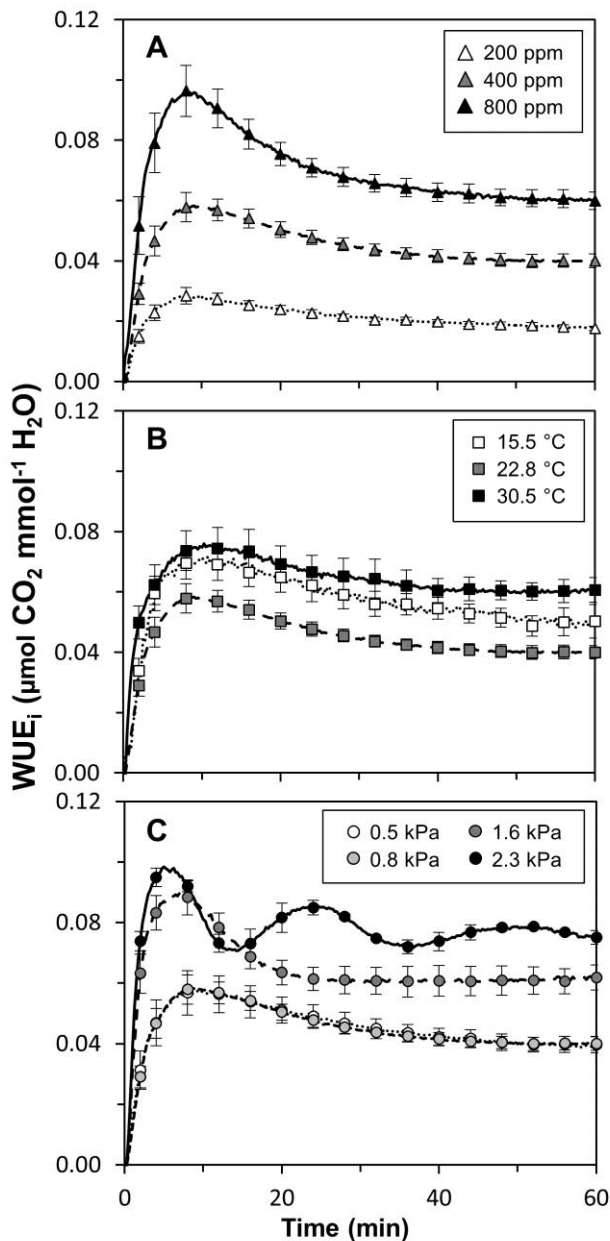


Fig. 3.2. Intrinsic water use efficiency ( $WUE_i$ ) during photosynthetic induction, as affected by  $C_a$  (A),  $T_{\text{leaf}}$  (B) and  $VPD_{\text{leaf-air}}$  (C). Average  $\pm$  SE ( $n = 5$ )

of induction, and relaxed rapidly within the first 10-15 minutes. The extent, as well as the rates of buildup and relaxation of diffusional and biochemical limitation scaled negatively with  $C_a$  (Fig. 3.3A, B). Diffusional limitation was clearly higher in low compared to intermediate  $C_a$ , while that difference was not visible when comparing biochemical limitation between these treatments. High  $C_a$  led to a smaller extent of diffusional limitation and to faster decreases of biochemical limitation in the first ten minutes of induction than both low and intermediate  $C_a$  (Fig. 3.3A, B). At the time that biochemical limitation had disappeared entirely at high  $C_a$  (~10 minutes), ~10% of biochemical limitation still remained at intermediate and low  $C_a$ , which took another ten minutes to relax (Fig. 3.3B). High  $T_{\text{leaf}}$  induced strong diffusional limitation (Fig. 3.3C), while

maintaining slightly positive effects on the rates of relaxation of biochemical limitation (Fig. 3.3D). The effects of high  $VPD_{leaf-air}$  (1.6 and 2.3 kPa) on  $g_s$  translated into very different kinetics of diffusional limitations during induction than moderate  $VPD_{leaf-air}$ . The 1.6 kPa treatment led to a faster decrease in diffusional limitation than the 0.5 and 0.8 kPa treatments, while the 2.3 kPa treatment produced oscillating diffusional limitation (Fig. 3.3E). Biochemical limitation was less affected, although it tended to relax more slowly in elevated  $VPD_{leaf-air}$  (Fig. 3.3F).

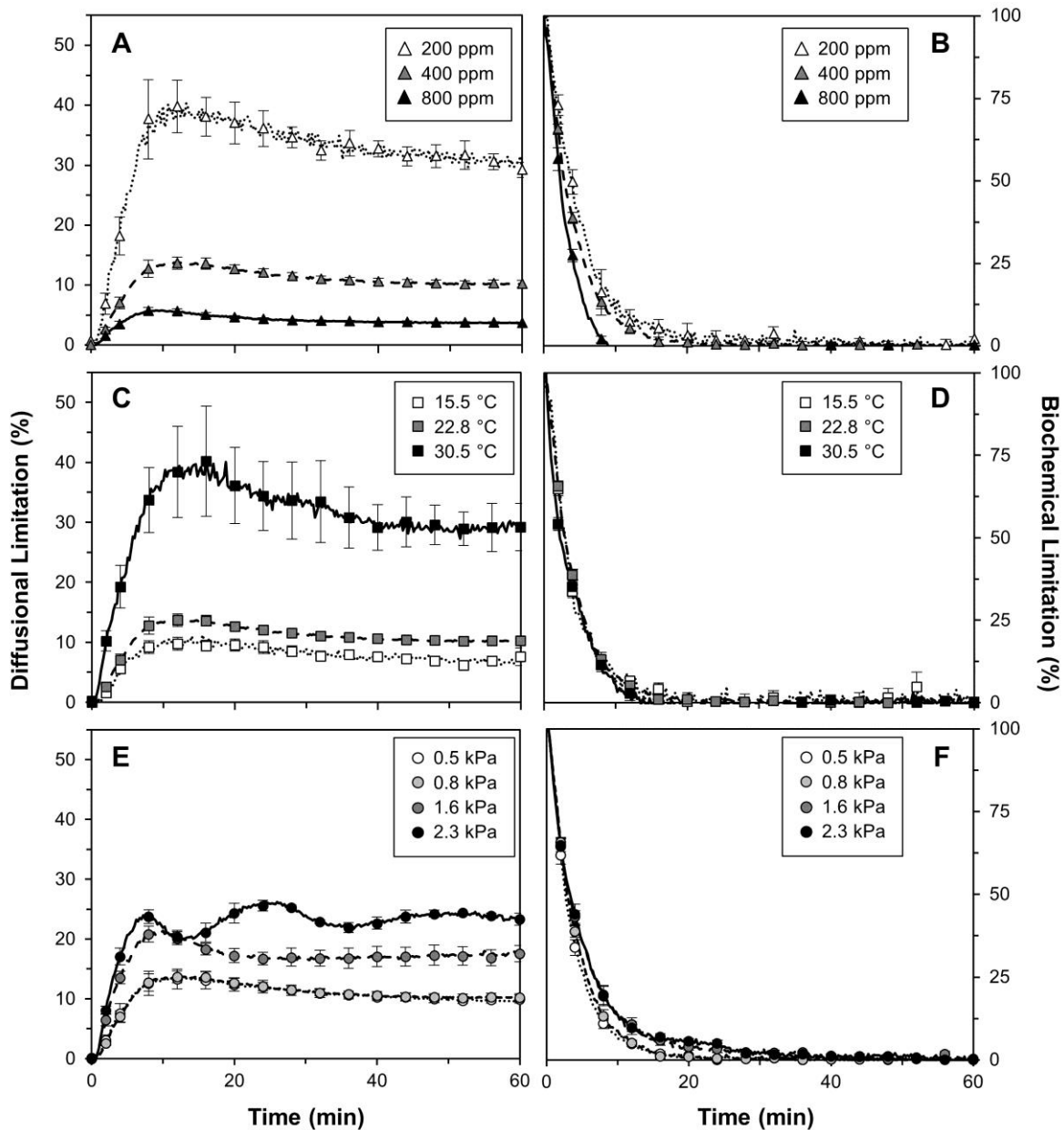


Fig. 3.3. Diffusional limitation (A, C, E) and biochemical limitation (B, D, F) during photosynthetic induction, as affected by  $C_a$  (A, B),  $T_{leaf}$  (C,D) and  $VPD_{leaf-air}$  (E, F). In panels B, D and F, the first 30 minutes of induction are shown. Average  $\pm$  SE ( $n = 5$ )

### Time constants of Rubisco activation

The time constants for Rubisco activation ( $\tau_R$ ), defined as the time to reach 63% of final Rubisco activation, decreased with increasing  $C_a$  (Fig. 3.4A), reflecting faster activation of Rubisco with increased abundance of  $\text{CO}_2$ . Compared to  $\tau_R$  in low  $C_a$ , average values for  $\tau_R$  at intermediate and high  $C_a$  were 20 and 56% lower, respectively. Leaf temperature did not

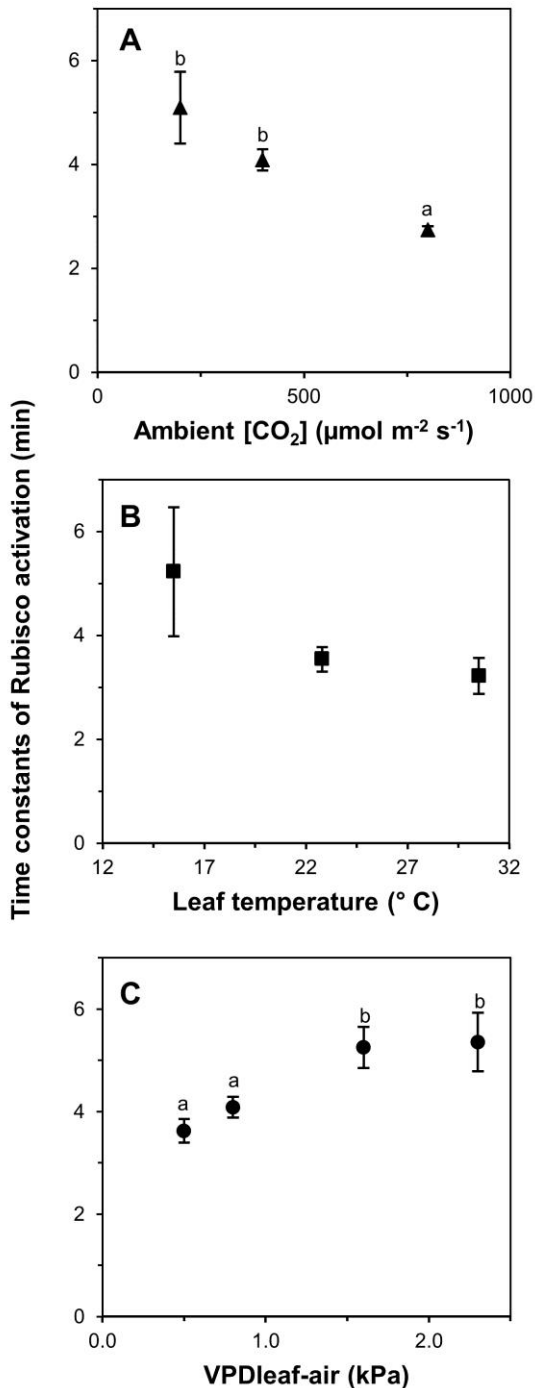


Fig. 3.4. Time constants of Rubisco activation ( $\tau_R$ ) during photosynthetic induction, as affected by  $C_a$  (A),  $\text{VPD}_{\text{leaf-air}}$  (B) and leaf temperature (C). Small letters denote significant differences between treatments, error bars denote  $\pm$  SE (n = 5)

have a statistically significant effect on  $\tau_R$ , however there was a trend towards higher  $\tau_R$  in low  $T_{\text{leaf}}$  (Fig. 3.4B). Elevated  $\text{VPD}_{\text{leaf-air}}$  produced a significant increase in  $\tau_R$  of 45 and 48% in the 1.6 and 2.3 kPa treatments (compared with 0.5 kPa; Fig. 3.4C). Most likely, lower Rubisco activation rates observed in elevated  $\text{VPD}_{\text{leaf-air}}$  were related to lower values of  $C_i$ , because of less open stomata compared to low  $\text{VPD}_{\text{leaf-air}}$ . It was observed that the decrease in  $C_i$  at the start of induction was stronger in elevated compared to low  $\text{VPD}_{\text{leaf-air}}$ . When plotting  $\tau_R$  against the relative rates of decrease in  $C_i$ , a positive relationship emerged (Fig. 3.5A). Data from the  $C_a$  treatments showed a similar trend (Fig. 3.5A). Also, at the time of induction when  $C_i$  reached its lowest point,  $C_c$  was calculated in an attempt to estimate the lowest  $\text{CO}_2$  concentration reached at the site of carboxylation. When plotting  $\tau_R$  against this  $C_c$ , a negative relationship emerged (Fig. 3.5B), possibly reflecting the fact that very low  $C_c$  during induction slows down the activation of Rubisco.

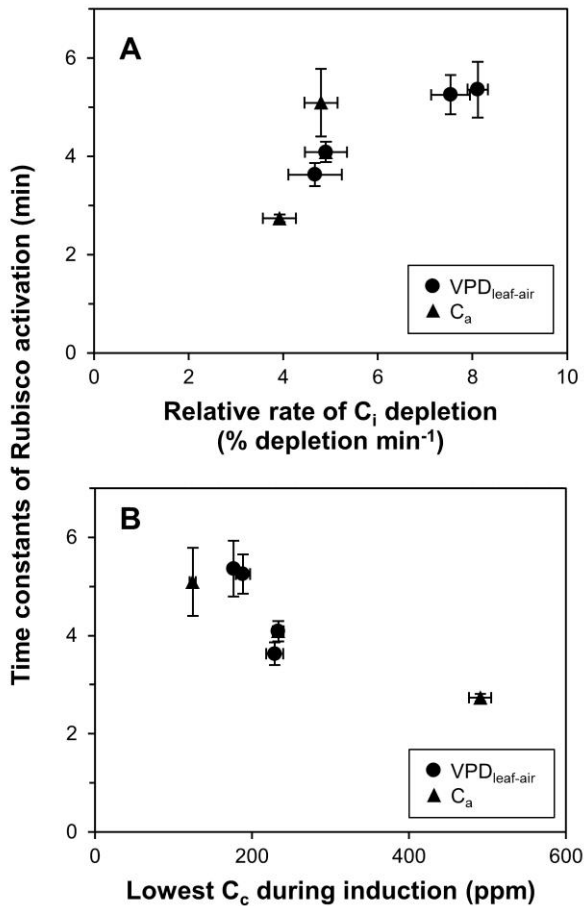


Fig. 3.5. Relationships between  $\tau_R$  in the  $\text{VPD}_{\text{leaf-air}}$  and  $C_a$  treatments and A) the rate of  $C_i$  depletion ( $\frac{\Delta C_i / \Delta t}{C_{i(t_0)}} * (-100)$ ), normalised by  $C_i$  in darkness ( $C_{i(t_0)}$ ) during the first 5 minutes of induction and B) the lowest value of  $C_c$  during induction, using the lowest value of  $C_i$  during induction and corresponding values of  $A_n$  and  $g_m$ , then calculating  $C_c = C_i - \frac{A_n}{g_m}$ . Average  $\pm$  SE ( $n = 5$ )

### Mesophyll conductance

Mesophyll conductance ( $g_m$ ) increased markedly during induction in all treatments. The most rapid changes in  $g_m$  were observed in the first ten minutes of induction. Mesophyll conductance showed a much stronger increase and higher steady-state levels at low than at high  $C_a$  (Fig. 3.6A). When induction was performed at different leaf temperatures,  $g_m$  increased with  $T_{leaf}$  (Fig. 3.6C). The index indicating the sensitivity of  $g_m$  estimations,  $dC_c/dA_{gr}$ , showed rapid increases in the first minute after the step irradiance increase that strongly exceeded the threshold level of 50 (Fig. 3.6B, D). Depending on the treatment, the index decreased to levels below 50 within 2-12 minutes, except for the 800 ppm treatment, where it remained above 50 throughout induction (Fig. 3.6B).

### $\Phi_{PSII}$ and NPQ

In dark-adapted leaves, the maximum, dark-adapted quantum efficiency of electron transport through photosystem II ( $F_v/F_m$ ) ranged between 0.79 and 0.82 across  $C_a$  and  $T_{leaf}$  treatments. During induction,  $\Phi_{PSII}$  increased to its steady-state level within 20 minutes. Between minutes 2 and 14, relative rates of  $\Phi_{PSII}$  increase were significantly higher in high

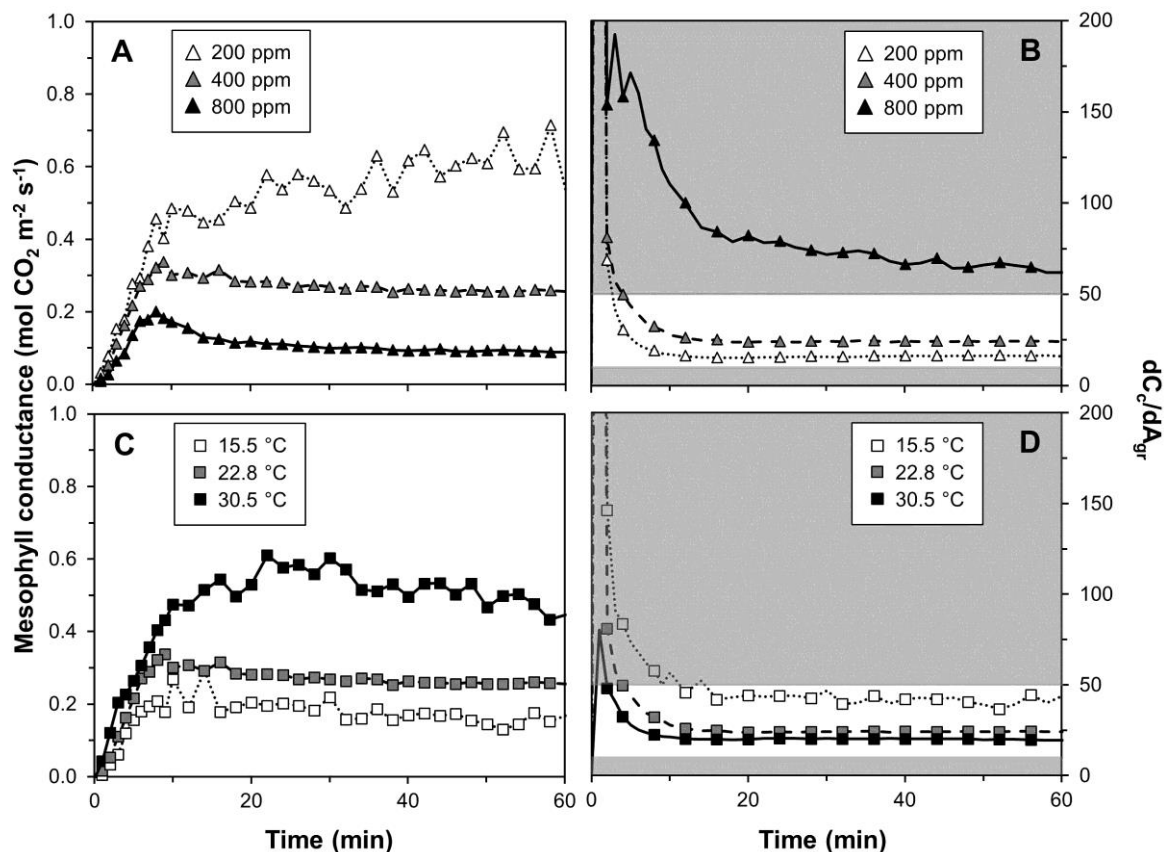


Fig. 3.6. Changes in mesophyll conductance ( $g_m$ ) during photosynthetic induction (A, C) and the sensitivity of  $g_m$  to parameter estimations (B, D), affected by  $C_a$  (A, B) and  $T_{leaf}$  (C, D). Unshaded areas in B and D indicate  $g_m$  data with a  $dC_c/dA_{gr}$  between 10 and 50, which refer to reliable  $g_m$  estimates according to Harley et al. (1992)

compared to low  $C_a$ . Furthermore, steady-state levels of  $\Phi_{\text{PSII}}$  were highest in intermediate  $C_a$  (0.35), followed by the high (0.33) and low  $C_a$  treatments (0.28; Fig. 3.7A). During induction, NPQ initially increased fast towards a peak of  $\sim 2$  after 5 minutes. This peak was followed by a decline, which was most pronounced at intermediate  $C_a$  (Fig. 3.7C). The lowest value of NPQ (1.5) was found at intermediate  $C_a$  and occurred after  $\sim 15$  minutes in all  $C_a$  treatments, after which NPQ increased slowly. This last phase was similar at all  $\text{CO}_2$  concentrations, but values of NPQ were highest in low  $C_a$  (NPQ of 2), followed by high  $C_a$  (1.8) and the lowest value of NPQ (1.7) was found at intermediate  $C_a$  (Fig. 3.7C). Between minutes 2 and 5, high leaf temperature increased the relative rate of change of  $\Phi_{\text{PSII}}$  compared to low  $T_{\text{leaf}}$ . Furthermore, steady-state  $\Phi_{\text{PSII}}$  values scaled positively with  $T_{\text{leaf}}$ , reaching 0.42 in high, 0.35 in intermediate and 0.22 in low  $T_{\text{leaf}}$  (Fig. 3.7B). At intermediate and high  $T_{\text{leaf}}$  and varying  $C_a$  the time courses of NPQ during induction were similar, rising rapidly to a maximum within 1-4 minutes, after which there was a decline to a minimum at  $\sim 20$  minutes (Fig. 3.7C, D), followed by a rise to the steady-state value, except for the  $30.5^\circ\text{C}$  treatment in which the final rise to the steady-state was replaced by a continuous decline (Fig. 3.7D). At low  $T_{\text{leaf}}$  the response was different: an initial rapid increase in NPQ was less pronounced and was followed by a slow increase that did not reach a stable value

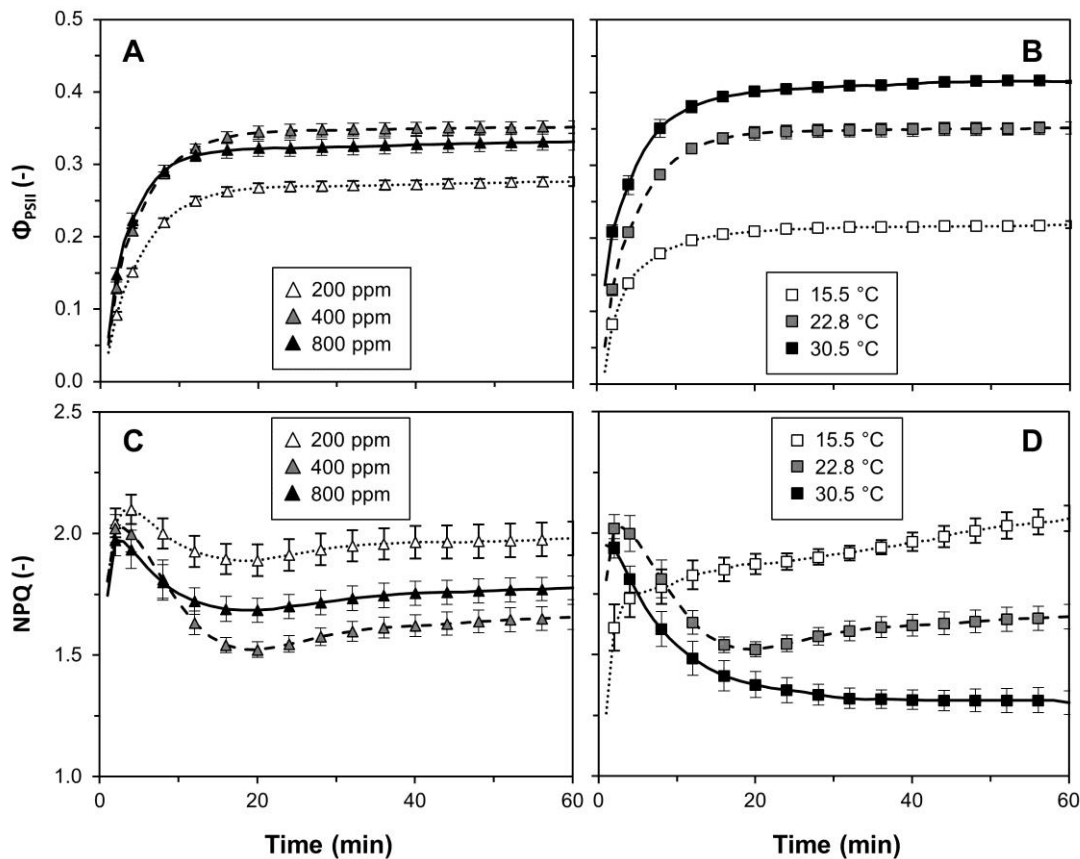


Fig. 3.7. Changes in  $\Phi_{\text{PSII}}$  (A, B) and NPQ (C, D) during photosynthetic induction, as affected by  $C_a$  (A, C) and  $T_{\text{leaf}}$  (B, D). Average  $\pm$  SE ( $n = 5$ )

during the duration of the experiment. Final NPQ values were therefore highest in low  $T_{\text{leaf}}$  ( $\sim 2$ ), followed by intermediate (NPQ of 1.7) and high  $T_{\text{leaf}}$  (1.3). While changes in qP paralleled  $\Phi_{\text{PSII}}$  and were of the same magnitude (Fig S3.11A, B), changes in  $F_v'/F_m'$  were rather small (Fig. S3.4). As a result,  $\Phi_{\text{PSII}}$  correlated linearly and positively with qP, while  $F_v'/F_m'$  strongly and negatively correlated with NPQ (data not shown).

### *Electron transport and gross photosynthesis rates*

Regressions of gross photosynthesis ( $A_{\text{gr}} = A_n + R_d$ ) vs. ETR were predominantly linear (Fig. 3.8), however the slopes of this relationship increased with  $C_a$  and decreased slightly with  $T_{\text{leaf}}$  (Fig. 3.8). Additionally, at low  $C_a$  and at high  $T_{\text{leaf}}$ , increases in  $A_{\text{gr}}$  became progressively independent of increases in ETR at high values of ETR and  $A_{\text{gr}}$  (Fig. 3.8).

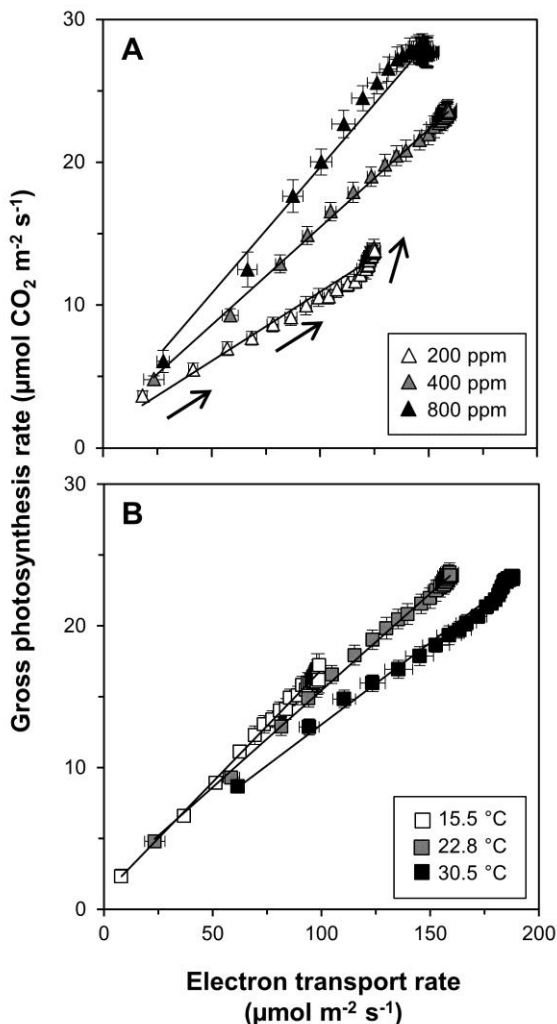


Fig. 3.8. Relationship between ETR and gross photosynthesis rate ( $A_n + R_d$ ) during photosynthetic induction, as affected by  $C_a$  (A) and  $T_{\text{leaf}}$  (B). Arrows indicate the direction of change over time. Average  $\pm$  SE ( $n = 5$ )

## Discussion

The environmental factors CO<sub>2</sub> concentration, temperature and VPD<sub>leaf-air</sub> had significant impacts on rates of photosynthetic induction, as well as on underlying diffusional, carboxylation and electron transport processes. For the first time, the effects of these environmental factors have been compared using the same experimental set-up. These results can help indicate the maximum gains that improvements in dynamic photosynthesis would have in various environments.

### *Environmental factor effects: comparison with other species*

While the effects of C<sub>a</sub> (Chazdon and Pearcy, 1986; Leakey *et al.*, 2002; Naumburg and Ellsworth, 2000; Naumburg *et al.*, 2001; Tomimatsu and Tang, 2012; Tomimatsu *et al.*, 2014) and T<sub>leaf</sub> (Carmo-Silva and Salvucci, 2013; Küppers and Schneider, 1993; Leakey *et al.*, 2003; Pepin and Livingston, 1997; Yamori *et al.*, 2012) on photosynthetic induction have been studied several times before, the effect of VPD<sub>leaf-air</sub> has only been studied once (Tinoco-Ojanguren and Pearcy, 1993a). By combining data from different publications, Kaiser *et al.* (2015) deduced that C<sub>a</sub> generally decreased t<sub>A90</sub> without decreasing t<sub>A50</sub>. Both t<sub>A50</sub> and t<sub>A90</sub> showed parabolic relationships with T<sub>leaf</sub>, with an optimum at ~30 °C. Overall, our results agree with this, however here t<sub>A50</sub> was increased by low C<sub>a</sub> and t<sub>A90</sub> decreased much more in elevated C<sub>a</sub> than the overall trend in Kaiser *et al.* (2015) suggests. It could be that the stronger response to C<sub>a</sub> observed here is caused by the use of a C<sub>3</sub> crop with high photosynthesis rates, compared to most species used in the various studies summarized by Kaiser *et al.* (2015).

Surprisingly, varying blue light (0-20%) had no effect on photosynthetic induction or stomatal opening. Blue light generally promotes rapid stomatal opening when combined with red light, and is thought to be a cue for overall radiation load (Shimazaki *et al.*, 2007). It could be that in the current experiment, 1000 μmol m<sup>-2</sup> s<sup>-1</sup> provided such a strong stimulus for stomatal opening, that the rate of opening could not have been accelerated by increasing the percentage of blue light. Assmann and Grantz (1990a, b), however, superimposed blue light on 900 μmol m<sup>-2</sup> s<sup>-1</sup> red light in sugarcane and soybean and found an additional opening response (data on photosynthesis were not shown in these studies). The reported effects of blue light on photosynthetic induction are ambiguous: Košvancová-Zitová *et al.* (2009) reported faster induction in beech (*Fagus sylvatica* L.) with increasing blue light (25-75% blue light in 800 μmol m<sup>-2</sup> s<sup>-1</sup>), while data reported in Zhang *et al.* (2011) for the orchid *Cyripedium flavum* showed the opposite (0- 100% blue light in 250 μmol m<sup>-2</sup> s<sup>-1</sup>). The effects of blue light on induction are therefore variable with no clear



correlations between the effects of blue light and other environmental responses or preferences.

### *Methodological considerations*

Diffusional and biochemical limitation were calculated assuming a curvilinear  $A_n/C_i$  relationship instead of a linear relationship, which so far was used in similar studies (e.g. Allen and Pearcy, 2000; Jackson *et al.*, 1991; Woodrow and Mott, 1989). This affected the estimation of stomatal limitation at all  $C_a$  levels, but especially at 800 ppm (Supplementary material 3.2). Calculations of biochemical limitation and Rubisco activation time constants ( $\tau_R$ ) are affected by estimated  $A_n$  corrected for changes in  $C_i$  during induction, and therefore by the assumed  $A_n/C_i$  relationship. Most studies that calculated a measure of stomatal or biochemical limitation, or time constants of Rubisco activation, were performed with atmospheric or below-atmospheric  $C_a$ . For such a situation, the assumption of a linear  $A_n/C_i$  relationship is reasonable. However, some authors also used a linear relationship at  $C_a$  of 700 ppm or higher (Kořvancová-Zitová *et al.*, 2009; Tomimatsu and Tang, 2012). Their measures of stomatal limitation in high  $C_a$  are most likely substantial overestimations.

In light-adapted leaves, the conventionally measured  $F_m'$  (obtained by a single saturating pulse) underestimated 'true'  $F_m'$  (obtained by multiple saturating pulses), by ca. 4%. We show for the first time that this underestimation develops within ten minutes after a dark-light transition (Fig. S3.1). Interestingly, steady-state measurements on climate-chamber grown tobacco, pea and maize leaves (grown at 300  $\mu\text{mol m}^{-2} \text{s}^{-1}$ ) showed underestimations of  $F_m'$  of comparable extent, translating into underestimations of  $\Phi_{\text{PSII}}$  (Loriaux *et al.*, 2013). Here, steady-state  $\Phi_{\text{PSII}}$  would have even been underestimated by 8-15% if single rather than multi-phase pulses had been used. Furthermore, if  $\Phi_{\text{PSII}}$  values from underestimated  $F_m'$  were used to calculate  $g_m$ , the values would have been much larger (300-800%) or even impossible (e.g. negative  $g_m$  in high temperature). Similar effects for  $g_m$  were reported by Loriaux *et al.* (2013).

### *Mesophyll conductance*

Estimating  $g_m$  is notoriously difficult, as each method makes questionable assumptions. This is certainly true for the method used here, though it is one of the most commonly used methods and relies on measurements of photosynthetic gas exchange and chlorophyll fluorescence (Harley *et al.*, 1992). In darkness  $C_c$  (and thus  $g_m$ ) cannot be estimated, as there is neither electron transport nor photosynthetic  $\text{CO}_2$  fixation. So, though  $g_m$  is shown to increase from zero (Fig. 3.6) this is at best a mathematical convenience and it is highly

unlikely that in the earliest stages of induction  $g_m$  really does increase as the data suggest, because the starting point of that increase is unknown. However,  $g_m$  changes of similar speed after stepwise changes in  $C_a$  have been demonstrated (Flexas *et al.*, 2007; Tazoe *et al.*, 2011). We used a method proposed by Harley *et al.* (1992; Eqn. 13) to analyse the change in  $g_m$  sensitivity to errors in parameter estimations. Application of this method (Fig. 3.6B, D) seems to confirm that the apparent  $g_m$  changes in the first 2-12 minutes (depending on treatment) are derived from transiently unreliable measurements. When comparing steady-state data in this paper to responses of  $g_m$  to different leaf temperatures, the increase of  $g_m$  with leaf temperature compares well to Bernacchi *et al.* (2002, measured in 21% oxygen) and to von Caemmerer and Evans (2015, measured in 2% oxygen), both obtained in tobacco, which is closely related to tomato. Also, both species are typically grown in warm conditions. So, despite the problems of measuring  $g_m$  changes after a dark-light transition, these results are similar to previous work. In some species,  $g_m$  increased with temperature, while in others it did not (von Caemmerer & Evans, 2015). With a  $Q_{10}$  of 2 - 2.3 for steady-state  $g_m$  (which is very close to that of tobacco, Bernacchi *et al.* 2002), our data suggest that tomato belongs to the first group and that enzymatic regulation is involved (Bernacchi *et al.*, 2002). As for the direction and magnitude of  $C_a$  effects on  $g_m$ , especially at low  $C_a$ , there is disagreement in previous literature, even between species within the same investigation (Flexas *et al.*, 2007a). Using tunable diode laser spectroscopy, it was shown that changes in  $g_m$  following changes in  $C_a$  were much larger in 21% compared to 2% oxygen (Tazoe *et al.*, 2011). This suggests that photorespiration strongly affects  $g_m$ , but the diffusional properties of leaves remain unchanged by a change in  $C_a$  (Tholen *et al.*, 2012). Unfortunately, this possibility cannot be ruled out here. Estimates of  $g_m$  are more strongly affected by parameter errors when  $C_i$  is  $>300$  ppm (Harley *et al.*, 1992); this may explain why the  $g_m$  sensitivity index was always  $>50$  in the high  $C_a$  treatment (Fig. 3.6B). Mesophyll conductance is especially sensitive to estimates of  $\Gamma^*$  (Harley *et al.*, 1992). Sensitivity analysis of steady-state  $g_m$  to  $\Gamma^*$  revealed that across  $C_a$  and  $T_{\text{leaf}}$  treatments,  $g_m$  was much less sensitive to underestimations than to overestimations in  $\Gamma^*$  (Figs. S3.5-6).

### *Rubisco activation*

Rubisco activated faster with increases in  $\text{CO}_2$  concentrations and leaf temperature (Carmo-Silva and Salvucci, 2011; 2013; Mott and Woodrow, 1993; Woodrow *et al.*, 1996), while elevated  $\text{VPD}_{\text{leaf-air}}$  slowed down Rubisco activation. A  $\text{VPD}_{\text{leaf-air}}$  effect on Rubisco activation rates has, to the authors' knowledge, not been found before. We argue that slower Rubisco activation is due to decreases in  $C_i$  during induction, as both the relative

rate of  $C_i$  decrease and the lowest concentration of  $C_c$  reached during induction seemed to correlate with Rubisco activation rates (Fig. 3.5). Further support for this hypothesis comes from studies on water stress: short-term leaf desiccation, leading to strong stomatal closure, decreased both  $C_c$  and Rubisco activity (Flexas *et al.*, 2006). Rubisco deactivation happened at  $C_c < 100$  ppm (Flexas *et al.*, 2006), so at lower  $C_c$  than in Fig. 3.5. Also, in a meta-analysis on drought-stressed leaves, decreased  $g_s$  correlated with decreased Rubisco activity (Flexas & Medrano, 2002). Furthermore, Rubisco activation rates after increases in irradiance correlated positively with  $C_i$  (Mott and Woodrow 1993; Woodrow *et al.* 1996).

### *Combined gas exchange and chlorophyll fluorescence during photosynthetic induction: insights*

During photosynthetic induction, gross photosynthesis rate and ETR showed linear correlations, whose slopes increased with  $CO_2$  concentration and decreased with leaf temperature (Fig. 3.8). ETR reflects the reductant and ATP needed to metabolise the products of carboxylation and oxygenation of RuBP, while  $A_{gr}$  reflects the rate of carboxylation of RuBP minus half the rate of oxygenation. Hence, the slope of the ETR/ $A_{gr}$  relationship increases as the rate of oxygenation decreases relative to the rate of carboxylation, e.g. in increasing  $C_a$  and decreasing  $T_{leaf}$ . Furthermore, deviations from linearity of the ETR/ $A_{gr}$  relationship imply changes of some of the underlying limitations to photosynthesis: For example, increases in  $A_{gr}$  without strong increases in ETR, as seen in later phases of induction in low  $C_a$  and high  $T_{leaf}$  (Fig. 3.8) imply decreases in photorespiration, most likely due to increases in  $C_i$ , which are brought about by stomatal opening. The fact that at the start of induction none of the slopes deviated strongly from linearity may imply that neither changes in  $g_s$  nor  $g_m$  limited induction, as in such a case  $C_c$  would have dropped momentarily (oxygenation would have increased relative to carboxylation).

Changes in  $\Phi_{PSII}$  during induction were primarily explained by changes in photochemical quenching (qP) rather than  $F_v'/F_m'$ . Overall, this suggests that changes in NPQ, acting via decreases in  $F_v'/F_m'$ , did not contribute substantially to the changes in  $\Phi_{PSII}$  (Baker *et al.*, 2007); the total span of changes of  $F_v'/F_m'$  was 0.55 – 0.65, while that for qP was 0.05 – 0.7 (Fig. S3.4). Steady-state  $\Phi_{PSII}$  was slightly higher in ambient compared to high  $C_a$  (Fig. 3.7A), while NPQ was slightly higher in high compared to ambient  $C_a$  (Fig. 3.7C). This may be explained by triose phosphate utilisation limitation slowing down ETR in high  $C_a$ .

Non-photochemical quenching is comprised of several components that activate and deactivate on different time scales (Ruban *et al.*, 2012). The fastest component is termed

energy-dependent quenching (qE), and depends on the pH gradient across the thylakoid membrane (Ruban *et al.*, 2012). qE is a complex process that is sensitive to lumen pH via protonation by PsbS, which is a rapidly responding process. This pH sensitivity is increased by zeaxanthin (i.e. there is more NPQ at the same lumen pH as zeaxanthin concentration increases; Rees *et al.*, 1989); this is a slower process. Here, all C<sub>a</sub> and T<sub>leaf</sub> treatments (except low T<sub>leaf</sub>) produced initial overshoots in NPQ during induction (Fig. 3.7). It is hypothesized that low photochemical quenching, due to deactivated Calvin cycle biochemistry, led to a rapid acidification of the lumen, quickly activating the qE component of NPQ. Upon the subsequent activation of Calvin cycle enzymes and increase in linear electron transport, the lumen pH increased and qE decreased, lowering NPQ. The slow build-up of zeaxanthin during induction, by enhancing the effect of pH on NPQ, would then have produced a slower increase in qE, visible between minutes 20 and 60 in all treatments except high T<sub>leaf</sub>. Leaves that contained fully activated Rubisco in low light did not exhibit an NPQ overshoot when transferred to high light (Carmo-Silva & Salvucci, 2013), demonstrating the indirect link between activation state of Calvin cycle biochemistry and development of the NPQ overshoot. In leaves containing less Rubisco activase, NPQ kept increasing throughout induction, indicating that Rubisco activation, and by implication photochemical quenching, required much more time to increase (Yamori *et al.*, 2012).

#### *VPD<sub>leaf-air</sub> effects on stomatal conductance*

Tinoco-Ojanguren and Pearcy (1993a) recognised three phases of g<sub>s</sub> changes during induction in leaf understory plants: lag time, rapid opening and slower opening. Also, leaves exposed to high VPD<sub>leaf-air</sub> (1.8 kPa) showed a larger lag time and an absence of the third, slower phase of stomatal opening, than leaves exposed to low VPD<sub>leaf-air</sub> (0.6 kPa). Also, in our study, a lag time and the absence of a slow increase towards maximum g<sub>s</sub> was visible at elevated VPD<sub>leaf-air</sub> (Fig. 3.1F). Similar to our findings, Tinoco-Ojanguren and Pearcy (1993a) reported that high VPD decreased steady-state g<sub>s</sub> before and after the increase in irradiance, slowed down photosynthetic induction and increased stomatal limitations, especially in high-light grown plants. High VPD induced stomatal oscillations that dampened out during induction, an often-observed phenomenon whose mechanisms are still under debate (Kaiser and Paoletti, 2014). These oscillations are triggered by a transient ‘wrong way’ response of stomatal opening upon an increase in evaporative demand, which can be explained by the loss of turgor of epidermal cells, leading to reduced back-pressure on guard cells (Buckley, 2005). Guard cells react upon this by inducing a closing response, which is counteracted by another opening response, inducing oscillations which continue until a new equilibrium is reached. Another explanation for the oscillations

may be patchy stomatal behaviour, although this has more often been shown to occur after decreases in irradiance (Cardon *et al.*, 1994; Eckstein *et al.*, 1996).

### *Improving crop photosynthesis in fluctuating irradiance: why and how?*

Improving crop productivity via photosynthetic efficiency is considered a crucial pathway for future global food security (Zhu *et al.*, 2010). One process worth improving is the regulation of Rubisco activity, as this would increase overall photosynthesis rates in fluctuating irradiance (Carmo-Silva *et al.*, 2015). Considering that in nature, incident irradiance often fluctuates, improvement of transient photosynthesis is highly relevant to improving overall plant productivity. Our data suggest that average photosynthesis rates during photosynthetic induction could be increased by up to 6-10% in ambient  $C_a$  (Table 3.3), if the transient increase of Rubisco activation was replaced by its steady-state value. Rubisco activation may be sped up by manipulating the isoform composition of Rubisco activase (Carmo-Silva & Salvucci, 2013). Maximising stomatal opening would improve average photosynthesis rates by up to 1-2% in ambient  $C_a$  and across air humidities and leaf temperatures (except at 30.5 °C, where rapid stomatal opening would increase photosynthesis by up to 3.4%, Table 3.3). Thus, from these data it seems that increasing the kinetics of Rubisco activation is a more useful strategy than increasing  $g_s$ , especially since higher  $g_s$  would decrease  $WUE_i$  while more rapid Rubisco activation would strongly increase  $WUE_i$  (Table 3.3). However, a transition from completely inactivated photosynthesis in darkness to near-saturating irradiance does not represent natural conditions, and the modulation of dynamic photosynthesis by environmental factors and

Table 3.3. Maximum gains in photosynthesis rates or intrinsic water use efficiency ( $WUE_i$ ) that an instantaneous increase in Rubisco activation or stomatal opening to their respective steady-states would have. Values are averaged over whole (60 minutes) induction curves. Average  $\pm$  SE (n = 5)

Treatment	Photosynthesis rates				$WUE_i$			
	Rubisco kinetics		Stomatal opening		Rubisco kinetics		Stomatal opening	
200 ppm	9.4	$\pm$ 1.5	4.4	$\pm$ 0.5	30.6	$\pm$ 2.1	-31.4	$\pm$ 2.0
400 ppm	7.4	$\pm$ 0.4	1.4	$\pm$ 0.2	16.3	$\pm$ 1.1	-20.3	$\pm$ 1.4
800 ppm	4.3	$\pm$ 0.6	0.6	$\pm$ 0.1	9.5	$\pm$ 0.9	-19.6	$\pm$ 2.2
15.5 °C	7.1	$\pm$ 0.6	1.6	$\pm$ 0.2	15.3	$\pm$ 2.2	-24.3	$\pm$ 6.2
22.8 °C	7.4	$\pm$ 0.4	1.4	$\pm$ 0.2	16.3	$\pm$ 1.1	-20.3	$\pm$ 1.4
30.5 °C	5.9	$\pm$ 0.8	3.4	$\pm$ 1.3	15.0	$\pm$ 1.5	-13.7	$\pm$ 2.6
0.5 kPa	6.8	$\pm$ 0.4	1.7	$\pm$ 0.5	16.0	$\pm$ 1.6	-23.0	$\pm$ 3.6
0.8 kPa	7.4	$\pm$ 0.4	1.4	$\pm$ 0.2	16.3	$\pm$ 1.1	-20.3	$\pm$ 1.4
1.6 kPa	9.5	$\pm$ 0.6	1.1	$\pm$ 0.4	24.2	$\pm$ 2.4	-15.5	$\pm$ 2.5
2.3 kPa	9.8	$\pm$ 0.8	1.0	$\pm$ 0.4	22.6	$\pm$ 2.4	-13.6	$\pm$ 2.0

the benefits of faster Rubisco activation or stomatal opening may be smaller when photosynthesis is somewhat induced. Therefore, these numbers can only be used to provide a first guess for the increase in Rubisco activation rate or stomatal opening rate could have on dynamic photosynthesis in various environments.

### *Conclusions*

The environmental factors CO<sub>2</sub> concentration, temperature and humidity had substantial effects on rates of induction and its underlying processes and limitations after a dark-light transition, while blue light had no effects. Increases in CO<sub>2</sub> concentration led to faster photosynthetic induction, by decreasing diffusional limitation and by speeding up the relaxation of biochemical limitation. Increases in leaf temperature led to slightly higher induction rates, by means of faster relaxation of biochemical limitation. Increases in leaf-to-air vapour pressure deficit mainly lowered the relaxation rates of biochemical limitation, by slowing down Rubisco activation via decreased availability of CO<sub>2</sub>. These insights can provide first guesses of the comparative effects of environmental factors on dynamic photosynthesis and on the benefits that increasing Rubisco activation or stomatal conductance would have on dynamic photosynthesis.

### **Funding**

This work was carried out within the research programme of BioSolar Cells, co-financed by the Dutch Ministry of Economic Affairs. Additionally, this work was supported by Essent.

### **Acknowledgements**

We thank Shizue Matsubara, Tracy Lawson, Tsu-Wei Chen and Alejandro Morales for useful discussions.

**Supplementary material 3.1: additional figures**

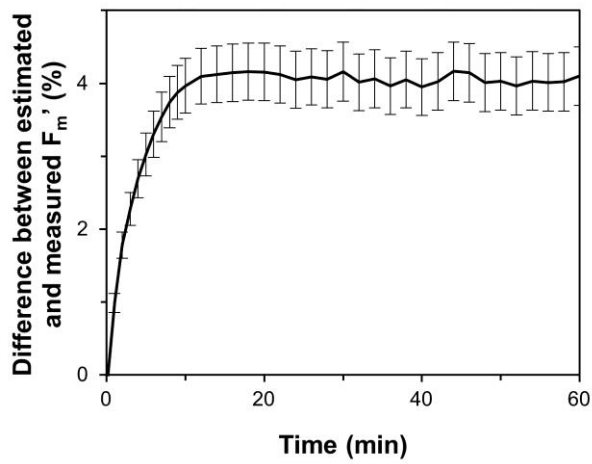


Fig. S3.1. Measured  $F_m'$  underestimates true  $F_m'$  in light-adapted, but not in dark-adapted leaves

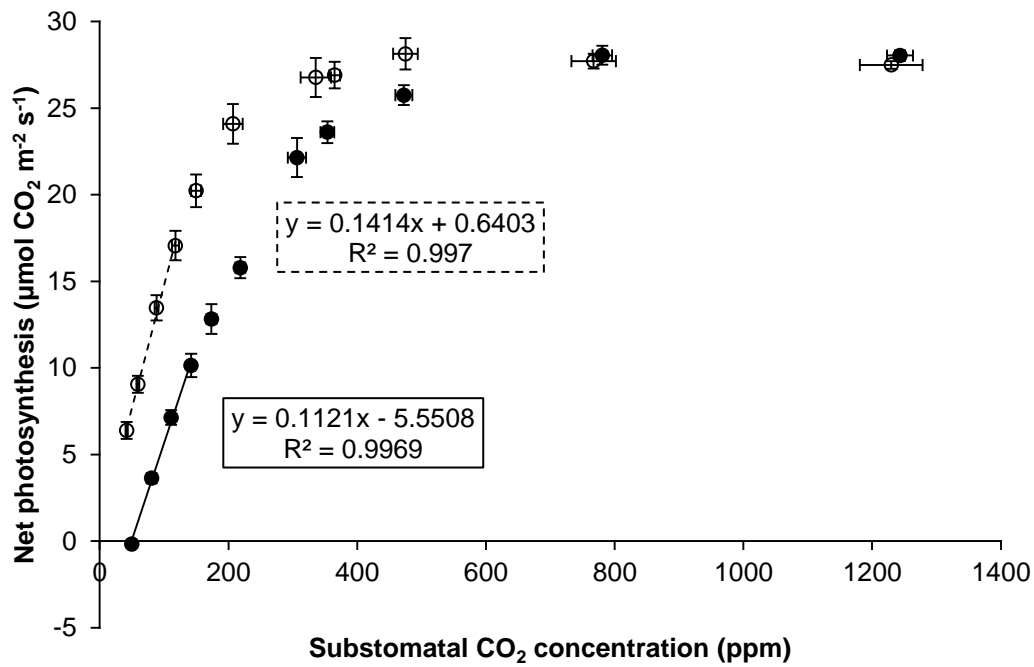


Fig. S3.2.  $A_n/C_i$  relationship in 21% (closed circles) and 2% oxygen (open circles). Regression lines highlight the values used for calculation of the chloroplast  $CO_2$  compensation point in the absence of day respiration (Yin *et al.*, 2009). Average  $\pm$  SE (n = 3-5)

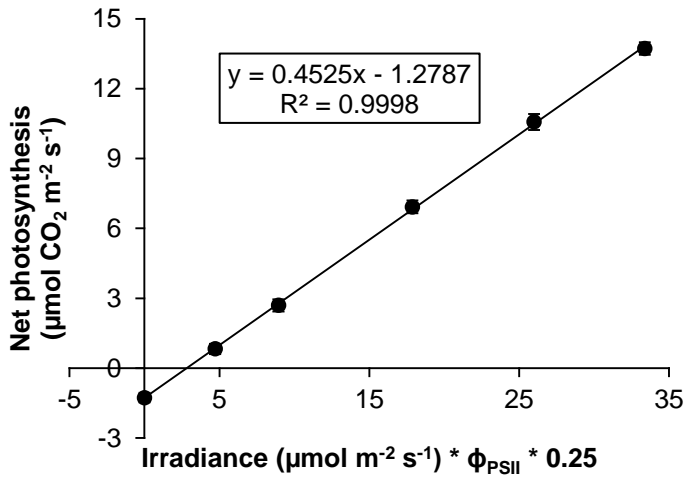


Fig. S3.3. Relationship between net photosynthesis and irradiance \*  $\Phi_{PSII}$  \* 0.25, as in Yin et al. (2009), measured in 2% O<sub>2</sub>. Average  $\pm$  SE (n = 4). The slope equals a calibration factor ( $s$ ), which is used to scale  $\Phi_{PSII}$  to ETR

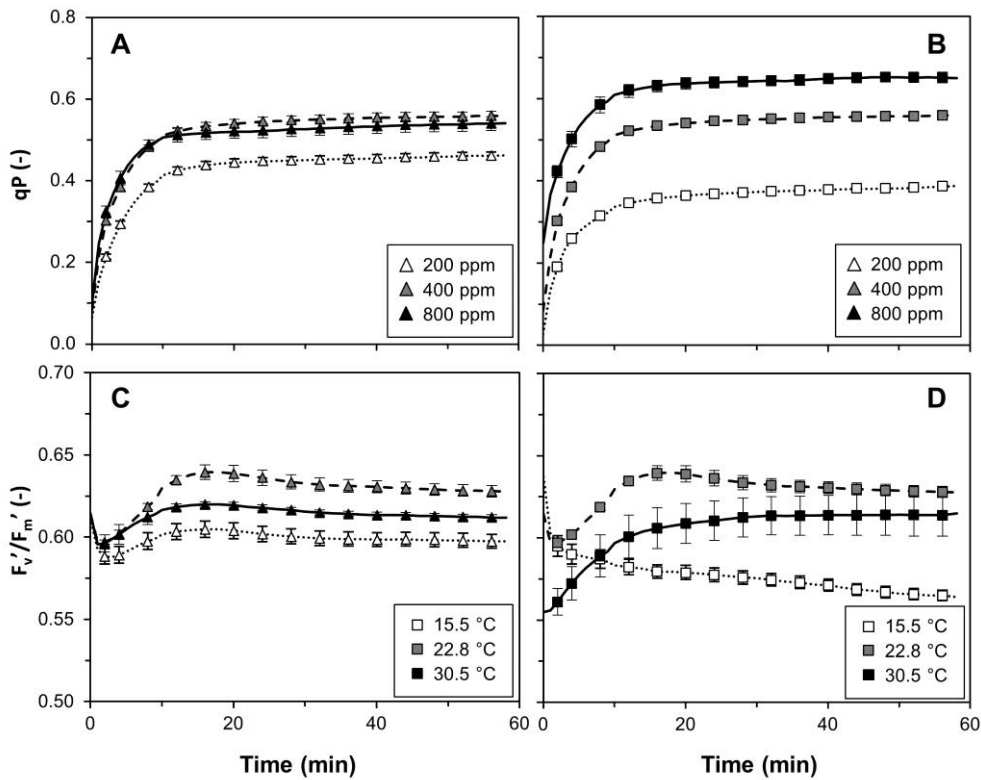


Fig. S3.4.  $qP$  (A,B) and  $F_v/F_m'$  (C,D) during photosynthetic induction and as affected by  $C_a$  (A, C) and  $T_{leaf}$  (B, D)



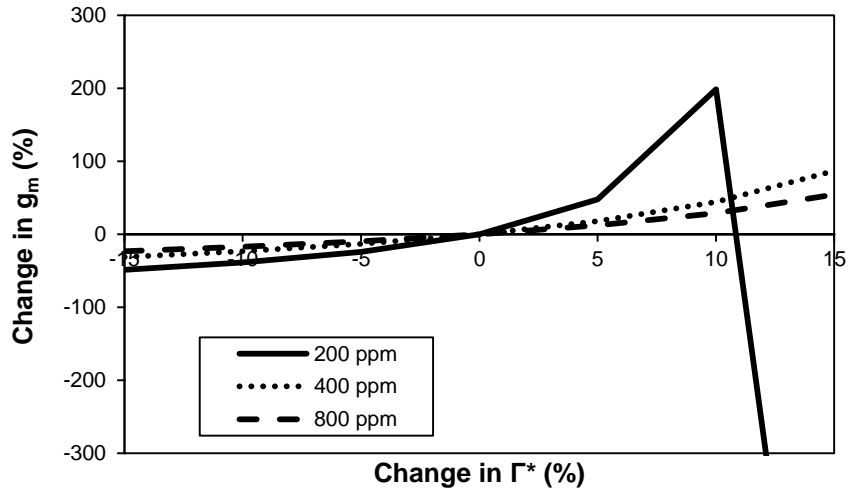


Fig. S3.5. Sensitivity of  $g_m$  to changes in  $\Gamma^*$ , and as affected by  $C_a$

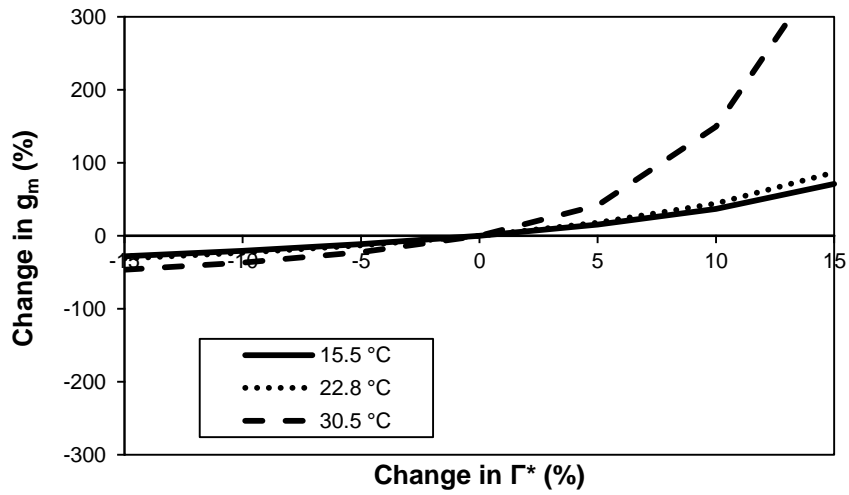


Fig. S3.6. Sensitivity of  $g_m$  to changes in  $\Gamma^*$ , and as affected by  $T_{leaf}$

### Supplementary material 3.2: Implications of using curvilinear instead of linear $A_n/C_i$ relationships

If a linear relationship between  $A_n$  and  $C_i$  is assumed, the formula used for calculating transient net photosynthesis rates corrected for changes in  $C_i$  during induction ( $A_{n(t)C_i}$ ) is simply (Woodrow & Mott, 1989):

$$A_{n(t)C_i} = A_{n(t)} * \frac{C_i(t_f)}{C_i(t)} \quad (\text{S3.1})$$

The implications of the type of  $A_n/C_i$  relationship for calculations of stomatal limitation are best exemplified when comparing  $C_a$  effects on stomatal limitation during induction (Figs. 3.S7-9):

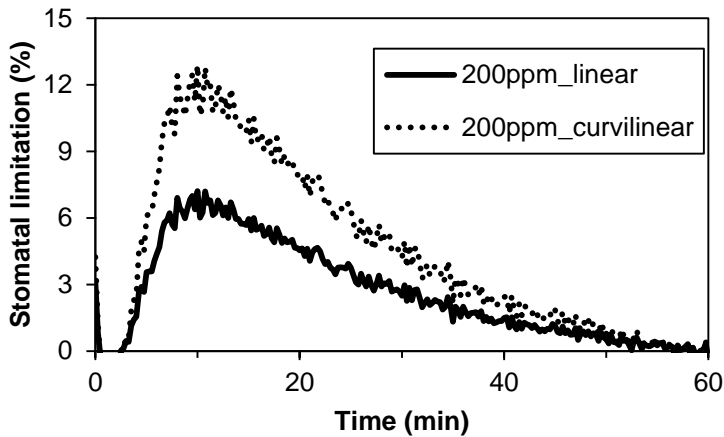


Fig. S3.7. Stomatal limitation during induction at 200 ppm  $C_a$ , as calculated assuming a linear (solid line) or a curvilinear  $A_n/C_i$  relationship (dotted line)

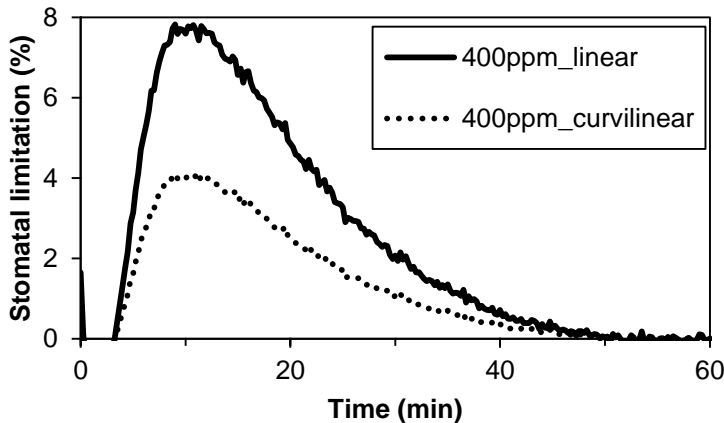


Fig. S3.8. Stomatal limitation during induction at 400 ppm  $C_a$ , as calculated assuming a linear (solid line) or a curvilinear  $A_n/C_i$  relationship (dotted line)

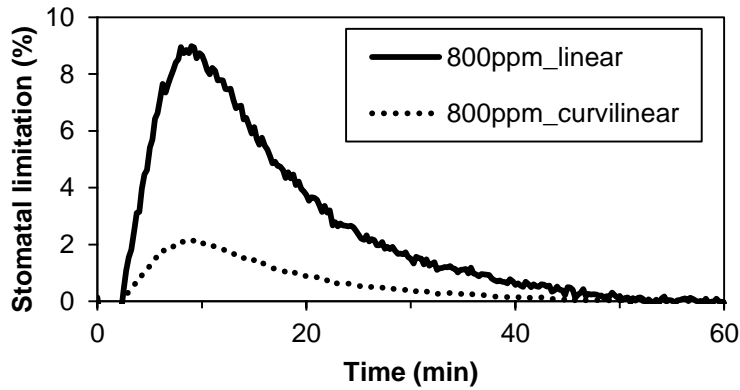


Fig. S3.9 Stomatal limitation during induction at 800 ppm  $C_a$ , as calculated assuming a linear (solid line) or a curvilinear  $A_n/C_i$  relationship (dotted line)

Clearly, the assumption of a linear relationship underestimates stomatal limitation in low  $C_a$  (by ca. 50%), while the opposite is true in intermediate (overestimation ca. 100%) and high  $C_a$  (overestimation ca. 350%). Due to these under- and overestimations, biochemical limitation and time constants of Rubisco activation ( $\tau_R$ ) would also be affected. Here, this would result in calculated values of  $\tau_R$  that would have been +8, -14 and -27% different for the 200, 400 and 800 ppm treatments, respectively.



## **CHAPTER 4**

Elevated CO<sub>2</sub> increases photosynthesis in fluctuating irradiance irrespective of photosynthetic induction state

**Authors:**

Elias Kaiser

Dianfan Zhou

Ep Heuvelink

Jeremy Harbinson

Alejandro Morales

Leo F.M. Marcelis

To be submitted

**Abstract**

Leaves are often exposed to fluctuating irradiance, which limits integrated assimilation. Elevated CO<sub>2</sub> enhances the rate of dynamic photosynthesis beyond its effects on steady-state photosynthesis rates. Studying its role in enhancing dynamic photosynthesis is important for understanding whole-canopy responses to rising CO<sub>2</sub> concentrations. The rise of photosynthesis after increases in irradiance (1000 μmol m<sup>-2</sup> s<sup>-1</sup>), the loss of photosynthetic induction after irradiance decreases and dynamic rates of photosynthesis during sinusoidal changes in irradiance were studied in tomato (*Solanum lycopersicum* L.) leaves, using three CO<sub>2</sub> concentrations (200, 400 and 800 ppm). Low irradiance was varied (0-200 μmol m<sup>-2</sup> s<sup>-1</sup>) to vary initial induction levels. Elevated CO<sub>2</sub> concentration enhanced the rates of increase of photosynthesis by 4-12% and decreased the loss of photosynthetic induction (21-25%) across photosynthetic induction states, while increasing relative photosynthesis rates during sine waves by 14%. Additionally, transient limitations on CO<sub>2</sub> diffusion and leaf biochemistry were lowered by elevated CO<sub>2</sub>. Elevated CO<sub>2</sub> concentration enhances the rates of dynamic photosynthesis regardless of photosynthetic induction state. Therefore, rising ambient CO<sub>2</sub> concentrations will similarly benefit integrated assimilation in naturally fluctuating irradiance in whole canopies, where different leaf layers are exposed to very different irradiance regimes.

## Introduction

Carbon dioxide (CO<sub>2</sub>) is the substrate of the carboxylation reaction that results in photosynthetic carbon fixation. It is indispensable for sugar synthesis and, ultimately, growth of cyanobacteria, algae and plants. The positive effects of elevated CO<sub>2</sub> concentration ([CO<sub>2</sub>]) on steady-state photosynthesis have long been recognized, and are due to an increased velocity of the carboxylation reaction, and a reduction of the wasteful oxygenation reaction (Long *et al.*, 2004). However, importantly, there is another beneficial aspect of elevated [CO<sub>2</sub>] that is often overlooked: an increase in [CO<sub>2</sub>] enhances the rate of photosynthesis in fluctuating irradiance more strongly than can be expected from steady-state characteristics (reviewed in Kaiser *et al.*, 2015). Due to fossil fuel consumption and changes in land use, atmospheric [CO<sub>2</sub>] currently increases by approx. 1-2 ppm year<sup>-1</sup> (IPCC, 2013). Much effort has been directed towards understanding plant, crop and ecosystem behavior under elevated [CO<sub>2</sub>] (Long *et al.*, 2004; Ainsworth & Rogers, 2007). Knowledge of how elevated [CO<sub>2</sub>] changes photosynthesis in fluctuating irradiance is important in this context, but to date is still incomplete.

Irradiance incident on a given leaf often fluctuates due to the movement of the sun, clouds and canopies (Percy, 1990; Smith & Berry, 2013). Changes in irradiance change the rate of linear electron transport, the activity of key enzymes in the Calvin cycle and sugar metabolism, and stomatal conductance (*g<sub>s</sub>*, Stitt & Grosse, 1988; Percy *et al.*, 1996; Kaiser *et al.*, 2015). Average photosynthesis rates in fluctuating irradiance are usually lower compared to a hypothetical leaf that responds instantaneously to changes in irradiance, though the ratio between an instantaneous and a delayed response depends on the induction state of the leaf (Percy *et al.*, 1996) and the frequency of the fluctuations (Pons & Percy, 1992). The rate with which photosynthesis responds to increases in irradiance is determined by its induction state, which in turn is determined by the irradiance history of the leaf (Percy *et al.*, 1996): the higher the induction state, the faster photosynthesis responds to increases in irradiance. Because most irradiance is captured by the top layers of canopies, it decreases exponentially and its availability varies approx. 50-fold in closed canopies (e.g. Sarlikioti *et al.*, 2011; Niinemets, 2007). Hence, photosynthetic induction state in the lower layers of a canopy is likely lower than in upper layers, and leaves acclimated to shade do not generally show faster induction rates than leaves acclimated to high irradiance (Urban *et al.*, 2007). Furthermore, total photosynthetic activity in the lower layers of a canopy depends more strongly on fluctuations in irradiance than that of upper layers, due to generally low irradiance levels in the understory (Percy *et al.*, 1990).

Several studies have investigated the effects of [CO<sub>2</sub>] on transient photosynthesis and *g<sub>s</sub>* (Chazdon & Percy, 1986; Leakey *et al.*, 2002; Naumburg & Ellsworth, 2000; Naumburg *et*

*al.*, 2001; Košvancová *et al.*, 2009; Holišová *et al.*, 2012; Tomimatsu & Tang, 2012; Tomimatsu *et al.*, 2014). The beneficial effects of elevated [CO<sub>2</sub>] (~700 ppm) on carbon gain after step changes in irradiance have been estimated to be in the order of 5-7% (Leakey *et al.*, 2002; Tomimatsu *et al.*, 2014). These increases are additional to enhancement effects of [CO<sub>2</sub>] in the steady state. They are partly due to faster photosynthetic induction after increases in irradiance, and partly due to higher rates of post-illumination CO<sub>2</sub> fixation, as well as a decreased post-illumination CO<sub>2</sub> burst, after decreases in irradiance (Leakey *et al.*, 2002; Tomimatsu *et al.*, 2014). Furthermore, the loss of photosynthetic induction during the first 5-12 minutes after a decrease in irradiance was reduced by elevated [CO<sub>2</sub>] (Naumburg & Ellsworth, 2000; Leakey *et al.*, 2002). An important limitation on the research conducted so far is that all studies have only used stepwise changes between two irradiance levels: a low irradiance (background irradiance) and a high, typically saturating, irradiance (inducing irradiance). However, it may be that the initial photosynthetic induction state of a leaf interacts with the beneficial effects of elevated [CO<sub>2</sub>], both after increases and after decreases in irradiance. If this were true, then predictions of whole-canopy photosynthesis rates in fluctuating irradiance were greatly complicated by the fact that different induction states of different leaf layers would have to be accounted for when considering [CO<sub>2</sub>] effects.

We used tomato (*Solanum lycopersicum* L.) leaves to study the effects of [CO<sub>2</sub>] on photosynthesis in fluctuating irradiance. We rigorously compared photosynthetic responses to stepwise increases and decreases in irradiance, using three levels of [CO<sub>2</sub>] and four levels of background irradiance. Additionally, we exposed leaves to sinusoidal changes in irradiance of several periods. The results showed that elevated [CO<sub>2</sub>] increases the rate with which photosynthesis reacts to an increase in irradiance (by 4-12%) regardless of initial activation state, that it slows down the loss of induction by 20-25% and that it enhances the dynamics of photosynthesis rates during sine waves by 14%.



## Material and methods

### *Plant material*

Tomato seeds (cv. 'Cappricia'; Rijk Zwaan, De Lier, NL) were germinated in Rockwool plugs (Grodan, Roermond, NL), which after a week were transferred to Rockwool cubes (10 cm \* 10 cm \* 7 cm; Grodan). Plants were grown in a climate chamber in 16/8 h photoperiod, 22/20 °C (day/night) temperature, 70% relative air humidity and 320  $\mu\text{mol m}^{-2} \text{s}^{-1}$  photosynthetically active radiation (PAR; irradiance at table height). Irradiance was provided by a mixture of white, red and far-red LEDs with emission peaks at 440, 550, 660 and 735 nm. Rockwool cubes were standing in a layer (height: 1-2 cm) of nutrient solution (Yara Benelux B.V., Vlaardingen, the Netherlands), which was replenished every 1-2 days and contained 12.4 mM  $\text{NO}_3^-$ , 7.2 mM  $\text{K}^+$ , 4.1 mM  $\text{Ca}^{2+}$ , 3.3 mM  $\text{SO}_4^{2-}$ , 1.8 mM  $\text{Mg}^{2+}$ , 1.2 mM  $\text{NH}_4^+$ , 1.1 mM  $\text{P}^{3-}$ , 30  $\mu\text{M}$   $\text{B}^{3+}$ , 25  $\mu\text{M}$   $\text{Fe}^{3+}$ , 10  $\mu\text{M}$   $\text{Mn}^{2+}$ , 5  $\mu\text{M}$   $\text{Zn}^{2+}$ , 0.75  $\mu\text{M}$   $\text{Cu}^+$  and 0.5  $\mu\text{M}$   $\text{Mo}^{2+}$  (EC 2.1 dS  $\text{m}^{-1}$ , pH 5.5). When plants were between five and six weeks old, leaves 4 or 5, counting from the bottom, were used for experiments. At this stage, growth of these leaves had slowed down strongly compared to initial growth rates (data not shown).

### *Experiments and measurements*

Experiments were performed in a lab, using the LI-6400 photosynthesis system (Li-Cor Biosciences, Lincoln, Nebraska, USA) equipped with a fluorescence chamber (Li-Cor Part No. 6400-40, area: 2  $\text{cm}^2$ ). In all experiments,  $\text{CO}_2$  was a treatment factor and was used in three concentrations: low (200 ppm), ambient (400 ppm) and elevated [ $\text{CO}_2$ ] (800 ppm). Other conditions in the measuring cuvette were:  $22 \pm 0.2$  °C cuvette temperature,  $70 \pm 3\%$  relative humidity and flow rate of 500  $\mu\text{mol s}^{-1}$ . All data were corrected for leaks of  $\text{CO}_2$  into or out of the cuvette, by using dried leaves (Long & Bernacchi, 2003).

Photosynthetic induction was analyzed by using stepwise changes between two irradiances, whereby the inducing irradiance was always 1000  $\mu\text{mol m}^{-2} \text{s}^{-1}$ . The background irradiance was used as a treatment factor and was applied in four levels: 0, 50, 100 and 200  $\mu\text{mol m}^{-2} \text{s}^{-1}$ . Irradiance was provided by a mixture of red (90%, peak intensity: 635 nm) and blue LEDs (10%, peak intensity: 465 nm). Leaves were adapted to the background irradiance until  $g_s$  was stable (60-120 minutes). Then, irradiance was increased and gas exchange parameters were recorded every 1-2 seconds for 60 minutes. Furthermore, to analyze changes in electron transport, saturating flashes of  $\sim 7000 \mu\text{mol m}^{-2} \text{s}^{-1}$  intensity and 1 s duration were applied once every minute in the first ten minutes of induction, and once every two minutes thereafter. After completing the measurements, it was found that the parameters of the saturating flashes were inappropriate to yield accurate electron transport

data, and these data were therefore omitted from further analysis. However, the regular application of saturating flashes did not affect gas exchange rates (see Table S4.1 for details). Loss of photosynthetic induction was analyzed by using the same irradiance intensities as for photosynthetic induction. After photosynthesis rates and  $g_s$  were at steady-state at  $1000 \mu\text{mol m}^{-2} \text{s}^{-1}$ , leaves were exposed to a given background irradiance for 0.5, 1, 2, 3, 5, 10, 20 or 60 minutes. Then, irradiance was returned to  $1000 \mu\text{mol m}^{-2} \text{s}^{-1}$  and the ratio of photosynthesis rates that were reached 60 seconds after re-illumination, divided by steady-state photosynthesis rates at  $1000 \mu\text{mol m}^{-2} \text{s}^{-1}$ , were used to describe the loss of photosynthetic induction (see below). The order of exposure to different durations of background irradiance was randomized, with the exception of the 60 minute period, which was applied at the end of the sequence.

To test the dynamic behavior of photosynthesis in response to changes in irradiance, leaves adapted to  $300 \mu\text{mol m}^{-2} \text{s}^{-1}$  were exposed to sine wave oscillations in irradiance between 100 and  $500 \mu\text{mol m}^{-2} \text{s}^{-1}$  for 30 minutes, using three different periods (1, 3 and 5 minutes).

### Calculations

The relative increase in net photosynthesis rate, following a step increase in irradiance (RI, %) was calculated as:

$$RI = \frac{A_n(t) - A_n(t_0)}{A_n(t_f) - A_n(t_0)} * 100 \quad (4.1)$$

Where  $A_{n(t)}$  is  $A_n$  (net photosynthesis rate,  $\mu\text{mol m}^{-2} \text{s}^{-1}$ ) at time  $t$  after the increase in irradiance,  $A_{n(t_0)}$  is average  $A_n$  before the increase in irradiance and  $A_{n(t_f)}$  is average, final steady-state  $A_n$  in inducing irradiance. This index (RI) was used to describe a) the relative increase of photosynthesis during induction and b) the loss of photosynthetic induction of leaves exposed to background irradiance, 60 seconds after they were re-exposed to inducing irradiance (RI<sub>60</sub>). A sigmoidal function (Zipperlen & Press, 1997) was fitted to the time courses of induction and loss of induction:

$$x = \frac{X_{initial} - X_{final}}{1 + (t/i)^s} + final \quad (4.2)$$

Where  $x$  is the value of the given process at time  $t$  (minutes),  $X_{initial}$  and  $X_{final}$  are the asymptotic minimum and maximum of the process, respectively;  $i$  is the inflection point and  $s$  is a shape parameter. The best fit of the model was determined by minimizing the

root mean squared error (RMSE) of the residuals between model and data. The RMSE was calculated as:

$$RMSE = \sqrt{\frac{1}{n} \sum_{i=1}^n (y_i - \hat{y}_i)^2} \quad (4.3)$$

Where  $n$  is the number of observed values,  $y_i$  is the observed value for the  $i^{\text{th}}$  observation, and  $\hat{y}$  is the predicted value based on the sigmoidal function. The sigmoidal function reproduced changes in RI well, with average RMSE of 1.9% (Table S4.2). The index  $RI_{60}$  was reproduced slightly worse, with RMSE of 3.6%.

Diffusional limitation was calculated as the percentage by which  $A_n$  would increase if  $CO_2$  concentration at the site of carboxylation ( $C_c$ ) was equal to leaf external  $CO_2$  concentration ( $C_a$ ), i.e. without any limitation to  $CO_2$  diffusion into the leaf. For this,  $A_n$  was corrected for transient changes in leaf diffusion ( $A_{n(t)Ca}$ ), by calculating  $A_n$  at  $C_a$ , and  $A_n$  at transient  $C_i$  ( $C_{i(t)}$ ) during the time course of photosynthetic induction and using previously determined  $A_n/C_i$  parameters:

$$A_{n(t)Ca} = A_{n(t)} * \frac{\min\{A_{n(c)}(C_a), A_{n(j)}(C_a), A_{n(TPU)}(C_a)\}}{\min\{A_{n(c)}(C_{i(t)}), A_{n(j)}(C_{i(t)}), A_{n(TPU)}(C_{i(t)})\}} \quad (4.4)$$

Rubisco activity-limited  $A_n$  ( $A_{n(c)}$ ), electron transport-limited  $A_n$  ( $A_{n(j)}$ ) and triose phosphate utilization-limited  $A_n$  ( $A_{n(TPU)}$ ) were determined according to Sharkey et al. (2007):

$$A_{n(c)} = V_{Cmax} \left( \frac{C_i - \Gamma^*}{C_i + K_c * \left(1 + \frac{O}{K_o}\right)} \right) - R_d \quad (4.5)$$

$$A_{n(j)} = J_{max} \left( \frac{C_i - \Gamma^*}{4 * C_i + 8 * \Gamma^*} \right) - R_d \quad (4.6)$$

$$A_{n(TPU)} = 3 * TPU - R_d \quad (4.7)$$

Where  $V_{Cmax}$  ( $85 \mu\text{mol m}^{-2} \text{s}^{-1}$ ) is maximum rate of carboxylation,  $\Gamma^*$  is the chloroplast  $CO_2$  compensation point (53 ppm) in the absence of day respiration ( $R_d$ ;  $1.2 \mu\text{mol m}^{-2} \text{s}^{-1}$ ),  $O$  (21 kPa) is the chloroplast  $O_2$  concentration,  $K_c$  (21.4 Pa) and  $K_o$  (15.4 kPa) are the Michaelis-Menten constants of Rubisco for  $CO_2$  and for  $O_2$ , respectively,  $J_{max}$  ( $148 \mu\text{mol m}^{-2} \text{s}^{-1}$ ) is the maximum rate of electron transport and TPU ( $10.3 \mu\text{mol m}^{-2} \text{s}^{-1}$ ) is the maximum rate of triose phosphate utilization. Parameters  $V_{Cmax}$ ,  $J_{max}$  and TPU were estimated after Sharkey et al. (2007; Fig. S4.1),  $R_d$  and  $\Gamma^*$  after Yin et al. (2009; Figs. S4.1, S4.2). Additionally,  $R_d$  was corrected for respiration under the gasket of the gas exchange

cuvette (Pons & Welschen, 2002). Parameters  $K_c$  and  $K_o$  were taken from Sharkey et al. (2007). Diffusional limitation (%) was determined as

$$\text{Diffusional limitation} = \frac{A_{n(t)C_a} - A_{n(t)}}{A_{n(tf)} - A_{n(t_0)}} * 100 \quad (4.8)$$

Biochemical limitation was calculated by using  $A_{n(t)}$  corrected for changes in transient  $C_i$  ( $A_{n(t)C_i}$ ). Thus, instead of using  $C_a$  in the numerator of Eqn. 4.4, steady-state  $C_i$  ( $C_{i(tf)}$ ) was used. Then, biochemical limitation was calculated as (Tinoco-Ojanguren & Pearcy, 1993b)

$$\text{Biochemical limitation} = \frac{A_{n(tf)} - A_{n(t)C_i}}{A_{n(tf)} - A_{n(t_0)}} * 100 \quad (4.9)$$

Using  $A_{n(t)C_i}$ , the apparent time constant of Rubisco activation ( $\tau_R$ ), denoting the time required to reach 63% of full activation, was calculated after Woodrow and Mott (1989)

$$\tau_R = \frac{\Delta \text{time}}{\Delta \ln(A_{n(tf)} - A_{n(t)C_i})} \quad (4.10)$$

where  $\Delta \text{time}$  is the duration used for determination of  $\tau_R$ . Instead of using a fixed duration for the linear correlation between time and  $\ln(A_{n(tf)} - A_{n(t)C_i})$ , as was done in Woodrow and Mott (1989), the duration of the correlation was varied based on visual observation for every replicate (Fig. S4.3, Table S4.3). This was necessary, as the length and starting point of the linear part of this correlation varied greatly with background irradiance and [CO<sub>2</sub>]. These correlations yielded an average  $R^2$  of 0.97 (Table S4.3), with the lowest  $R^2$  being 0.90.

### *Statistical analysis*

The sigmoidal function used on RI and RI<sub>60</sub> (Eqn. 2) was fitted separately to each replicate. Then, the same function was used to determine the time to reach 50% ( $t_{50}$ ) or 90% ( $t_{90}$ ) of change in RI, and to calculate enhancement effects of elevated [CO<sub>2</sub>] compared to ambient [CO<sub>2</sub>]. Effects of background irradiance and [CO<sub>2</sub>] on parameters of the sigmoidal function (Table 4.1), and on  $t_{50}$  and  $t_{90}$ , were then analyzed using two-way ANOVA (Genstat 16<sup>th</sup> Ed., VSN International, Hempstead, UK). In case of non-significant interactions between the two factors, single-factor effects were analyzed using Fisher's protected least significant difference tests (Genstat). Single-factor effects on simulated RI and RI<sub>60</sub> were determined by varying the parameters of the sigmoidal model that were significantly affected by each factor level. Then, 1000 random numbers with normal distribution and centered on a given

average of a parameter, with the standard error of means (SEM) of that parameter as the standard deviation of the distribution, were generated. The 2.5<sup>th</sup> and the 97.5<sup>th</sup> percentile of those 1000 samples was used to generate the 95% confidence interval around the mean of a given effect.

Table 4.1. Effects of background irradiance, CO<sub>2</sub> concentration and their interaction on parameters of sigmoidal fits. The sigmoidal function was fitted to data describing the gain and loss of photosynthetic induction (Eqn. 2). Symbols: \*\*\* = P<0.001, \*\* = P<0.01, \* = P<0.05. Lack of symbol denotes lack of statistically significant effect

Irradiance change	Index	Parameter	Background irradiance	CO <sub>2</sub> concentration	Background irradiance X CO <sub>2</sub> concentration
Step increase	Relative increase in net photosynthesis rate (%)	initial			
		final		**	
		inflection	***	***	
		shape	**	***	
Step decrease	Relative increase in net photosynthesis rate 60 s after re-illumination (%)	initial			
		final	***	***	
		inflection	**		
		shape		**	

## Results

### *Effects of [CO<sub>2</sub>] and background irradiance on photosynthetic induction and loss of photosynthetic induction*

There was no interaction between [CO<sub>2</sub>] and background irradiance on parameters of the sigmoidal function fitted to RI and RI<sub>60</sub> data (Table 4.1). Therefore, average [CO<sub>2</sub>] effects across background irradiances (and vice versa) on rates of photosynthetic induction and loss of photosynthetic induction, could be explored (Fig. 4.1). Elevated [CO<sub>2</sub>] (800 ppm) had a stimulating effect on the relative increase in photosynthesis rates between ~2.5 and 25 minutes after a step increase in irradiance (Fig. 4.1A; Fig. 4.2). The average responses at ambient (400 ppm) and low [CO<sub>2</sub>] (200 ppm) did not differ from each other. The time to reach 50 and 90% (t<sub>50</sub>, t<sub>90</sub>) of final steady-state photosynthesis rates decreased with each increase in [CO<sub>2</sub>] (Table 4.2). t<sub>50</sub> almost doubled, while t<sub>90</sub> was almost four times larger in low compared to elevated [CO<sub>2</sub>].

Between ~1.5 and 4 minutes after the irradiance increase, leaves that were adapted to darkness showed a significantly slower increase in relative photosynthesis rates than leaves that had been adapted to shade (i.e. 50, 100 and 200 μmol m<sup>-2</sup> s<sup>-1</sup>), which did not differ in their responses (Fig. 4.1C). This was also illustrated in t<sub>50</sub> and t<sub>90</sub> values, which were much larger in dark-adapted leaves than in shade-adapted leaves (Table 4.2). t<sub>50</sub> was approx. four times larger in dark-adapted leaves than that of leaves in 200 μmol m<sup>-2</sup> s<sup>-1</sup>, while t<sub>90</sub> was almost twice as large.

Average loss of photosynthetic induction was slowed down by elevated [CO<sub>2</sub>] within ~2.5 – 7.5 minutes after an irradiance decrease, while responses at ambient and low [CO<sub>2</sub>] were not different from each other (Fig. 4.1B). After this initial period, there was a tendency towards decreased loss of induction at elevated [CO<sub>2</sub>], but because of the large uncertainty around the mean, this was not significant. However, plotting loss of induction as affected by the various background irradiances (Fig. 4.3) revealed that after ~15 minutes of exposure to low irradiance, effects of elevated [CO<sub>2</sub>] were more positive on RI<sub>60</sub> in leaves exposed to shade levels (Fig. 4.3B-D) than in leaves exposed to darkness (Fig. 4.3A). Approx. 10 minutes after the decrease in irradiance, the induction state was similar across the different irradiances, except for leaves exposed to darkness where it was comparatively lower (Fig. 4.1D, Fig. 4.3).

### *Relative increases in photosynthesis and its limitations*

Across all background irradiances, [CO<sub>2</sub>] increased the rate of relative increases in photosynthesis, after a step increase in irradiance (Fig. 4.2). Steady-state photosynthesis rates increased linearly with irradiance in the range 0-200 μmol m<sup>-2</sup> s<sup>-1</sup>, and additionally

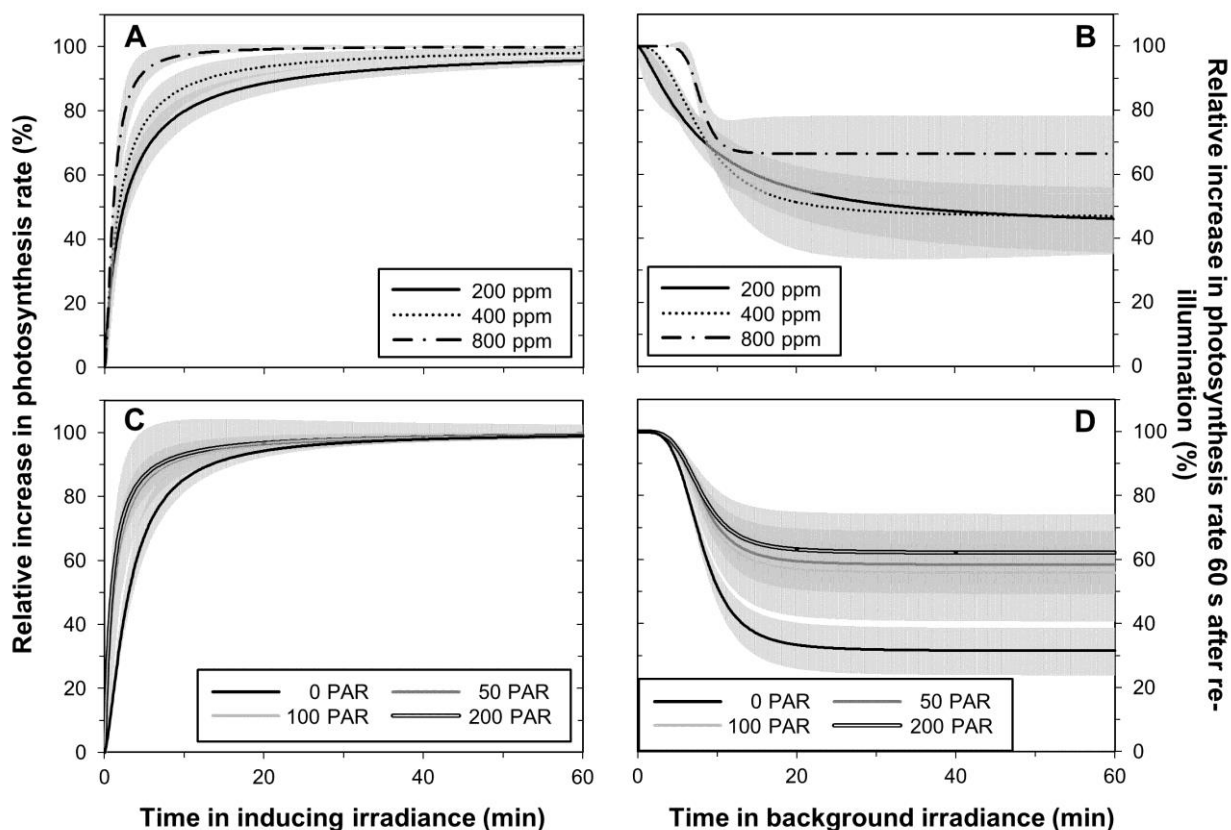


Fig. 4.1. Average effects of CO<sub>2</sub> concentration (A, B) and background irradiance (C, D) on the relative increase in photosynthesis rate after a step increase in irradiance (A, C) and on loss of photosynthetic induction, depicted as relative increase in photosynthesis rate 60 seconds after re-illumination (B, D). Shown are averages  $\pm$  95% confidence interval. Simulations were conducted by using a sigmoidal model (Eqn. 4.2) and by varying the parameters that were significantly affected by CO<sub>2</sub> concentration or background irradiance, while keeping the other parameters constant. **A)** initial (0), final (100), inflection (200 ppm = 2.4; 400 ppm = 1.8; 800 ppm = 1.1), shape (200 ppm = 1.0; 400 ppm = 1.1; 800 ppm = 1.7). **B)** initial (0), final (100), inflection (0 PAR = 1.5; 50 and 100 PAR = 1.1; 200 PAR = 0.9), shape (0 PAR = 1.5; 50, 100 and 200 PAR = 1.1). **C)** initial (100), final (200 ppm = 42.4; 400 ppm = 46.6; 800 ppm = 66.4), inflection (7.9), shape (200 ppm = 1.3; 400 ppm = 2.5; 800 ppm = 7.7). **D)** initial (100), final (0 PAR = 31.4; 50 PAR = 58.3; 100 PAR = 55.8; 200 PAR = 62.1), inflection (8.0), shape (3.9)

scaled with [CO<sub>2</sub>] (Fig. S4.4). The increase in stomatal conductance ( $g_s$ ) after irradiance increases generally scaled negatively with background irradiance, i.e. it was stronger in low background irradiance (Fig. S4.5, left panel). In elevated [CO<sub>2</sub>],  $g_s$  showed a smaller amplitude between initial and final  $g_s$ , and initial  $g_s$  exhibited the smallest modulation due to background irradiance ( $\sim 0.2 \text{ mol m}^{-2} \text{ s}^{-1}$  in  $0\text{--}200 \mu\text{mol m}^{-2} \text{ s}^{-1}$  irradiance). Initial  $g_s$  in low [CO<sub>2</sub>], on the other hand, was more strongly affected by background irradiance, ranging from  $\sim 0.2 \text{ mol m}^{-2} \text{ s}^{-1}$  in darkness to  $\sim 0.4 \text{ mol m}^{-2} \text{ s}^{-1}$  in  $200 \mu\text{mol m}^{-2} \text{ s}^{-1}$ . Transient photosynthesis rates and  $g_s$  changes determined the time course of  $C_i$  (data not shown). Together, those data were used to calculate time courses of diffusional and biochemical limitation.

Table 4.2. Time (minutes) to reach 50% ( $t_{50}$ ) or 90% ( $t_{90}$ ) of final net photosynthesis rates after a step increase in irradiance, as affected by CO<sub>2</sub> concentration and background irradiance. Different letters denote statistically significant differences ( $P < 0.05$ ) within either CO<sub>2</sub> concentration or background irradiance treatments, as determined by Fisher's protected least significant difference (L.S.D.) tests. L.S.D. values (in italics) are also supplied for comparison

Factor	Level	$t_{50}$		$t_{90}$	
CO <sub>2</sub> concentration (ppm)	200	1.91	c	14.7	c
	400	1.62	b	10.0	b
	800	1.02	a	3.9	a
	<i>L.S.D.</i>	<i>0.27</i>		<i>3.1</i>	
Background irradiance ( $\mu\text{mol m}^{-2} \text{s}^{-1}$ )	0	2.72	c	13.1	b
	50	1.03	b	7.6	a
	100	0.89	ab	7.0	a
	200	0.64	a	8.0	a
	<i>L.S.D.</i>	<i>0.33</i>		<i>3.9</i>	

Diffusional limitation is an estimation of the absolute decrease in net photosynthesis rates due to obstacles to CO<sub>2</sub> diffusion between the outside of the leaf and the site of carboxylation. Diffusional limitation therefore includes effects of stomatal and mesophyll conductance, both during transients and in the steady state, and therefore does not decrease to zero in a fully induced leaf. While the final level of diffusional limitation was strongly affected by [CO<sub>2</sub>], the rate of its initial buildup increased with increases in background irradiance (Fig. 4.4, left panel). Also, after the initial buildup, diffusional limitation exhibited a decrease that was more pronounced when the background irradiance and [CO<sub>2</sub>] were lower. To analyze whether [CO<sub>2</sub>] and background irradiance affected the transient diffusional limitation during photosynthetic induction, we averaged the fraction of diffusional limitation that was above the final, steady-state level for each replicate (grey area in Fig. 4.4A). This analysis showed that the average of the additional diffusional limitation was significantly ( $P < 0.001$ ) lower in 800 ppm (0.6%) than in both 400 ppm (1.5%) and 200 ppm (1.7%), which were not significantly different from each other. Also, additional diffusional limitation was significantly ( $P < 0.001$ ) larger in dark-adapted (1.8%) than in shade-adapted (0.7-1.1%) leaves. Steady-state diffusional limitation increased with irradiance, and decreased with [CO<sub>2</sub>] levels (Fig. S4.6A). Steady-state net photosynthesis rates at different irradiances showed curvilinear relationships with diffusional limitation, in which diffusional limitation increased with increases in photosynthesis, but decreased strongly with each [CO<sub>2</sub>] level (Fig. S4.6B). Steady-state  $g_s$  and diffusional limitation showed a positive near-linear relationship that was irrespective of [CO<sub>2</sub>] (Fig. S4.6C).

Here, biochemical limitation is defined as an additional limitation to photosynthesis rates after an increase in irradiance, due to an initially low activation state of enzymes, mostly in the Calvin cycle. Thus, by definition, biochemical limitation decreases towards zero as pho-



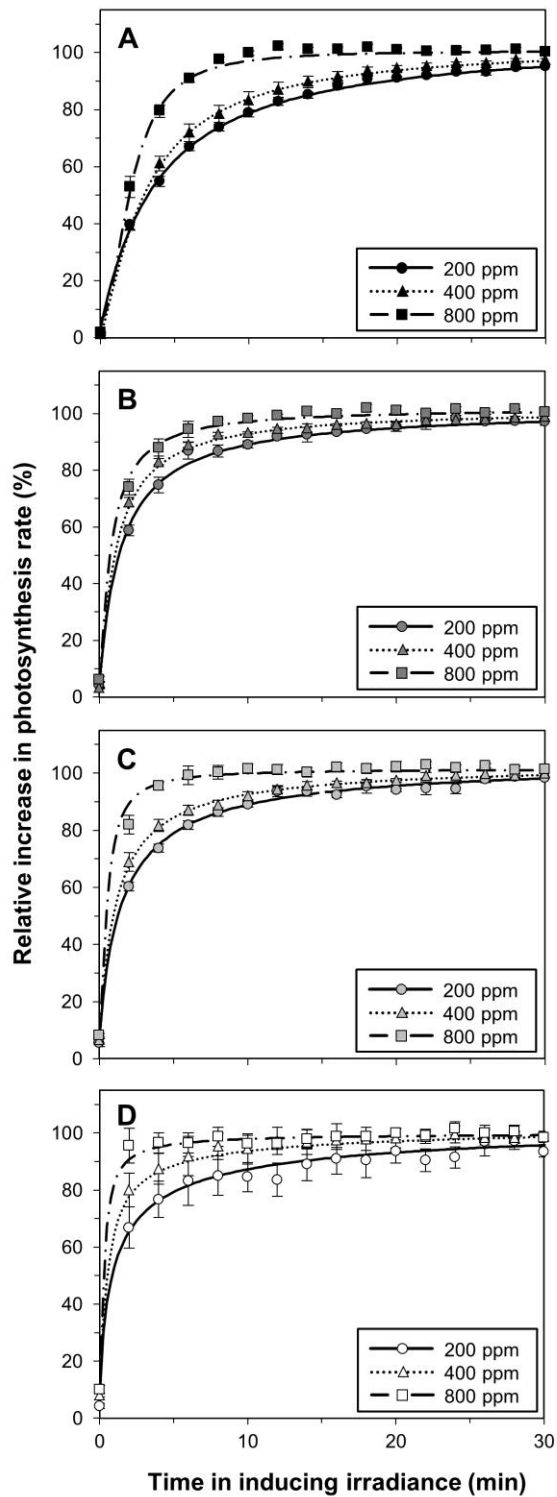


Fig. 4.2. Relative increase in photosynthesis rate after a step increase in irradiance at three CO<sub>2</sub> concentrations. Background irradiance was 0 (A), 50 (B), 100 (C) or 200  $\mu\text{mol m}^{-2} \text{s}^{-1}$  (D); inducing irradiance was 1000  $\mu\text{mol m}^{-2} \text{s}^{-1}$ . Lines denote sigmoidal fits (Eqn. 4.2), symbols denote average  $\pm$  SEM,  $n = 3-5$

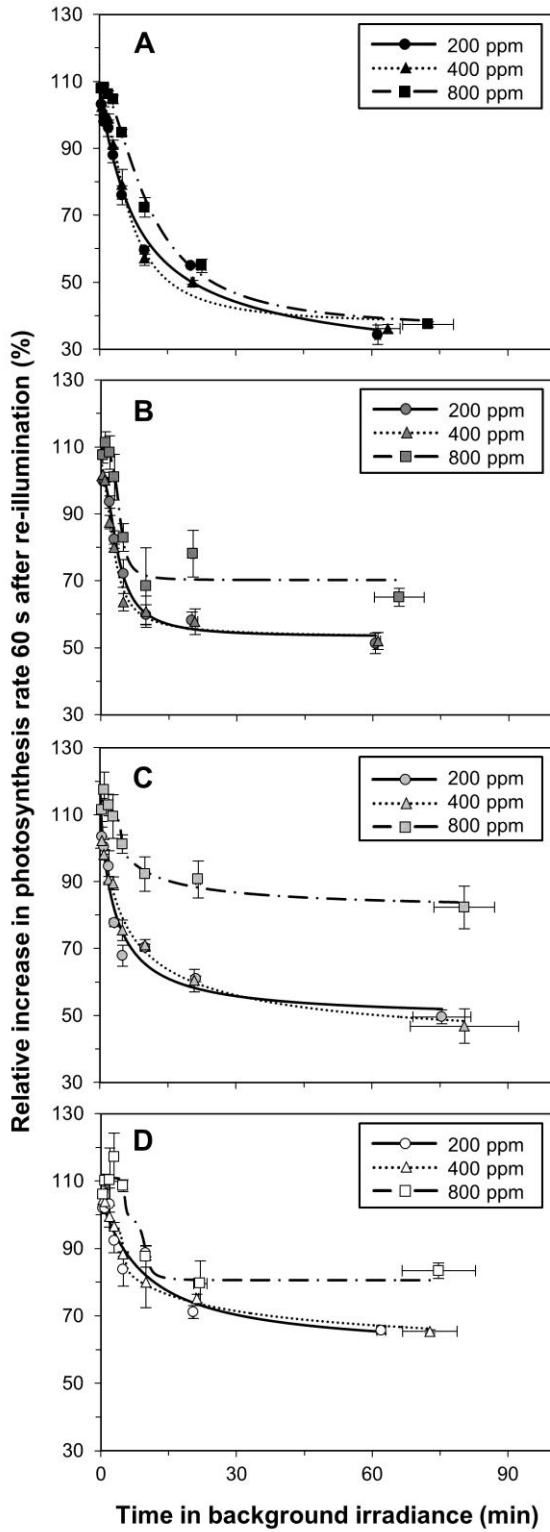


Fig. 4.3. Loss of photosynthetic induction after step decreases in irradiance at three CO<sub>2</sub> concentrations. Background irradiance was 0 (A), 50 (B), 100 (C) or 200 μmol m<sup>-2</sup> s<sup>-1</sup> (D); inducing irradiance was 1000 μmol m<sup>-2</sup> s<sup>-1</sup>. Loss of photosynthetic induction is depicted as the relative increase in net photosynthesis rate 60 s after re-illumination (RI<sub>60</sub>). Lines denote sigmoidal fits (Eqn. 4.2), symbols denote average ± SEM, n = 3-4

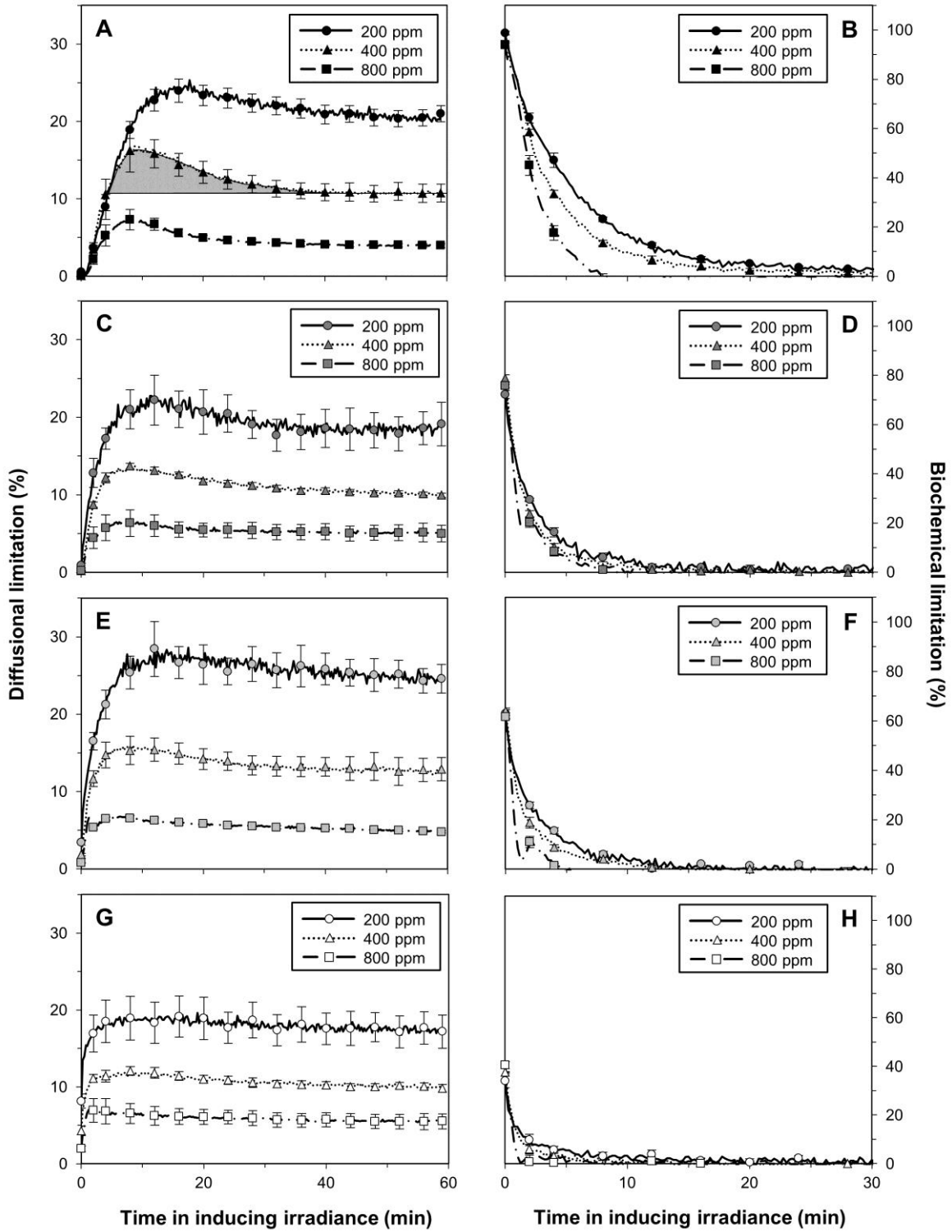


Fig. 4.4. Changes in diffusional (left panel) and biochemical limitation (right panel) after a step increase in irradiance at three CO<sub>2</sub> concentrations. Background irradiance was 0 (A, B), 50 (C, D), 100 (E, F) or 200  $\mu\text{mol m}^{-2} \text{s}^{-1}$  (G, H); inducing irradiance was 1000  $\mu\text{mol m}^{-2} \text{s}^{-1}$ . The shaded area in A) depicts the transient additional increase in diffusional limitation above steady-state levels. Lines and symbols denote average, error bars denote  $\pm$  SEM,  $n = 3-5$

tosynthesis rates approach full induction. Because of their different definitions, diffusional and biochemical limitations are not additive. The initial level of biochemical limitation decreased with background irradiance (Fig. 4.4, right panel). Biochemical limitation relaxed faster the higher the previous background irradiance had been, and was positively modulated by [CO<sub>2</sub>]. There was a significant ( $P=0.001$ ) interaction between background irradiance and [CO<sub>2</sub>] affecting average biochemical limitation, causing [CO<sub>2</sub>] to have smaller effects on biochemical limitation with increases in background irradiance (Table 4.3). The apparent time constant of Rubisco activation ( $\tau_R$ ) decreased with [CO<sub>2</sub>] (Fig. 4.5A) and background irradiance (Fig. 4.5B). Both affected  $\tau_R$  with similar magnitude ( $\sim 70\%$  difference between the smallest and largest value).

### *Photosynthetic responses to sine waves*

Photosynthesis followed the sinusoidal input in irradiance, however with a delay that was relatively larger in shorter sine waves (Fig. 4.6). Because of this delay, net photosynthesis rates in the half-cycles during which irradiance decreased were  $\sim 25\%$  higher than during half-cycles of increasing irradiance. Additionally, [CO<sub>2</sub>] strongly affected the amplitude (i.e. maximum minus minimum value) of photosynthesis, and this was further modulated by sine wave period. For example, in elevated [CO<sub>2</sub>] the amplitude of photosynthesis rates was  $\sim 14.1 \mu\text{mol m}^{-2} \text{s}^{-1}$  for sine waves with a 1 minute period (Fig. 4.6A),  $\sim 17.9 \mu\text{mol m}^{-2} \text{s}^{-1}$  for sine waves with a 3 minutes period (Fig. 4.6B) and  $\sim 18.3 \mu\text{mol m}^{-2} \text{s}^{-1}$  for sine waves with a 5 minutes period (Fig. 4.6C). The relative difference in amplitudes between [CO<sub>2</sub>] levels was similar irrespective of sine wave duration, i.e. the amplitude of net photosynthesis rates at 200 ppm was always  $\sim 60\%$  lower than that at 800 ppm, and at 400 ppm was always  $\sim 30\%$  lower.

When constructing “dynamic irradiance response curves” from transient photosynthesis rates during sine waves, the curvilinearity that would be expected from steady-state irradiance response curves in this irradiance range ( $100\text{--}500 \mu\text{mol m}^{-2} \text{s}^{-1}$ ) was visible from data at 3 and 5 minute periods, but not during short sine waves (Fig. 4.7). When splitting the data depending on the direction of irradiance change (i.e. whether irradiance was within the increasing or the decreasing portion of the sine wave), the hysteresis of photosynthesis in fluctuating irradiance became apparent (Fig. S4.7). Photosynthesis rates were hardly affected by the direction of irradiance change in sine waves with 5 minute periods, especially in low [CO<sub>2</sub>] (Fig. S4.7C). In contrast to this, in sine waves of 1 minute period, transient photosynthesis rates were much higher in the decreasing irradiance portion of the sine wave than in the increasing portion, and this was further modulated by [CO<sub>2</sub>] (Fig. S4.7A). Because of the hysteresis in photosynthesis rates, there was a gain in in-

Table 4.3. Average biochemical limitation (%) after stepwise increases in irradiance, as affected by CO<sub>2</sub> concentration and background irradiance. Letters denote statistically significant differences (P<0.05) within rows as determined by Fisher's protected least significant difference (LSD) tests. LSD values (in italics) are also supplied for comparison

Background irradiance ( $\mu\text{mol m}^{-2} \text{s}^{-1}$ )	CO <sub>2</sub> concentration (ppm)			L.S.D.
	200	400	800	
0	10.3 a	7.6 b	3.5 c	<i>1.5</i>
50	4.4 b	3.0 ab	1.7 a	<i>1.9</i>
100	2.8 b	2.0 b	-0.1 a	<i>1.9</i>
200	1.9 a	0.9 a	0.7 a	<i>1.9</i>

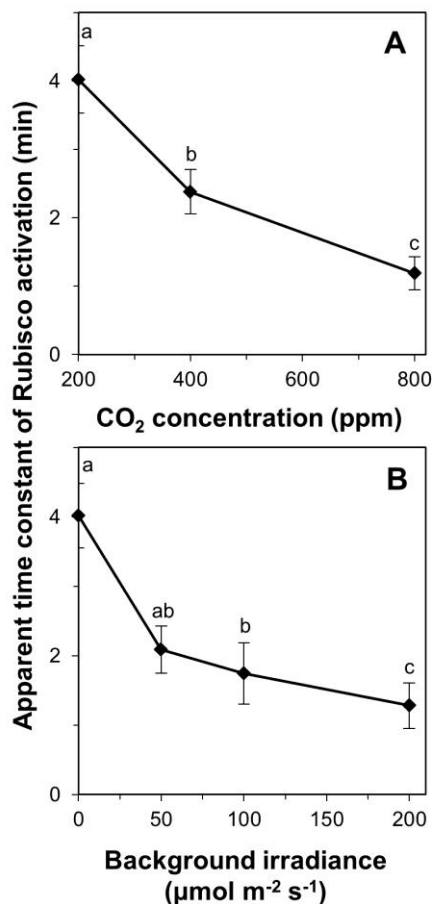


Fig. 4.5. Apparent time constant of Rubisco activation after a step increase in irradiance, as affected by CO<sub>2</sub> concentration (A) and background irradiance (B). Different letters denote statistically significant (P<0.05) differences between treatment levels, symbols denote average  $\pm$  SEM, n = 3-5

egrated assimilation during the half cycle of decreasing irradiance relative to the other half-cycle (Fig. S4.8). This relative gain decreased with cycle period, and was modulated by [CO<sub>2</sub>]: While there was no [CO<sub>2</sub>] effect at the longest period, in sine waves with 1 and 3 minute periods, intermediate and elevated [CO<sub>2</sub>] produced a stronger gain than low [CO<sub>2</sub>].

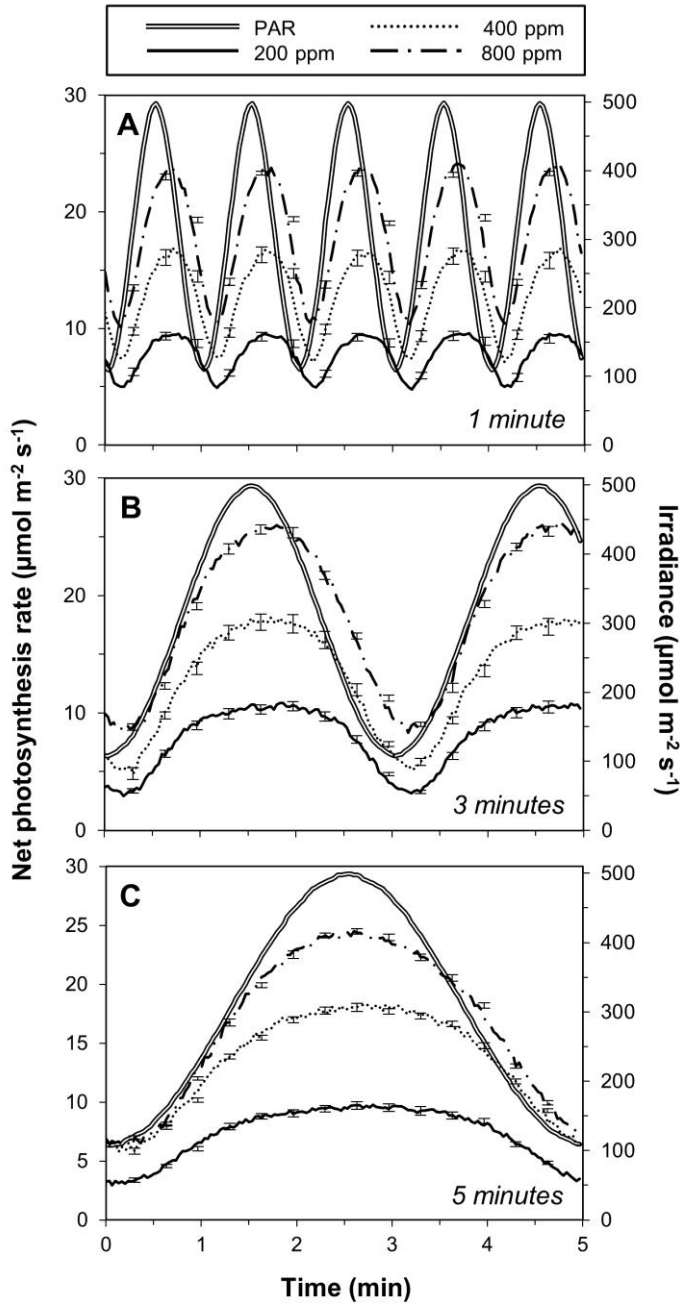


Fig. 4.6. Response of net photosynthesis rate to sinusoidal changes in irradiance, as affected by period of irradiance changes and [CO<sub>2</sub>]. Sine wave periods (minutes) are shown in the bottom right corner of every figure. Lines depict average values, error bars depict  $\pm$  SEM at selected time points,  $n = 12-15$

#### *Enhancement effects of elevated [CO<sub>2</sub>]*

To what extent did elevated [CO<sub>2</sub>] stimulate rates of dynamic photosynthesis, compared to ambient [CO<sub>2</sub>]? To answer that question, sigmoidal fits to data after stepwise increases and decreases in irradiance (lines in Figs. 4.2 and 4.3) and average irradiance responses during sine waves (Fig. 4.7) were used.

The relative increase in net photosynthesis rates was enhanced by  $\sim 12\%$  when comparing

averages of the first 15 minutes after a stepwise increase in irradiance, and diminished to ~7% and ~4% after 30 and 60 minutes, respectively (Table 4.4). This was so because the difference between relative rates at elevated and ambient  $[\text{CO}_2]$  was largest in the first minutes following the stepwise increase in irradiance (Fig. 4.2). Photosynthetic induction state after a stepwise decrease to low irradiance was ~21-25% higher in elevated compared to ambient  $[\text{CO}_2]$  (Table 4.4). Here, the positive effect of elevated  $[\text{CO}_2]$  increased with time in low irradiance (Table 4.4).

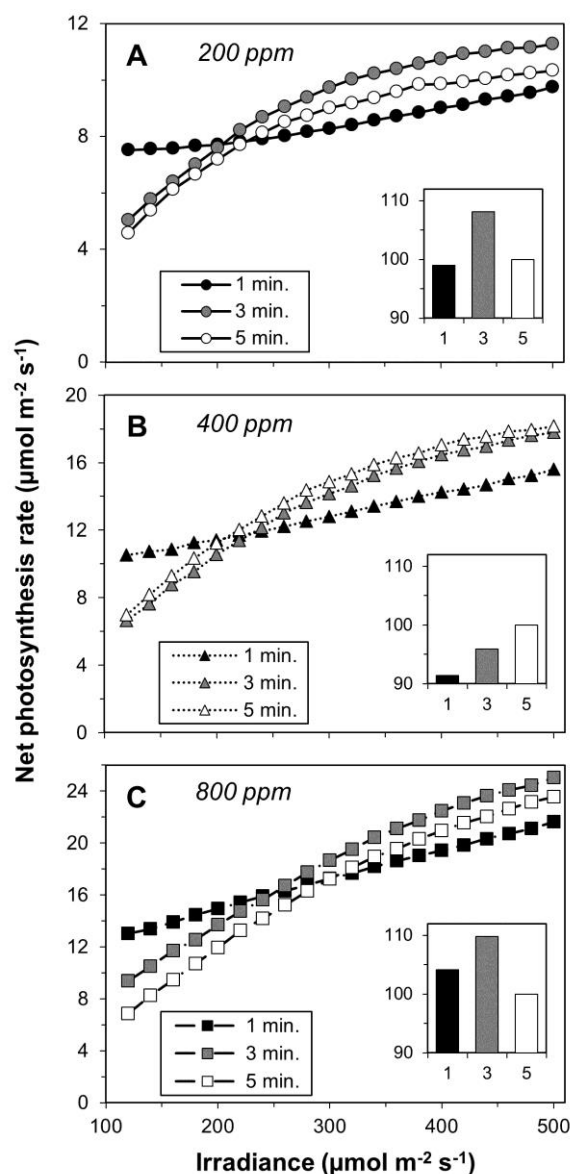


Fig. 4.7. Average net photosynthesis rate during sinusoidal changes in irradiance, plotted against irradiance, at 200 (A), 400 (B) and 800 ppm (C). Responses to three periods of sine wave (1, 3 and 5 minutes) are shown. Note the different scales of y-axes between subplots. Insets: bar charts depict relative net photosynthesis rate, averaged over the complete dynamic irradiance response and expressed relative to the response at 5 minutes sine wave period (set to 100%)

The enhancement effect of elevated [CO<sub>2</sub>] during sine waves was quantified by firstly taking an average of the dynamic response to irradiance at all periods, and by secondly expressing this value at 1 and 3 minute periods relative to the one at 5 minute period (insets in Fig. 4.7). The second step was done assuming that assimilation rates at 5 minute periods were close to steady-state rates (Fig. S4.7C), thereby forming a baseline to which the more dynamic rates at 1 and 3 minute periods could be compared. This analysis revealed that relative rates of dynamic photosynthesis were increased in elevated [CO<sub>2</sub>] by ~14% in both 1 and 3 minute periods, respectively.

Table 4.4. Enhancement effects (%) of elevated (800 ppm) over ambient (400 ppm) CO<sub>2</sub> concentration, 15-60 minutes after stepwise increases or decreases in irradiance

Direction of irradiance change	No. of minutes after irradiance change		
	15	30	60
Increase	12.1	7.1	3.8
Decrease	20.6	22.8	25.4



## Discussion

### *Elevated [CO<sub>2</sub>] speeds up photosynthetic induction, and decreases the loss of photosynthetic induction, regardless of background irradiance*

This study aimed to analyze how the dynamics of photosynthesis in various irradiance environments were affected by CO<sub>2</sub> concentration. We found that regardless of the background irradiance that leaves were adapted to, higher [CO<sub>2</sub>] increased the rate of photosynthesis increases after a step change in irradiance (Figs. 4.1A and 4.2). Previous studies, which were conducted using a single background irradiance only, also found faster photosynthetic induction with increased [CO<sub>2</sub>] (Chazdon & Pearcy, 1986; Leakey *et al.*, 2002; Košvancová *et al.*, 2009; Tomimatsu & Tang, 2012; Tomimatsu *et al.*, 2014). Our study confirms these findings for a wider range of irradiances and [CO<sub>2</sub>] levels, and finds that elevated [CO<sub>2</sub>] speeds up reaction rates by 4-12% (Table 4.4).

Recently, Kaiser *et al.* (2015) summarized the published effects of [CO<sub>2</sub>] on the times to reach 50 and 90% of full photosynthetic induction ( $t_{50}$  and  $t_{90}$ , respectively). They found that across studies,  $t_{90}$  decreased with increases in [CO<sub>2</sub>], while  $t_{50}$  did not. In fact, Leakey *et al.* (2002) reported an *increase* in  $t_{50}$  with increased [CO<sub>2</sub>], while Chazdon and Pearcy (1986) reported unchanged  $t_{50}$  in the range 200-844 ppm. However, in some studies,  $t_{50}$  decreased with elevated [CO<sub>2</sub>] (Tomimatsu & Tang, 2012; Tomimatsu *et al.*, 2014), similar to the present study. Thus, while there is variability between studies (and species) regarding [CO<sub>2</sub>] effects on  $t_{50}$ , we show that in tomato both  $t_{50}$  and  $t_{90}$  decrease with increased [CO<sub>2</sub>], and that this is the case across all background irradiances tested (Table 4.2).

Elevated [CO<sub>2</sub>] (800 ppm) decreased the loss of photosynthetic induction, regardless of background irradiance. Again, this confirms previous studies showing the beneficial effects of high [CO<sub>2</sub>] on the loss of induction (Naumburg & Ellsworth, 2000; Leakey *et al.*, 2002). Importantly, the current study finds that photosynthetic induction state in darkness or low irradiance is 20-25% higher in elevated compared to ambient [CO<sub>2</sub>]. Thus, while elevated [CO<sub>2</sub>] increases the *velocity* of photosynthesis increases after irradiance increases, it additionally enhances the *photosynthetic induction state* after irradiance decreases. In continuously changing irradiance (i.e. sine waves), the beneficial effect of elevated [CO<sub>2</sub>] on relative rates of photosynthesis (i.e. additional to effects on steady-state photosynthesis) was found to be 14%. This effect may be due to a combination of faster rates of increase of photosynthesis, higher post-illumination CO<sub>2</sub> fixation and decreased post-illumination CO<sub>2</sub> burst (Leakey *et al.*, 2002; Tomimatsu *et al.*, 2014).

*Elevated [CO<sub>2</sub>] alleviates transient limitations more quickly*

Of all studies linking elevated [CO<sub>2</sub>] and photosynthetic induction, one has attempted to analyze the changes in underlying limitations: Košvancová et al. (2009) compared the time required to completely remove transient stomatal and biochemical limitations in *Fagus sylvatica* and *Picea abies*, in 385 and 700 ppm. There was no [CO<sub>2</sub>] effect on biochemical limitation in either species, but a faster removal of stomatal limitation in 700 ppm in *P. abies* (Košvancová et al., 2009). Thus, unlike effects of elevated [CO<sub>2</sub>] on induction, reports of [CO<sub>2</sub>] effects on the underlying limitations of photosynthetic induction are sparse.

Here, we show that an increase in [CO<sub>2</sub>] decreases steady-state (Fig. S4.6) and transient (Fig. 4.4) diffusional limitations, and that high [CO<sub>2</sub>] alleviates additional diffusional limitations more quickly than intermediate and low [CO<sub>2</sub>], regardless of initial induction state. Furthermore, elevated [CO<sub>2</sub>] has positive effects on the speed of the relaxation of biochemical limitations (Fig. 4.4), and these effects were larger the lower the initial induction state had been (Table 4.3).

*[CO<sub>2</sub>] affects Rubisco activation rates irrespective of initial photosynthetic induction state*

The apparent time constant of Rubisco activation ( $\tau_R$ ) decreased with increases in both [CO<sub>2</sub>] and background irradiance (Fig. 4.5). As a result, our data agree with the findings of Woodrow et al. (1996) in spinach (*Spinacia oleracea* L.): the value of  $\tau_R$  decreased with the difference between initial and final induction states. Also for spinach, Jackson et al. (1991) described a roughly sigmoidal relationship between background irradiance and Rubisco activation, with a threshold of  $\sim 135 \mu\text{mol m}^{-2} \text{s}^{-1}$ : if background irradiance was below this threshold (including darkness),  $\tau_R$  was relatively insensitive to increases in background irradiance. However, at background irradiances above this threshold,  $\tau_R$  started to decrease steeply. The authors hypothesized that below  $135 \mu\text{mol m}^{-2} \text{s}^{-1}$ , the slow activation of Rubisco activase added to the time required to activate Rubisco, while above the threshold, Rubisco activase was largely active (Jackson et al., 1991). Such a sigmoidal pattern was clearly not visible in our data, where the steepest decline in  $\tau_R$  was found between 0 and  $50 \mu\text{mol m}^{-2} \text{s}^{-1}$ , and where, generally, the decrease in  $\tau_R$  followed a negative exponential pattern (Fig. 4.5B). In *Arabidopsis thaliana* (Colombia 0),  $\tau_R$  decreased near-linearly in the range  $0\text{-}130 \mu\text{mol m}^{-2} \text{s}^{-1}$  (Kaiser et al., unpublished results). Altogether, these differing patterns suggest large species-specific differences in the irradiance- Rubisco activation relationship. These may be explained by differences in the concentration of 2-carboxyarabinitol 1-phosphate (CA1P), a tight-binding inhibitor of Rubisco (Gutteridge et

*al.*, 1986). Concentrations of CA<sub>1</sub>P are high in dark-adapted leaves of tomato, but low in both spinach and *A. thaliana* (Moore *et al.*, 1991). Another explanation may lie in the interaction between Rubisco and Rubisco activase. The ATPase Rubisco activase is required to remove inhibitory compounds, such as CA<sub>1</sub>P, from uncarbamylation Rubisco (Salvucci *et al.*, 1985). Rubisco activase from spinach leaves was found to be compatible with Rubisco from *A. thaliana* (and many other species), but not with that of different Solanaceae species (including tomato), suggesting differences in the structure of the enzymes between different groups of species (Wang *et al.*, 1992).

In spinach, rates of photosynthetic increase were shown to be sensitive to [CO<sub>2</sub>] (C<sub>i</sub> range: 100-300 ppm) when differences between background and inducing irradiance (and therefore differences in Rubisco activation states) were rather small (Woodrow *et al.*, 1996). This was explained by [CO<sub>2</sub>] having large effects on carbamylation, but not on Rubisco activase-mediated removal of inhibitors from Rubisco (Woodrow *et al.*, 1996). In our study, an increase in [CO<sub>2</sub>] was similarly beneficial, at least in relative terms, for rates of Rubisco activation at every background irradiance level (Fig. 4.5A). Our data are therefore in disagreement with those of Woodrow *et al.* (1996), suggesting that the model of Woodrow *et al.* (1996) proposed for the role of [CO<sub>2</sub>] in Rubisco activation does not apply to tomato leaves.

#### *Differences in dark- vs. shade-adapted leaves: Hypotheses*

Rates of photosynthesis increase in dark-adapted leaves, and loss of photosynthetic induction in darkness, were substantially different from the same processes of leaves adapted to various shade levels (Fig. 4.1, Table 4.2). However, we also note that the distinct difference between dark- and shade-adapted tomato leaves may (partly) be species-specific, as spinach did not exhibit abrupt changes in induction rates between background irradiances of 0 and ~135 μmol m<sup>-2</sup> s<sup>-1</sup> (Jackson *et al.*, 1991; see discussion above), while *Alocasia macrorrhiza* lost photosynthetic induction much more quickly in darkness than in 10 μmol m<sup>-2</sup> s<sup>-1</sup> (Kirschbaum & Percy, 1988) and sunflower (*Helianthus annuus* L.) leaves showed faster increases in induction after adaptation to 10 μmol m<sup>-2</sup> s<sup>-1</sup> than to darkness (Kirschbaum *et al.*, 2005). There are three hypotheses that may explain the difference between dark- and shade adapted leaves. Those are a) the necessity for a buildup of RuBP pools, and excess production of reducing and phosphorylating equivalents, b) differences in Rubisco activase activation state and c) differences in diffusional limitation.

Below ~5 μmol m<sup>-2</sup> s<sup>-1</sup> background irradiance, the apparent quantum yield of photosynthesis is reduced (Kirschbaum *et al.*, 2004). Using simultaneous measurements of

O<sub>2</sub> and CO<sub>2</sub> exchange on sunflower leaves in non-photorespiratory conditions, it was found that there was a mismatch between calculated RuBP pools and calculated overall PGA reduction to triose phosphates after an increase in irradiance (Kirschbaum *et al.*, 2005). It was suggested that this difference was due to a slightly higher activation state of enzymes facilitating sucrose synthesis than of those regenerating RuBP (i.e. the Calvin cycle) in very low irradiance, and that this mismatch transiently drained the Calvin cycle of triose phosphates, leading to a slower buildup of RuBP pools (Kirschbaum *et al.*, 2005). The transient decrease of the apparent quantum yield relaxed to steady-state levels within 100 s after an increase in irradiance (Kirschbaum *et al.*, 2005). Here, the difference between  $t_{50}$  of dark-adapted leaves and that of leaves adapted to 50  $\mu\text{mol m}^{-2} \text{s}^{-1}$  was  $\sim 100$  s (Table 4.2), and it could be that the mechanisms described by Kirschbaum *et al.* (2005) were at least partly responsible for that delay.

As stated above, tomato can accumulate high levels of CA1P (Moore *et al.*, 1991). CA1P is not only produced in darkness, but also in irradiance up to 200  $\mu\text{mol m}^{-2} \text{s}^{-1}$  (Seemann *et al.*, 1990). In spinach leaves, Lan *et al.* (1992) found that Rubisco activase was inactive in darkness and fully active in  $\sim 300 \mu\text{mol m}^{-2} \text{s}^{-1}$ , with an approximately linear increase between 0 and 300  $\mu\text{mol m}^{-2} \text{s}^{-1}$ . Furthermore, they observed that after illuminating dark-adapted leaves, Rubisco activase reached full activity after  $\sim 7$  minutes (Lan *et al.*, 1992). From this, it can be hypothesized that unlike leaves in darkness, leaves in shade contained more active (initial) Rubisco and more rapidly activating Rubisco because a) in low irradiance, Rubisco activase was at least partly active, removing inhibitors from Rubisco's catalytic sites and b) after a stepwise increase in irradiance, less residual Rubisco activase required activation, and the totality of Rubisco activase therefore probably took less time to reach a full activation state.

The additional diffusional limitation during photosynthetic induction (depicted as grey area in Fig. 4.3A) was larger in dark-adapted than in shade-adapted leaves, due to lower initial  $g_s$  in darkness than in shade (Fig. S4.5). Unlike initial and final  $g_s$ , the rate of stomatal opening was not affected by [CO<sub>2</sub>] and background irradiances (data not shown). Thus, due to lower initial  $g_s$ , but not due to slower increase in  $g_s$ , there was larger additional diffusional limitation, which may have decreased the rates of photosynthetic induction in dark-adapted leaves.

### *Conclusions*

In conclusion, we show here that elevated CO<sub>2</sub> concentration enhances the rates of dynamic photosynthesis (additional to its positive effects on steady-state photosynthesis rates), regardless of photosynthetic induction state, and that it does so to a considerable

extent. This means that future increases in ambient CO<sub>2</sub> concentration will benefit overall carbon gain in naturally fluctuating irradiance in whole canopies, in which different leaf layers are exposed to very different irradiance regimes.

### **Acknowledgements**

This work was carried out within the research programme of BioSolar Cells, co-financed by the Dutch Ministry of Economic Affairs. Additionally, this work was supported by Essent.

**Supplementary material 4.1**

Table S4.1. To exclude the possibility that saturating flashes affected photosynthetic induction or rates of stomatal opening, parameters from gas exchange responses (after a 0→1000  $\mu\text{mol m}^{-2} \text{s}^{-1}$  step increase) with and without the regular application of saturating flashes were compared. Only two parameters were significantly different between data sets: initial  $g_s$  in darkness in 400 ppm (which was unaffected by saturating flashes, since they were applied after dark adaptation), and final  $g_s$  in light in 200 ppm, where  $g_s$  was 0.1  $\text{mol m}^{-2} \text{s}^{-1}$  lower in the data set where saturating flashes had been applied. All other parameters being the same, this difference seemed small enough to carry on with the analysis of gas exchange data.

Effects of application of saturating flashes on parameters of photosynthetic induction and stomatal conductance, average  $\pm$  SEM ( $n = 5$ ). Parameters were derived from gas exchange measurements on dark-adapted leaves after 0→1000  $\mu\text{mol m}^{-2} \text{s}^{-1}$  step increases. Parameters from induction curves without flashes ("No Flashes") have been derived from an Chapter 3, while parameters derived from induction curves with periodic (every 1-2 minutes during 60 minutes) application of saturating flashes ("Flashes") are derived from the current Chapter. Stars (\* =  $P < 0.05$ ) denote statistically significant difference between Flashes and No Flashes, absence of stars denotes lack of significant difference. Abbreviations:  $IS_{60}$ ; induction state (%) 60 seconds after illumination,  $t_{IS50}$  and  $t_{IS90}$ ; time (minutes) to reach 50 and 90% of full photosynthetic induction, respectively,  $t_{gs50}$  and  $t_{gs90}$ ; time (minutes) to reach 50 and 90% of final stomatal conductance, respectively,  $A_{n(0)}$  and  $A_{n(tf)}$ , steady-state photosynthesis rate ( $\mu\text{mol m}^{-2} \text{s}^{-1}$ ) in darkness and in 1000  $\mu\text{mol m}^{-2} \text{s}^{-1}$ , respectively,  $g_{s(0)}$  and  $g_{s(tf)}$ ; steady-state stomatal conductance in darkness and in 1000  $\mu\text{mol m}^{-2} \text{s}^{-1}$ , respectively,  $\tau_R$ ; apparent time constant of Rubisco activation (minutes)

	CO <sub>2</sub> concentration					
	200 ppm		400 ppm		800 ppm	
	No Flashes	Flashes	No Flashes	Flashes	No Flashes	Flashes
$IS_{60}$	25.7 $\pm$ 1.4	22.6 $\pm$ 1.9	21.6 $\pm$ 1.2	21.2 $\pm$ 1.0	21.9 $\pm$ 1.9	27.5 $\pm$ 2.7
$t_{A50}$	3.2 $\pm$ 0.3	3.4 $\pm$ 0.3	2.6 $\pm$ 0.1	2.6 $\pm$ 0.2	2.2 $\pm$ 0.1	1.8 $\pm$ 0.1
$t_{A90}$	18.5 $\pm$ 1.8	18.7 $\pm$ 1.3	10.8 $\pm$ 0.6	13.7 $\pm$ 1.6	6.2 $\pm$ 0.1	5.9 $\pm$ 0.3
$t_{qs50}$	19.8 $\pm$ 0.5	19.0 $\pm$ 1.3	18.7 $\pm$ 1.4	17.5 $\pm$ 1.0	18.2 $\pm$ 1.0	15.8 $\pm$ 0.5
$t_{qs90}$	46.7 $\pm$ 0.6	45.0 $\pm$ 1.9	38.2 $\pm$ 2.5	36.7 $\pm$ 2.2	39.9 $\pm$ 2.1	34.8 $\pm$ 1.9
$A_{n(0)}$	-1.1 $\pm$ 0.2	-1.6 $\pm$ 0.2	-1.6 $\pm$ 0.1	-1.2 $\pm$ 0.2	-1.3 $\pm$ 0.3	-1.3 $\pm$ 0.2
$A_{n(tf)}$	11.7 $\pm$ 0.6	12.2 $\pm$ 0.4	22.2 $\pm$ 0.6	22.0 $\pm$ 0.4	27.1 $\pm$ 1.0	25.5 $\pm$ 0.9
$g_{s(0)}$	0.2 $\pm$ 0.0	0.2 $\pm$ 0.0	0.3 $\pm$ 0.0	0.2 $\pm$ 0.0	0.2 $\pm$ 0.0	0.2 $\pm$ 0.0
$g_{s(tf)}$	0.7 $\pm$ 0.0	0.6 $\pm$ 0.0 *	0.6 $\pm$ 0.0	0.5 $\pm$ 0.1	0.5 $\pm$ 0.0	0.4 $\pm$ 0.0
$\tau_R$	5.1 $\pm$ 0.7	6.1 $\pm$ 0.6	4.1 $\pm$ 0.2	3.8 $\pm$ 0.3	2.7 $\pm$ 0.1	2.2 $\pm$ 0.2

Table S4.2. Goodness of fit of sigmoidal function, as illustrated by the root mean squared error (RMSE, Eqn. 4.3). The sigmoidal function was fitted to the index RI (relative increase in net photosynthesis rate) during a period of 60 minutes after a stepwise increase in irradiance, and to the index RI<sub>60</sub> (relative increase in net photosynthesis rate 60 seconds after re-illumination) as a function of time since the stepwise decrease in irradiance. Displayed are the averages, plus the 1<sup>st</sup> and 3<sup>rd</sup> percentile of single-replicate values, across [CO<sub>2</sub>] and background irradiance treatments (n = 38-42)

Irradiance change	Index	Root mean squared error (%)		
		Average	1 <sup>st</sup> percentile	3 <sup>rd</sup> percentile
Step increase	Relative increase in net photosynthesis rate (%)	1.9	1.3	2.4
Step decrease	Relative increase in net photosynthesis rate 60 s after re-illumination (%)	3.6	2.4	4.2

Table S4.3. Parameters describing the correlations between  $\ln(A_{n(t_f)} - A_{n(t)_{Ci}})$  and time after a step increase in irradiance to determine the apparent time constant of Rubisco activation ( $\tau_R$ ). Average  $\pm$  SEM (n = 3-5). Start and end (and therefore duration) of correlations was varied with time (see Fig. S4.3), in order to obtain highly linear correlations (signified by R<sup>2</sup>)

Background irradiance ( $\mu\text{mol m}^{-2} \text{s}^{-1}$ )	CO <sub>2</sub> concentration (ppm)	Start (min.)		End (min.)		Duration (min.)		R <sup>2</sup>	
			$\pm$		$\pm$		$\pm$		$\pm$
0	200	1.13	$\pm$ 0.05	3.87	$\pm$ 0.38	2.74	$\pm$ 0.34	0.98	$\pm$ 0.01
0	400	1.19	$\pm$ 0.04	4.57	$\pm$ 0.12	3.38	$\pm$ 0.08	0.98	$\pm$ 0.00
0	800	1.15	$\pm$ 0.00	4.45	$\pm$ 0.00	3.30	$\pm$ 0.00	0.99	$\pm$ 0.00
50	200	0.50	$\pm$ 0.00	4.45	$\pm$ 0.00	3.95	$\pm$ 0.00	0.97	$\pm$ 0.01
50	400	0.50	$\pm$ 0.00	4.45	$\pm$ 0.00	3.95	$\pm$ 0.00	0.98	$\pm$ 0.00
50	800	0.12	$\pm$ 0.07	1.23	$\pm$ 0.07	1.12	$\pm$ 0.09	0.98	$\pm$ 0.01
100	200	0.78	$\pm$ 0.17	4.95	$\pm$ 0.00	4.17	$\pm$ 0.17	0.95	$\pm$ 0.01
100	400	0.10	$\pm$ 0.00	1.72	$\pm$ 0.12	1.62	$\pm$ 0.12	0.99	$\pm$ 0.00
100	800	0.22	$\pm$ 0.06	0.97	$\pm$ 0.02	0.75	$\pm$ 0.06	0.97	$\pm$ 0.01
200	200	0.20	$\pm$ 0.06	2.45	$\pm$ 1.01	2.25	$\pm$ 1.04	0.91	$\pm$ 0.01
200	400	0.03	$\pm$ 0.02	1.55	$\pm$ 0.34	1.52	$\pm$ 0.34	0.98	$\pm$ 0.00
200	800	0.00	$\pm$ 0.00	0.83	$\pm$ 0.17	0.83	$\pm$ 0.17	0.97	$\pm$ 0.01

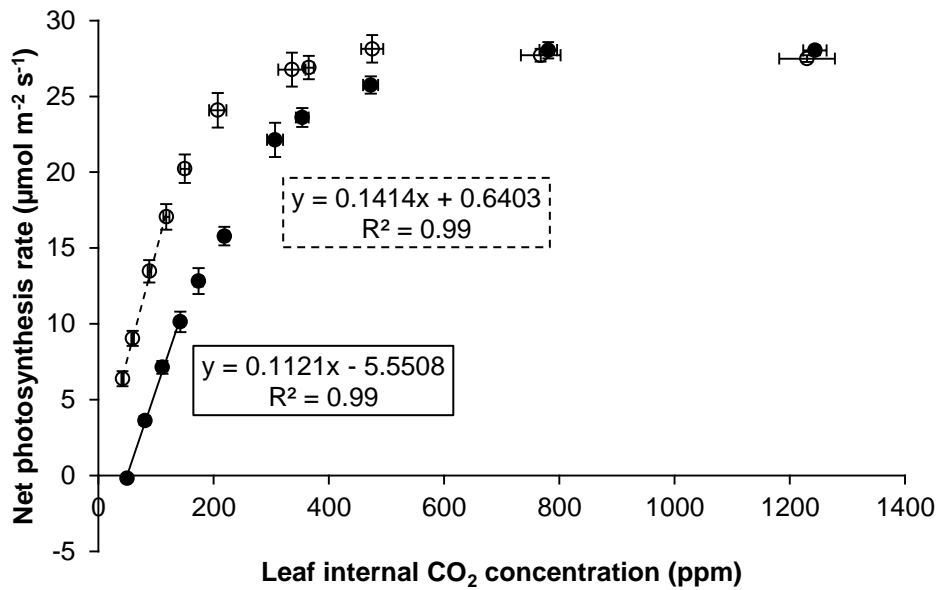


Fig. S4.1. Data used for determination of the parameters  $V_{C_{max}}$ ,  $J_{max}$ , TPU and  $\Gamma^*$ .  $A_n/C_i$  relationships in 21% (closed circles) and 2% oxygen (open circles). Leaves were exposed to 11 different [CO<sub>2</sub>] values between 50 and 1500 ppm. Data were logged every 5 seconds, and averages of 10 values at each [CO<sub>2</sub>] step, after steady-state photosynthesis had visibly been reached, were used. Other cuvette conditions were: 1000  $\mu\text{mol m}^{-2} \text{s}^{-1}$  PAR, 0.8 kPa  $\text{VPD}_{\text{leaf-air}}$  and 23 °C  $T_{\text{leaf}}$ . Parameters  $V_{C_{max}}$ ,  $J_{max}$  and TPU were estimated using the curve-fitting procedure by Sharkey *et al.* (2007). The chloroplast CO<sub>2</sub> compensation point in the absence of day respiration,  $\Gamma^*$ , was calculated using the slopes of the regression lines depicted in the figure, after Yin *et al.* (2009). Average  $\pm$  SEM ( $n = 3-5$ )

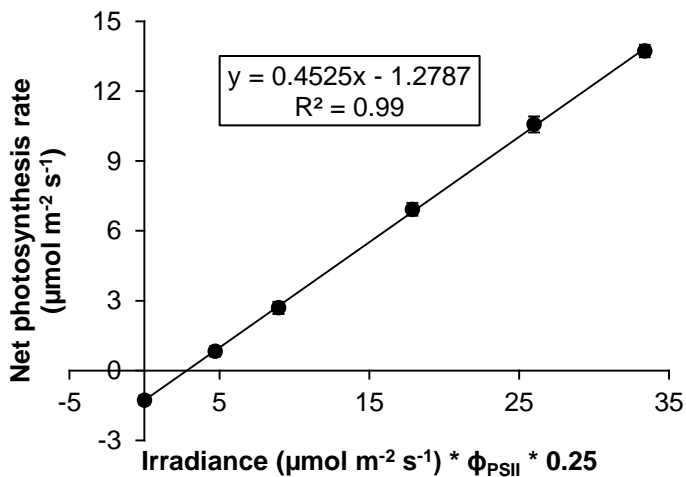


Fig. S4.2. Data used for the determination of the rate of day respiration ( $R_d$ ). Relationship between net photosynthesis rates and irradiance \*  $\phi_{\text{PSII}}$  \* 0.25, as in Yin *et al.* (2009), measured in 2% O<sub>2</sub>. Leaves were adapted to 200  $\mu\text{mol m}^{-2} \text{s}^{-1}$ , until  $A_n$  and  $g_s$  were stable. Then, leaves were exposed to a range of PAR values between 0 and 200  $\mu\text{mol m}^{-2} \text{s}^{-1}$ . Data were logged every 5 seconds, and averages of 10 values at each irradiance step, after steady-state photosynthesis had visibly been reached, were used. Other cuvette conditions were: 400 ppm [CO<sub>2</sub>], 0.8 kPa  $\text{VPD}_{\text{leaf-air}}$  and 22 °C  $T_{\text{leaf}}$ . The intercept of the resulting relationship was assumed to equal  $R_d$  (Yin *et al.*, 2009). Average  $\pm$  SEM ( $n = 4$ )



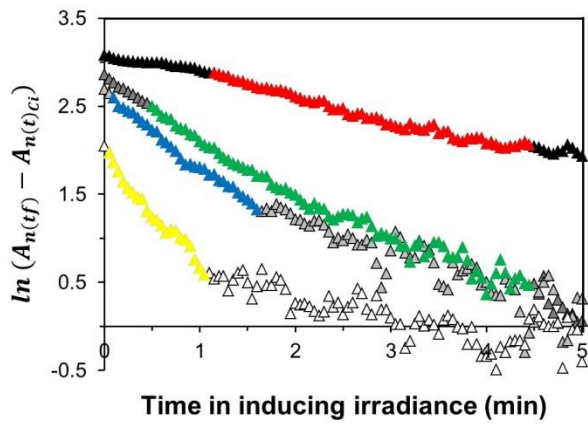


Fig. S4.3. Examples of determination of the apparent time constant of Rubisco activation ( $\tau_R$ ), in four induction curves (at 400 ppm  $\text{CO}_2$ ), as affected by background irradiance. Data were calculated as the natural logarithm ( $\ln$ ) of the difference of steady-state net photosynthesis rate in inducing irradiance ( $A_{n(t_f)}$ ) and transient net photosynthesis rate after a step increase in irradiance, corrected for changes in leaf internal  $\text{CO}_2$  concentration ( $A_{n(t_{ci})}$ ). Black-and-white symbols show the complete range of data in the first 5 minutes after a step increase in irradiance, color symbols show the range chosen for a linear correlation between  $\ln(A_{n(t_f)} - A_{n(t_{ci})})$  and time. Black and red symbols:  $0 \rightarrow 1000 \mu\text{mol m}^{-2} \text{s}^{-1}$ , dark grey and green symbols:  $50 \rightarrow 1000 \mu\text{mol m}^{-2} \text{s}^{-1}$ , light grey and blue symbols:  $100 \rightarrow 1000 \mu\text{mol m}^{-2} \text{s}^{-1}$ , white and yellow symbols:  $200 \rightarrow 1000 \mu\text{mol m}^{-2} \text{s}^{-1}$

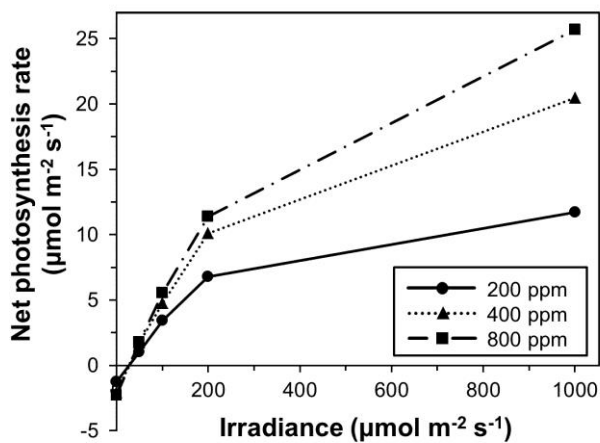


Fig. S4.4. Effect of  $\text{CO}_2$  concentration on the steady-state response of net photosynthesis rate to irradiance. Symbols denote average  $\pm$  SEM,  $n = 27-126$

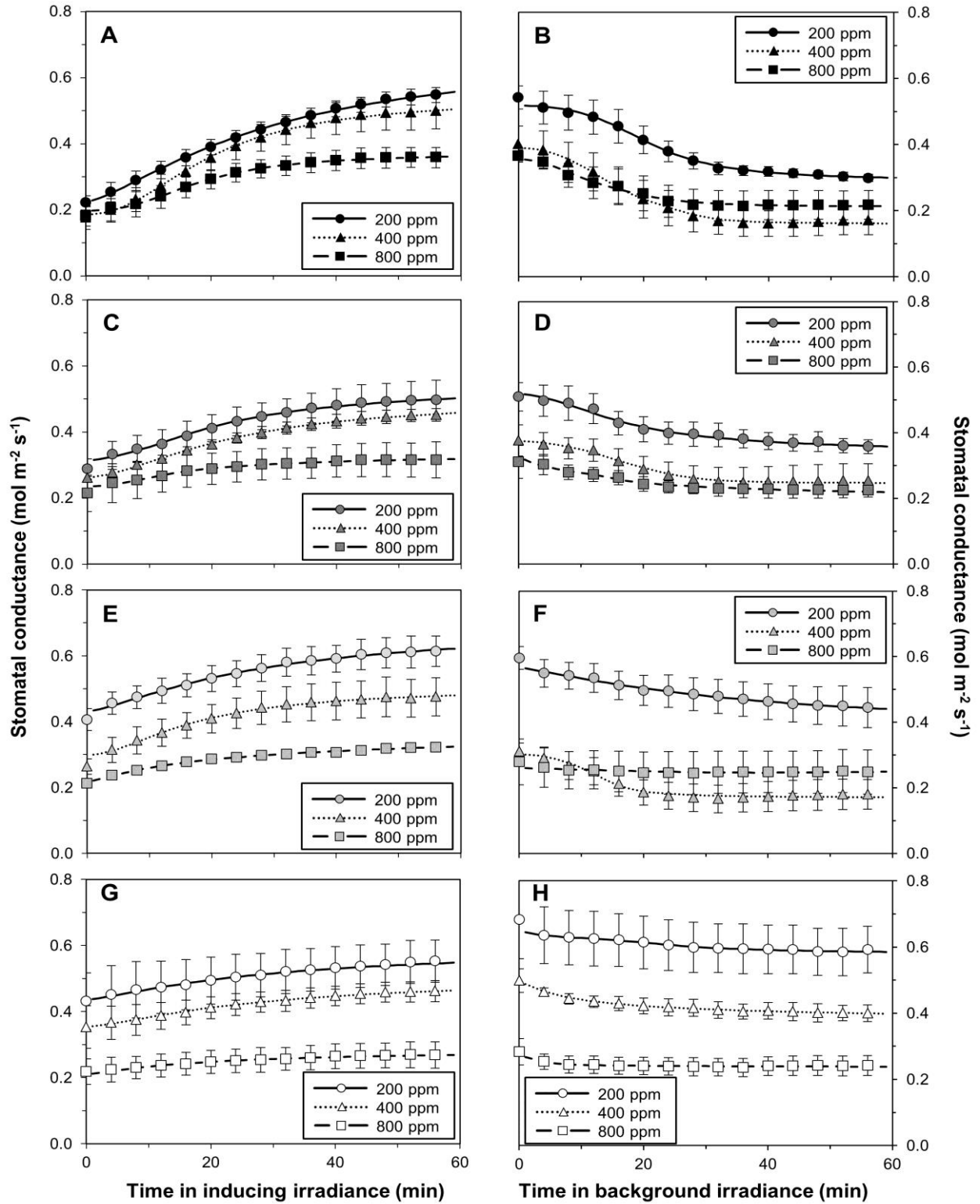


Fig. S4.5. Changes in stomatal conductance (mol m<sup>-2</sup> s<sup>-1</sup>) after step increases (A, C, E, G) and decreases (B, D, F, H) in irradiance, and as affected by 0 (A, B), 50 (C, D), 100 (E, F) or 200 μmol m<sup>-2</sup> s<sup>-1</sup> (G, H) background irradiance and [CO<sub>2</sub>]. Lines denote sigmoidal fits (Eqn. 2), symbols denote data (average ± SEM, n = 3-5)

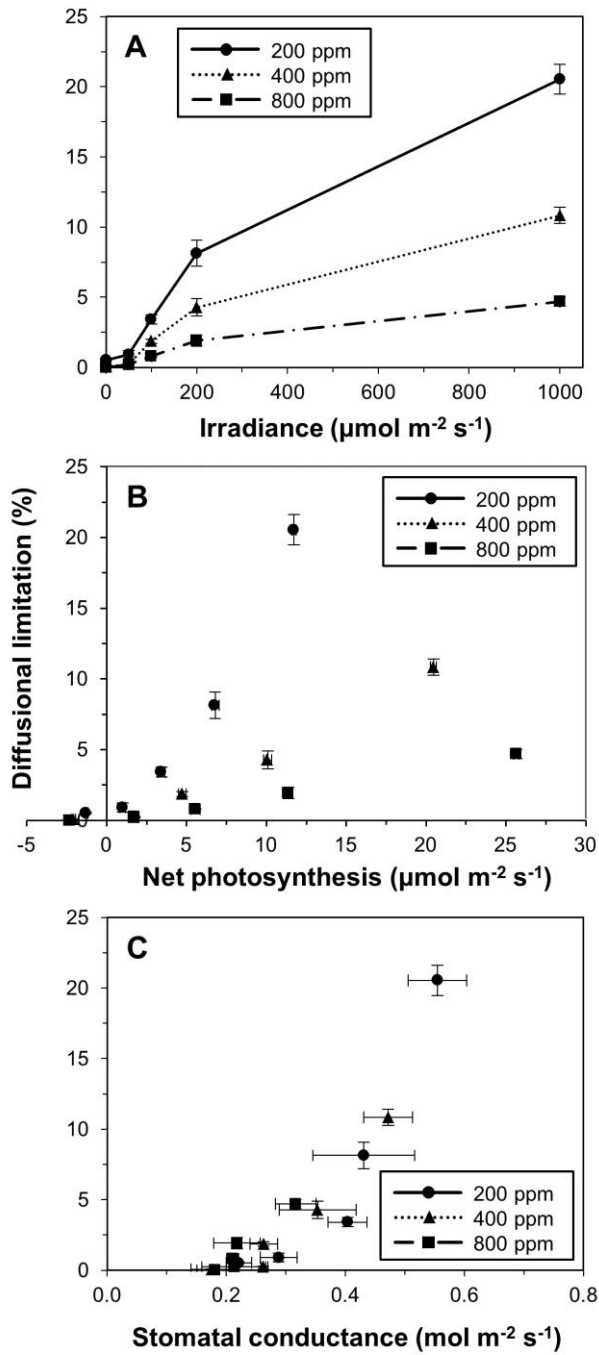


Fig. S4.6. Relationships between steady-state diffusional limitation, irradiance (A), steady-state net photosynthesis rates (B) and steady-state stomatal conductance (C). Symbols depict average  $\pm$  SEM,  $n = 3-14$

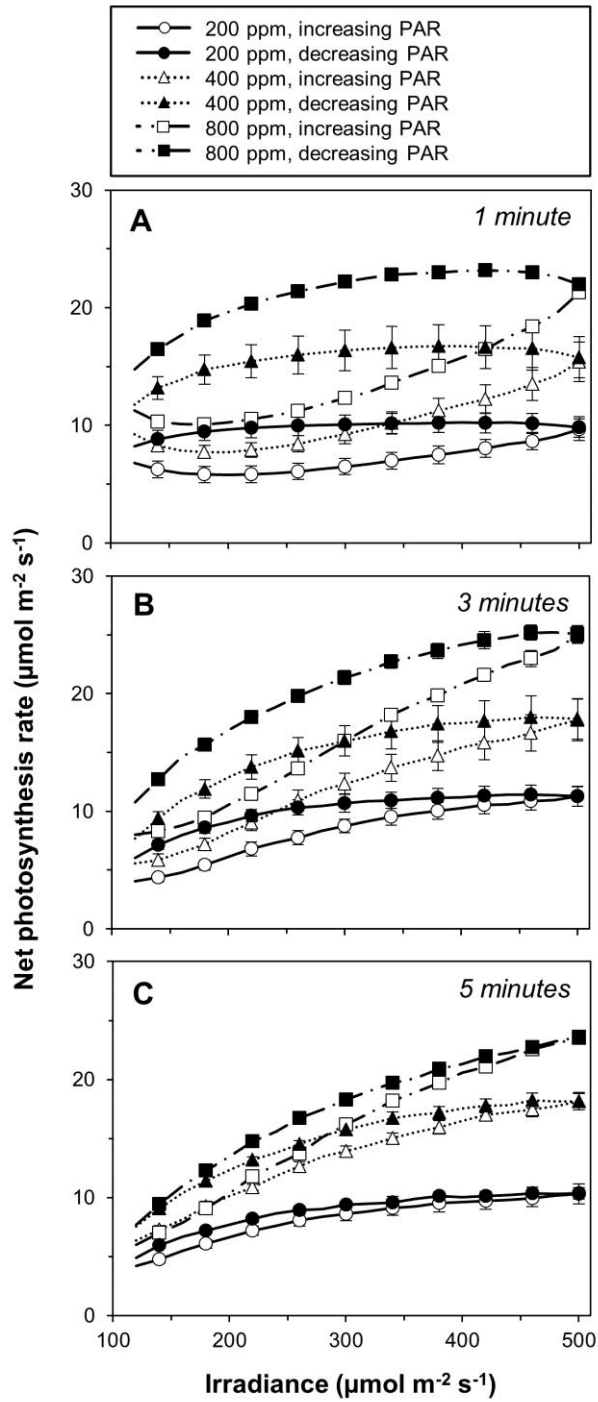


Fig. S4.7. Dynamic irradiance response of photosynthesis rate to sinusoidal changes in irradiance, as affected by periods of irradiance changes, direction of irradiance changes (increasing or decreasing) and CO<sub>2</sub> concentrations. Symbols denote average  $\pm$  SEM, n = 3

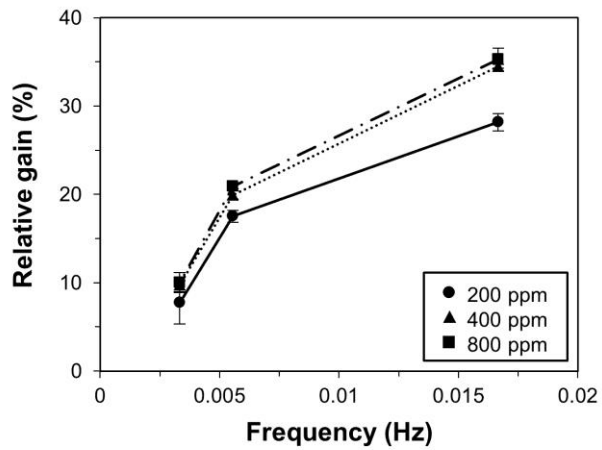


Fig. S4.8. Relative gain of net photosynthesis rate during sinusoidal changes in irradiance (integrated over time), as affected by sine wave frequency (inverse of sine wave period) and CO<sub>2</sub> concentration. Calculated as  $\text{Relative gain} = (A_{n\_decr}/A_{n\_incr}) * 100$ , where  $A_{n\_decr}$  is integrated net photosynthesis rate during half-cycles of decreasing irradiance, and  $A_{n\_incr}$  is average net photosynthesis rate during half-cycles of increasing irradiance. Symbols denote average  $\pm$  SEM,  $n = 3$



## **CHAPTER 5**

Strongly increased stomatal conductance in tomato does not speed up photosynthetic induction in ambient CO<sub>2</sub> concentration

**Authors:**

Elias Kaiser

Jeremy Harbinson

Ep Heuvelink

Leo F.M. Marcelis

To be submitted

**Abstract**

Irradiance-dependent opening and closure of stomata is usually slow. Therefore, stomatal conductance ( $g_s$ ) is typically assumed to limit photosynthesis in fluctuating irradiance, particularly when leaves adapted to low irradiance or darkness are exposed to large increases in irradiance. This transient limitation may reduce crop productivity in natural environments, where irradiance incident on a leaf can fluctuate rapidly. To test this assumption, photosynthetic gas exchange in *flacca*, a mutant with very high  $g_s$ , was compared with its wildtype, cv. Rheinlands Ruhm. Steady-state photosynthesis responses to leaf internal  $\text{CO}_2$  concentrations were similar, indicating similar photosynthetic capacity between genotypes. Surprisingly, when exposing dark-adapted leaves at ambient  $\text{CO}_2$  concentration (400 ppm) to a stepwise increase in irradiance, photosynthetic induction was not faster in *flacca* than in the wildtype, despite *flacca* having 3.5 times higher  $g_s$  in darkness. The same was true for leaves at 800 ppm. At 200 ppm, photosynthetic induction was significantly faster in *flacca*. These findings are discussed with respect to the general assumption that  $g_s$  limits photosynthesis in fluctuating irradiance. Additionally, several indices of transient stomatal limitation are compared and diffusional limitation, a new index, is proposed to be most useful.



## Introduction

In the leaves of higher plants, stomata are the gateways that balance carbon uptake against water loss. They achieve this balance by dynamically regulating their aperture in response to intrinsic and extrinsic factors. Typically, stomatal guard cells reduce their aperture (and therefore conductance) in low irradiance or darkness, and increase it in high irradiance. Stomatal opening after sudden increases in irradiance is comparatively slow, with time constants in the range of 4-29 minutes (Vico *et al.*, 2011). Stomatal conductance ( $g_s$ ) is often assumed to be one of the three main limitations of photosynthesis in fluctuating irradiance, because of its initially low value and because of slow stomatal opening. The other two main limitations are the activation of RuBP regeneration and Rubisco activation (reviewed in Pearcy *et al.*, 1996; Way & Pearcy, 2012).

Several studies indicate that stomata do not always limit the induction of photosynthesis after stepwise increases in irradiance (Valladares *et al.*, 1997; Ögren & Sundin, 1996; Tausz *et al.*, 2005). In fact, for most studies conducted on photosynthetic induction so far it is unclear whether, and to what extent, stomata limit the transient increase in photosynthesis, because the data are often not analysed to that end (Kaiser *et al.*, 2015). Several indices for assessing the limitations imposed by stomata in fluctuating irradiance have been described. These are a) transient  $A_n/C_i$  curves (Küppers & Schneider, 1993; Ögren & Sundin, 1996; Valladares *et al.*, 1997; Urban *et al.*, 2008), b) stomatal limitation (Tinoco-Ojanguren & Pearcy, 1993b; Allen & Pearcy, 2000b; Urban *et al.*, 2007; 2008) and c) the relationship between initial  $g_s$  and the time required to reach 90% of full induction (Valladares *et al.*, 1997; Allen & Pearcy, 2000a; Naumburg & Ellsworth, 2000). Previously published data could be re-analysed to evaluate stomatal limitation dependent on e.g. species, growth conditions, or geographic origin. However, what is lacking so far is a proper evaluation and comparison of these indices.

One way to test whether stomata limit photosynthetic induction is to use genotypes that strongly differ in  $g_s$  (but not in other photosynthesis-related traits), and to test whether their responses to an increase in irradiance differ (Tomimatsu & Tang, 2012). The tomato (*Solanum lycopersicum* L.) cv. Rheinlands Ruhm *flacca* mutant has a 80-90% lower abscisic acid (ABA) content than its wildtype (Tal & Nevo, 1973). *Flacca* leaves therefore exhibit very high  $g_s$  (almost) independent of irradiance, without affecting the response of photosynthesis to leaf internal  $CO_2$  concentration ( $C_i$ ; Bradford *et al.*, 1983). This suggests that the photosynthetic capacity of *flacca* leaves is unaffected by changes in hormonal balance (Bradford *et al.*, 1983), making these plants an ideal model for studying the effects of stomatal limitations in leaves with moderately high rates of photosynthesis.

We used the *flacca* mutant and its wildtype to test to what extent stomata limit the transient increase in photosynthesis after a stepwise increase in irradiance. We hypothesized that in ambient (400 ppm) and reduced [CO<sub>2</sub>] (200 ppm), wildtype leaves would exhibit slower rates of photosynthetic induction than *flacca* leaves, and that this relative reduction would be due to comparably low  $g_s$  in wildtype leaves. Furthermore, we hypothesized that in elevated [CO<sub>2</sub>] (800 ppm), rates of induction would be similar between genotypes, because of a larger gradient for CO<sub>2</sub> diffusion into the leaf. Data were also used to evaluate and compare several indices of assessing stomatal limitation during photosynthetic induction.

## Materials and Methods

### *Plant material*

Seeds of tomato cv. Rheinlands Ruhm wildtype (LA0535) and *flacca* (LA0673) were obtained from the Tomato Genetics Resource Center (University of California, Davis, USA). Seeds were germinated in Rockwool plugs (Grodan, Roermond, NL). A week after sowing, they were transferred to Rockwool cubes (10 cm \* 10 cm \* 7 cm; Grodan). Plants were grown in a climate chamber in 16/8 h photoperiod, 22/20 °C (day/night) temperature, 70% relative air humidity and 320  $\mu\text{mol m}^{-2} \text{s}^{-1}$  photosynthetically active radiation (PAR; irradiance at table height). Irradiance was provided by white, red and far-red LEDs with emission peaks at 440, 550, 660 and 735 nm. Rockwool cubes were standing in a layer (height: 1-2 cm) of nutrient solution (Yara Benelux B.V., Vlaardingen, the Netherlands), which was replenished every 1-2 days and contained 12.4 mM  $\text{NO}_3^-$ , 7.2 mM  $\text{K}^+$ , 4.1 mM  $\text{Ca}^{2+}$ , 3.3 mM  $\text{SO}_4^{2-}$ , 1.8 mM  $\text{Mg}^{2+}$ , 1.2 mM  $\text{NH}_4^+$ , 1.1 mM  $\text{P}^{3-}$ , 30  $\mu\text{M}$   $\text{B}^{3+}$ , 25  $\mu\text{M}$   $\text{Fe}^{3+}$ , 10  $\mu\text{M}$   $\text{Mn}^{2+}$ , 5  $\mu\text{M}$   $\text{Zn}^{2+}$ , 0.75  $\mu\text{M}$   $\text{Cu}^+$  and 0.5  $\mu\text{M}$   $\text{Mo}^{2+}$  (EC 2.1 dS  $\text{m}^{-1}$ , pH 5.5). Between one and three weeks after sowing, *flacca* plants were sprayed daily with a solution containing 10  $\mu\text{M}$  ABA, 0.01% (w/v) Triton-X and 0.1% (v/v) ethanol (Bradford *et al.*, 1983). Wildtype plants were sprayed with a mock solution containing 0.01% Triton-X and 0.1% ethanol. All chemicals were purchased from Sigma (St. Louis, USA). Plants were sprayed until drop-off and using commercially available gardening spray bottles. When plants were between five and six weeks old, leaves 4 and 5, counting from the bottom, were used for experiments.

### *Measurements*

Measurements were performed in a lab, using the LI-6400 photosynthesis system (Li-Cor Biosciences, Lincoln, Nebraska, USA) equipped with the fluorescence chamber (Li-Cor Part No. 6400-40, area: 2  $\text{cm}^2$ ). Conditions in the measuring cuvette were:  $22 \pm 0.2$  °C cuvette temperature,  $70 \pm 3$  % relative humidity and flow rate of 500  $\mu\text{mol s}^{-1}$ . Irradiance was provided by LEDs as 90 / 10% red / blue light mixture, with peak intensities at wavelengths of 635 and 465 nm. In all measurements, 3 biological replicates were used.

### *Photosynthetic induction*

To assess the response of gas exchange to a step increase in irradiance, leaves were first dark-adapted until  $g_s$  was constant (60-120 minutes). Then, irradiance was increased to 1000  $\mu\text{mol m}^{-2} \text{s}^{-1}$  in a step change and gas exchange values were logged every second for 60 minutes.  $\text{CO}_2$  concentration was used as a treatment factor and was applied in three levels: 200, 400 and 800 ppm. Treatments were applied in a completely randomized fashion.

### *CO<sub>2</sub> response curves*

To assess steady-state responses of gas exchange to various leaf internal CO<sub>2</sub> concentrations (C<sub>i</sub>), leaves were adapted for ~30 min to 1000 μmol m<sup>-2</sup> s<sup>-1</sup> PAR and 400 ppm external CO<sub>2</sub> concentration. External CO<sub>2</sub> concentration was then decreased stepwise until 50 ppm, each step taking 2-3 minutes. Thereafter, the external CO<sub>2</sub> concentration was raised to 400 ppm, and after waiting for ~15 minutes, leaves were exposed to stepwise increases in CO<sub>2</sub> until 1500 ppm, each step taking ~4 minutes. Values were logged every 5 s and the last 60 s of every CO<sub>2</sub> step were used to calculate average values of C<sub>i</sub> and net photosynthesis rates (A<sub>n</sub>, μmol m<sup>-2</sup> s<sup>-1</sup>).

### *Calculations*

The photosynthetic induction state (IS, %) was calculated as the transient rate of photosynthesis (A<sub>n(t)</sub>, μmol m<sup>-2</sup> s<sup>-1</sup>) as a percentage of the steady-state rate in 1000 μmol m<sup>-2</sup> s<sup>-1</sup> PAR (A<sub>n(tf)</sub>), corrected for leaf CO<sub>2</sub> exchange in darkness (A<sub>n(t0)</sub>):

$$IS = \frac{A_{n(t)} - A_{n(t0)}}{A_{n(tf)} - A_{n(t0)}} * 100 \quad (5.1)$$

Then, IS reached 60 s after the stepwise increase in irradiance (IS<sub>60</sub>, %) and the time (minutes) to reach 50 and 90% of full induction state (t<sub>50</sub> and t<sub>90</sub>, respectively) were calculated.

In order to calculate stomatal limitation, transient A<sub>n</sub> was first corrected for changes in transient C<sub>i</sub> (C<sub>i(t)</sub>) during induction (A<sub>n(t)C<sub>i</sub></sub>; Urban *et al.*, 2007) using steady-state C<sub>i</sub> in high irradiance (C<sub>i(tf)</sub>). However, instead of using a linear A<sub>n</sub>/C<sub>i</sub> relationship (as in Urban *et al.*, 2007), a curvilinear relationship, using previously determined A<sub>n</sub>/C<sub>i</sub> parameters, was used:

$$A_{n(t)C_i} = A_{n(t)} * \frac{\min\{A_{n(c)}(C_{i(tf)}), A_{n(j)}(C_{i(tf)}), A_{n(TPU)}(C_{i(tf)})\}}{\min\{A_{n(c)}(C_{i(t)}), A_{n(j)}(C_{i(t)}), A_{n(TPU)}(C_{i(t)})\}} \quad (5.2)$$

Rubisco activity-limited A<sub>n</sub> (A<sub>n(c)</sub>), electron transport-limited A<sub>n</sub> (A<sub>n(j)</sub>) and triose phosphate utilization-limited A<sub>n</sub> (A<sub>n(TPU)</sub>) were determined according to Sharkey *et al.* (2007):

$$A_{n(c)} = V_{Cmax} \left( \frac{C_i - \Gamma^*}{C_i + K_c * \left(1 + \frac{\Gamma^*}{K_o}\right)} \right) - R_d \quad (5.3)$$

$$A_{n(j)} = J_{max} \left( \frac{C_i - \Gamma^*}{4 * C_i + 8 * \Gamma^*} \right) - R_d \quad (5.4)$$

$$A_{n(TPU)} = 3 * TPU - R_d \quad (5.5)$$

Where  $V_{C_{max}}$  ( $91 \mu\text{mol m}^{-2} \text{s}^{-1}$ ) is maximum rate of carboxylation,  $\Gamma^*$  is the chloroplast  $\text{CO}_2$  compensation point (53 ppm) in the absence of day respiration ( $R_d$ ;  $1.4 \mu\text{mol m}^{-2} \text{s}^{-1}$ ),  $O$  (21 kPa) is the chloroplast  $\text{O}_2$  concentration,  $K_c$  (21.4 Pa) and  $K_o$  (15.4 kPa) are the Michaelis-Menten constants of Rubisco for  $\text{CO}_2$  and for  $\text{O}_2$ , respectively,  $J_{max}$  ( $135 \mu\text{mol m}^{-2} \text{s}^{-1}$ ) is the maximum rate of electron transport and TPU ( $8.2 \mu\text{mol m}^{-2} \text{s}^{-1}$ ) is the maximum rate of triose phosphate utilization. Parameters  $V_{C_{max}}$ ,  $J_{max}$  and TPU were estimated after Sharkey et al. (2007) from  $A_n/C_i$  curves of both genotypes (Fig. 5.1). As there were no significant differences between genotypes for these parameters, average values between genotypes were used.  $R_d$  was taken from literature (Bradford *et al.*, 1983) as an average value reported, since in their study (Bradford *et al.*, 1983),  $R_d$  did not differ significantly between genotypes.  $\Gamma^*$  was calculated from data on leaves of cv. Cappricia after Yin et al. (2009). This was assumed to be acceptable, because  $\text{CO}_2$  responses of cv. Rheinlands Ruhm and cv. Cappricia were very similar in the Rubisco activity-limited range (0-300 ppm, Fig. S5.1). Parameters  $K_c$  and  $K_o$  were taken from Sharkey et al. (2007). Stomatal limitation (%) was determined as

$$\text{Stomatal limitation} = \frac{A_{n(t)C_i} - A_{n(t)}}{A_{n(tf)} - A_{n(t0)}} * 100 \quad (5.6)$$

Diffusional limitation (%) was calculated similarly to stomatal limitation (Eqns. 5.2-5.6), but instead of using  $C_{i(tf)}$  in the numerator of Eqn. 2, the leaf external  $\text{CO}_2$  concentration ( $[\text{CO}_2]$ ) was used. The apparent time constant of Rubisco activation ( $\tau_R$ ), denoting the time required to reach 63% of full activation, was calculated after Woodrow and Mott (1989), by using net photosynthesis corrected for changes in  $C_i$  ( $A_{n(t)C_i}$ ):

$$\tau_R = \frac{\Delta t}{\Delta \ln(A_{n(tf)} - A_{n(t)C_i})} \quad (5.7)$$

where  $\Delta t$  is the duration used for determination of  $\tau_R$ . Data in the range of 1-5 minutes after the stepwise irradiance increase were used to calculate  $\tau_R$ .

*Statistical analysis*

Steady-state  $A_n$  and  $g_s$  in dark- and high-irradiance adapted leaves, indices of induction rates ( $IS_{60}$ ,  $t_{50}$ ,  $t_{90}$ ) and  $\tau_R$  were compared for the various  $CO_2$  concentrations between genotypes using a 2-sided Student's  $t$ -test, assuming equal variances (Microsoft Excel). Furthermore, using one-sided  $t$ -tests, it was analysed whether single transient values of diffusional and stomatal limitation during photosynthetic induction were significantly larger than the value at the end of induction (at steady state, 60 minutes after irradiance increase).

## Results

### *Steady-state responses of photosynthesis and stomatal conductance to CO<sub>2</sub> concentration and irradiance*

Photosynthesis in wildtype and *flacca* leaves showed similar relationships with leaf internal CO<sub>2</sub> concentrations ( $C_i$ ; Fig. 5.1). In darkness, *flacca* leaves showed consistently higher respiration rates than wildtype leaves, irrespective of [CO<sub>2</sub>] (Table 5.1). Steady-state photosynthesis rates at 1000  $\mu\text{mol m}^{-2} \text{s}^{-1}$  were similar between genotypes in reduced (200 ppm) and elevated [CO<sub>2</sub>] (800 ppm), but were significantly higher in *flacca* in ambient [CO<sub>2</sub>] (400 ppm). Stomatal conductance ( $g_s$ ) was consistently higher in *flacca* compared to wildtype leaves, by factors of 3.5-4.6 in dark-adapted leaves (initial  $g_s$ ), and 2.1-2.6 in leaves adapted to 1000  $\mu\text{mol m}^{-2} \text{s}^{-1}$  (Table 5.1, Fig. S5.3).

### *Photosynthetic induction at ambient, reduced and elevated CO<sub>2</sub> concentrations*

Rates of photosynthetic induction in ambient and elevated [CO<sub>2</sub>] were not faster in *flacca* than in wildtype leaves (Fig. 5.2B, C; Table 5.2), despite much higher initial  $g_s$  in *flacca* (Table 5.1). In reduced [CO<sub>2</sub>], *flacca* showed higher rates of photosynthetic induction than

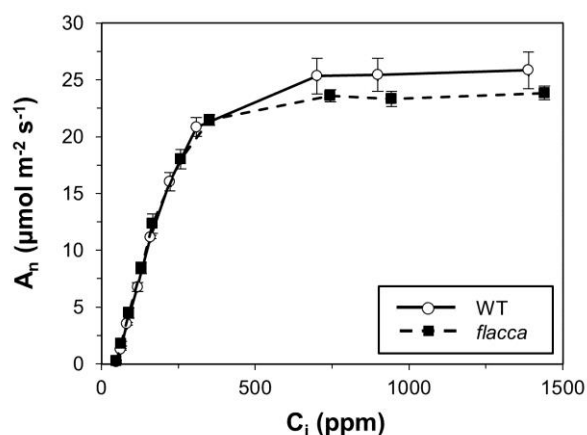


Fig. 5.1. Steady-state relationship between net photosynthesis rate ( $A_n$ ) and leaf internal CO<sub>2</sub> concentration ( $C_i$ ) in wildtype (WT) and *flacca* leaves of tomato. Irradiance was 1000  $\mu\text{mol m}^{-2} \text{s}^{-1}$ . Symbols denote average, error bars denote  $\pm$  SEM,  $n = 3$

Table 5.1. Steady-state values of net photosynthesis rate ( $A_n$ ) and stomatal conductance ( $g_s$ ) in wildtype (WT) and *flacca* leaves of tomato, as affected by irradiance and CO<sub>2</sub> concentration. Averages  $\pm$  standard error of the mean (SEM),  $n = 3$ . Stars within rows denote a significant difference between genotypes: \*\*\* =  $P < 0.001$ , \*\* =  $P < 0.01$ , \* =  $P < 0.05$ , n.s. = not significant

Irradiance ( $\mu\text{mol m}^{-2} \text{s}^{-1}$ )	CO <sub>2</sub> concentration (ppm)	$A_n$ ( $\mu\text{mol m}^{-2} \text{s}^{-1}$ )		$g_s$ ( $\text{mol m}^{-2} \text{s}^{-1}$ )	
		WT	<i>flacca</i>	WT	<i>flacca</i>
0	200	-1.5 $\pm$ 0.1	-2.5 $\pm$ 0.2 *	0.25 $\pm$ 0.03	0.96 $\pm$ 0.02 ***
	400	-1.7 $\pm$ 0.4	-3.9 $\pm$ 0.3 *	0.26 $\pm$ 0.03	0.90 $\pm$ 0.01 ***
	800	-0.9 $\pm$ 0.4	-2.7 $\pm$ 0.1 *	0.20 $\pm$ 0.04	0.93 $\pm$ 0.04 ***
1000	200	11.1 $\pm$ 0.1	13.5 $\pm$ 0.9 n.s.	0.56 $\pm$ 0.02	1.21 $\pm$ 0.04 ***
	400	20.7 $\pm$ 0.4	23.5 $\pm$ 0.4 **	0.51 $\pm$ 0.05	1.18 $\pm$ 0.07 **
	800	24.0 $\pm$ 1.4	27.5 $\pm$ 1.3 n.s.	0.40 $\pm$ 0.02	1.06 $\pm$ 0.04 ***

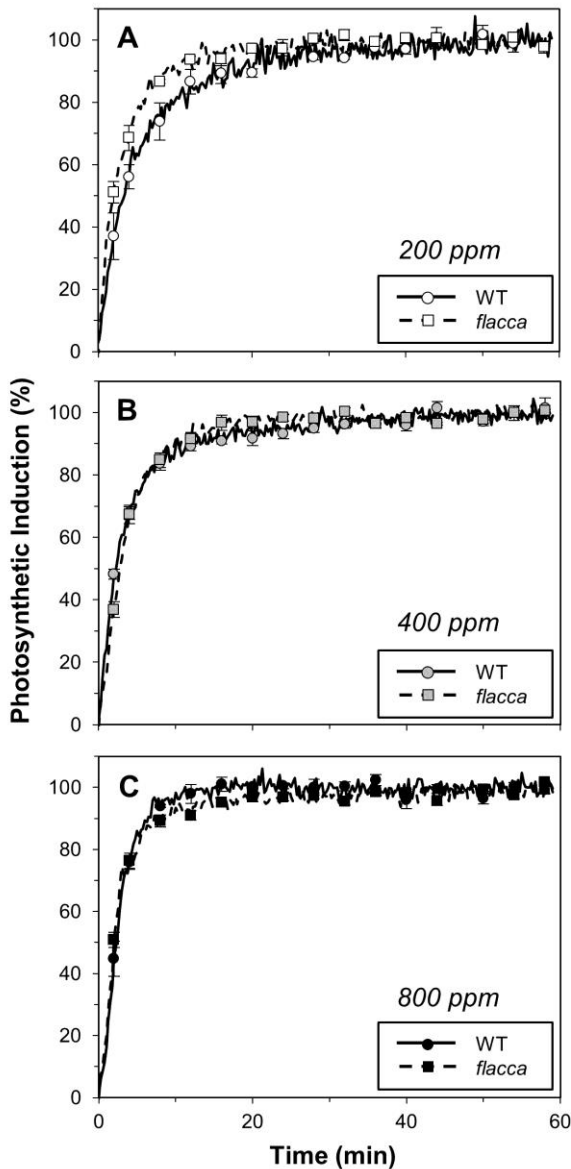


Fig. 5.2. Photosynthetic induction after a single-step increase in irradiance ( $0 \rightarrow 1000 \mu\text{mol m}^{-2} \text{s}^{-1}$ ) in wildtype (WT) and *flacca* leaves of tomato, as affected by  $\text{CO}_2$  concentration: 200 (A), 400 (B) and 800 ppm (C). Lines and symbols denote average, error bars denote  $\pm$  SEM,  $n = 3$

WT within the first  $\sim 15$  min. (Fig. 5.2A). As a reflection of this,  $\text{IS}_{60}$  in *flacca* almost doubled compared to wildtype leaves, while  $t_{90}$  halved (Table 5.2). Furthermore, the apparent time constant of Rubisco activation was significantly larger in reduced  $[\text{CO}_2]$  in wildtype leaves compared to *flacca* (Fig. 5.3), reflecting slower activation of the enzyme in reduced  $[\text{CO}_2]$ .

#### *Comparison of indices of transient stomatal limitation*

Three indices were used to evaluate the limitation of rates of photosynthetic induction by stomata: a) diffusional limitation, b) stomatal limitation and c) dynamic  $A_n/C_i$  curves.

Diffusional limitation, reflecting the total limitation to net photosynthesis rates by stomatal



Table 5.2. Indices describing photosynthetic induction rate after a stepwise increase in irradiance ( $0 \rightarrow 1000 \mu\text{mol m}^{-2} \text{s}^{-1}$ ) in wildtype (WT) and *flacca* leaves of tomato, as affected by  $\text{CO}_2$  concentration.  $\text{IS}_{60}$ , induction state 60 seconds after irradiance increase;  $t_{50}$  and  $t_{90}$ , time to reach 50 and 90% of full photosynthetic induction, respectively. Averages  $\pm$  SEM,  $n = 3$ . Stars within rows denote a significant difference between genotypes: \*\*\* =  $P < 0.001$ , \*\* =  $P < 0.01$ , \* =  $P < 0.05$ , n.s. = not significant

$\text{CO}_2$ concentration (ppm)	Index	WT		<i>flacca</i>		
200	$\text{IS}_{60}$ (%)	19.11	$\pm 4.80$	35.21	$\pm 2.39$	*
	$t_{50}$ (min)	3.14	$\pm 0.50$	1.78	$\pm 0.22$	n.s.
	$t_{90}$ (min)	19.42	$\pm 3.70$	8.49	$\pm 0.66$	*
400	$\text{IS}_{60}$ (%)	24.40	$\pm 3.26$	16.21	$\pm 1.73$	n.s.
	$t_{50}$ (min)	2.18	$\pm 0.10$	2.69	$\pm 0.17$	n.s.
	$t_{90}$ (min)	14.01	$\pm 1.34$	10.17	$\pm 1.38$	n.s.
800	$\text{IS}_{60}$ (%)	16.47	$\pm 4.28$	20.11	$\pm 1.06$	n.s.
	$t_{50}$ (min)	2.17	$\pm 0.21$	1.99	$\pm 0.00$	n.s.
	$t_{90}$ (min)	5.56	$\pm 0.60$	8.04	$\pm 0.98$	n.s.

and mesophyll resistance, was lower in *flacca* than in wildtype leaves, and lower in ambient than in reduced  $[\text{CO}_2]$  (Fig. 5.4). Furthermore, in wildtype leaves in reduced  $[\text{CO}_2]$ , several time points showed a significantly larger diffusional limitation than at steady state (marked by stars in Fig. 5.4A), while this was neither the case in ambient  $[\text{CO}_2]$  in wildtype leaves nor in both  $[\text{CO}_2]$  in *flacca* leaves. Because both genotypes were completely limited by triose phosphate utilisation in elevated  $[\text{CO}_2]$ , diffusional limitation (and stomatal limitation, see below) was nonexistent in elevated  $[\text{CO}_2]$  (data not shown).

Stomatal limitation, i.e. the apparent limitation to induction rates due to incompletely opened stomata, exhibited similar patterns (Fig. 5.5). These showed a decrease to negative values in the first five minutes, followed by an increase to a maximum in the first 10-20 minutes, which was followed by a gradual decrease towards zero at the end of photosynthetic induction. Maximum stomatal limitation was much higher in the wildtype

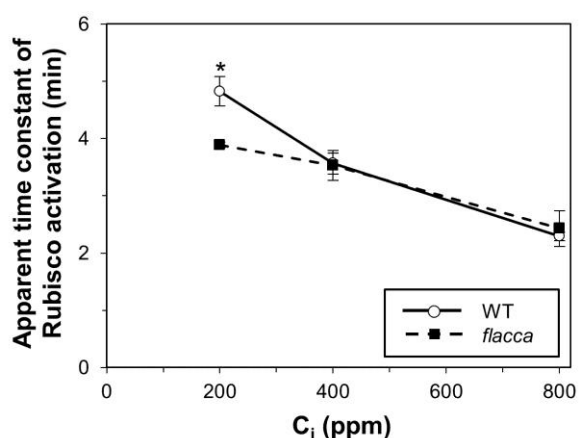


Fig. 5.3. Apparent time constant of Rubisco activation after a single-step increase in irradiance ( $0 \rightarrow 1000 \mu\text{mol m}^{-2} \text{s}^{-1}$ ) in wildtype (WT) and *flacca* leaves of tomato, as affected by  $\text{CO}_2$  concentration. The star denotes a significant difference ( $P < 0.05$ ) between genotypes at 200 ppm. Symbols denote average, error bars denote  $\pm$  SEM,  $n = 3$

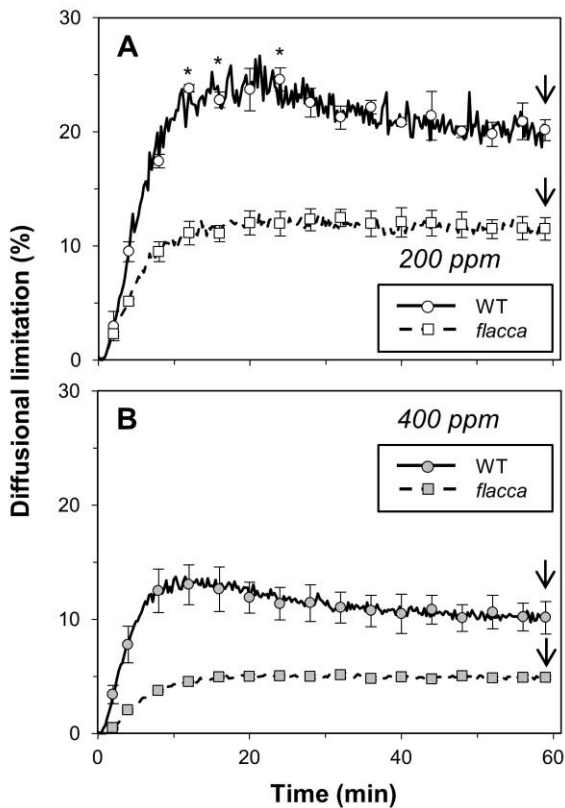


Fig. 5.4. Diffusional limitation after a single-step increase in irradiance ( $0 \rightarrow 1000 \mu\text{mol m}^{-2} \text{s}^{-1}$ ) in wildtype (WT) and *flacca* leaves of tomato, as affected by CO<sub>2</sub> concentration: 200 (A) and 400 (B). Diffusional limitation was absent in both genotypes in 800 ppm (due to triose phosphate utilisation limitation) and is therefore omitted here. Lines and symbols denote average, error bars denote  $\pm$  SEM,  $n = 3$ . Stars above single time points denote a significantly higher value ( $P < 0.05$ ) compared to the time point at the end of induction; this last time point is marked by an arrow

than in *flacca*, and higher in reduced compared to ambient [CO<sub>2</sub>]. Furthermore, stomatal limitation was significantly larger at most time points compared to steady-state values in the wildtype, and at several time points in *flacca*, in both [CO<sub>2</sub>] (Fig. 5.5).

Dynamic  $A_n/C_i$  curves, i.e. transient net photosynthesis rates ( $A_n$ ) versus transient  $C_i$  values during photosynthetic induction, revealed distinctly different patterns between the two genotypes (Fig. 5.6). In the wildtype, the initial increase in  $A_n$  towards the steady-state  $A_n/C_i$  relationship exhibited a simultaneous decrease in  $C_i$ , due to a faster rate of consumption of CO<sub>2</sub> than of CO<sub>2</sub> supply. Thereafter, wildtype  $A_n$  in reduced and ambient [CO<sub>2</sub>] increased much more slowly along the steady-state  $A_n/C_i$  relationship, due to stomatal opening (Fig. 6A, B). In elevated [CO<sub>2</sub>], this was not the case (Fig. S5.2). In *flacca* leaves, on the other hand,  $A_n$  showed a linear increase independent of  $C_i$ , indicating that supply of CO<sub>2</sub> did not limit photosynthesis at either reduced, ambient or elevated [CO<sub>2</sub>] (Fig. 5.6).

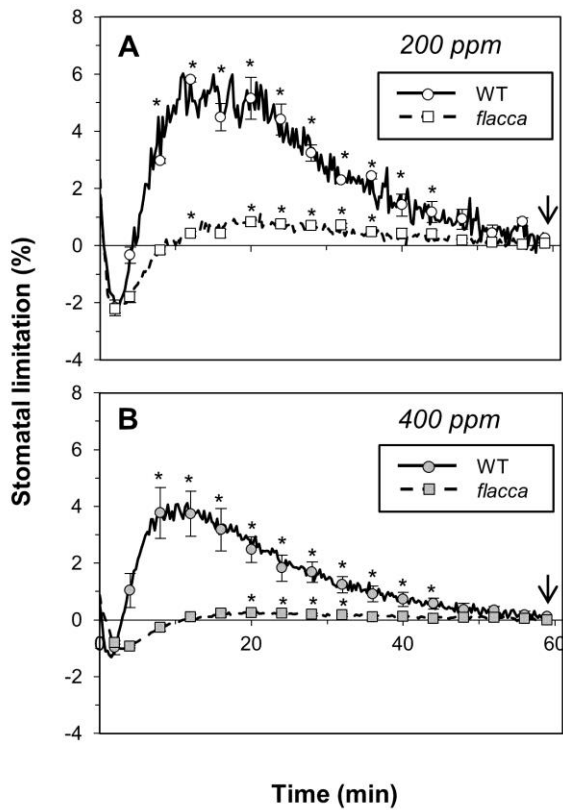


Fig. 5.5. Stomatal limitation after a single-step increase in irradiance ( $0 \rightarrow 1000 \mu\text{mol m}^{-2} \text{s}^{-1}$ ) in wildtype (WT) and *flacca* leaves of tomato, as affected by CO<sub>2</sub> concentration: 200 (A) and 400 (B). Stomatal limitation was absent in both genotypes in 800 ppm (due to triose phosphate utilisation limitation) and is therefore omitted here. Lines and symbols denote average, error bars denote  $\pm$  SEM,  $n = 3$ . Stars above single time points denote a significantly higher value ( $P < 0.05$ ) compared to the time point at the end of induction, marked by an arrow

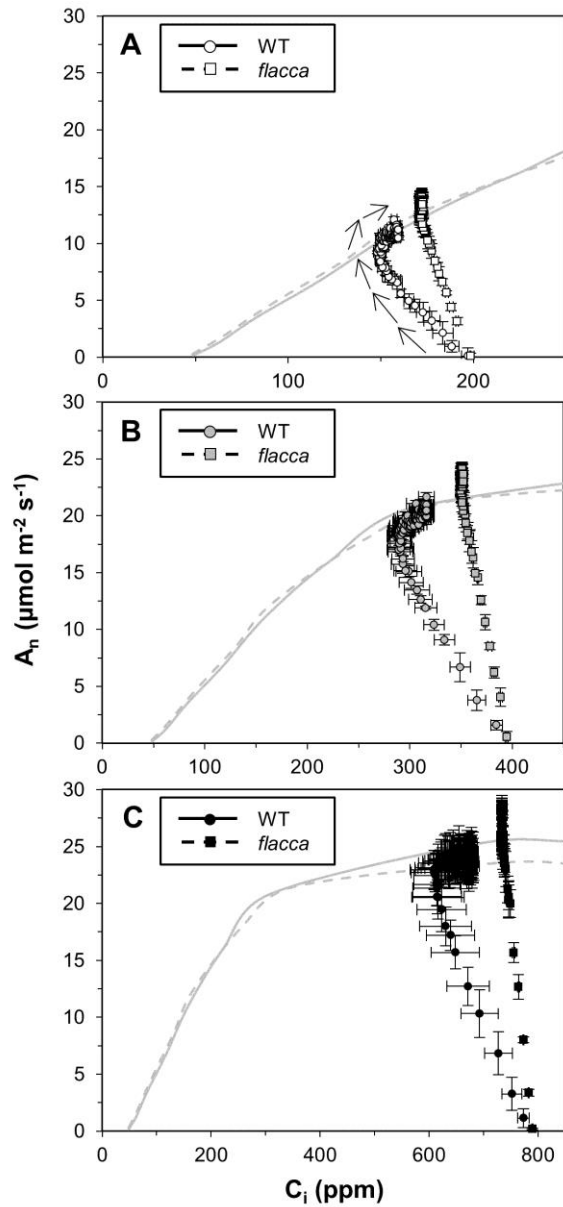


Fig. 5.6. Relationship between transient net photosynthesis rate ( $A_n$ ) and leaf internal  $\text{CO}_2$  concentration ( $C_i$ ) in wildtype (WT) and *flacca* leaves of tomato during photosynthetic induction after a single-step increase in irradiance ( $0 \rightarrow 1000 \mu\text{mol m}^{-2} \text{s}^{-1}$ ), in 200 (A), 400 (B) and 800 ppm (C) leaf external  $\text{CO}_2$  concentration. Grey lines represent the steady-state  $A_n/C_i$  relationship (as in Fig. 5.1). Note the different scales of X-axes in subplots. Arrows in A) are an example of time courses of  $A_n$  and  $C_i$  during induction. Symbols denote average, error bars denote  $\pm$  SEM,  $n = 3$

## Discussion

### *Lack of stomatal limitation in ambient [CO<sub>2</sub>]*

In agreement with our hypotheses, rates of photosynthetic induction in wildtype leaves were slower in reduced [CO<sub>2</sub>] and similar in elevated [CO<sub>2</sub>], compared to leaves of the high-g<sub>s</sub> mutant *flacca* (Fig. 5.2, Table 5.2). Surprisingly, in ambient [CO<sub>2</sub>], there was no difference in induction rates between genotypes. To the best of our knowledge, this has not been shown before and suggests that low initial stomatal conductance (g<sub>s</sub>) in dark-adapted tomato leaves does not limit rates of induction in ambient [CO<sub>2</sub>]. This challenges the common assumption that g<sub>s</sub> is one of the three main limitations of photosynthesis in fluctuating irradiance (e.g. Pearcy *et al.*, 1996; Way & Pearcy, 2012). This lack of limitation is despite the fact that wildtype leaves exhibited moderately high net photosynthesis rates (A<sub>n</sub>) in 1000 μmol m<sup>-2</sup> s<sup>-1</sup> (~21 μmol m<sup>-2</sup> s<sup>-1</sup> in ambient [CO<sub>2</sub>]; Table 5.1), and despite g<sub>s</sub> being low in darkness (~0.26 mol m<sup>-2</sup> s<sup>-1</sup>) and increasing slowly after the stepwise irradiance increase (Fig. S5.3). Leaves of both genotypes exhibited similar steady-state CO<sub>2</sub> responses (Fig. 5.1; Bradford *et al.*, 1983) and similar apparent time constants of Rubisco activation in ambient and elevated [CO<sub>2</sub>] (Fig. 5.3). Therefore, it is unlikely that a hypothetically larger transient stomatal limitation in the wildtype was offset by a hypothetically larger transient biochemical limitation in the *flacca* mutant.

### *Indices for assessing transient stomatal limitation: an evaluation*

Our data enabled us to compare several indices for assessing stomatal limitation during photosynthetic induction. Basically, any method correctly reflecting transient stomatal limitation should show a limitation at reduced [CO<sub>2</sub>] in wildtype leaves, and no limitations at ambient or elevated [CO<sub>2</sub>]. Furthermore, this method should show an absence of a transient stomatal limitation in *flacca*, irrespective of [CO<sub>2</sub>]; the reasoning for this is that initial g<sub>s</sub> in *flacca* was approx. 1.5 times larger than g<sub>s</sub> in wildtype leaves adapted to high irradiance, while final, steady-state A<sub>n</sub> was similar in both genotypes or slightly higher in *flacca* (Table 5.1). Therefore, initial g<sub>s</sub> in *flacca* was highly unlikely to be limiting during photosynthetic induction.

Stomatal limitation, a frequently used index (Roden & Pearcy, 1993; Tinoco-Ojanguren & Pearcy, 1993b; Allen & Pearcy, 2000b; Urban *et al.*, 2007; 2008), did not fulfil the above requirements. Instead, data in Fig. 5.5 suggest that almost all transient values during photosynthetic induction were significantly larger in wildtype leaves in ambient [CO<sub>2</sub>]. Furthermore, the values for *flacca* leaves suggested a mild form of stomatal limitation in both ambient and reduced [CO<sub>2</sub>] at several time points (Fig. 5.5). A general problem of this index is that it approaches zero by definition; this is so because steady-state and transient

$C_i$  values are used to correct transient  $A_n$  (Eqn. 2), and transient  $C_i$  approaches steady-state  $C_i$  towards the end of photosynthetic induction. This artificially reduces any biological variation of average values as they approach zero. Therefore, many comparisons between different time points of transient and steady-state stomatal limitation yielded significant differences (Fig. 5.5) that were not corroborated by comparisons of rates of photosynthetic induction between both genotypes (Fig. 5.2). Also, this index often reaches negative values in the beginning of induction, because transient  $C_i$  is larger than final  $C_i$  (Urban *et al.*, 2007), making it less credible. Because limitations during the induction phase can be partitioned into stomatal and biochemical contributions (Allen & Pearcy, 2000b; Urban *et al.*, 2007), this index is very convenient to use. However, our data suggest that it can easily be misleading.

The dynamic  $A_n/C_i$  curve of wildtype leaves in ambient  $[CO_2]$  suggested  $g_s$  to be limiting, as part of  $A_n$  during induction increased along the steady-state  $A_n/C_i$  relationship (Fig. 5.6B). Considering that induction rates did not differ between wildtype and *flacca* leaves (Fig. 5.2B), this is misleading. Furthermore, the dynamic  $A_n/C_i$  approach does not yield a quantitative analysis of transient stomatal limitation and therefore is of limited use.

Additionally, values from single replicates of initial  $g_s$  and the time required to reach 90% of full induction ( $t_{90}$ ) were plotted against each other (Fig. S5.4). These values have been shown to be highly correlated before (Valladares *et al.*, 1997; Allen & Pearcy, 2000a). However, just like the dynamic  $A_n/C_i$  curves, this analysis suffers from the drawback of an inability to quantify stomatal limitation. Furthermore, to obtain useful correlations, a large gradient in responses, using many different replicates (and genotypes) is necessary, and those were not available here.

Diffusional limitation has often been used to describe limitations due to any barriers to  $CO_2$  diffusion towards the site of carboxylation in studies of steady-state photosynthesis (e.g. Grassi & Magnani, 2005; Diaz-Espejo *et al.*, 2007; Chen *et al.*, 2014). However, to our knowledge, this index has not been used before in studies of photosynthetic induction, probably due to the convenience of using stomatal limitation (see above). Here, diffusional limitation correctly showed significantly larger values during photosynthetic induction in the wildtype in reduced, but not in ambient,  $[CO_2]$  (Fig. 5.4). Furthermore, it did not show any additional transient diffusional limitation in *flacca*. From this analysis, it seems that diffusional limitation is the most useful index, because it eliminates the weaknesses of the above indices. It is quantitative, works even if only a small number of replicates are used, and does not come with the same problems for statistical comparisons as stomatal limitation does. A possible weakness of this index is that it includes mesophyll conductance ( $g_m$ ). If  $g_m$  was to change during photosynthetic induction, then transient changes of

diffusional limitation would be due to a combination of changes in  $A_n$ ,  $g_s$  and  $g_m$ . The difficulty in estimating  $g_m$  (e.g. Tholen *et al.*, 2012; Gu & Sun, 2014), and especially transient  $g_m$ , would greatly complicate matters. However, data from previous experiments with tomato leaves (Chapter 3) suggest that changes in  $g_m$  during photosynthetic induction are unlikely. We therefore recommend to use diffusional limitation when analysing transient stomatal limitations of photosynthesis in fluctuating irradiance.

### *Conclusions*

This study provides evidence of a lack of stomatal limitation during photosynthetic induction in tomato leaves at ambient  $[CO_2]$ , challenging the common assumption of stomatal conductance being one of the three predominant limitations to photosynthesis in fluctuating irradiance. Furthermore, several indices for assessing stomatal limitation during photosynthetic induction were compared, and diffusional limitation, a new index for assessing transient stomatal limitation, was found to be the most useful.

### **Acknowledgements**

This work was carried out within the research programme of BioSolar Cells, co-financed by the Dutch Ministry of Economic Affairs. Additionally, this work was supported by Essent.

**Supplementary material 5.1**

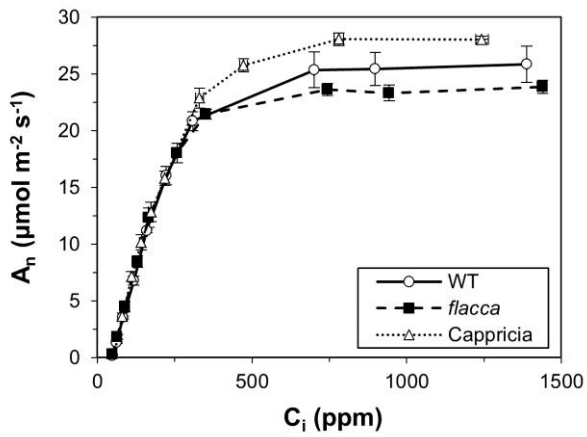


Figure S5.1.  $A_n/C_i$  response of tomato leaves: cv. Cappricia, cv. Rheinlands Ruhm wildtype (WT), and cv. Rheinlands Ruhm *flacca*. Symbols denote average, error bars denote  $\pm$  SEM,  $n = 3-5$

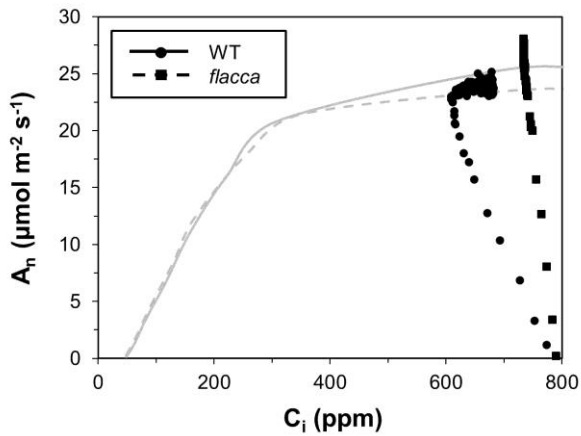


Figure S5.2. Dynamic  $A_n/C_i$  relationship in elevated  $[CO_2]$ , plotted without error bars, to emphasize the increase in  $C_i$  without an increase in  $A_n$  in the wildtype



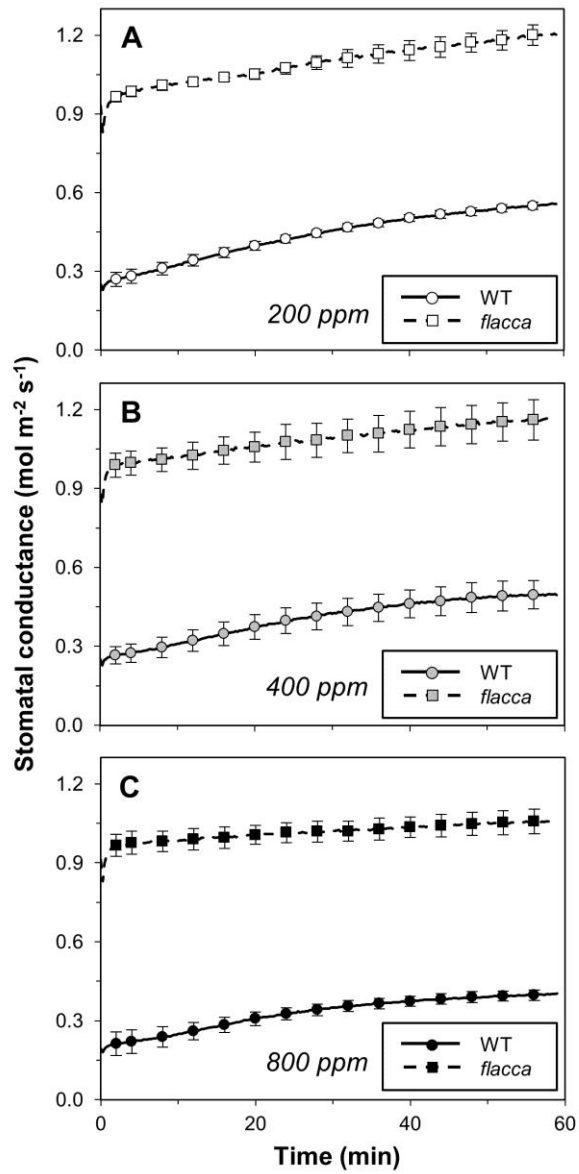


Figure S5.3. Time course of stomatal conductance after a stepwise increase in irradiance ( $0 \rightarrow 1000 \mu\text{mol m}^{-2} \text{s}^{-1}$ ) in wildtype (WT) and *flacca* leaves, as affected by  $\text{CO}_2$  concentration. Symbols denote average, error bars denote  $\pm$  SEM,  $n = 3$

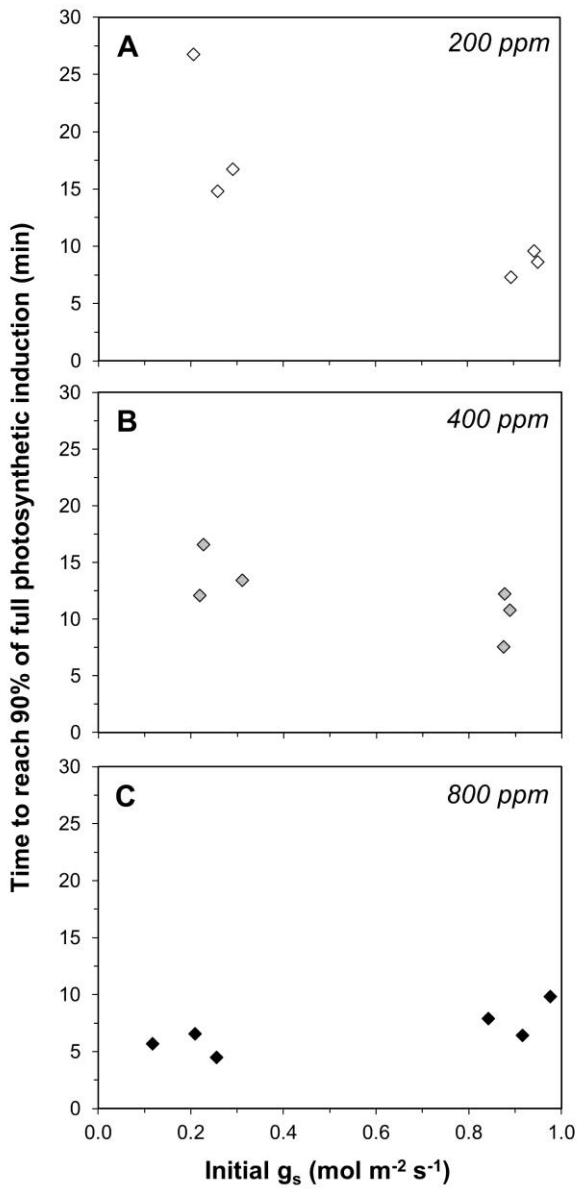


Figure S5.4. Relationships between initial (dark-adapted) stomatal conductance and the time required to reach 90% of full photosynthetic induction state in single replicates of wildtype and *flacca* leaves, as affected by [CO<sub>2</sub>]

## CHAPTER 6

Metabolic and diffusional limitations of  
photosynthesis in fluctuating irradiance in  
*Arabidopsis thaliana*

**Authors:**

Elias Kaiser

Alejandro Morales

Jeremy Harbinson

Ep Heuvelink

Aina E. Prinzenberg

Leo F.M. Marcelis

Under review

**Abstract**

A better understanding of the metabolic and diffusional limitations of photosynthesis in fluctuating irradiance can help identify targets for improving crop yields. We used different genotypes of *Arabidopsis thaliana* to characterise the importance of Rubisco activase (Rca), stomatal conductance ( $g_s$ ), non-photochemical quenching of chlorophyll fluorescence (NPQ) and sucrose phosphate synthase (SPS) on photosynthesis in fluctuating irradiance. Leaf gas exchange and chlorophyll fluorescence were measured in leaves exposed to stepwise increases and decreases in irradiance, including periodic, symmetrical lightflecks. *rwt43*, which has a constitutively active Rubisco enzyme (except in darkness), showed faster increases than Colombia-o (Col-o) in photosynthesis rates after step increases in irradiance. *rca-2*, having decreased Rca concentration, showed the opposite response. In *aba2-1*, high  $g_s$  increased transient photosynthesis rates and lightfleck use efficiency, while in C24, low  $g_s$  tended to decrease transient photosynthesis rates. Differences in transient photosynthesis rates between Col-o and plants with low levels of NPQ (*npq1-2*, *npq4-1*) or SPS (*spsa1*) were negligible. In Col-o, the regulation of Rubisco activation and levels of  $g_s$  were limiting for photosynthesis in fluctuating irradiance, while levels of NPQ or SPS were not. This suggests Rubisco activase and  $g_s$  as targets for improvement of photosynthesis of plants in fluctuating irradiance.

## Introduction

Plants grow in a variable environment, with changes occurring within seconds and upwards. Of the factors important for photosynthesis, irradiance changes most quickly (Pearcy, 1990), causing a lag between changes in irradiance and the regulation of photosynthesis (Pearcy *et al.*, 1996). This lag decreases light-use efficiency relative to the steady state and transiently increases excess irradiance, possibly harming the photosynthetic apparatus (Kono & Terashima, 2014). Leaves use various mechanisms in response to fluctuating irradiance. Among the best known mechanisms are the regulation of enzymes of carbon fixation and sucrose metabolism, excess energy dissipation and stomatal conductance (g<sub>s</sub>; Pearcy *et al.*, 1996; Kaiser *et al.*, 2015). Adjusting these mechanisms to changes in irradiance takes time and can impose transient limitations, which reduce plant productivity (Küppers & Pfiz, 2009). Reductions in assimilation due to these physiological limitations can be up to 35% per day (subject to light environment and genotype; Naumburg & Ellsworth, 2002), and understanding them better may pave the road towards higher yields (Murchie & Niyogi, 2011; Carmo-Silva *et al.*, 2014). Past achievements in understanding metabolic constraints of photosynthesis in fluctuating irradiance (dynamic photosynthesis) have mainly come from biochemical studies (e.g. Seemann *et al.*, 1988; Stitt & Grosse, 1988; Sassenrath-Cole & Pearcy, 1992), with less use being made of genetic diversity. Naturally occurring ecotypes, mutations, cultivars and genetically modified accessions offer a range of genotypes with specific properties, that could be used to study dynamic photosynthesis (Kaiser *et al.*, 2015). *Arabidopsis thaliana* possesses a wide, well documented genotypic diversity, which has been extended by selecting for mutations and by transgenic modifications.

Rubisco catalyses the first reaction of CO<sub>2</sub> assimilation. Its activation is a relatively slow process that often limits assimilation after irradiance increases (Seemann *et al.*, 1988; Woodrow & Mott, 1989). In the chloroplast stroma, several inhibitory compounds can bind to Rubisco. To maintain sufficient Rubisco activity, these inhibitors need to be removed from the active sites by the ATPase Rubisco activase (Rca, Salvucci *et al.*, 1985). In *Arabidopsis thaliana*, there are two isoforms of Rca, the larger  $\alpha$ -isoform and the smaller  $\beta$ -isoform (Salvucci *et al.*, 1987). The  $\alpha$ -isoform, which contains two additional Cys residues, is redox-activated via thioredoxin-f, increasing the ADP sensitivity of the  $\alpha$ -isoform but not that of the  $\beta$ -isoform (Zhang & Portis, 1999). In low irradiance (i.e. high ADP/ATP ratio), the  $\alpha$ -isoform is less active and the rate of overall Rubisco activation is low. The  $\beta$ -isoform is not sensitive to ADP, but the  $\alpha$ -isoform indirectly controls the  $\beta$ -isoform (Zhang & Portis, 1999; Zhang *et al.*, 2002). Since Rca is a central regulator of Rubisco activity, how

these isoforms, or their concentration affect dynamic photosynthesis is an important yet unresolved question.

After CO<sub>2</sub> assimilation by Rubisco, a fraction of the triose phosphates leaves the chloroplast in exchange for orthophosphate (P<sub>i</sub>) from the cytosol. In the cytosol, triose phosphate is converted to sucrose, and sucrose phosphate synthase (SPS) plays a central role in this pathway (reviewed in Stitt *et al.*, 2010). In certain circumstances, such as photosynthetic induction in saturating CO<sub>2</sub>, activation of SPS can be slower than that of Calvin cycle enzymes, making the Calvin cycle transiently P<sub>i</sub>-limited (Stitt & Grosse, 1988). Furthermore, after irradiance decreases, an overshoot in sucrose synthesis can transiently drain metabolites from the Calvin cycle, transiently decreasing carbon gain (Prinsley *et al.*, 1986). Plants with reduced SPS concentration may therefore exhibit slower increases in photosynthesis after irradiance increases, and a lower CO<sub>2</sub> burst after irradiance decreases. Leaves protect themselves from absorbed irradiance that is in excess of the capacity of photochemistry using non-photochemical quenching (NPQ). This protection, however, may come at a price. Slow NPQ relaxation after irradiance decreases may result in transient limitations of the quantum efficiency of photosystem II for electron transport ( $\Phi_{\text{PSII}}$ ). Model calculations indicate that this transient limitation could decrease canopy photosynthesis by ~13-32% (Zhu *et al.*, 2004). NPQ has been shown to limit assimilation in genotypes with faster NPQ buildup after irradiance increases (Hubbart *et al.*, 2012) or slower NPQ relaxation after irradiance decreases (Armbruster *et al.*, 2014). Thus, genotypes with constitutively low NPQ may have increased dynamic photosynthesis rates, principally as a result of less limitation on assimilation following a decrease in irradiance. In many plants, stomata open when irradiance increases. Typically, stomatal opening is slow, transiently limiting the increase in assimilation produced by an increase in irradiance (Vico *et al.*, 2011). Genotypes with constitutively high g<sub>s</sub> may not impose this limitation (Allen & Pearcy, 2000a), and may therefore be more productive in environments with a high proportion of fluctuating irradiance.

We used several genotypes, i.e. plants containing point mutations, transformants, T-DNA insertion lines (SALK lines, Alonso *et al.*, 2003) and naturally occurring accessions of *A. thaliana*, to analyse how metabolic (Rubisco activation, NPQ, sucrose synthesis) and diffusional (g<sub>s</sub>) limitations affect dynamic photosynthesis. Additional to measuring their steady-state photosynthetic irradiance and CO<sub>2</sub> responses, we exposed these genotypes to stepwise increases and decreases in irradiance and to symmetrical lightflecks of several frequencies and amplitudes, while measuring gas exchange and chlorophyll fluorescence. To investigate the effects of Rca regulatory properties or concentrations, we used the genetically modified genotype *rwt43* (lacks the  $\alpha$ -isoform of Rca and is therefore ADP-

insensitive; Zhang *et al.*, 2002) and the leaky allele mutation *rca-2* (decreased Rca concentration; Shan *et al.*, 2011). To analyze the effect of SPS, we used *spsa1* (80% reduction in maximum SPS activity; Sun *et al.*, 2011). The effect of low NPQ was investigated by using *npq4-1* (lacks PsbS, greatly diminishing NPQ; Li *et al.*, 2000) and *npq1-2* (lacks zeaxanthin deepoxidase and therefore violaxanthin, greatly diminishing NPQ; Niyogi *et al.*, 1998). Effects of high and low  $g_s$  were analyzed by using *aba2-1* (impaired abscisic acid (ABA) synthesis, leading to constitutively high  $g_s$ ; Leon-Kloosterziel *et al.*, 1996) and the natural accession C24 (comparably low  $g_s$ , Brosché *et al.*, 2010), respectively. All genotypes were compared to Col-0, which is the progenitor of all genotypes except C24.

## Materials and methods

### *Plant material*

Seeds of *npq4-1*, *spsa1* (SALK\_148643C) and *rca-2* (SALK\_003204C) were obtained from NASC (University of Nottingham, Loughborough, UK; Scholl *et al.*, 2000). C24 (CS76106) was obtained from the Arabidopsis Biological Resource Center (ABRC, Ohio State University, USA). Seeds of Col-o and *aba2-1* were obtained from Corrie Hanhart (Wageningen University, the Netherlands), *npq1-2* was obtained from Dr. Shizue Matsubara (Forschungszentrum Jülich, Germany) and *rwt43* was obtained from Dr. Elizabete Carmo-Silva (Rothamsted Research, UK).

### *Growth conditions*

Plants were grown in 0.37 L pots using soil with a 4:1 peat:perlite mixture (Horticoop, Katwijk, the Netherlands). Pots were placed on irrigation mats, and mats were saturated daily to full capacity. Plants were fertilized weekly using a nutrient solution especially developed for Arabidopsis (van Rooijen *et al.*, 2015). To inhibit algal growth, the soil was covered with black plastic film. Plants were grown in a growth chamber in short-day conditions (8 hours of light) to delay flowering (Gibeaut *et al.*, 1997) and thus ensure that leaves were large enough for gas-exchange measurements. Irradiance was  $172 \pm 4 \mu\text{mol m}^{-2} \text{s}^{-1}$  as supplied by LED lights (GreenPower LED production module deep red/white 120; Philips, Eindhoven, the Netherlands; Fig. S6.1). Temperature was 23/18 °C (day/night) and relative humidity was 70%. Mutants lacking ABA (*aba2-1*) were sprayed with an aqueous solution containing  $10 \mu\text{mol mol}^{-1}$  ABA (Sigma, St. Louis, U.S.A.) when plants were 2, 4 and 6 weeks old. This increases rosette growth compared to untreated *aba2-1* plants (data not shown). There was a period of 15 days between the last application of ABA and the first measurements on *aba2-1* plants.

Single genotypes were grown in sequential batches, by approx. one batch per week. Five plants per batch were used for measurements. To monitor the quality of the growth system over time, Col-o was grown in three batches, each batch separated by several weeks. The number of replicates was therefore 15 for Col-o, and 5 for all other genotypes. The growth system produced very reproducible photosynthetic phenotypes of Col-o (Fig. S6.2).

### *Measurements*

Measurements were performed using the LI-6400 portable photosynthesis system (Li-Cor Biosciences, Lincoln, Nebraska, USA) equipped with the leaf chamber fluorometer (Part No. 6400-40) on single leaves of plants that were 6-8 weeks old. Leaves large enough to cover the leaf chamber gasket (area: 2 cm<sup>2</sup>, diameter: 1.6 cm) were used. Conditions in



the cuvette were as follows: 23 °C air temperature, 70% relative humidity, 90/10% red/blue light mixture and 500  $\mu\text{mol s}^{-1}$  air flow rate. Except for the  $\text{CO}_2$ -response curves, the  $\text{CO}_2$  mole fraction ( $C_a$ ) was kept at 400 ppm and the oxygen mole fraction at 21%.

### *Stepwise increases in irradiance*

Leaves were adapted to several low irradiances (0, 70 or 130  $\mu\text{mol m}^{-2} \text{s}^{-1}$ ; hereafter: background irradiances) for 30-60 minutes (always 60 minutes in darkness), and then exposed to single-step increases in irradiance, namely 0→1000, 70→800 and 130→600  $\mu\text{mol m}^{-2} \text{s}^{-1}$ . Gas exchange was logged nominally every second. Logging was stopped when  $g_s$  reached a new steady state (this took a minimum of 30 minutes after the step increase), or 60 minutes after switching to 1000  $\mu\text{mol m}^{-2} \text{s}^{-1}$ . Before and after the 0→1000  $\mu\text{mol m}^{-2} \text{s}^{-1}$  increase,  $\Phi_{\text{PSII}}$  and NPQ were measured, using a measuring beam intensity of 5  $\mu\text{mol m}^{-2} \text{s}^{-1}$  and a saturating pulse of  $\sim 7600 \mu\text{mol m}^{-2} \text{s}^{-1}$  intensity and 1 s duration. In preliminary measurements on Col-0, the saturating pulse was sufficient to saturate  $F_m'$ . The  $F_o$  and  $F_m$  relative fluorescence yields were measured in dark-adapted leaves. After the increase in irradiance, the  $F_m'$  relative fluorescence yield was measured every minute for the first ten minutes, and every 2 minutes thereafter. The steady-state relative fluorescence yield,  $F_s$ , was measured continuously. Dark-adapted  $F_v/F_m$ ,  $\Phi_{\text{PSII}}$  and NPQ were calculated as  $F_v/F_m = (F_m - F_o)/F_m$ ,  $\Phi_{\text{PSII}} = (F_m' - F_s)/F_m'$  and  $\text{NPQ} = (F_m - F_m')/F_m'$ , respectively.

The time to reach 10, 20...90% (i.e.  $t_{10}$ ,  $t_{20}$ ... $t_{90}$ ) of steady-state net photosynthesis rate ( $A_n$ ) and  $g_s$  was calculated for each irradiance increase. To increase robustness of these indices to experimental noise and outliers, time series were smoothed using a local polynomial regression with a span of 5% (Cleveland *et al.*, 1992). This means that, for each point in the time series, a polynomial of degree 2 was fitted using weighted least squares to a data window of size equal to 5% of the total size of the time series; the weight assigned to each point decreases with the distance from the central point. The apparent time constant of Rubisco activation ( $\tau_R$ ) was computed by linearizing the transients, which had been corrected for changes in  $C_i$  (see below), and then fitting a linear regression model (Woodrow & Mott, 1989). The range of data used for calculating  $\tau_R$  differed between background irradiances, and in some cases between genotypes (Fig. S6.3). This was due to differences in the rate of change of photosynthesis, and included 120 data points in the case of 0→1000  $\mu\text{mol m}^{-2} \text{s}^{-1}$  (all genotypes) and 40 (for *rwt43*) or 60 (all other genotypes) in the case of 70→800 and 130→600  $\mu\text{mol m}^{-2} \text{s}^{-1}$ . These ranges were selected by visual inspection.

For diffusional and biochemical limitations during photosynthetic induction, values of  $A_n$  were corrected by the difference between  $C_i$  at each time point and  $C_a$  (when calculating

diffusional limitation) and  $C_i$  at the end of induction (when calculating biochemical limitation and  $\tau_R$ ). The relative effects of  $C_i$  on photosynthesis were taken from the steady-state  $A_n/C_i$  curve by fitting a local polynomial regression in the range 50-500 ppm. From time series of  $A_n$  corrected for changes in  $C_i$ , the change in biochemical limitation during photosynthetic induction was calculated after Allen & Pearcy (2000b). Throughout induction, this index decreases from 100 to 0%, and therefore indicates the additional limitation imposed on photosynthesis due to incomplete activation of several enzymes. Changes in diffusional limitation during induction were calculated as the difference between transient  $A_n$  and  $A_n$  at ambient  $CO_2$  concentration (i.e. without limitation to  $CO_2$  diffusion into the leaf). This means that diffusional limitation is a combination of possible changes in stomatal and mesophyll conductance ( $g_m$ ) during induction, and that this index does not decrease to 0% at the end of induction, but rather gives an indication of steady-state limitations due to  $g_s$  and  $g_m$ . Therefore, biochemical and diffusional limitations do not add up, and are to be interpreted separately.

### *Split-line regression analysis*

To investigate how the transition between limiting and non-limiting initial  $g_s$  was changed by background irradiance and at different time-points after step irradiance increases, a split-line regression analysis (Genstat 17<sup>th</sup> Ed., VSN International, Hempstead, UK) with initial  $g_s$  vs.  $t_{A10}$ ,  $t_{A20}$  ...  $t_{A90}$  was carried out using data from genotypes affecting  $g_s$ . The split-line regression assigned two linear fits to the data: A non-horizontal line on the left side of the plot and a horizontal line on the right side. To evaluate when this approach yielded reliable results, the variance accounted for by the split-line model was used: Only fits that accounted for >40% of the variance were assumed to be reliable (the threshold of 40% was determined by trial and error to be the most useful).

### *Stepwise decreases in irradiance*

Irradiance was decreased in the following steps: 800→130 and 600→200  $\mu\text{mol m}^{-2} \text{s}^{-1}$ . Post-illumination  $CO_2$  fixation (Pons *et al.*, 1992) and post-illumination  $CO_2$  bursts (Vines *et al.*, 1983) were quantified. The former implies that photosynthesis is above the steady-state value during the transient, while the latter implies a lower assimilation rate than at steady state. Values were estimated by integrating the difference between time series of photosynthesis and the steady-state value at the end of the transient (Tomimatsu *et al.*, 2014).

### *Lightfleck use efficiency*

Leaves adapted to  $300 \mu\text{mol m}^{-2} \text{s}^{-1}$  were exposed to lightfleck sequences, i.e. series of symmetrical square wave irradiance fluctuations with amplitudes of 50, 100 and  $250 \mu\text{mol m}^{-2} \text{s}^{-1}$  centred on  $300 \mu\text{mol m}^{-2} \text{s}^{-1}$ . Each lightfleck cycle consisted of one step increase to higher irradiance (first half of the cycle) and one step decrease to lower irradiance (second half of the cycle). Durations of single lightfleck cycles were 120, 60 and 10 s and the number of lightfleck cycles used were, respectively, 5, 10 and 60, so each treatment lasted 600 s (Fig. 6.1). The order of amplitudes was randomized for each leaf. Between amplitudes, assimilation was allowed to return to steady state. The last 2, 4 and 24 lightfleck cycles of the 120, 60 and 10 s durations were used to calculate the lightfleck use efficiency (LFUE), defined as  $\text{LFUE} = 100 \times (A_{n(\text{lf})} / A_{n(\text{ss})})$ .  $A_{n(\text{lf})}$  is average  $A_n$  during a cycle, while  $A_{n(\text{ss})}$  is steady-state  $A_n$  at ( $300 \mu\text{mol m}^{-2} \text{s}^{-1}$ ). This definition of LFUE differs from earlier definitions, which used values of steady-state  $A_n$  at both irradiances used during the lightfleck as a baseline (e.g. Pons & Pearcy, 1992). For calculation of partial LFUE, which accounted for the portion of LFUE gained after increases or decreases in irradiance, average carbon gain during the corresponding half of the lightfleck cycle was used instead of  $A_{n(\text{lf})}$ .

### *Irradiance response curves*

When  $A_n$  was at a steady state, i.e. before step changes in irradiance or at the end of a measurement sequence, 120 data points were used to extract average  $A_n$  at a given irradiance. The resulting values were used to construct steady-state irradiance response curves.

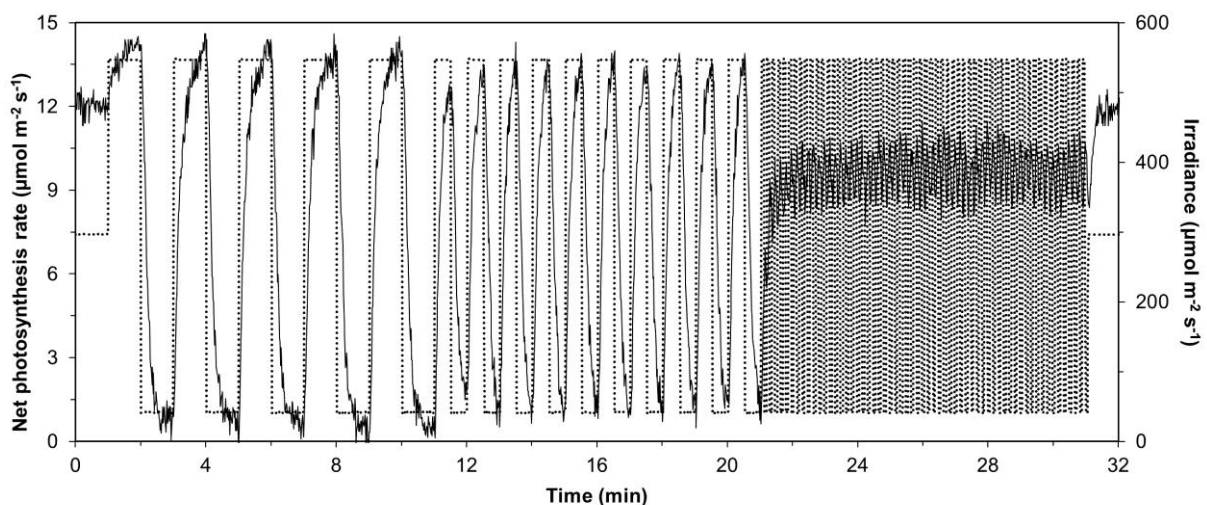


Fig. 6.1. Example of net photosynthesis rates (continuous line) and irradiance (dotted line) during a series of lightflecks ( $300 \pm 250 \mu\text{mol m}^{-2} \text{s}^{-1}$ )

### *CO<sub>2</sub> response curves*

To assess steady-state responses of assimilation and electron transport to various leaf internal CO<sub>2</sub> concentrations (C<sub>i</sub>), leaves were adapted for ~30 min to 1000 μmol m<sup>-2</sup> s<sup>-1</sup> (saturating irradiance, Fig. 6.2) and 500 ppm C<sub>a</sub>. C<sub>a</sub> was then decreased stepwise until 50 ppm, each step taking 2-3 minutes. Thereafter, C<sub>a</sub> was raised to 500 ppm, and after waiting for ~15 minutes, leaves were exposed to stepwise increases in C<sub>a</sub> until 1500 ppm, each step taking ~4 minutes. Values were logged every 5 s and the last 60 s of every CO<sub>2</sub> step used to calculate average ± SEM (standard error of the mean) of C<sub>i</sub> and A<sub>n</sub>. Φ<sub>PSII</sub> was determined at the end of each step as described above. Photosynthesis in all genotypes was corrected for CO<sub>2</sub> leaks using dried leaves of Col-o (Long & Bernacchi, 2003). Parameters V<sub>cmax</sub> (maximum carboxylation rate by Rubisco), J<sub>max</sub> (maximum rate of electron transport in the absence of regulation) and TPU (maximum rate of triose phosphate utilisation) were calculated from A<sub>n</sub>/C<sub>i</sub> curves after Sharkey et al. (2007). Mitochondrial respiration in the light was assumed to be identical to genotype-specific steady-state respiration in the dark. For g<sub>m</sub>, a value of 0.071 mol m<sup>-2</sup> s<sup>-1</sup> was used for all genotypes, which was an average value taken from literature corresponding to two different methods to determine g<sub>m</sub> on 6-7 week old plants of Col-o (Flexas *et al.*, 2007b).

### *Statistical analysis*

Each genotype was compared to Col-o using a Student's *t*-test (Microsoft Excel, function t.test, assuming 2-tailed distribution and two-sample equal variance).

## Results

### *Steady-state responses to irradiance and CO<sub>2</sub>*

In the mutant containing less Rubisco activase, *rca-2*, the maximum photosynthesis rate was lower than for Col-o, and saturation occurred around 600  $\mu\text{mol m}^{-2} \text{s}^{-1}$  (Fig. 6.2A). The lower  $A_n/C_i$  response in *rca-2* (Fig. 6.2B) resulted in significantly decreased  $V_{\text{cmax}}$  (-25%),  $J_{\text{max}}$  (-14%) and TPU (-7%) compared to Col-o (Table 6.1). Assimilation in the transformant lacking the  $\alpha$ -isoform of Rca, *rwt43*, had a similar irradiance response, but slightly different  $A_n/C_i$  curvature compared to Col-o (Fig. 6.2A, B), resulting in significantly enhanced  $J_{\text{max}}$  (+8%, Table 6.1). The ABA-deficient mutant, *aba2-1*, showed larger irradiance- and CO<sub>2</sub>-saturated photosynthesis rates compared to Col-o, while the accession C24 showed the opposite (Fig. 6.2C-D).  $A_n/C_i$  parameters were therefore larger in *aba2-1* ( $V_{\text{cmax}}$ : +12%,  $J_{\text{max}}$ : +19%, TPU: +20%), while they were smaller in C24 ( $V_{\text{cmax}}$ : -18%,  $J_{\text{max}}$ : -21%, TPU: -23%, Table 6.1). The supply lines (Fig. 6.2D) emphasize differences in  $g_s$  between C24, Col-o and *aba2-1*: the steeper the slope, the smaller the difference between  $C_a$  and  $C_i$ , and the larger  $g_s$ . Irradiance and  $C_i$  responses of photosynthesis of low-NPQ mutants (*npq1-2*, *npq4-1*) were similar to Col-o (Fig. 6.2E-F). Assimilation in the mutant with less SPS (*spsa1*) did not differ from Col-o in its irradiance response (Fig. 6.2G), but was strongly reduced at high  $C_i$  (Fig. 6.2H), resulting in decreased  $J_{\text{max}}$  (-13%) and TPU (-23%, Table 6.1). The response of  $\Phi_{\text{PSII}}$  to  $C_i$  largely paralleled that of  $A_n$ , with the exception that  $\Phi_{\text{PSII}}$  decreased at high  $C_i$  in many genotypes (except *rca-2* and *npq4-1*; Fig. S6.4). This decrease in  $\Phi_{\text{PSII}}$  was most marked, and started at a lower  $C_i$ , in *spsa1* (Fig. S6.4D).

### *Responses to stepwise increases in irradiance*

Photosynthetic induction in dark-adapted leaves was initially similar between all genotypes (except *rwt43*) until ~60% induction was reached (Fig. 6.3). *rwt43* reached 50% of photosynthetic induction ( $t_{A50}$ ) significantly faster than Col-o (Table 6.2). Induction remained faster in *rwt43* until it reached ~80% (Fig. 6.3A). In *rca-2*, the rate of induction slowed after 60% completion and then increased in a nearly linear fashion rather than the more exponential increase shown by all other genotypes (Fig. 6.3A). This increased the time to reach 90% of photosynthetic induction ( $t_{A90}$ ) by ~10 minutes compared to Col-o (Table 6.2). *aba2-1* exhibited faster induction, halving the  $t_{A90}$  (Table 6.2) of Col-o, while induction in C24 was identical to that of Col-o (Fig. 6.3B). Induction in *npq1-2* and *npq4-1* was identical to Col-o (Fig. 6.3C). *spsa1* showed slightly slower induction rates (Fig. 6.3D), increasing  $t_{A90}$  by ~5 min compared to Col-o (Table 6.2).

Differences in photosynthetic induction for genotypes affecting Rca and  $g_s$  were also visible in the time series of  $C_i$ , diffusional limitation and biochemical limitation (Fig. 6.4). While

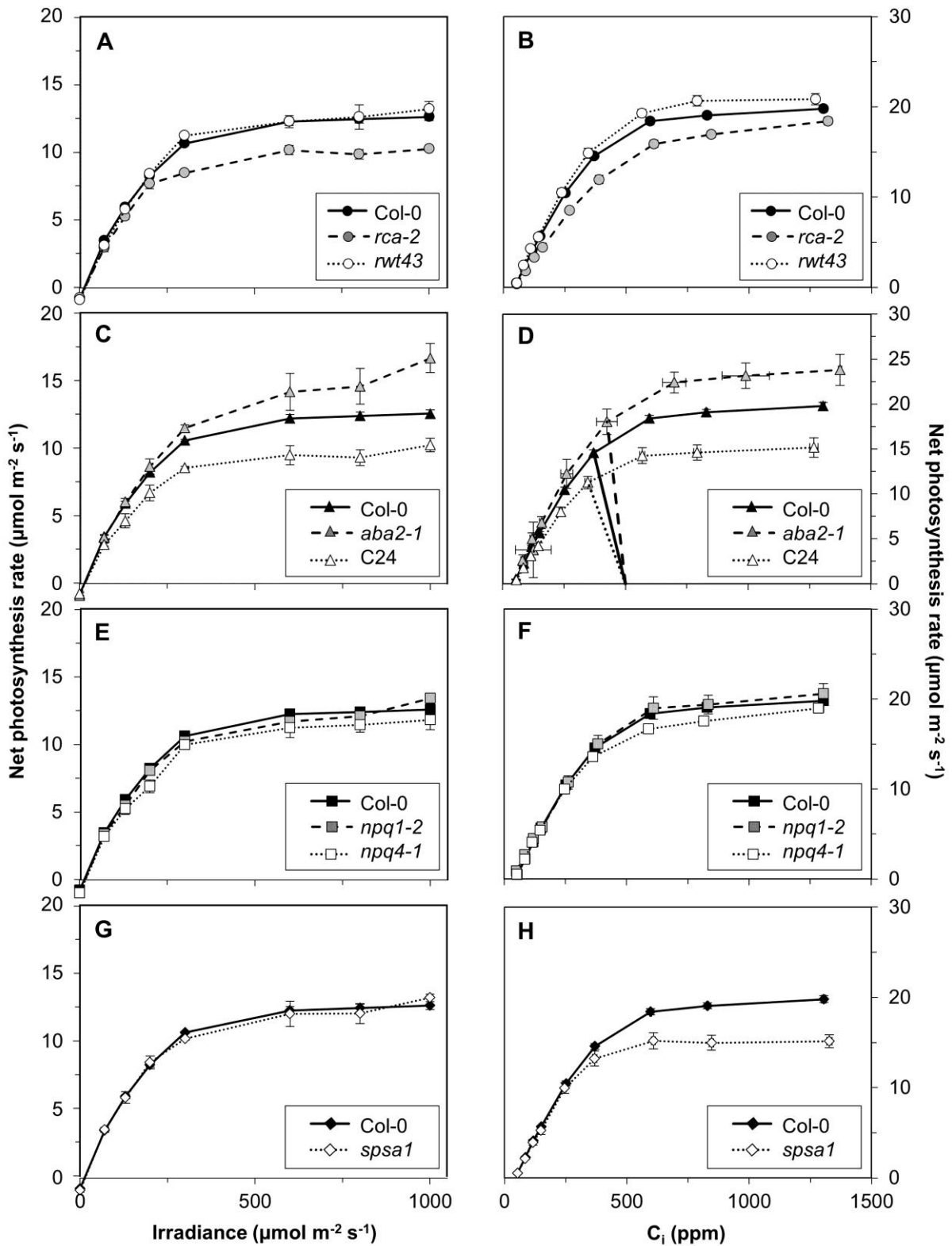


Fig. 6.2. Irradiance (A, C, E, G) and  $\text{CO}_2$  response (B, D, F, H) of net photosynthesis rates in *rca-2* and *rwt43* (A, B), *aba2-1* and C24 (C, D), *npq1-2* and *npq4-1* (E, F) and *spsa1* (G, H). Col-0 is included in each subplot for ease of comparison. In D), supply lines (Farquhar & Sharkey, 1982) between  $C_a = 500$  and the corresponding  $A_n/C_i$  relationships are shown to emphasize stomatal effects of *aba2-1*, C24 and Col-0 on  $C_i$ . Averages  $\pm$  SEM,  $n = 5-15$

Table 6.1. Parameters derived from  $A_n/C_i$  curves.  $V_{cmax}$ , maximum carboxylation rate by Rubisco ( $\mu\text{mol CO}_2 \text{ m}^{-2} \text{ s}^{-1}$ );  $J_{max}$ , maximum rate of electron transport in the absence of regulation ( $\mu\text{mol electrons m}^{-2} \text{ s}^{-1}$ ); TPU, maximum rate of triose phosphate utilisation ( $\mu\text{mol CO}_2 \text{ m}^{-2} \text{ s}^{-1}$ ). The sum of squares of the differences between measurement and model during curve fitting (Sharkey *et al.*, 2007) is shown as an estimation of the overall goodness of fit. Averages  $\pm$  SEM,  $n = 5-15$ . Stars within columns denote significance levels compared to Col-0: \*\*\* =  $P < 0.0001$ , \*\* =  $P < 0.01$ , \* =  $P < 0.05$ . Absence of stars denotes lack of significant difference with Col-0

	$V_{cmax}$	$J_{max}$	TPU	Sum of squares
Col-0	54 $\pm$ 1	103 $\pm$ 2	7.3 $\pm$ 0.1	4.2 $\pm$ 0.4
<i>rca-2</i>	41 $\pm$ 2 ***	88 $\pm$ 2 ***	6.8 $\pm$ 0.1 *	4.1 $\pm$ 1.0
<i>rwt43</i>	60 $\pm$ 3	111 $\pm$ 3 *	7.7 $\pm$ 0.2	5.2 $\pm$ 0.3
<i>aba2-1</i>	61 $\pm$ 3 *	123 $\pm$ 7 ***	8.8 $\pm$ 0.6 **	6.8 $\pm$ 1.3 *
C24	45 $\pm$ 2 **	81 $\pm$ 5 ***	5.6 $\pm$ 0.4 ***	2.4 $\pm$ 0.5 *
<i>npq1-2</i>	55 $\pm$ 3	106 $\pm$ 6	7.6 $\pm$ 0.4	8.1 $\pm$ 1.3 **
<i>npq4-1</i>	55 $\pm$ 1	96 $\pm$ 2	7.1 $\pm$ 0.2	5.2 $\pm$ 0.7
<i>spsa1</i>	57 $\pm$ 5	89 $\pm$ 5 **	5.7 $\pm$ 0.3 ***	3.8 $\pm$ 0.5

$C_i$  in Col-0 and *rwt43* dropped by  $\sim 130$  ppm within 10 minutes and then increased by 30-40 ppm following stomatal opening, in *rca-2* it never dropped below its final value (Fig. 6.4A). Diffusional limitation reached its maximum within  $\sim 10$  minutes in Col-0 and *rwt43* and then relaxed, while in *rca-2* its increase was much slower and levelled off after  $\sim 30$  minutes (Fig. 6.4C). Biochemical limitation during induction relaxed almost completely within  $\sim 10$  minutes in Col-0 and *rwt43*, while in *rca-2* it was generally greater and the same extent of relaxation took  $\sim 40$  minutes (Fig. 6.4E). Comparing Col-0 and C24, the responses of  $C_i$  were indistinguishable, while in *aba2-1* the initial decrease in  $C_i$  was smaller, ranging from 50-60% of that found in Col-0 (Fig. 6.4B). Buildup and relaxation of diffusional limitation were much smaller in *aba2-1* (Fig. 6.4D), while relaxation of biochemical limitation was similar between Col-0, *aba2-1* and C24 (Fig. 6.4F).

The relative responses of  $A_n$  after intermediate irradiance increases ( $70 \rightarrow 800$  and  $130 \rightarrow 600 \mu\text{mol m}^{-2} \text{ s}^{-1}$ ) were qualitatively similar to those after the  $0 \rightarrow 1000 \mu\text{mol m}^{-2} \text{ s}^{-1}$  increase (Fig. S6.5). *rwt43* exhibited a faster increase, and *rca-2* a much slower increase than Col-0 (Fig. S56.A-B). This reduced  $t_{A50}$ , but not  $t_{A90}$ , in *rwt43*, while  $t_{A50}$  and  $t_{A90}$  in *rca-2* were larger than Col-0 (Table 6.2). C24 tended to increase photosynthesis more slowly compared to Col-0 (Fig. S56.C-D), leading to a larger  $t_{A50}$  after the  $70 \rightarrow 800 \mu\text{mol m}^{-2} \text{ s}^{-1}$  step increase and larger  $t_{A50}$  and  $t_{A90}$  after the  $130 \rightarrow 600 \mu\text{mol m}^{-2} \text{ s}^{-1}$  step increase (Table 6.2). Assimilation responses in NPQ and SPS mutants to intermediate irradiance increases were similar to Col-0.

Dark-adapted  $F_v/F_m$  was  $0.805 \pm 0.002$  (Avg  $\pm$  SEM) in Col-o. In *rca-2*, C24 and *npq4-1*,  $F_v/F_m$  was marginally, but significantly, smaller while in *spsa1* it was slightly but significantly higher than in Col-o (Fig. S6.6). Changes in  $\Phi_{PSII}$  after  $0 \rightarrow 1000 \mu\text{mol m}^{-2} \text{s}^{-1}$  in-

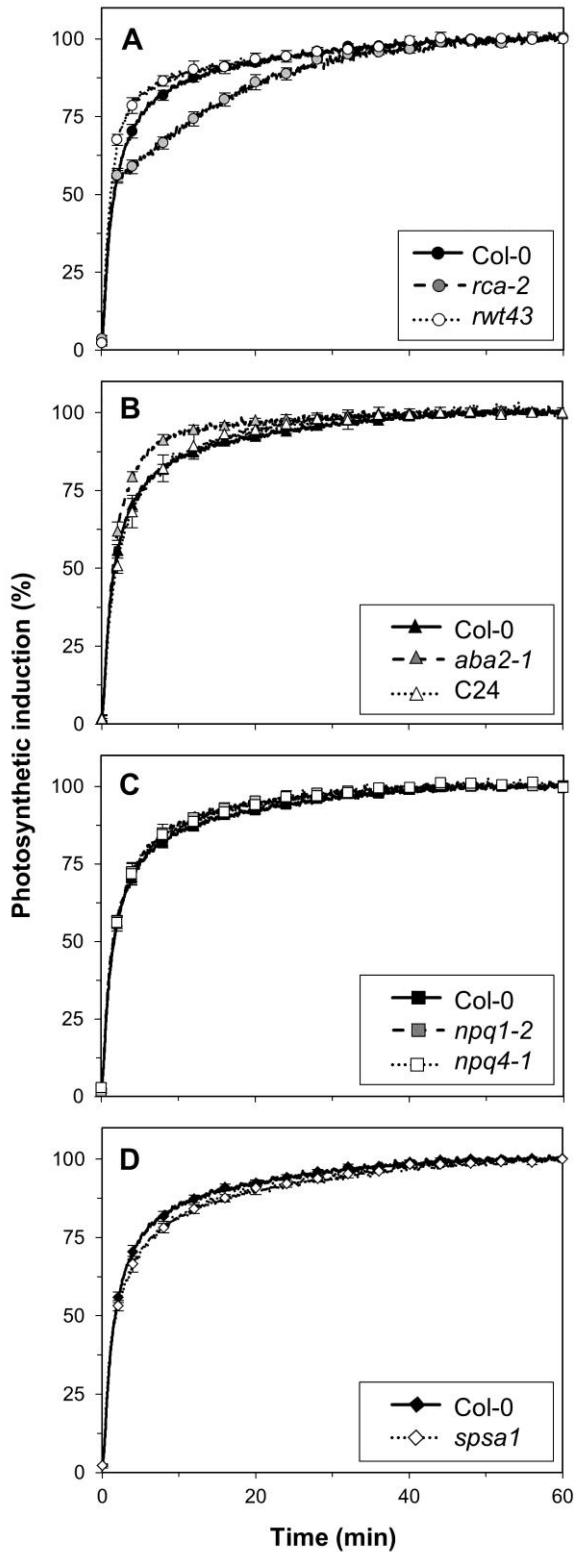


Fig. 6.3. Relative response of photosynthesis to a step increase in irradiance from 0 to  $1000 \mu\text{mol m}^{-2} \text{s}^{-1}$  in *rca-2* and *rwt43* (A), *aba2-1* and C24 (B), *npq1-2* and *npq4-1* (C) and *spsa1* (D). Col-0 is included in each subplot for ease of comparison. Averages  $\pm$  SEM,  $n = 5-15$



Table 6.2. Time (minutes) to reach 50 and 90% of steady-state photosynthesis rates ( $t_{A50}$ ,  $t_{A90}$ ) after step increases in irradiance. Averages  $\pm$  SEM,  $n = 5-15$ . Stars within columns denote significance levels compared to Col-0: \*\*\* =  $P < 0.0001$ , \*\* =  $P < 0.01$ , \* =  $P < 0.05$ . Absence of stars denotes lack of significant difference with Col-0

Genotype	0 $\rightarrow$ 1000 $\mu\text{mol m}^{-2} \text{s}^{-1}$		70 $\rightarrow$ 800 $\mu\text{mol m}^{-2} \text{s}^{-1}$		130 $\rightarrow$ 600 $\mu\text{mol m}^{-2} \text{s}^{-1}$	
	$t_{A50}$	$t_{A90}$	$t_{A50}$	$t_{A90}$	$t_{A50}$	$t_{A90}$
Col-0	1.6 $\pm$ 0.1	14.7 $\pm$ 1.2	1.3 $\pm$ 0.1	10.2 $\pm$ 1.1	0.6 $\pm$ 0.0	9.0 $\pm$ 2.2
<i>rca-2</i>	1.5 $\pm$ 0.2	25.5 $\pm$ 1.5 ***	6.3 $\pm$ 0.4 ***	30.9 $\pm$ 2.0 ***	4.0 $\pm$ 0.7 ***	29.8 $\pm$ 1.7 ***
<i>rwt43</i>	1.2 $\pm$ 0.1 **	14.2 $\pm$ 2.6	0.5 $\pm$ 0.0 ***	16.2 $\pm$ 6.1	0.3 $\pm$ 0.0 ***	18.8 $\pm$ 6.1
<i>aba2-1</i>	1.4 $\pm$ 0.1	7.3 $\pm$ 0.5 **	1.3 $\pm$ 0.1	7.7 $\pm$ 2.6	0.8 $\pm$ 0.1	15.1 $\pm$ 5.8
C24	1.9 $\pm$ 0.1	15.0 $\pm$ 3.2	1.7 $\pm$ 0.3 *	13.3 $\pm$ 2.7	0.9 $\pm$ 0.2 *	29.4 $\pm$ 5.1 ***
<i>npq1-2</i>	1.4 $\pm$ 0.1	11.7 $\pm$ 1.7	1.3 $\pm$ 0.1	10.7 $\pm$ 2.9	0.7 $\pm$ 0.0	14.6 $\pm$ 8.6
<i>npq4-1</i>	1.5 $\pm$ 0.1	14.8 $\pm$ 2.6	1.1 $\pm$ 0.1	6.1 $\pm$ 0.7	0.6 $\pm$ 0.0	15.3 $\pm$ 11.0
<i>spsa1</i>	1.6 $\pm$ 0.1	19.5 $\pm$ 1.3 *	1.3 $\pm$ 0.1	14.1 $\pm$ 7.2	0.6 $\pm$ 0.1	13.7 $\pm$ 6.9

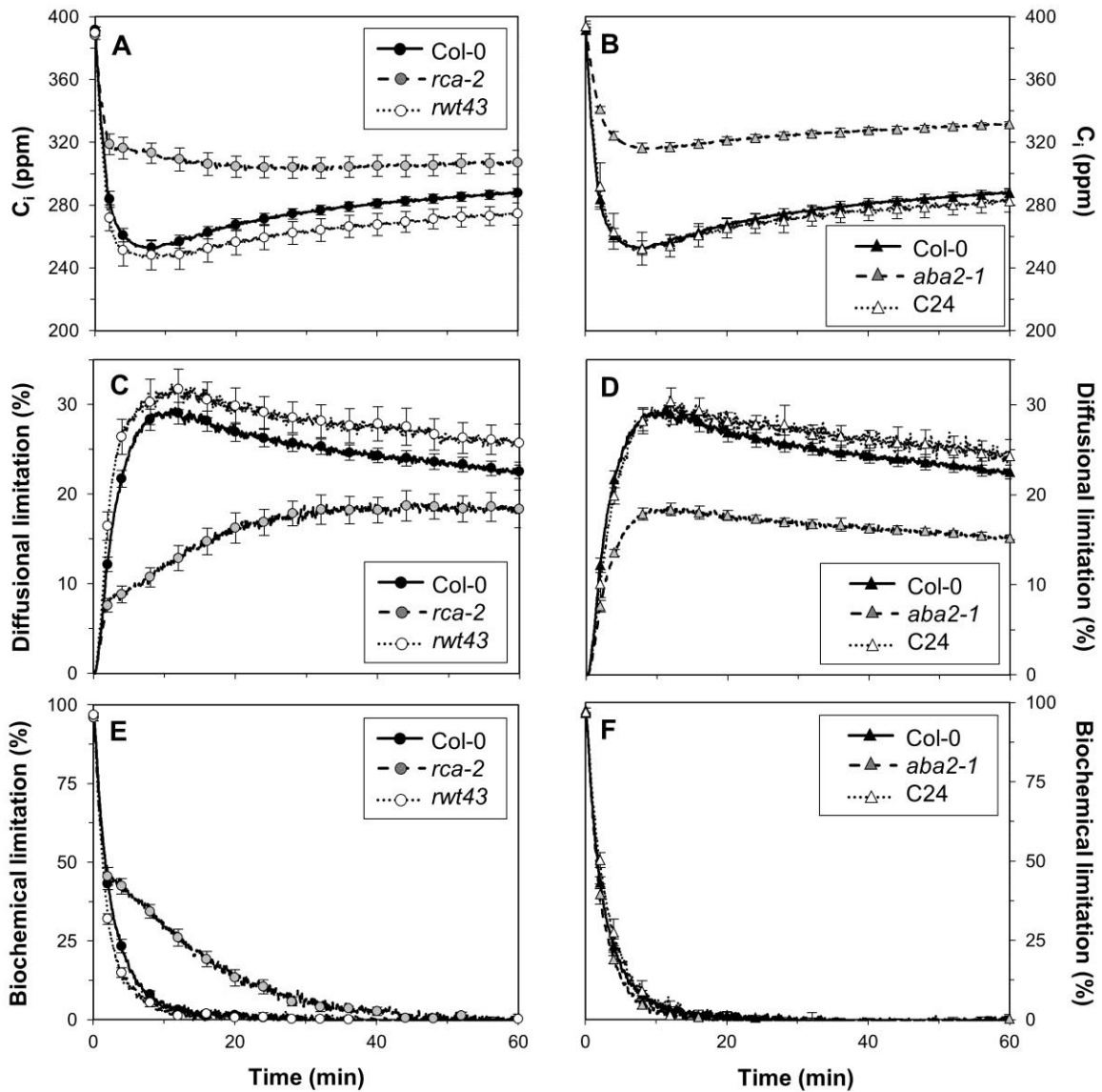


Fig. 6.4. Leaf internal CO<sub>2</sub> concentration (C<sub>i</sub>), diffusional limitation and biochemical limitation after a step increase in irradiance from 0 to 1000  $\mu\text{mol m}^{-2} \text{s}^{-1}$  in Col-0, *rca-2* and *rwt43* (A, C, E) and Col-0, *aba2-1* and C24 (B, D, F). Averages  $\pm$  SEM,  $n = 5-15$

creases largely paralleled those of  $A_n$  (Fig. 6.5). In *rwt43*, the increase in  $\Phi_{\text{PSII}}$  was slightly faster than in Col-o, while in *rca-2*, it was slower and steady-state  $\Phi_{\text{PSII}}$  was lower (Fig. 6.5A), paralleling its lower steady-state  $A_n$  (Fig. 6.2A). *aba2-1* showed increased steady-state  $\Phi_{\text{PSII}}$  levels, while in C24 they were reduced compared to Col-o (Fig. 6.5C), similar to the differences in steady-state assimilation (Fig. 6.2C). In *npq4-1*,  $\Phi_{\text{PSII}}$  was slightly smaller during induction than in *npq1-2* and Col-o (which were not different from each other). Despite slightly larger  $\Phi_{\text{PSII}}$  throughout induction in *spsa1*, final values were not significantly different from Col-o ( $P = 0.09$ , Fig. 6.5G). Gross photosynthesis rate ( $A_{\text{gr}}$ ) showed a linear or slightly curvilinear relationship with electron transport rate (ETR) during induction, with the curvilinearity being greatest at the beginning of induction. Considering that these first values of the  $A_{\text{gr}}/\text{ETR}$  relationship coincided with high  $C_i$ , this explains the initially higher irradiance use efficiency during early stages of induction. Genotypes differing in Rca, NPQ or SPS had similar  $A_{\text{gr}}/\text{ETR}$  relationships (Fig. S6.7). Amongst the genotypes affecting  $g_s$ , *aba2-1* showed higher  $A_{\text{gr}}$  for the same ETR than Col-o, which in turn exhibited a higher  $A_{\text{gr}}$  than C24 (Fig. S6.7B). This reflects differences in  $C_i$  between those genotypes.

Non-photochemical quenching (NPQ) in *rca-2* increased more quickly to its steady-state level, which was larger than that of Col-o and *rwt43* (Fig. 6.5B). NPQ in *aba2-1* was lower than in Col-o and C24 (which were not significantly different from each other, Fig. 6.5D). As expected, *npq1-2* and *npq4-1* developed much lower NPQ levels than Col-o, and the time-course of NPQ buildup was slower compared to Col-o, but similar in both *npq1-2* and *npq4-1* (Fig. 6.5F). There was no difference between *spsa1* and Col-o (Fig. 6.5H).

#### *Apparent time constants of Rubisco activation*

The apparent time constants of Rubisco activation ( $\tau_R$ ), denoting the time to reach 63% of total change in Rubisco activation state, decreased with increasing background irradiance (Fig. 6.6). Genotypes differing in  $g_s$ , NPQ and SPS did not differ in  $\tau_R$  (data not shown). However,  $\tau_R$  tended to be larger in *spsa1* than in Col-o;  $P$ -values ranged from 0.07 to 0.09. Of the genotypes affecting Rca regulation, *rca-2* exhibited the biggest differences in  $\tau_R$ , both compared with Col-o ( $P < 0.001$  in all cases) and between background irradiances, with  $\sim 22$  minutes in dark-adapted leaves to  $\sim 4$  minutes at  $130 \mu\text{mol m}^{-2} \text{s}^{-1}$  (Fig. 6.6A). In *rwt43*,  $\tau_R$  of dark-adapted leaves was not significantly different to that of Col-o, but was significantly ( $P < 0.001$ ) smaller at 70 and  $130 \mu\text{mol m}^{-2} \text{s}^{-1}$  background irradiance (Fig. 6.6B).

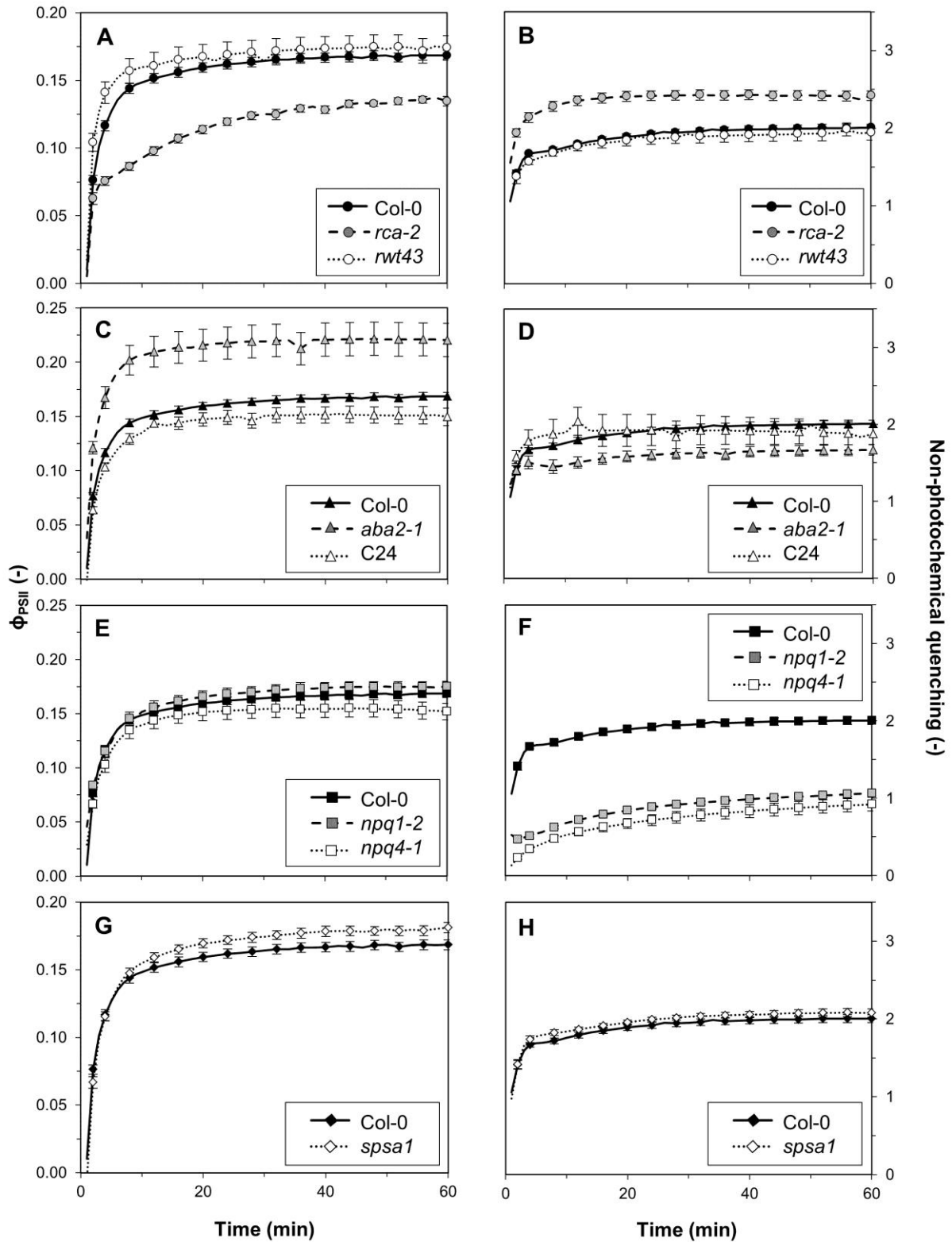


Fig. 6.5. Quantum yield of photosystem II ( $\Phi_{\text{PSII}}$ ) and non-photochemical quenching (NPQ) after a step increase in irradiance from 0 to  $1000 \mu\text{mol m}^{-2} \text{s}^{-1}$  in *rca-2* and *rwt43* (A, B), *aba2-1* and C24 (C, D), *npq1-2* and *npq4-1* (E, F) and *spsa1* (G, H). Col-0 is included in each subplot for ease of comparison. Averages  $\pm$  SEM,  $n = 5-15$

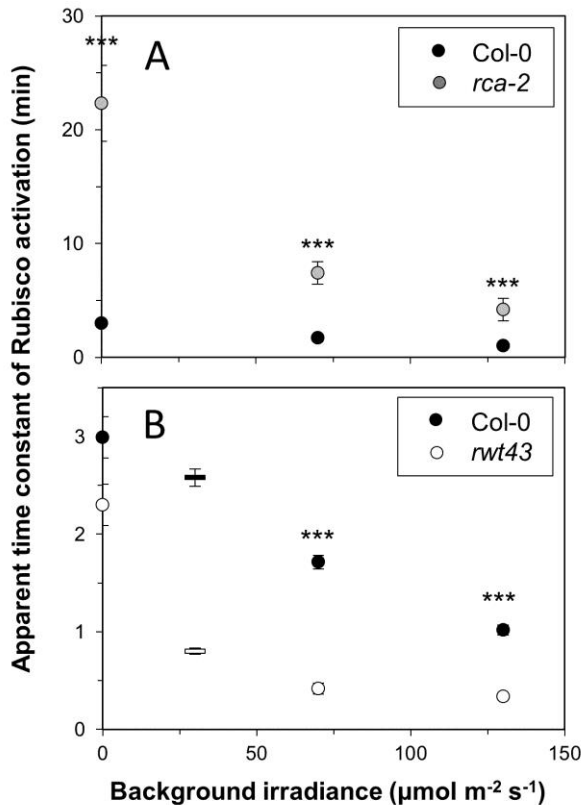


Fig. 6.6. Apparent time constant of Rubisco activation in *rca-2* (A) and *rwt43* (B), compared to Col-0. Note the different scales of Y-axes in A) and B). Averages  $\pm$  SEM,  $n = 5-15$ . Bars in B) at  $30 \mu\text{mol m}^{-2} \text{s}^{-1}$  background irradiance included from Carmo-Silva and Salvucci (2013). Stars denote significance levels of single genotypes compared to Col-0: \*\*\* =  $P < 0.001$

### *Stomatal limitations after irradiance increases*

Before and after stepwise increases in irradiance,  $g_s$  was considerably higher in *aba2-1* than in Col-0 and C24 (Fig. S6.8). In dark-adapted leaves of Col-0 and C24,  $g_s$  was similar (Fig. S6.8A), but in leaves adapted to 70 or  $130 \mu\text{mol m}^{-2} \text{s}^{-1}$ , it was almost twice as high in Col-0 compared to C24 (Fig S6.8B-C). This spread in  $g_s$  was used to explore the transition from limiting to non-limiting initial  $g_s$  for the rates of photosynthesis increase. For example, after the  $0 \rightarrow 1000 \mu\text{mol m}^{-2} \text{s}^{-1}$  increase,  $t_{A90}$  decreased with increases in initial  $g_s$  up to  $\sim 0.13 \text{ mol m}^{-2} \text{s}^{-1}$ , but when initial  $g_s$  was higher,  $t_{A90}$  did not decrease any further (Fig. 6.7). This shows that initial  $g_s > 0.13 \text{ mol m}^{-2} \text{s}^{-1}$  was non-limiting in this case. A split-line analysis was applied to investigate the relationship of initial  $g_s$  with the relative increase in  $A_n$  at specific time points after irradiance increases. Generally, the fit of the regression increased with the percentage of final  $A_n$  (Fig. 6.8A). In dark-adapted leaves, the variance accounted for by the split-line regression was higher towards the end of photosynthetic induction (50-90% of steady-state  $A_n$ ), than at 70 or  $130 \mu\text{mol m}^{-2} \text{s}^{-1}$  background irradiance (Fig 6.8A). The transition from limiting to non-limiting initial  $g_s$  was remarkably robust between between 0.09 and  $0.17 \text{ mol m}^{-2} \text{s}^{-1}$  (Fig. 6.8B).

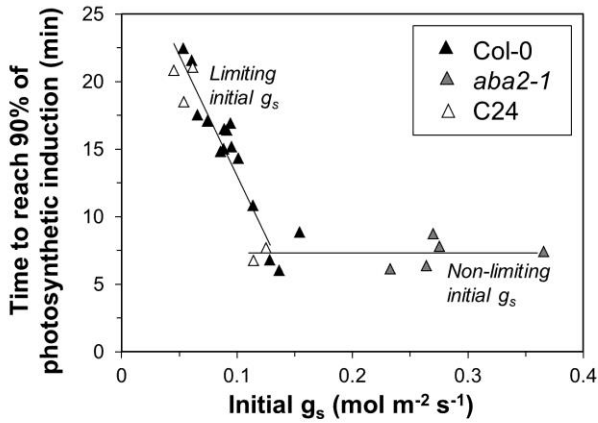


Fig. 6.7. Relationship between initial  $g_s$  and the time to reach 90% of final photosynthesis rates after a step increase in irradiance ( $0-1000 \mu\text{mol m}^{-2} \text{s}^{-1}$ ) in single replicates of Col-0, *aba2-1* and C24

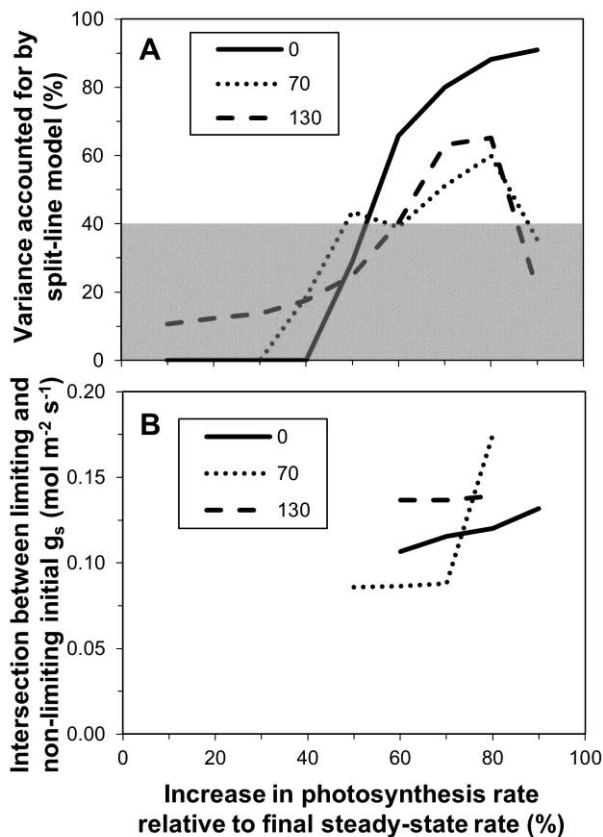


Fig. 6.8. Results of split-line regression analysis between initial  $g_s$  and time to reach 10 to 90% of steady-state photosynthesis rates of leaves in 0, 70 and  $130 \mu\text{mol m}^{-2} \text{s}^{-1}$  background irradiance. A) Percentage of variance accounted for by the split-line regression, versus the percentage increase in final photosynthesis rate. The shaded area represents the range that was deemed unreliable for calculations of parameters. B) Intersection point between the horizontal and non-horizontal line on the X-axis ( $g_s$ )

After the  $0 \rightarrow 1000 \mu\text{mol m}^{-2} \text{s}^{-1}$  increase,  $g_s$  increased (Fig. S6.8A). In C24 and Col-0, stomatal opening and  $t_{A90}$  correlated positively (Fig. 6.9). Because initial  $g_s$  in *aba2-1* was high, it was non-limiting to rates of increase in photosynthesis after irradiance increases, and stomatal opening did not correlate with  $t_{A90}$  (data not shown).

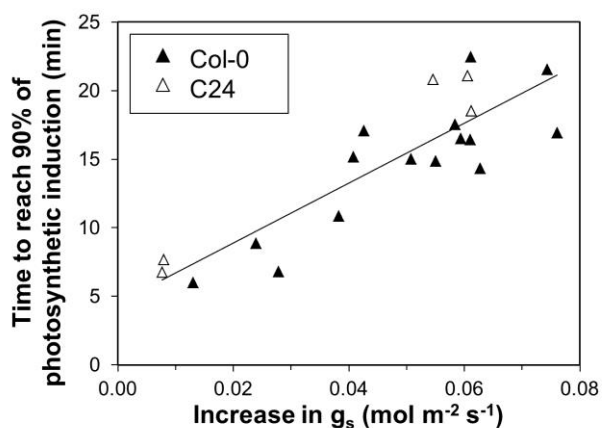


Fig. 6.9. Relationship between the increase in  $g_s$  and the time to reach 90% of final photosynthesis rates after a step increase in irradiance ( $0-1000 \mu\text{mol m}^{-2} \text{s}^{-1}$ ) in single replicates of Col-0 and C24 ( $R^2 = 0.75$ )

### *Responses to stepwise decreases in irradiance*

After step decreases in irradiance ( $600 \rightarrow 200$ ,  $800 \rightarrow 130 \mu\text{mol m}^{-2} \text{s}^{-1}$ ), relative changes in transient photosynthesis rates were similar between genotypes (Fig. S6.9), and there were no significant differences in either post-illumination  $\text{CO}_2$  fixation or the post-illumination  $\text{CO}_2$  burst (data not shown), including the NPQ mutants (Fig. 6.10).

### *Lightfleck use efficiency (LFUE)*

The only genotypes showing significant differences in LFUE, compared to Col-0, were *rca-2* and *aba2-1* (Table 6.3). In low and intermediate amplitudes in irradiance ( $50$  and  $100 \mu\text{mol m}^{-2} \text{s}^{-1}$ ), *rca-2* showed higher LFUE than Col-0 regardless of cycle duration. In short and intermediate lightflecks ( $10$  and  $60$  s cycles) this difference was attributable to a higher partial LFUE both in high-irradiance and low-irradiance half-cycles. In long lightflecks ( $120$  s cycles) of low and intermediate amplitudes, partial LFUE was higher only in low-irradiance half-cycles. In lightflecks with high amplitude ( $250 \mu\text{mol m}^{-2} \text{s}^{-1}$ ) and short or intermediate duration, LFUE was reduced in *rca-2*, which was attributable to either lower partial LFUE in high-irradiance half-cycles ( $60$  s cycles) or low-irradiance half-cycles ( $10$  s cycles). LFUE in long cycles with  $250 \mu\text{mol m}^{-2} \text{s}^{-1}$  amplitude was similar between Col-0 and *rca-2*, but *rca-2* showed significantly higher LFUE during low-irradiance half cycles and significantly lower LFUE in high-irradiance half cycles, the relative gain in low irradiance offsetting the relative loss in high irradiance. *aba2-1* had significantly higher LFUE in long lightflecks of intermediate amplitude ( $120$  s,  $100 \mu\text{mol m}^{-2} \text{s}^{-1}$ ), which was caused by a higher partial LFUE in high irradiance, but not in low irradiance. *aba2-1* showed higher partial LFUE during the high irradiance portion of long lightflecks in all amplitudes.

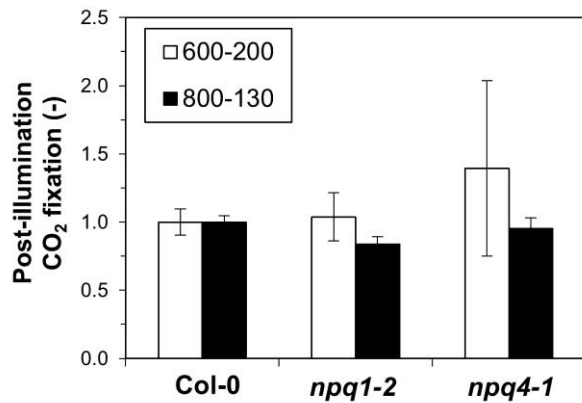


Fig. 6.10. Relative post-illumination CO<sub>2</sub> fixation in Col-0, *npq1-2* and *npq4-1*. Values are expressed relative to Col-0, which was  $52 \pm 5 \mu\text{mol m}^{-2}$  after  $600 \rightarrow 200 \mu\text{mol m}^{-2} \text{ s}^{-1}$  step decreases (white bars) and  $76 \pm 3 \mu\text{mol m}^{-2}$  after  $800 \rightarrow 130 \mu\text{mol m}^{-2} \text{ s}^{-1}$  step decreases (black bars). Averages  $\pm$  SEM,  $n = 5-15$

Table 6.3. Lightfleck use efficiency (LFUE, %) of Col-0, *rca-2* and *aba2-1*. Averages  $\pm$  SEM,  $n = 5-15$ . Stars denote significance levels within rows compared to Col-0: \*\*\* =  $P < 0.0001$ , \*\* =  $P < 0.01$ , \* =  $P < 0.05$ . Absence of stars denotes lack of significant difference with Col-0

	Amplitude (PAR)	Duration (s)	Col-0			<i>rca-2</i>			<i>aba2-1</i>		
Full lightfleck	50	10	100.9	$\pm$ 0.3	104.2	$\pm$ 2.5	*	101.9	$\pm$ 0.9		
	50	60	99.3	$\pm$ 0.3	102.7	$\pm$ 2.0	*	100.6	$\pm$ 0.7		
	50	120	98.7	$\pm$ 0.2	101.2	$\pm$ 1.6	*	100.0	$\pm$ 0.5	**	
	100	10	98.4	$\pm$ 0.4	102.6	$\pm$ 3.2	*	97.9	$\pm$ 0.7		
	100	60	94.7	$\pm$ 0.3	98.8	$\pm$ 2.3	**	94.2	$\pm$ 0.7		
	100	120	94.3	$\pm$ 0.3	97.7	$\pm$ 2.0	**	93.5	$\pm$ 0.7		
	250	10	80.5	$\pm$ 0.7	77.6	$\pm$ 0.6	*	80.6	$\pm$ 1.0		
	250	60	65.5	$\pm$ 0.6	60.4	$\pm$ 0.6	***	67.2	$\pm$ 1.7		
	250	120	61.7	$\pm$ 0.5	60.6	$\pm$ 0.7		63.5	$\pm$ 1.5		
Half lightfleck: PAR increases	50	10	100.3	$\pm$ 0.3	103.8	$\pm$ 2.4	*	101.4	$\pm$ 1.0		
	50	60	100.6	$\pm$ 0.3	103.5	$\pm$ 1.9	*	101.9	$\pm$ 0.7		
	50	120	102.8	$\pm$ 0.2	103.1	$\pm$ 1.7		105.9	$\pm$ 0.4	***	
	100	10	97.3	$\pm$ 0.4	101.4	$\pm$ 3.0	*	96.3	$\pm$ 0.7		
	100	60	97.6	$\pm$ 0.3	100.9	$\pm$ 2.4	*	97.3	$\pm$ 1.0		
	100	120	103.0	$\pm$ 0.3	102.3	$\pm$ 1.8		105.4	$\pm$ 1.7	*	
	250	10	77.0	$\pm$ 0.7	74.5	$\pm$ 0.5		76.7	$\pm$ 0.8		
	250	60	76.4	$\pm$ 0.7	66.5	$\pm$ 0.6	***	78.6	$\pm$ 2.9		
	250	120	90.3	$\pm$ 0.5	83.2	$\pm$ 0.8	***	94.7	$\pm$ 3.3	*	
	Half lightfleck: PAR decreases	50	10	101.3	$\pm$ 0.3	105.0	$\pm$ 2.5	*	102.6	$\pm$ 0.9	
50		60	98.0	$\pm$ 0.3	101.9	$\pm$ 2.0	**	99.2	$\pm$ 0.8		
50		120	94.7	$\pm$ 0.3	99.3	$\pm$ 1.6	***	94.2	$\pm$ 1.1		
100		10	99.5	$\pm$ 0.4	103.9	$\pm$ 3.0	*	99.0	$\pm$ 0.7		
100		60	91.7	$\pm$ 0.4	96.7	$\pm$ 2.3	**	91.2	$\pm$ 0.6		
100		120	85.6	$\pm$ 0.4	93.1	$\pm$ 2.2	***	81.6	$\pm$ 1.2	***	
250		10	83.9	$\pm$ 0.6	79.6	$\pm$ 0.6	**	83.9	$\pm$ 1.3		
250		60	54.6	$\pm$ 0.6	54.3	$\pm$ 0.7		55.9	$\pm$ 0.7		
250		120	33.2	$\pm$ 0.7	38.1	$\pm$ 1.0	**	32.2	$\pm$ 0.8		

## Discussion

Making use of the genetic diversity available for *A. thaliana*, we elucidated several physiological limitations of dynamic photosynthesis. This analysis revealed that altered Rubisco activation kinetics or stomatal conductance affect photosynthesis in a dynamic irradiance environment greatly, while alterations in non-photochemical quenching or sucrose synthesis do not.

### *Rubisco activase concentration and isoform affect dynamic photosynthesis*

Changes affecting Rubisco activase (Rca) concentration (*rca-2*) or isoform (*rwt43*) had strong effects on dynamic photosynthesis. The observed effects were likely caused by different kinetics of Rubisco activation, as the initial increase in assimilation after dark-light transitions (first minute in Fig. 6.3A) was similar between genotypes, implying a similar limitation due to activation of ribulose-1,5-bisphosphate (RuBP) regeneration (Sassenrath-Cole & Pearcy, 1992). Furthermore, these genotypes had similar  $g_s$  (data not shown). Lower steady-state irradiance and CO<sub>2</sub> responses in *rca-2* may have been caused by a reduced steady-state activation of Rubisco (Mate *et al.*, 1993).

Intriguingly,  $\tau_R$  decreased with background irradiance (Fig. 6.6). While this decrease was linear in Col-o, it resembled a negative exponential in *rwt43*. Data obtained from Carmo-Silva and Salvucci (2013) agreed with this pattern (Fig. 6.6B). Rubisco activation states in Col-o increased linearly with irradiance in the range 0-130  $\mu\text{mol m}^{-2} \text{s}^{-1}$  (Brooks & Portis, 1988; Carmo-Silva & Salvucci, 2013; Scales *et al.*, 2014). In *rwt43*, Rubisco activation state was similar to Col-o in dark-adapted leaves, but close to full activation in low irradiance (Zhang *et al.*, 2002; Carmo-Silva & Salvucci, 2013; Scales *et al.*, 2014). Thus, relationships between  $\tau_R$  and background irradiance in Col-o and *rwt43* resemble the inverse of relationships between Rubisco activation state and background irradiance. One interpretation of this phenomenon is that the rate of Rubisco activation, when limited by Rca, depends on the total difference in activation states of Rubisco before and after irradiance increases (Woodrow *et al.*, 1996), and on the amount of activase. Another interpretation is that differences in the activity of Rca, rather than that of Rubisco, caused  $\tau_R$  to decrease with background irradiance. Rca activity increased linearly between 0 and 300  $\mu\text{mol m}^{-2} \text{s}^{-1}$  in intact spinach leaves (Lan *et al.*, 1992), and should be high in *rwt43* except in darkness (see above). The mechanism(s) behind the  $\tau_R$  - background irradiance relationship require further research.

Even though photosynthesis in *rwt43* increased more quickly after step increases in irradiance (Fig. S6.5), its LFUE was not higher than that of Col-o. This may be because at 300  $\mu\text{mol m}^{-2} \text{s}^{-1}$ , Rubisco activation state is high in Col-o (Brooks & Portis, 1988), and



because the periods of low irradiance between lightflecks were short (the longest gap was 60 s). With a  $\tau$  of 22-30 minutes for Rubisco deactivation (Percy, 1990; Percy *et al.*, 1997), the Rubisco activity in Col-o would have decreased by only ~2-4% in 60 s, which may not affect  $A_n$ . Additionally, after small changes in Rubisco activity, its activation kinetics are thought to be limited by carbamylation rather than the action of Rca (Woodrow *et al.*, 1996). In contrast to *rwt43*, *rca-2* showed increased LFUE in lightflecks of small amplitudes, which was probably caused by post-lightfleck enhancement of carbon fixation. In long lightflecks with high amplitude, increased post-illumination CO<sub>2</sub> fixation may have compensated for losses during high irradiance. Considering that absolute steady-state  $A_n$  before the start of lightfleck sequences were lower in *rca-2* than in Col-o (Fig. 6.2A), we believe that the Rubisco activation state was also lower. The Rubisco activation state affects RuBP concentrations: In a null mutant of Rca (*rca*), RuBP pools were 3-7 times larger than in Col-o (Zhang *et al.*, 2002). Also, in *rwt43* in low irradiance, RuBP pools were 2-3 times lower than in Col-o (Carmo-Silva & Salvucci, 2013). Since the concentration of RuBP and other metabolites affects post-illumination CO<sub>2</sub> fixation (Sharkey *et al.*, 1986), a lower activation state of Rubisco, leading to a higher concentration of RuBP, could result in a higher post-illumination CO<sub>2</sub> fixation in *rca-2* compared to Col-o. In summary, redox-regulation of the  $\alpha$ -isoform of Rca in the wildtype decreases dynamic photosynthesis, but not when time in low irradiance is short or in dark-adapted leaves. Furthermore, decreased Rca concentration leads to slower Rubisco activation and higher LFUE, most likely due to enhanced post-illumination CO<sub>2</sub> fixation.

#### *High initial $g_s$ increases dynamic photosynthesis*

Genotypes with different  $g_s$ , *aba2-1* and C24, had steady-state characteristics that differed from those of Col-o. While the steady-state irradiance response (Fig. 6.2C) may partly be attributed to differences in  $g_s$ , the  $C_i$  response (Fig. 6.2D; Table 6.1) cannot, as differences in  $g_s$  are included in the value of  $C_i$ . Thus, not only stomatal, but also biochemical characteristics may differ between these genotypes. Also,  $g_m$  may have been affected, as it has been observed to scale with  $g_s$  (Flexas *et al.*, 2013a). Furthermore, higher  $C_i$  (due to higher  $g_s$ ) likely decreased photorespiration. This was visible from higher  $A_{gr}$  in *aba2-1* compared to C24, at identical ETR (Fig. S6.7). This could mean that photosynthetic responses to fluctuating irradiance were partially affected by differences in leaf biochemistry or diffusivity, potentially making the interpretation of our data more difficult. However, because biochemical limitations during induction (Fig. 6.4F) and  $\tau_R$  after step increases in irradiance were similar between those genotypes, we believe that the

differences after increases in irradiance and during lightflecks can indeed be attributed to differences in  $g_s$  (Fig. S6.8).

Compared to natural fluctuations in irradiance, stomata open and close slowly (Fay & Knapp, 1993). Low initial  $g_s$  can become a limitation to carbon fixation after a step change in irradiance (Percy, 1990), because of comparably rapid activation of RuBP regeneration and Rubisco. The peak of this limitation is typically reached within ~10 minutes due to Rubisco activation without similarly large increases in  $g_s$ , after which it relaxes due to stomatal opening (Fig. 6.4D). The mutant with high initial  $g_s$  (*aba2-1*) did not show such large differences in stomatal opening, but still had much higher rates of  $A_n$  increases when irradiance was raised. Additionally, *aba2-1* had a higher LFUE during the high irradiance half-cycle of lightflecks. Therefore, we argue that initial  $g_s$  is more important for dynamic photosynthesis than rapid stomatal opening. Also, the transition between limiting and non-limiting  $g_s$  for rates of photosynthesis increase could be used as a phenotypic marker, to be used for breeding of cultivars with non-limiting  $g_s$  in fluctuating irradiance. It proved to be consistent at different time points of increases in photosynthesis rates and between background irradiances (Fig. 6.8B). Previous findings indicate that this transition shows no diurnal variation (Allen & Percy, 2000a), and that it is unchanged by water stress (Allen & Percy, 2000a) or growth light conditions (Valladares *et al.*, 1997). An open question that remains is whether this transition is species-specific (Allen & Percy, 2000) or not (Valladares *et al.*, 1997). Very likely, high initial  $g_s$  correlates with constitutively high  $g_s$ , and higher dynamic photosynthesis rates could be reached at a lower intrinsic water use efficiency ( $WUE_i$ ). Rapid screening for high  $g_s$  could be achieved by thermal imaging (McAusland *et al.*, 2013). In summary, wildtype  $g_s$  is limiting for dynamic photosynthesis in *Arabidopsis*, and improvements would be possible but at the expense of  $WUE_i$ .

### *Reduced NPQ does not affect photosynthesis in fluctuating irradiance*

The NPQ mutants *npq1-2* (lacking violaxanthin de-epoxidase, Niyogi *et al.*, 1998) and *npq4-1* (lacking PsbS) exhibited a much lower buildup of NPQ after a dark-light transition. However, they showed negligible differences in gas exchange to Col-0, neither in their steady-state responses to irradiance and CO<sub>2</sub> (Fig. 6.2E-F) nor in their responses to step increases in irradiance (Figs. 6.3C, S6.5E-F). Similar to our findings, reduced PsbS content in transgenic rice plants strongly reduced NPQ but had limited effects on carbon gain during a 5-min induction period (Hubbart *et al.*, 2012). Overexpressors with 2-4 fold increases in PsbS showed ~15% lower  $A_n$  during induction, demonstrating that increased energy dissipation can have adverse effects on assimilation (Hubbart *et al.*, 2012). Recently, *A. thaliana* antisense mutants with reduced thylakoid membrane K<sup>+</sup> flux capacities showed

less rapid relaxation of NPQ after irradiance decreases, reducing electron transport and assimilation (Armbruster *et al.*, 2014). These findings provide empirical proof of the theory put forward by Zhu *et al.* (2004) that slow relaxation of NPQ can reduce  $A_n$  after decreases in irradiance. Importantly, our data revealed no differences between *npq1-2*, *npq4-1* and Col-o with respect to post-illumination CO<sub>2</sub> fixation (Fig. 6.10), and therefore do not seem to support the theory of Zhu *et al.* (2004).

#### *Reduced SPS has negligible effects on photosynthesis in fluctuating irradiance*

The SPS antisense mutant *spsa1* has a 80% lower maximum SPS activity than Col-o (Sun *et al.*, 2011). Similar to our findings, Sun *et al.* (2011) found no photosynthetic differences between *spsa1* and Col-o, except for a strong reduction in CO<sub>2</sub>-saturated  $A_n$  (~23%). Importantly, the decrease in SPS hardly affected photosynthetic responses to fluctuating irradiance. The only significant difference was a longer time to reach 90% of full induction after dark-light transitions (Table 6.2). However, no such differences were observed in transitions from low to higher irradiance. *spsa1* would probably show decreased rates of dynamic photosynthesis in elevated  $C_a$ . Furthermore, it may be that the absence of a measurable effect of *spsa1* on the post-illumination CO<sub>2</sub> burst, which is partly affected by the rate of sucrose synthesis (Prinsley *et al.*, 1986), was masked by the photorespiratory portion of the CO<sub>2</sub> burst, which is most pronounced in C<sub>3</sub> plants (Kaiser *et al.*, 2015). Clearly, wildtype SPS activities are far from limiting for dynamic photosynthesis at ambient CO<sub>2</sub>.

#### *Absence of RuBP-regeneration limitation in $\Phi_{PSII}/C_i$ data*

The relationship between the light-use efficiency of linear electron transport ( $\Phi_{PSII}$ ) and the  $A_n/C_i$  response has three phases: When assimilation is limited by Rubisco,  $\Phi_{PSII}$  increases with  $C_i$ , when it is limited by RuBP regeneration,  $\Phi_{PSII}$  is constant with increases in  $C_i$  and when it is limited by TPU,  $\Phi_{PSII}$  decreases with increasing  $C_i$  (Long & Bernacchi, 2003; Sharkey *et al.*, 2007). Most genotypes in our study did not show the plateau in  $\Phi_{PSII}$  that would signify a phase of RuBP regeneration limitation, with *spsa1* showing an extreme form of that behaviour (Fig. S6.4). This suggests that a) TPU occurs at a lower  $C_i$  than visible from gas exchange, b) different limitations occur simultaneously within different layers of the leaf or c) with increasing  $C_i$  during the phase of limitation by RuBP regeneration photosynthetic electron transport is sometimes restricted, and  $\Phi_{PSII}$  is reduced, due to the increased inhibition of starch synthesis following the inhibition of phosphoglucoisomerase by phosphoglycerate (T. D. Sharkey, pers. comm.). However, these results have to be interpreted with caution because a)  $\Phi_{PSII}$  was not at steady-state at

the time of taking the measurements (this takes ~20 minutes at each CO<sub>2</sub> step; Kaiser *et al.*, unpublished results) and b) more data points between the end of Rubisco limitation and the onset of TPU may lead to different conclusions. We propose that this topic warrants further research.

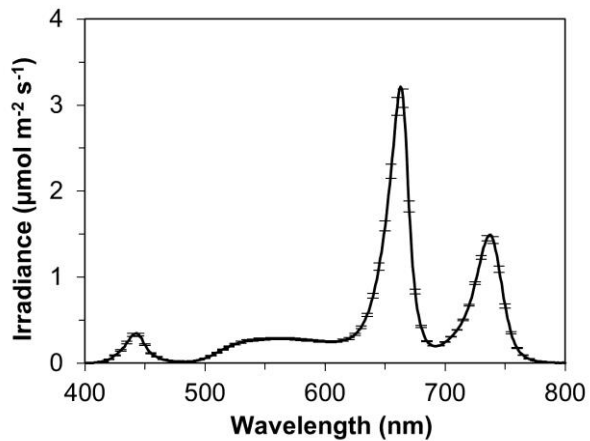
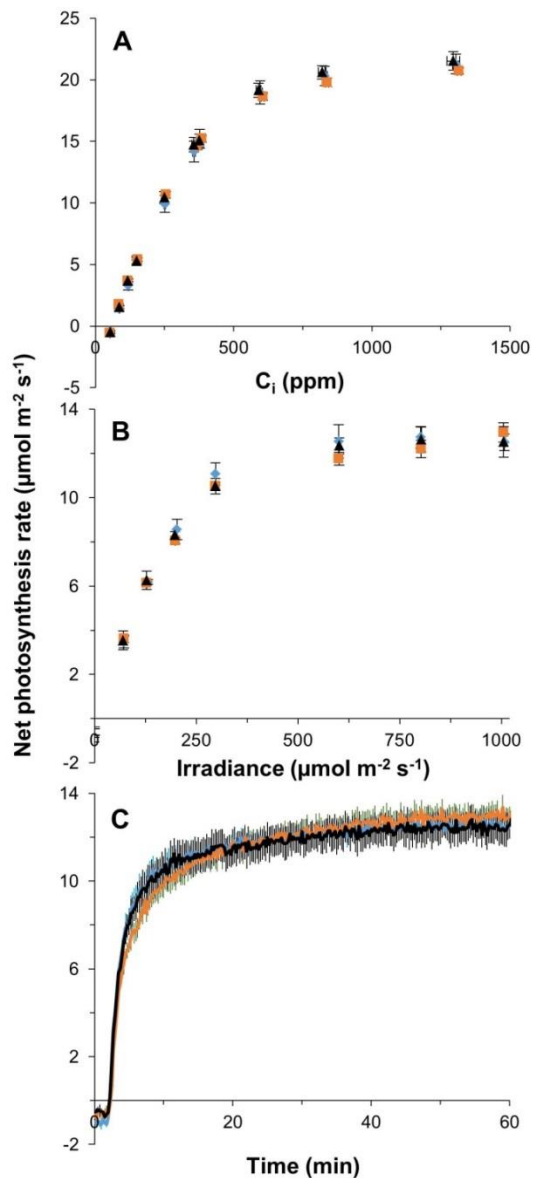
### *Conclusions*

In *A. thaliana*, the presence of the redox-regulated  $\alpha$ -isoform of Rca in the wildtype, and wildtype levels of  $g_s$ , are limiting for dynamic photosynthesis. Furthermore, reductions in Rca strongly decrease dynamic photosynthesis. We also show that wildtype levels of NPQ and SPS are not limiting in *A. thaliana*. This suggests Rca and  $g_s$  as targets for improvement of photosynthesis in fluctuating irradiance.

### **Acknowledgements**

We thank the Nottingham Arabidopsis Stock Centre, Corrie Hanhart, Elizabete Carmo-Silva and Shizue Matsubara for providing *A. thaliana* seeds. Also, we thank Sasan Aliniaiefard for help with the growth system. We thank Shizue Matsubara and Tom Sharkey for helpful discussions. This work was carried out within the BioSolar Cells programme. It was funded by the Dutch Ministry of Economic Affairs and Essent.

## Supplementary material 6.1

Fig. S6.1. Irradiance spectrum in the growth chamber. Average  $\pm$  SEM,  $n = 4$ Fig. S6.2. CO<sub>2</sub> response (A), irradiance response (B) and photosynthetic induction (C) in three batches of Col-0, grown sequentially in the same growth system. Batch 1, blue symbols; batch 2, orange symbols; batch 3, black symbols. Average  $\pm$  SEM,  $n = 5$

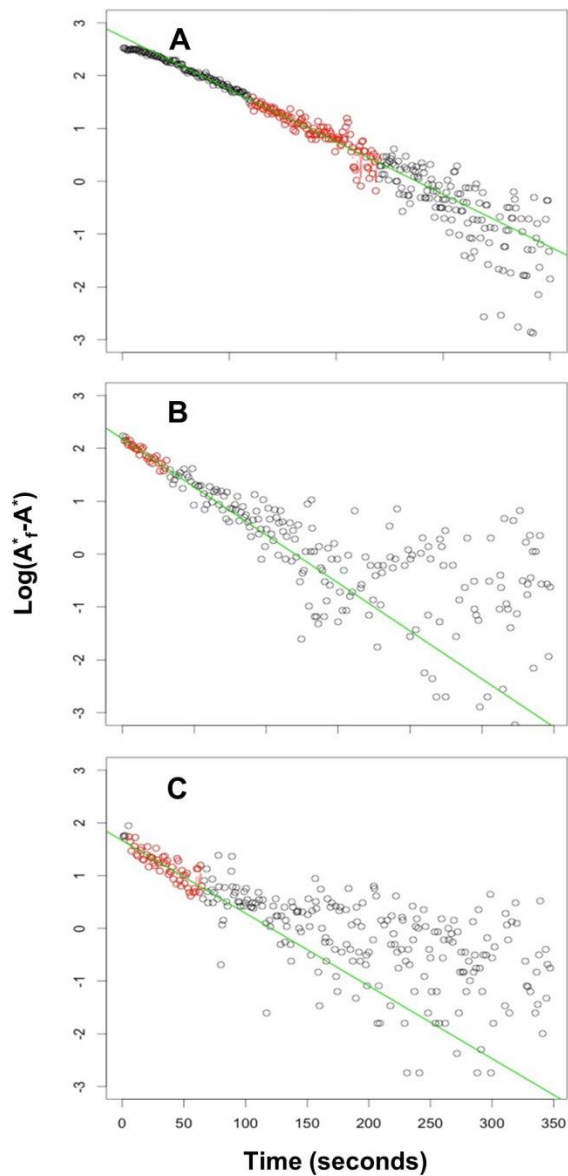


Fig. S6.3. Example of data used to calculate the apparent time constant of Rubisco activation ( $\tau_R$ ) after step increases in irradiance A)  $0 \rightarrow 1000$ , B)  $70 \rightarrow 800$  and C)  $130 \rightarrow 600 \mu\text{mol m}^{-2} \text{s}^{-1}$ . Red dots indicate the data points used to calculate  $\tau_R$ , which is equal to the inverse of the slope of the green line. Explanation of abbreviations on Y-axis: log, natural logarithm;  $A_{f_i}^*$ , steady-state net photosynthesis rate at full photosynthetic induction;  $A^*$ , transient net photosynthesis rate after irradiance increase, corrected for changes in substomatal  $\text{CO}_2$  concentration

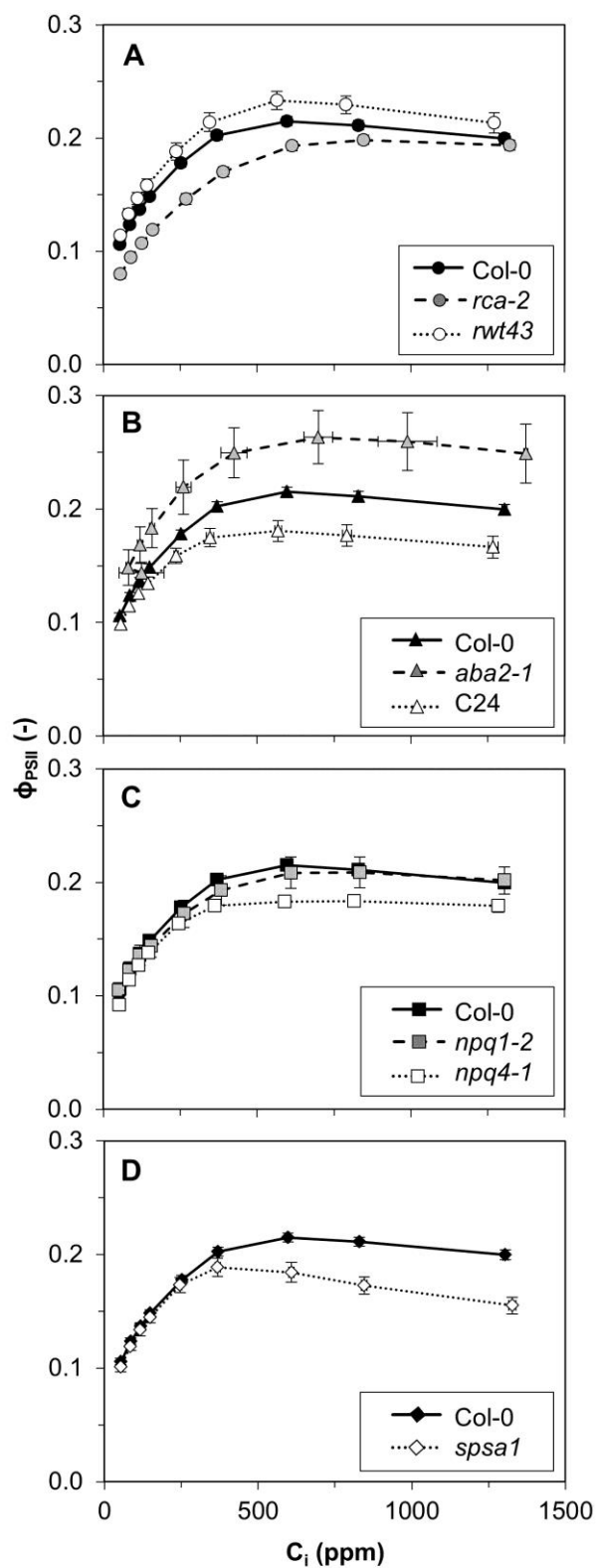


Fig. S6.4. CO<sub>2</sub> response of  $\Phi_{PSII}$  in Arabidopsis genotypes. Averages  $\pm$  SEM, n = 5-15

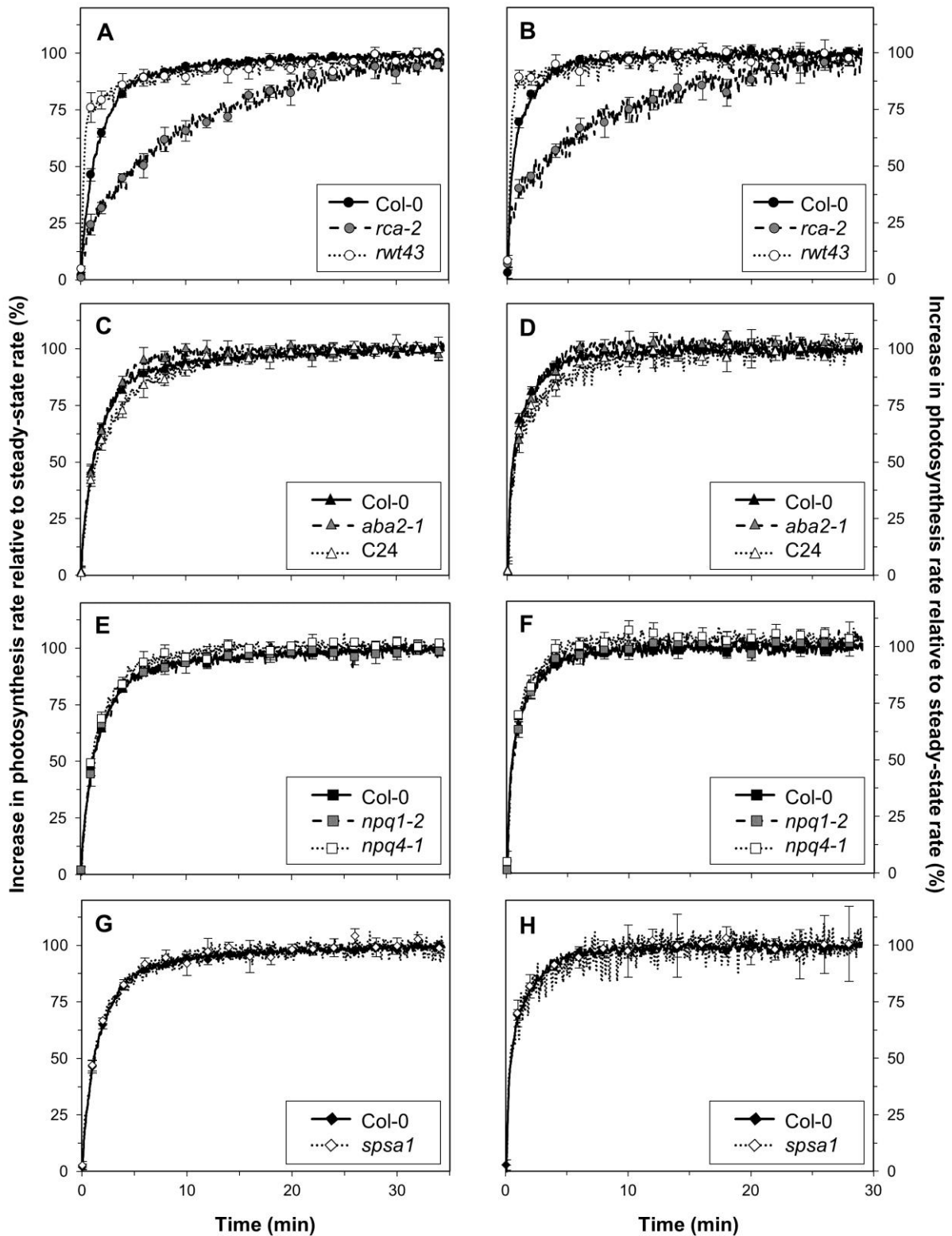


Fig. S6.5. Relative responses of net photosynthesis rates to increases in irradiance, from 70 to 800 (left panel: A, C, E, G) and from 130 to 600  $\mu\text{mol m}^{-2} \text{s}^{-1}$  (right panel: B, D, F, H). Averages  $\pm$  SEM,  $n = 5-15$



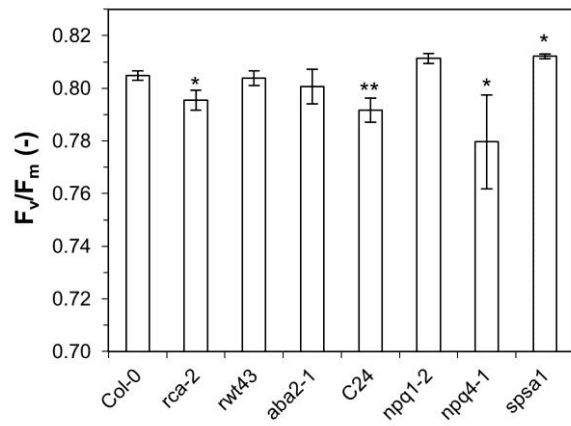


Fig. S6.6. Dark-adapted  $F_v/F_m$  in *Arabidopsis* genotypes after 60 dark adaptation. Stars denote significant difference from Col-0, as  $P < 0.05$  (\*) and  $P < 0.01$  (\*\*). Averages  $\pm$  SEM,  $n = 5-15$

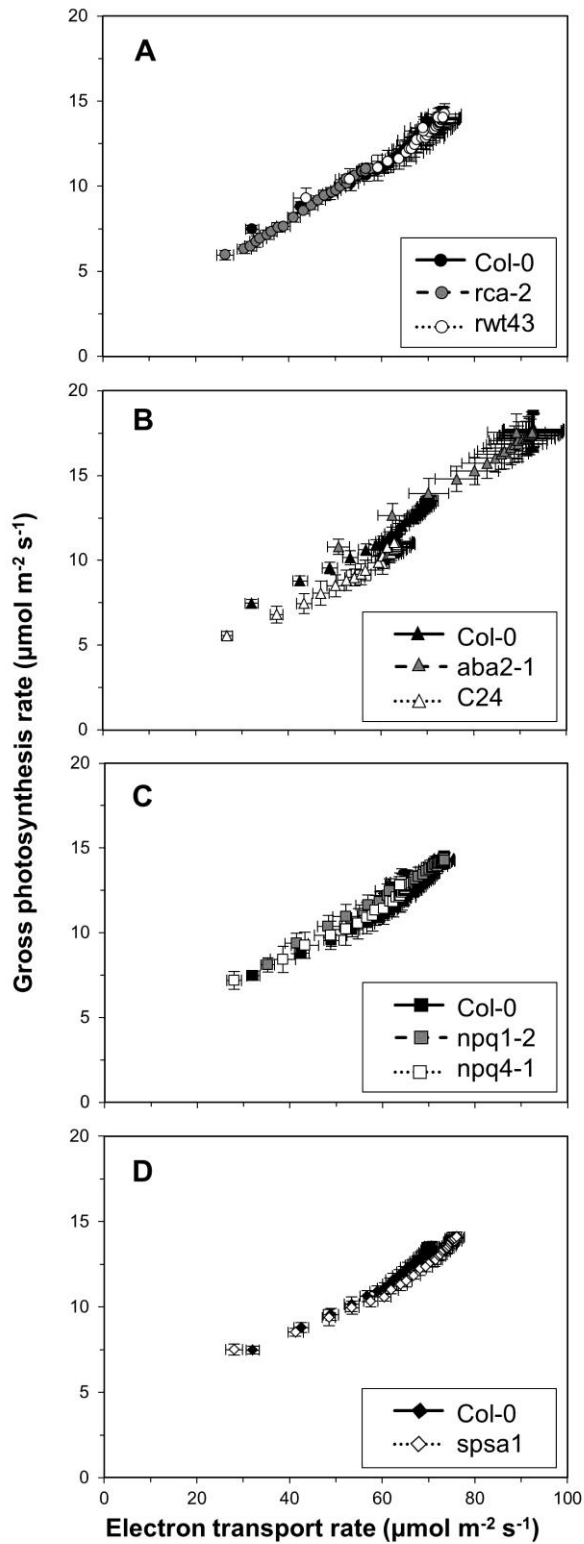


Fig. S6.7. Gross photosynthesis rate ( $A_n$  + dark respiration) as affected by electron transport rate through photosystem II (ETR) during photosynthetic induction after a  $0 \rightarrow 1000 \mu\text{mol m}^{-2} \text{s}^{-1}$  irradiance increase. ETR was calculated as  $\text{ETR} = \text{PAR} * \Phi_{\text{PSII}} * 0.84 * 0.5$  (e.g. Hubbart *et al.*, 2012). Averages  $\pm$  SEM,  $n = 5-15$

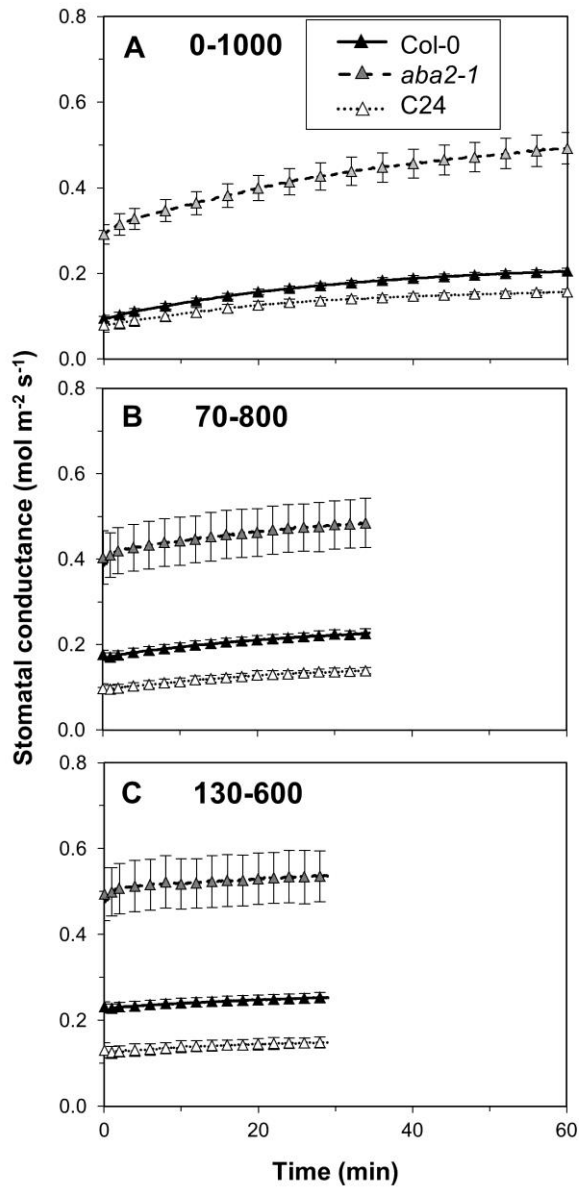


Fig. S6.8. Increases in stomatal conductance in Col-0, *aba2-1* and C24 after step increases in irradiance, A) 0→1000, (B) 70→800 and C) 130→600  $\mu\text{mol m}^{-2} \text{s}^{-1}$ . Averages  $\pm$  SEM, n = 5-15

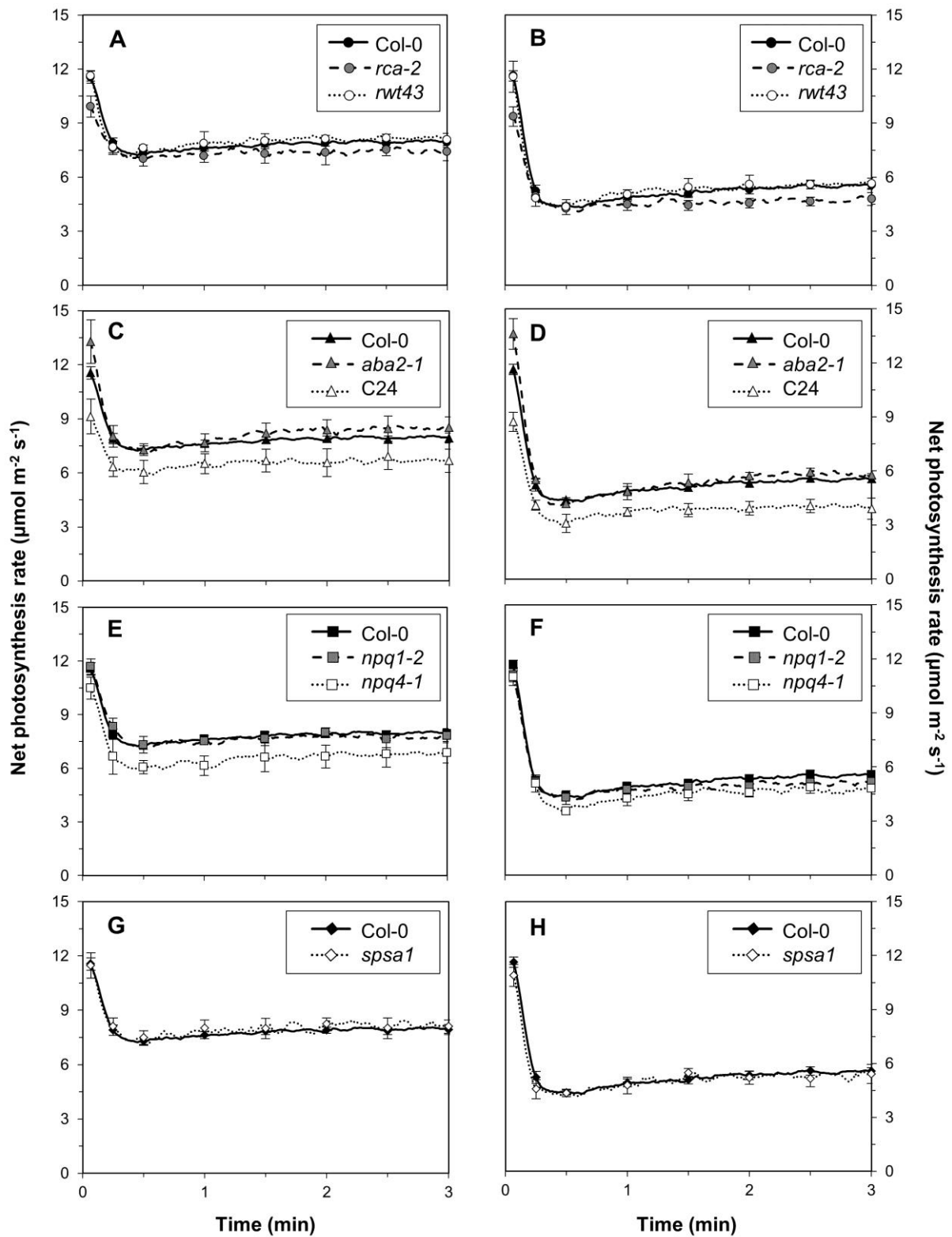


Fig. S6.9. Responses of net photosynthesis rates to step decreases in irradiance, from 600 to 200 (left panel: A, C, E, G) and from 800 to 130  $\mu\text{mol m}^{-2} \text{s}^{-1}$  (right panel: B, D, F, H). Averages  $\pm$  SEM,  $n = 5-15$

## **CHAPTER 7**

Modelling the effects of non-photochemical quenching and metabolic regulation on dynamic leaf photosynthesis

Alejandro Morales  
Elias Kaiser  
Xinyou Yin  
Jeremy Harbinson  
Jaap Molenaar  
Paul C. Struik

To be submitted

**Abstract**

A dynamical model of leaf photosynthesis was developed as an extension of existing steady-state biochemical models of photosynthesis. The dynamics of photosynthesis at the leaf level were reproduced by simulating the regulation of electron transport, non-photochemical quenching and activation state of Rubisco. The model was calibrated using gas exchange and fluorescence data of *Arabidopsis thaliana* ecotype col-0, and mutants in Rubisco activase (*rca-2*), non-photochemical quenching (NPQ; *npq4-1*), abscisic acid formation (*aba2-1*) and sucrose-phosphate synthase (*spsa1*). The model fitted the measurements on the wildtype and the effect of mutants was reproduced with minimal adjustments of parameter values. The model predicted that most of the NPQ build-up during induction was due to the fast mechanism of heat dissipation. This fast mechanism contributed to transient limitations of photosynthesis after decreases in light, but delays in the release of photorespiratory CO<sub>2</sub> were responsible for most of the limitations to net exchange of CO<sub>2</sub>. Predictions of dynamic photosynthesis under symmetrical, periodical lightflecks were successfully validated and the model reproduced the relative effects of the mutations, specifically the large decrease in lightfleck use efficiency due to lower Rubisco activase content in the *rca-2* mutant. We conclude that the model can accurately predict the dynamics of leaf photosynthesis and NPQ under different irradiances and that the successful reproduction of the effect of mutants proves that the assumptions of the model are sound and represent the underlying mechanisms correctly.

**Keywords**

Lightflecks, Rubisco activase, NPQ, CO<sub>2</sub> assimilation, fluctuating light conditions.

## Introduction

Most of the leaves inside a canopy are exposed to fluctuating light, due to transient direct exposure to the sun or shading by clouds. Proper quantification of the effects of these fluctuations on plant performance requires the integration of dynamic photosynthesis over time. Simulation models are an important tool for such purposes.

There are a small group of comprehensive models that describe parts of the metabolism of photosynthesis in detail (e.g. Laisk *et al.*, 2006; Hills *et al.*, 2012; Zaks *et al.*, 2012; Zhu *et al.*, 2013). While these models are of great interest to understanding the functioning of photosynthesis, the large number of parameters involved has prevented attempts to calibrate them against specific species or growing conditions. More parsimonious models, requiring fewer data for calibration and validation, are needed.

Most published photosynthesis models focus on steady-state behaviour and are derived from the mathematical principles postulated by Farquhar *et al.* (1980). The original formulation has been extended by adding a phosphate recycling limitation (Sharkey, 1985a) and including cyclic and pseudocyclic electron transport (Yin *et al.*, 2006). These models have proven to be successful and have been used for a wide range of applications (von Caemmerer, 2013). However, when they are used to calculate photosynthesis in fluctuating light environments, they tend to overestimate measured photosynthesis (Pearcy *et al.*, 1997; Naumburg *et al.*, 2001; Naumburg & Ellsworth, 2002).

A few phenomenological models have been published with the aim of simulating dynamic photosynthesis and/or transpiration in fluctuating light (Pearcy *et al.*, 1997; Kirschbaum *et al.*, 1998; Noe & Giersch, 2004). However, these models lack the effects of non-photochemical quenching (NPQ) on photosynthesis (Zhu *et al.*, 2004; Armbruster *et al.*, 2014), or the limitations due to phosphate recycling at high CO<sub>2</sub> (Sharkey, 1985a) and use empirical models to describe regulation of Rubisco activity (von Caemmerer & Edmondson, 1986; Mott & Woodrow, 2000).

In this study, we propose a novel model of dynamic photosynthesis at the leaf level. The model was calibrated and validated with experimental data by Kaiser *et al.* (unpublished results, Chapter 6) including measurements of gas exchange and fluorescence for mutants of *Arabidopsis thaliana*. The aim of this study is to describe the model and to demonstrate its predictive power and ability to reproduce the effects of different mutations on key components of photosynthesis.

## Materials and Methods

### General description of the model

The model described in this publication is an extension of the steady-state model of photosynthesis proposed by Farquhar et al. (1980) for  $C_3$  plants. At any given moment, the rate of carboxylation ( $V_C$ ,  $\mu\text{mol m}^{-2} \text{s}^{-1}$ ) is calculated as the minimum of four potentially limiting factors:

$$V_C = \min(V_{C,J_2}, V_{C,RB}, V_{C,R}, V_{C,TPU}) \quad (7.1)$$

where the subscripts “ $J_2$ ”, “RB”, “R” and “TPU” refer to limitation by potential PSII electron transport, Rubisco kinetics, activity of enzymes responsible for RuBP regeneration in the Calvin cycle and triose phosphate utilisation (Fig. 7.1). The third limiting factor in the equation is generally not included in steady-state models of photosynthesis, as it cannot be distinguished from a limitation due to potential electron transport. However, the rate of activation of enzymes during light transients is known to limit dynamic photosynthesis (Percy *et al.*, 1996). The model simulates the regulation of enzyme activity in the Calvin cycle (both Rubisco and enzymes in the regeneration phase), the different forms of non-photochemical quenching (heat dissipation and changes in leaf-level light absorbance and photoinhibition). NPQ is calculated from irradiance and the difference between potential electron transport and the other limiting factors in Eqn. 7.1. Rubisco activity is calculated as the difference between potential electron transport and the other limiting factors in Eqn. 7.1. Accumulation of photorespiratory intermediates (PR) introduces a delay in  $\text{CO}_2$  release.  $\text{CO}_2$  from the air diffuses into the chloroplast via stomatal conductance

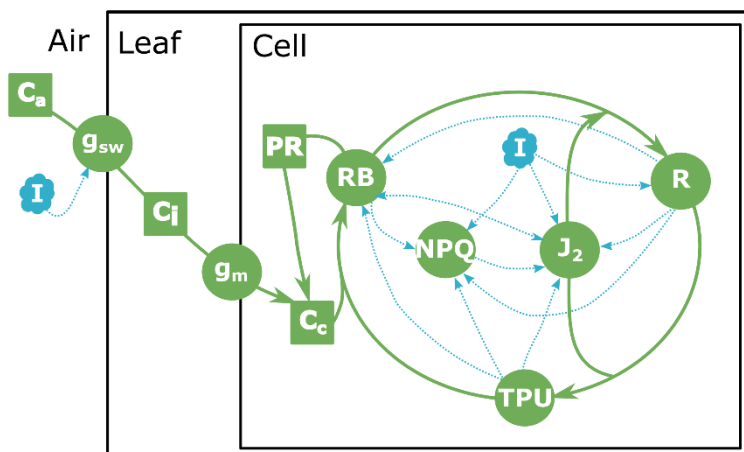


Fig. 7.1. Conceptual diagram of the model. The rate of carboxylation is limited by Rubisco kinetics (RB), activity of enzymes in the regeneration phase of the Calvin cycle (R), triose phosphate utilisation (TPU) and potential rate of electron transport ( $J_2$ ). NPQ is calculated from irradiance (I) and actual electron transport.  $\text{CO}_2$  diffuses from the air ( $C_a$ ), into the chloroplast ( $C_c$ ) as mediated by stomatal and mesophyll conductance ( $g_{sw}$  and  $g_m$ , respectively).  $\text{CO}_2$  emitted due to photorespiration (PR) is assumed to be delayed with respect to oxygenation



and depends on stomatal ( $g_{sw}$ ) and mesophyll conductance ( $g_m$ ). We did not simulate  $g_{sw}$  but rather used measured values as input into the model. Additionally, we included a temperature-dependent  $g_m$ . Photosynthesis ( $A$ ,  $\mu\text{mol m}^{-2} \text{s}^{-1}$ ) was calculated as the balance of carboxylation, photorespiratory intermediates ( $PR$ ,  $\mu\text{mol m}^{-2}$ ) and the rate at which they were converted to  $\text{CO}_2$  ( $K_{PR}$ ,  $\text{s}^{-1}$ ) and mitochondrial respiration ( $R_d$ ,  $\mu\text{mol m}^{-2} \text{s}^{-1}$ ) as

$$A = V_C - 0.5PR \cdot K_{PR} - R_d \quad (7.2)$$

In the following sections, the main assumptions and concepts of the model are presented in order to facilitate interpretation of the results. All equations of the model are discussed in detail in Supplementary Material 7.1.

### *Dynamic regulation of the electron transport chain*

Experimental evidence indicates that regulation of the quantum efficiency of PSII due to enhanced heat dissipation affects biomass production under fluctuating conditions (Külheim *et al.*, 2002). Part of this effect is associated with the photoprotective role of NPQ against photoinhibition (Murchie & Harbinson, 2014), but there is evidence that during high to low light transients, NPQ can limit photosynthesis (Hubbart *et al.*, 2012; Armbruster *et al.*, 2014; Ikeuchi *et al.*, 2014). We model regulation of heat dissipation using a teleonomic model that calculates the amount of NPQ required to reduce the excitation pressure on the reaction centre by a fixed fraction. This approach allows us to simulate the effects of irradiance and changes in metabolic demand on NPQ. We separate this heat dissipation into two components with different kinetics: a fast component that can be considered equivalent to qE (we denoted it as qD<sub>f</sub>) and a slow component that represents slower forms of NPQ (qD<sub>s</sub>) that are not associated with changes in leaf-level light absorbance (Nilkens *et al.*, 2010; Dall'Osto *et al.*, 2014). We assumed the effect of state transitions to be negligible.

Photoinhibition and other slowly reversible forms of NPQ may also limit photosynthesis under fluctuating light conditions, especially at low temperatures (Zhu *et al.*, 2004). We modelled photoinhibition using a first-order approximation as described by Campbell and Tyystjärvi (2012). Photoinhibition is assumed to contribute to slowly reversible NPQ (i.e. qI). In addition, we include the effect of chloroplast movement on leaf-level light absorbance (Kasahara *et al.*, 2002; Davis & Hangarter, 2012) and its contribution to NPQ is denoted qA.

### *Dynamic regulation of Rubisco activity*

Rubisco activity is regulated by irradiance and CO<sub>2</sub> concentration (von Caemmerer & Edmondson, 1986). This allows regulating the rate of carboxylation, considering that RuBP levels are not kinetically limiting in the steady state (Sharkey, 1989). In our model, the steady-state activation state of Rubisco is calculated by comparing the actual rate of carboxylation as defined by Eqn. 7.1 and the potential rate of carboxylation defined by the kinetics and amount of Rubisco as originally described by Farquhar (1979). The rate at which this activation state increases is assumed to follow second-order kinetics with respect to the amount of Rubisco activase as proposed by Mott and Woodrow (2000).

### *Regeneration of RuBP*

In addition to limitations due to potential production of NADPH associated with the potential rate of electron transport, we also include the limitation due to (i) maximum activity of enzymes in the regeneration phase of the Calvin cycle and (ii) maximum rate of triose phosphate utilisation for synthesis of sucrose and starch. Triose phosphate utilisation was assumed to be dependent on temperature (Sharkey *et al.*, 2007) but we did not simulate any dynamics associated with this limitation. We assumed that transient limitations to photosynthesis during light fluctuations could be caused by phosphoribulokinase or fructose-1,6-bisphosphatase (Sassenrath-Cole & Pearcy, 1992; Pearcy *et al.*, 1997; Kirschbaum *et al.*, 1998). Thus, we considered that the maximum activity was dependent on the irradiance and that changes in the activity of these enzymes follow first-order kinetics.

### *Parameter estimation*

The values for most of the parameters in the model were taken from the relevant literature (Table S7.1). However, some parameters in the model are specific to species and their growth environment. Thus, a reduced number of parameters were estimated by fitting the model to dynamic measurements of gas exchange and chlorophyll fluorescence on *Arabidopsis thaliana*. The measurements were performed on the ecotype col-o as well as on mutants of key components of photosynthesis derived from this ecotype. The use of mutants allowed us also to test the assumptions of the model. That is, if the model correctly captured the effect of the different processes that affect dynamic photosynthesis, it should be possible to reproduce the phenotypes of the different mutants by modifying only the parameters directly affected by the mutations. However, this is only possible with mutants that have no pleiotropic effects or when these effects are known *a priori*.

Measurements on the Rubisco activase mutant *rca-2* (Shan *et al.*, 2011) were used to test how well the model incorporates the effect of Rubisco activase. This mutant contains a “leaky” mutation that allows some residual expression of Rubisco activase (Shan *et al.*, 2011). Therefore, for practical purposes, it can be considered analogous to a Rubisco activase underexpressor plant. The only parameter assumed to change was the amount of Rubisco activase. The PsbS mutant *npq4-1* (Li *et al.*, 2000) was used to test the ability of the model to simulate the different components of NPQ correctly. This mutant lacks rapid, reversible NPQ (i.e. in terms of the model’s parameters this means a photoprotective efficiency of zero for the fast mechanism of regulated heat dissipation). In addition, the quantum yield of photodamage and the photoprotective efficiency of the slow mechanism of heat dissipation were assumed to vary based on previous observations of pleiotropic effects for this mutant (Nilkens *et al.*, 2010; Dall’Osto *et al.*, 2014).

The mutant with low endogenous ABA levels, *aba2-1* (Leon-Kloosterziel *et al.*, 1996), was used to test the effect of higher CO<sub>2</sub> concentrations during induction, as this mutant is characterised by higher  $g_{sw}$  compared with the wild-type. However, we had to take into account the fact that ABA is involved in additional processes relevant to dynamic photosynthesis. Thus, it was assumed that there was no chloroplast light avoidance movement (Rojas-Pierce *et al.*, 2014) and that the mesophyll conductance increased (Flexas *et al.*, 2008; Mizokami *et al.*, 2015). The analysis of the data performed by Kaiser *et al.* (Chapter 6) indicated that  $J_{max,25}$  and the amount of Rubisco were also up-regulated and, although we cannot explain the mechanism for such effects, it was necessary to allow these two parameters to increase in the *aba2-1* mutant in order to reproduce the observations. The mutant *spsa1* (Sun *et al.*, 2011) was used to test the concept of triose phosphate utilisation as implemented by the model. Only the *TPU* parameter was assumed to vary in *spsa1*.

In the experiment described by Kaiser *et al.* (Chapter 6), leaves of 6-week-old *A. thaliana* plants were used for measurements. Measurements were performed using a LI-6400 photosynthesis system (Li-Cor Biosciences, Lincoln, Nebraska, USA). Below, a summary of the measurement protocols is given. These protocols were applied to gather dynamic data on photosynthesis, chlorophyll fluorescence and  $g_{sw}$ :

- Photosynthetic induction: irradiance was increased stepwise from an initial irradiance (0, 70 or 130  $\mu\text{mol m}^{-2} \text{s}^{-1}$ ) to 1000, 800 or 600  $\mu\text{mol m}^{-2} \text{s}^{-1}$ , respectively. Leaves were adapted to the initial irradiance until gas exchange measurements reached a steady state. Fluorescence measurements were taken periodically, but only for the light transient starting from darkness. In the rest of the document, these measurements are referred to as “0-1000”, “70-800” and “130-600” light transients.

- Loss of induction: irradiance was decreased from an initial irradiance (800 or 600  $\mu\text{mol m}^{-2} \text{s}^{-1}$ ) to 130 or 200  $\mu\text{mol m}^{-2} \text{s}^{-1}$ , respectively. Leaves were adapted to the initial irradiance until gas exchange measurements reached a steady-state. Fluorescence was not measured. In the rest of the document, these measurements are referred to as “800-130” and “600-200” light transients.
- $\text{CO}_2$  response curves: steady-state measurements of photosynthesis and fluorescence were performed at a saturating irradiance of 1000  $\mu\text{mol m}^{-2} \text{s}^{-1}$  and the following  $\text{CO}_2$  concentrations: 50, 100, 150, 200, 350, 500, 750, 1000 and 1500  $\mu\text{mol mol}^{-1}$ . In the rest of the document this measurement is referred to as “A-Ci” response curve.

All measurements were done with a light source composed of 10% blue and 90% red. These measurements were repeated in five replicates per genotype, except for col-0 for which 15 replicates were used. The model was fitted to all data simultaneously, by minimising the weighted sum of absolute relative deviations between the model’s predictions and the measurements. The weights were chosen to compensate for the fact that the number of data points were different in each dataset, and that relative (as opposed to absolute) deviations were necessary as the scale of the different measured variables differ. The minimisation was done with the derivative-free trust region algorithm BOBYQA (Powell, 2009). In order to approximate the initial state of the leaf in each measurement, we assumed that leaves had been exposed for 40 minutes to the same environmental conditions as those used in the measurements. For every simulation, we used measured leaf temperature and  $g_{\text{sw}}$  as inputs. In order to calculate the mixing of gases in the open gas exchange chamber, we also took into account measured air temperature and transpiration. In the experimental data and for a given genotype and protocol there was a strong variation across the replicates (i.e. plant-to-plant variation). In the model fitting procedure, we assumed that all replicates within a particular genotype were characterised by the same parameter values. This is equivalent to assuming that we fitted the model to the average behaviour of each genotype. Therefore, the goodness-of-fit described in the Results and Discussion sections (i.e. mean absolute error and fraction of variance explained by the model) were calculated by comparing the predictions of the model with the observed average behaviour for each combination of genotype and type of measurement, rather than the measurements for each individual replicate.

### *Photosynthesis in fluctuating light*

In order to test the predictive power of a model fitted to experimental data, it is customary to validate the model with a second dataset that is statistically independent of the first one.

In this case, we were interested in the ability of the model to predict photosynthesis in fluctuating light conditions.

In order to achieve these objectives we used additional measurements from the experiments by Kaiser et al. (Chapter 6). In these measurements, irradiance was varied as a square wave. A square wave is a function of time that consists of a periodic repetition of cycles. Each cycle consist of two half-cycles of equal length. The total length of a cycle is called “period” and its inverse is the frequency of the wave. During each half-cycle, irradiance was kept constant. For each cycle, the irradiance of the first half-cycle was higher than in the second half-cycle. The difference between the irradiance of the first and second half-cycle is the amplitude. The average of the irradiances of the first and second half-cycle was always  $300 \mu\text{mol m}^{-2} \text{s}^{-1}$  but three amplitudes of 100, 200 and  $500 \mu\text{mol m}^{-2} \text{s}^{-1}$  were used. Each amplitude was combined with three periods (120, 60 and 10 s). This resulted in nine amplitude  $\times$  period combinations that were measured for each replicate.

The number of replicates used per genotype were the same as in the rest of the experiment. Using the parameter values estimated in the calibration step, we ran simulations with the model for all measurements of photosynthesis under fluctuating light intensities. As with the calibration step, we used measured leaf temperature and  $s g_{\text{sw}}$  as model inputs.

We compared simulations and measurements of average photosynthesis and compared how they were affected by genotype, amplitude and period in the experiment and in the simulations. When irradiance varies as a symmetrical, periodical function of time, the dynamics of the system can only contribute to average photosynthesis if the oscillations in photosynthesis become asymmetric (i.e. the rates of increase and decrease differ). Therefore, we also analyzed the behavior of the system during each half-cycle where irradiance increased or decreased.

In order to further understand how the dynamics of the system contributed to different average photosynthesis, we calculated the lightfleck utilisation efficiency (LFUE), defined as the ratio between observed (or simulated) average photosynthesis and the values we would obtain from a steady-state model (Percy, 1990; Pons & Percy, 1992). This index requires knowledge of steady-state photosynthesis at each irradiance of the square wave, for which we simulated steady-state light response curves for each genotype. Since  $g_{\text{sw}}$  barely changed during the measurements, we performed the light response curve at constant  $g_{\text{sw}}$ .

## Results and Discussion

### *Comparison of simulations and data*

The fraction of variance in measured photosynthesis explained by the model during light transients varied between 0.94 and 0.98 for the different genotypes, being lowest in *aba2-1*. The mean absolute error was more variable, with the smallest values found for *npq4-1* and *rca-2* (0.35 and 0.40  $\mu\text{mol m}^{-2} \text{s}^{-1}$ , respectively), higher values for *spsa1* and *col-0* (0.58 and 0.47  $\mu\text{mol m}^{-2} \text{s}^{-1}$ , respectively) and a significantly worse fit in the case of *aba2-1* (0.81  $\mu\text{mol m}^{-2} \text{s}^{-1}$ ). This worse fit in *aba2-1* was caused by an underestimation of photosynthesis at 1000  $\mu\text{mol m}^{-2} \text{s}^{-1}$  (Fig. 7.2C). This underestimation was present (but with smaller magnitude) in all other genotypes except *npq4-1* (Fig. 7.2B). However, this underestimation was not necessarily caused by errors in the model. We found that photosynthesis at the end of the 0-1000 light transient was always larger than the corresponding value interpolated from A-Ci curves, except for *npq4-1* (Fig. S7.1). The magnitude of this difference was very similar to the aforementioned underestimation by the model. However, given the variation in photosynthesis across replicates, the difference was not statistically significant at the 95% confidence probability. Since we cannot affirm that the difference is not caused by experimental error, we refrain from speculating on the possible nature of this difference. Furthermore, we cannot claim neither that the model underestimates nor that it correctly fits the true photosynthesis in the 0-1000 light transient.

Unfortunately, errors in predicting steady-state photosynthesis also affect the dynamics. Since the parameters were estimated by minimizing the distance between the model and data, an underestimation of the value at the end of a light transient will result in an overestimation of the rate constants associated with photosynthetic induction. This contributes to the model's overestimation of the relative rate of induction in the 0-1000 light transient. The other light transients were simulated accurately by the model.

The dynamics of NPQ during induction were simulated accurately by the model (Fig. 7.3) with mean absolute errors ranging from 0.04 (*npq4-1*) to 0.07 (*aba2-1*), except for *rca-2*, where the mean absolute error increased to 0.16 as the model underestimated NPQ during the first 15 minutes. Similarly, the fraction of variance explained by the model was only 0.68 in *rca-2*, but it ranged from 0.86 to 0.99 in the other genotypes. The model also fitted the A-Ci curve accurately (Fig. 7.4). The fraction of explained variance was always 0.99 and the mean absolute error varied between 0.25 (*col-0*) and 0.56 (*aba2-1*)  $\mu\text{mol m}^{-2} \text{s}^{-1}$ .

The model underestimated average photosynthesis (calculated for each cycle of the square wave) by 0.45  $\mu\text{mol m}^{-2} \text{s}^{-1}$  (Fig. 7.5) with a mean absolute error of 0.59  $\mu\text{mol m}^{-2} \text{s}^{-1}$ . Since the range of observed values (9.48  $\mu\text{mol m}^{-2} \text{s}^{-1}$ ) was much larger than the error, this meant

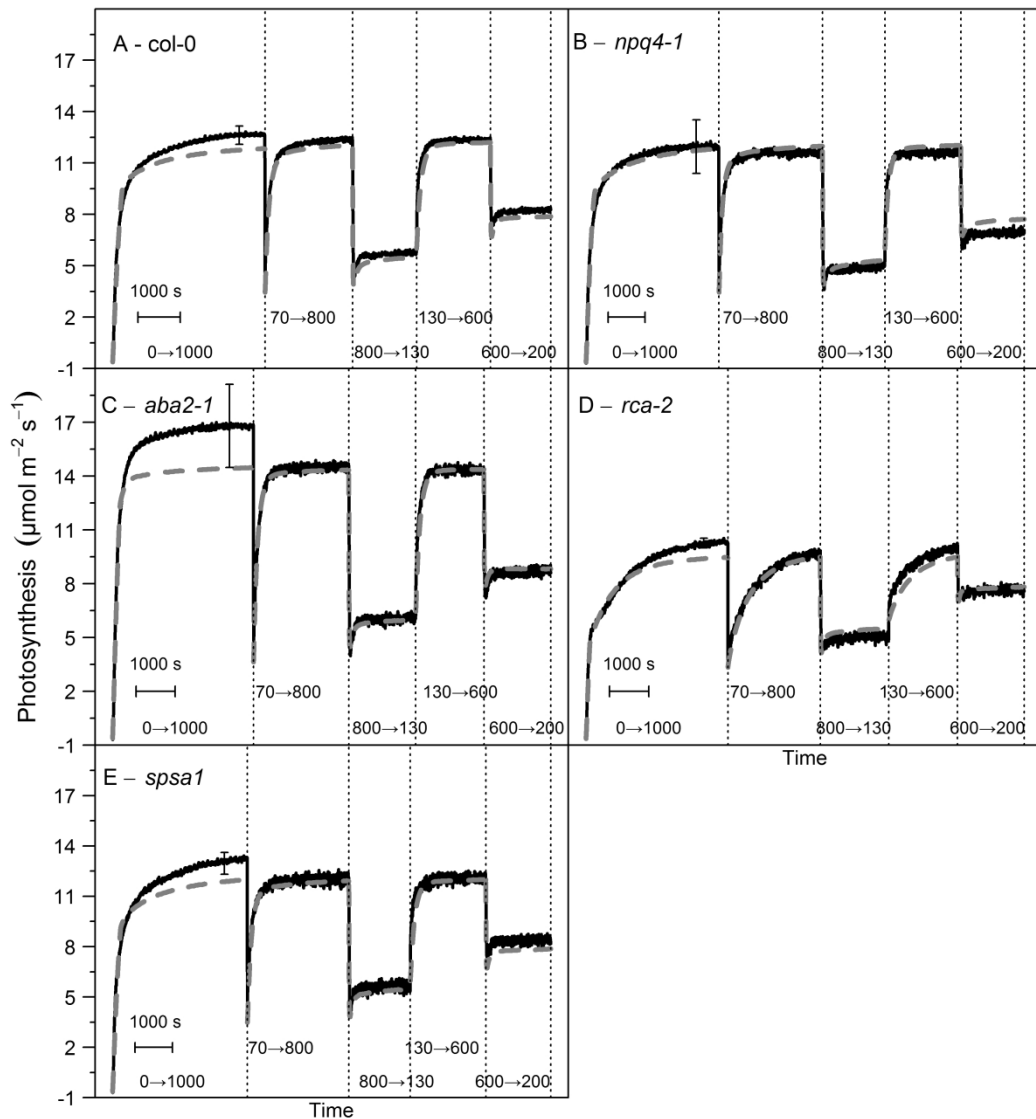


Fig. 7.2. Measured (black line) and simulated (grey line) photosynthesis during the different light transients (start and final irradiance indicated in subplots) in *col-0* (A), *npq4-1* (B), *aba2-1* (C), *rca-2* (D) and *spsa1* (E). Error bars indicate 95% confidence interval of the mean across replicates

that a high fraction of the total variation (0.86) was explained by the model. The goodness-of-fit measures varied across genotypes. The maximum bias was found for *col-0*, with an average underestimation of  $0.94 \mu\text{mol m}^{-2} \text{s}^{-1}$ , whereas there was no bias for *rca-2*. The mean absolute errors also varied, ranging from  $0.38 \mu\text{mol m}^{-2}$  in *aba2-1* to  $0.96 \mu\text{mol m}^{-2}$  in *col-0*. The lack of bias but similar absolute error in *rca-2* meant that only 66% of the variation in the data was explained by the model for this particular genotype, whereas predictions for *spsa1*, *aba2-1*, *npq4-1* and *col-0* accounted for 80%, 89%, 91% and 94% of the observed variation, respectively.

An analysis of variance of the measurements that included all main effects and interactions among genotype, amplitude and period revealed that 43% of the variation in the experimental data was explained by the amplitude and 21% was due to the genotype,

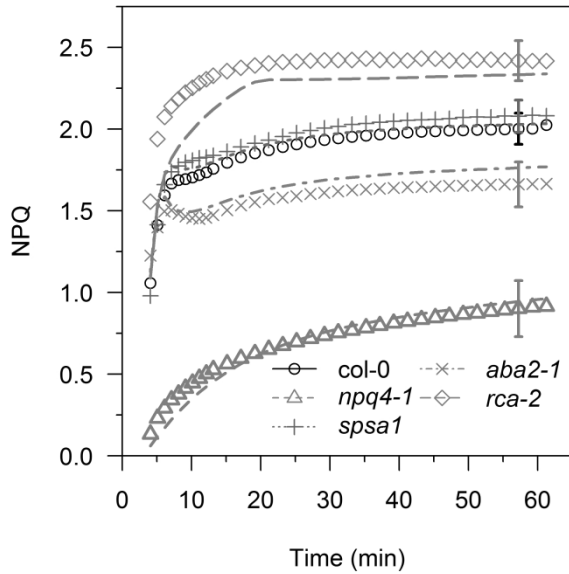


Fig. 7.3. Total measured (symbols) and simulated (lines) NPQ in the 0-1000 light transient. NPQ was calculated as  $F_m/F_m' - 1$ . Error bars indicate 95% confidence interval of the mean across replicates

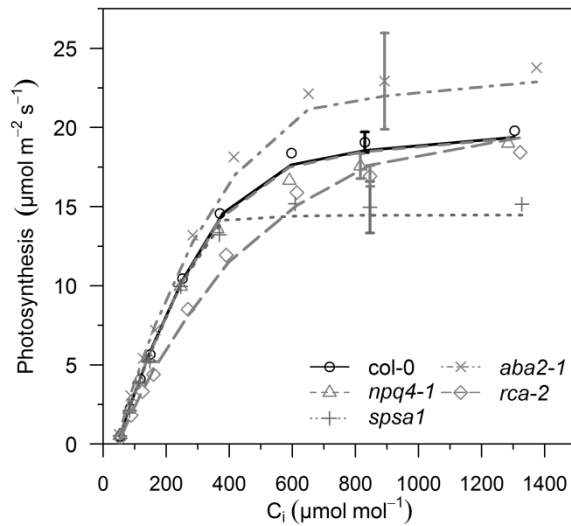


Fig. 7.4. Measured (symbols) and simulated (lines) response of steady-state photosynthesis to  $CO_2$ . Error bars represent the 95% confidence interval of the mean across replicates

although 32% of the variation remained unaccounted for. In the simulations, the genotype contributed to 77% of the variation, the amplitude contributed with 18%, whereas unexplained variation was minimal (3%). This suggests that the success of the model in explaining large fractions of the variance in the measurement is associated with its ability to predict correctly the effects of genotype and amplitude. The period had a small effect, except for the period of 10 s at the highest amplitude ( $500 \mu\text{mol m}^{-2} \text{s}^{-1}$ ).



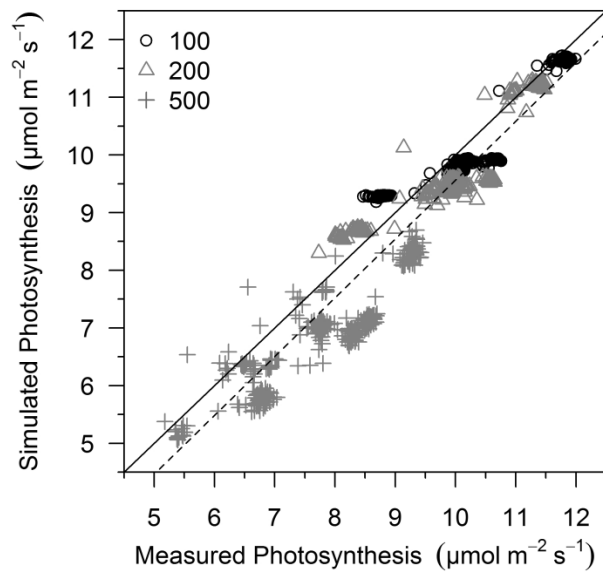


Fig. 7.5. Measured and simulated average photosynthesis under fluctuating light conditions for all amplitudes (100, 200 and 500  $\mu\text{mol m}^{-2} \text{s}^{-1}$ ) and periods of the square wave and genotypes. Each symbol represents the value for a specific cycle of the square wave, averaged over all replicates. The solid line represents the 1:1 line. The dashed line is the linear regression between simulated and measured average photosynthesis

### *Components of non-photochemical quenching*

Parameters associated with chloroplast movement were not estimated from our data, but taken from literature. At the end of the 0-1000 light transient, chloroplast movement contributed to NPQ with a qA component of 0.24 in the wild-type but only of 0.16 in *npq4-1* (Fig. 7.6), even though in both cases leaf-level light absorbance was reduced by 8%. qA is calculated as the difference between simulated NPQ (using the Stern-Volmer coefficient) and the NPQ that would have been obtained in the absence of chloroplast movement. Mathematically, this implies that the magnitude of qA depends on the the contribution of other NPQ mechanisms (see Supplementary Material 7.1 for details).

The difference between NPQ in *col-0* and *aba2-1* was almost entirely explained by the lack of chloroplast movement in *aba2-1*, as the other NPQ components were similar to *col-0* (Fig. 7.6). The ratio  $J_{max,25}/RB$  was higher in *aba2-1* compared with the wildtype (11.5 and 9.5, respectively. See Tables S7.1, S7.4 for details). A higher  $J_{max,25}/RB$  in *aba2-1* should result in a higher NPQ as it increases the imbalance between potential and metabolic-limited electron transport. However, the *aba2-1* mutant also had a higher  $\text{CO}_2$  concentrations in the chloroplast (due to enhanced  $g_{sw}$  and  $g_m$ ) which compensated for this effect. Such compensation did not occur in *rca-2*, where a strong decrease in the metabolic demand due to lower Rubisco activase content resulted in a larger total NPQ (Figs. 7.3, 7.6), even though the  $\text{CO}_2$  concentration in the chloroplast was also increased. This increase in  $\text{CO}_2$  concentration was not caused by higher stomatal or mesophyll conductan-

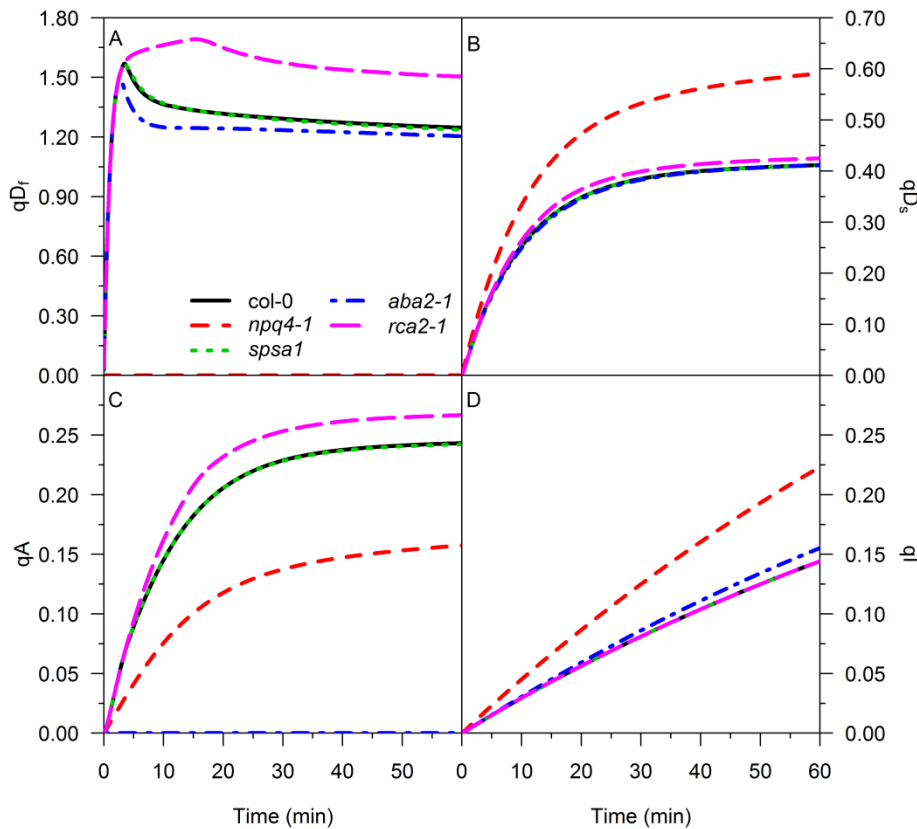


Fig. 7.6. Simulated components of NPQ during the 0 – 1000 light transient. Irradiance was varied in 2 s steps at the beginning of the experiment between 0 and  $1000 \mu\text{mol m}^{-2} \text{s}^{-1}$ .  $qD_f$  (A) and  $qD_s$  (B) represent the fast and slow mechanisms of heat dissipation,  $qA$  (C) is NPQ due to chloroplast movement and  $qI$  (D) is the contribution to NPQ of photoinhibition

ce but by the lower rate of photosynthesis.

The fraction of NPQ attributed to heat dissipation at the end of the 0-1000 light transient was 0.59 in *npq4-1* and varied between 1.61 in *aba2-1* (similar values for *spsa1* and *col-0*) to 1.92 in *rca-2* for the other mutants (Fig. 7.6). 75% of this component of NPQ was due to  $qD_s$ , which meant that  $qD_f$  represented 61-68% of total NPQ at the end of the induction curve. This fraction decreased with time as, 5 minutes after induction,  $qD_f$  represented 85% of total NPQ. The decrease in the relative contribution of  $qD_f$  was caused by both the decrease in  $qD_f$  and the increase in the other components (Fig. 7.6).

Our model predicted an overshoot of  $qD_f$  at the beginning of some induction curves and a slow decrease at the end of all induction curves (Fig. 7.6A). This prediction is a logical consequence of the concept of photoprotective efficiency as defined in this model: as metabolic demand increases and slow NPQ mechanisms are activated, the need for photoprotection from  $qD_f$  decreases. This is not an explicit assumption of the model, but rather the logical consequence of modelling  $qD$  as a function of redox state of the electron transport chain (Supplementary Material 7.1).  $qD_f$  may be considered analogous to the

rapid, reversible, energy-dependent fraction of NPQ (i.e. qE). Since it is not possible to perform direct measurements of the qE mechanism during induction, we cannot validate these patterns, but simulations with mechanistic models of qE (e.g. Zaks *et al.*, 2012) reproduce the initial overshoot (caused by a transient over-acidification of the lumen). We can also obtain this pattern if we subtract NPQ of *npq4-1* from the NPQ observed in the wildtype, although one should consider the differences in qI when performing such subtractions.

The amount of NPQ due to photoinhibition (qI) after one hour of exposure to 1000  $\mu\text{mol m}^{-2} \text{s}^{-1}$  in *col-0* was 0.14 and increased to 0.22 in *npq4-1* (Fig. 7.6D), which means that photoinhibition had a small contribution to total NPQ at the end of the 0-1000 light transient. This small contribution is in agreement with previous measurements of qI in *col-0* and *npq4-1* (Nilkens *et al.*, 2010; Dall'Osto *et al.*, 2014).

### *Limiting factors during dynamic photosynthesis*

The model predicted that the rate with which enzymes in the regeneration phase of the Calvin cycle were activated limited photosynthesis at the beginning of the 0-1000 light transient. This was followed by limitation due to activation of Rubisco. The transition between the two limitations can be appreciated as an abrupt change in the rate at which photosynthesis increases (Fig. 7.2). In the rest of transients where irradiance was increased, photosynthesis was only limited by activation of Rubisco. In the simulations, whether activation of enzymes in the regeneration phase limit photosynthesis or not and the extension of this limitation depended on the initial activities of Rubisco and enzymes in the regeneration phase of the Calvin cycle (results not shown). At low irradiances, the model predicted that the activities of enzymes in the regeneration phase were sufficiently high to no longer be limiting.

All measurements of high to low light transients were characterized by a short period of time during which photosynthesis was below the steady-state (Fig. 7.2), a phenomenon described as “post-illumination CO<sub>2</sub> burst” or PICB (Kaiser *et al.*, 2015). The model predicted that there are two processes that contribute to this phenomenon:

1. Delayed release of photorespired CO<sub>2</sub>.
2. Relaxation of NPQ that is in excess and transiently limits electron transport.

The effects of photorespiration on PICB have been studied extensively (see Kaiser *et al.*, 2015 for a review) and it was the only process responsible for PICB in previous models of dynamic photosynthesis (Percy *et al.*, 1997; Kirschbaum *et al.*, 1998). We incorporated this process as described by Percy *et al.* (1997) and hence reproduced the effects they observed.

However, recent publications have pointed to the importance of NPQ in limiting photosynthesis after decreases in irradiance. Armbruster et al. (2014) demonstrated that altering NPQ relaxation kinetics had an effect on photosynthesis during the PICB. Ikeuchi et al. (2014) used an antisense transformant of *Oryza sativa* with lower PsbS and observed higher rates of electron transport after decreases in irradiance, although they did not report CO<sub>2</sub> exchange. Hubbart et al. (2012) reported changes in photosynthesis under fluctuating light when they increased and decreased the levels of PsbS in *O. sativa*.

Our model confirms that after decreases in irradiance, relaxation of NPQ contributes to a decrease in photosynthesis, increasing the extension and magnitude of the PICB (Fig. S7.2). Most of the reduction attributed to NPQ was caused by relaxation of qD<sub>b</sub>, as this mechanism was responsible for most of the NPQ generated at high irradiances.

Interestingly, the 600-200 light transient in *rca-2* (both data and simulations) presented a lack of PICB (Figs. 7.2D, S7.2), even though qD<sub>f</sub> was larger in *rca-2* than in the wildtype. The difference in the simulation was caused by a lower amount of photorespiration intermediates in *rca-2* relative to other genotypes that presented a clear PICB (Fig. S7.2) as well as a slower decay of this pool. In the model, this phenomenon was a direct consequence of lower Rubisco activation state. These simulations indicate that the contribution of delayed photorespiration to PICB is larger than that of the fast mechanism of heat dissipation (i.e qE). Further research is required to test this hypothesis experimentally.

The total loss of CO<sub>2</sub> during PICB in *npq4-1* appears to be slightly smaller, especially in the 600-200 light transient (Figs. 7.2B, S7.2), but this difference was not statistically significant in the experimental data (Chapter 6). Measurements of PICB are always limited by the smoothing effect imposed by the open gas exchange system on any measurement of dynamic photosynthesis. From the specification of the manufacturer (Li-Cor, 2012) and the settings of the experiment (Chapter 6) we estimated a time constant of 6.53 s for our gas exchange system (see Supplementary Material 7.1, Section 4 for details). This value is similar to the 7.5 s measured for the same model by Leakey et al. (2003). With this time response, the smoothing effect, added to the measurement error, resulted in a similar PICB for *col-0* and *npq4-1*. Our simulations indicated that the differences in PICB between *col-0* and *npq4-1* disappeared once the smoothing effect was added to the simulations of photosynthesis. This could explain why it was not possible to measure a significant difference in PICB between the wildtype and *npq4-1*.

A different type of limitation is the one imposed by the slower components of NPQ (slow heat dissipation, chloroplast movement and qI). This effect was most notable in the simulations of *npq4-1*, where there is no fast mechanism of heat dissipation (as described in

the Materials and Methods) and slow components of NPQ are up-regulated. This resulted in a lower photosynthesis (relative to wildtype) in transients where irradiance was decreased. We also observed these differences in the experimental data (Fig. 7.2), although they were not statistically significant (Chapter 6). This type of inhibition by slowly reversible NPQ could have a strong effect on canopy photosynthesis, as predicted by the simulations performed by Zhu et al. (2004). Indeed, biomass production and fitness of *npq4-1* mutants was reported to be lower than wildtype levels when the plants were grown in fluctuating light conditions (Külheim *et al.*, 2002; Krah & Logan, 2010).

### *Photosynthesis in fluctuating light conditions*

Visual analysis of the time series of average photosynthesis during the square wave measurements indicated that there was sufficient time at each fluctuating regime for photosynthesis to reach a dynamic equilibrium (both in the simulations and the experiment). This allowed to calculate an average photosynthesis representative of each combination of genotype, amplitude and period. From this average, we calculated the lightfleck use efficiency as described in the Materials and Methods.

The simulated values of LFUE varied between 0.72 and 0.94 (Fig. 7.7). The variations in the average  $g_{sw}$  across difference replicates created some variation in the value of LFUE for each replicate (error bars in Fig. 7.7). When averaged over amplitude and period, the LFUE of the different genotypes were *col-0* (0.86), *aba2-1* (0.87), *rca-2* (0.78), *spsa1* (0.86) and *npq4-1* (0.85). Thus, only *rca-2* presented a significant difference with respect to the wildtype. Differences across genotypes increased with the amplitude of the square waves, as the LFUE of *rca-2* decreased while that of the other genotypes increased. In some of the mutants, there was an important variation around the mean (e.g. *spsa1* at low amplitudes, Fig. 7.8A). This was caused by variations in  $g_{sw}$  and leaf temperature in the measurements. In the absence of such variations, *spsa1* presented no difference with respect to *col-0*, as TPU never limited photosynthesis during lightflecks.

The effect of the amplitude of the square wave on LFUE was smaller than on average photosynthesis (compare Figs. 7.5 and 7.7). This is not a contradiction, as average irradiance under fluctuating light would decrease with the amplitude of the square wave in the absence of dynamics (i.e. for a steady-state model). This is simply the result of the non-linearity in the light response curve of photosynthesis. The shape of the light response curve of the different mutants barely changed with respect to the wildtype within the range of irradiances used in the experiment (data not shown). Thus, for all genotypes and in the absence of dynamics, we would obtain an average photosynthesis equal to 0.99, 0.96 and

0.67 times the steady-state photosynthesis at the average irradiance, for amplitudes of 100, 200 and 500  $\mu\text{mol m}^{-2} \text{s}^{-1}$ , respectively.

For the different genotypes, amplitudes and periods, the model always predicted that photosynthesis during the high-irradiance half-cycle of the square wave was limited by Rubisco kinetics and it would increase at a slow rate due to Rubisco activation (Fig. 7.8). During the low-irradiance half-cycle of the square wave, photosynthesis was limited by the potential rate of the electron transport. This resulted in an asymmetric pattern, with sharp transitions between limitations and the characteristic transient limitation associated with PICB.

However, the data did not display such patterns. Rather, there was always a smooth transition between the maximum and minimum photosynthesis for each cycle of the

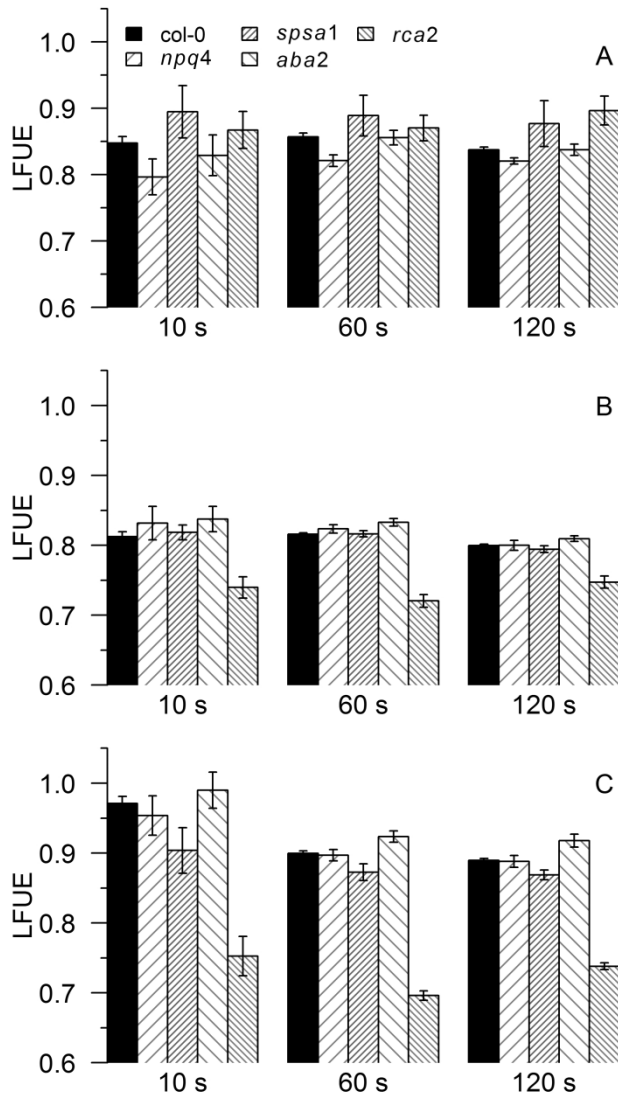


Fig. 7.7. Lightfleck use efficiency (LFUE) for each combination of genotype and period of the square wave for amplitudes of 100 (A), 200 (B) and 500 (C)  $\mu\text{mol m}^{-2} \text{s}^{-1}$ , averaged over all replicates. The error bars represent 95% confidence intervals of the mean across replicates. The variation across replicates was due to variations in stomatal conductance and leaf temperature

square wave. This is due to the effect that a slow time response of an open gas exchange system can have on measurements of dynamic photosynthesis. When we simulated the mixing of  $\text{CO}_2$ , we obtained a significant smoothing of the transients which more closely resembled the patterns in the measurements (Fig. 7.8).

This smoothing creates an apparent post-illumination  $\text{CO}_2$  fixation (PICF, higher values than in the steady state during high to low light transients) and absence of PICB. There is extensive evidence that, under different environmental conditions, leaves show PICF (Percy, 1990) and our simulations with added smoothing still underestimated the measurements in *rca-2* (Fig. 7.8B). However, PICF is reduced in leaves that have previously been exposed to intermediate or high irradiances (Percy *et al.*, 1996), so one should expect that the protocol used to apply the square waves should result in reduced PICF. We conclude that the smoothing effect resulted in an overestimation of the apparent PICF observed in the experiment, as well as an underestimation of the rate at which photosynthesis increased during the high irradiance phase of each cycle.

The phenomenon of PICF is caused by consumption of metabolites in the Calvin cycle, as the pools adjust to the new irradiance (Sharkey *et al.*, 1986; Percy, 1990). The concentrations of metabolites are known to vary with irradiance and  $\text{CO}_2$  concentrations (Badger *et al.*, 1984; von Caemmerer & Edmondson, 1986). Although previous models of leaf photosynthesis have included the dynamics of metabolites in the Calvin cycle (Percy *et al.*, 1997; Kirschbaum *et al.*, 1998) the equations used therein lacked mechanistic justification and contradicted modern hypotheses regarding the regulation of electron transport. Future research should extend the model described in this study in order to pro-

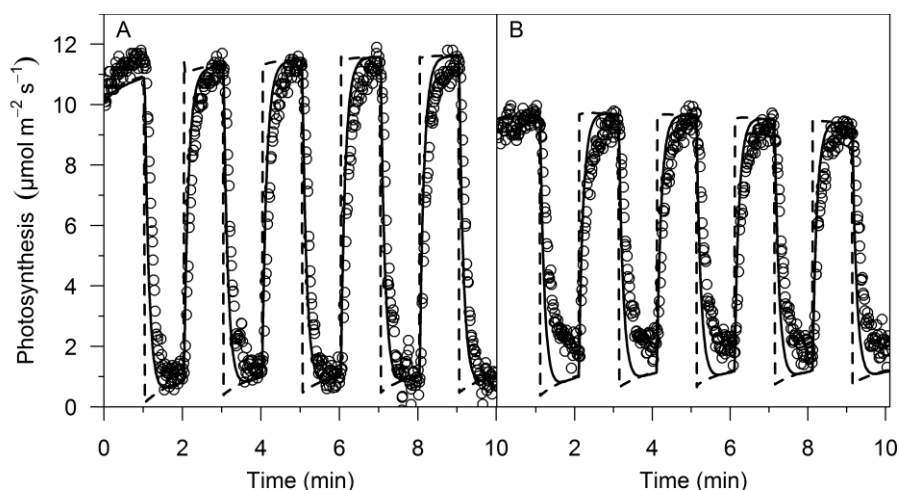


Fig. 7.8. Example of simulated and measured time series of photosynthesis during consecutive lightflecks at an amplitude of  $500 \mu\text{mol m}^{-2} \text{s}^{-1}$  and period of 120 s for *col-0* (A) and *rca-2* (B). The symbols represent measurements, the dashed line is modelled photosynthesis, whereas the solid line is modelled photosynthesis affected by the smoothing effects of the gas exchange system

vide a more accurate simulation of dynamic photosynthesis in conditions in which PICF is relevant.

### *Conclusions*

Despite its simplicity (few parameters), the model accurately predicted the dynamics of leaf photosynthesis and NPQ under a wide range of irradiances. Mutants with pleiotropic side-effects like *aba2-1* or *npq4-1* required recalibration of several parameters in order to reproduce the experimental observations. However, mutants without significant side-effects (*rca-2* and *spsa1*) could be simulated with recalibration of a single parameter that captured the effect of the mutation, which proves that the assumptions of the model are sound and represent the underlying mechanisms correctly. The model was calibrated and validated with measurements of gas exchange and fluorescence, which facilitates future adaptation to different species and growing conditions.

### **Acknowledgements**

This work was carried out within the IPOP Systems Biology programme financed by Wageningen University. This research was also financed in part by the BioSolar Cells open innovation consortium, supported by the Dutch Ministry of Economic Affairs, Agriculture and Innovation. We thank Steven Driever and Herman Berghuijs for helpful discussions during the development of the model and analysis of the data.



## Supplementary Material 7.1: Model Description

### 1 Introduction

This model is an extension of the model for steady-state  $C_3$  photosynthesis proposed by Farquhar et al. (1980). In that model, the rates of carboxylation and oxygenation were calculated according to a mechanistic kinetic model of Rubisco (Farquhar, 1979). However, it is assumed that, under certain conditions, carboxylation could also be limited by the potential production of NADPH (required to regenerate RuBP from the products of carboxylation and oxygenation). We also included the extension by Sharkey (Sharkey, 1985b) by adding a third limitation due to the release of free orthophosphate associated to the export of triose phosphates (this limitation is generally known as “triose phosphate utilisation”).

The model by Farquhar et al. (1980), with the third limitation mentioned above, does not consider how photosynthesis changes during transitions between steady states, nor what happens to processes that are not limiting in the steady state. For example, at low light, when potential NADPH production limits photosynthesis, the actual rate of carboxylation must be adjusted such that production and consumption of NADPH are equal. Similarly, NADPH production must be down-regulated when potential Rubisco kinetics or triose phosphate utilisation are limiting. These adjustments (hereafter called regulation) do not occur instantaneously. This implies that a process that is not limiting in the steady state may become transiently limiting as its actual rate is adjusted. Thus, the dynamics of these regulatory mechanisms affect the dynamics of photosynthesis during transitions between steady states as well as under fluctuating environmental conditions (i.e., when a steady state may not be reached). Therefore, the first step in extending a model of steady state photosynthesis into a model of dynamic photosynthesis is to incorporate dynamic changes in the potential rates of each process. This is described in Sections 2.1 through 2.3 of this document.

In addition, there is empirical evidence that light-dependent activation of enzymes in the regeneration phase of the Calvin cycle can limit photosynthesis during transients (Sassenrath-Cole & Pearcy, 1992; (Sassenrath-Cole *et al.*, 1994). This limitation on photosynthesis is exerted by a direct kinetic limitation by RuBP whose concentration is transiently lower than in the steady state.

In order to scale photosynthesis to the leaf level,  $CO_2$  diffusion into the chloroplasts must be taken into account. The diffusion of  $CO_2$  from the air into the chloroplast may be approximated by a series of resistances in analogy to Ohm's law; and the inverse of resistance is conductance, the term that is more commonly used. Because stomatal

conductance can be measured using porometry and the principles regulating its behaviour are not clear (Lawson *et al.*, 2014b), we decided not to include stomatal conductance in our models. This implies that any simulation will require measured stomatal conductance as input. We included a constant (though temperature-dependent) mesophyll conductance, as it may limit the rate of photosynthesis and also affects estimation of photosynthetic parameters. The net exchange of CO<sub>2</sub> between the leaf and its environment is also dependent on mitochondrial respiration and photorespiration. The equations describing CO<sub>2</sub> diffusion and the calculation of the net exchange of CO<sub>2</sub> are described in Section 3.

Finally, all the measurements used in this study were performed using an open gas exchange system (LI-6400; Li-Cor Biosciences, Lincoln, Nebraska, USA). This type of system introduces a series of artefacts on any dynamic measurement of CO<sub>2</sub> gas exchange and stomatal conductance, which need to be considered in comparisons between simulations and experimental data. In theory, this could be achieved either by correcting the measurements or by adding such artefacts to the simulations. We decided to choose the second option, and the equations required to simulate the perturbations of the measurements are described in Section 4.

The model is implemented as a system of differential equations according to the state-space model formalism, with 13 state variables, 58 parameters, and 6 dynamic inputs. The symbols and definitions of all parameters, state variables, and dynamic inputs are given in Tables S7.1, S7.2, and S7.3, respectively. In the following sections, all the equations in the model are given, along with brief explanatory texts that facilitate the interpretation of the equations and highlight the main assumptions of the model. The equations given below are sufficient to implement the model in any programming language or simulation software, but the source code of the model is also available from the corresponding author upon request. All simulations were performed using the CVODE numerical solver provided by the Sundials library (Hindmarsh *et al.*, 2005). Other ODE solvers may be used, but the user should take into account that the model is a stiff system of differential equations (i.e., the time constants associated to the different processes cover several timescales) and thus ODE solvers suitable for stiff problems are recommended (e.g., LSODA or ode15s).

In the following sections, all the equations of the model are presented and described in detail. Some of the equations used are taken from the literature. When that is the case, the original symbols are not used, but the symbols that correspond to our notation.

## **2 Limiting factors to dynamic photosynthesis**

At any given moment, the rate of carboxylation ( $V_C$ ,  $\mu\text{mol m}^{-2} \text{s}^{-1}$ ) is calculated as the minimum of four potentially limiting factors:

$$V_C = \min(V_{C,NADPH}, V_{C,RB}, V_{C,R}, V_{C,TPU}) \quad (S7.1)$$

where the subscripts “NADPH”, “RB”, “R” and “TPU” refer to limitation by NADPH production (Section 2.2), Rubisco kinetics (Section 2.1), activity of enzymes responsible for RuBP regeneration in the Calvin cycle (Section 2.4) and triose phosphate utilisation (Section 2.3).

## 2.1 Kinetics of carboxylation and oxygenation

### 2.1.1 Potential rate of carboxylation

The potential rate of carboxylation limited by Rubisco kinetics ( $V_{C,RB}$ ,  $\mu\text{mol m}^{-2} \text{s}^{-1}$ ) follows the model proposed by Farquhar (1979) modified to include the effect of partially active Rubisco as:

$$V_{C,RB} = \frac{RB \cdot f_{RB} \cdot K_C \cdot C_C}{C_C + K_M^C \left(1 + \frac{O_2}{K_M^O}\right)} \quad (S7.2)$$

where  $RB$  is the amount of Rubisco catalytic sites per unit of leaf area ( $\mu\text{mol m}^{-2}$ ),  $C_C$  is the  $\text{CO}_2$  concentration in the stroma of the chloroplast ( $\mu\text{M}$ ),  $f_{RB}$  is the fraction of Rubisco catalytic sites that are active (i.e. carbamylated and not occupied by inhibitors),  $K_C$  ( $\text{s}^{-1}$ ) is the rate constant of carboxylation,  $K_M^C$  and  $K_M^O$  are the Michaelis-Menten constants of Rubisco with respect to  $\text{CO}_2$  ( $\mu\text{M}$ ) and  $\text{O}_2$  ( $\text{mM}$ ), respectively. To convert molar fractions of  $\text{CO}_2$  and  $\text{O}_2$  into concentrations we multiplied by air pressure (101 kPa) and the Henry coefficients of  $\text{CO}_2$  and  $\text{O}_2$  ( $0.33 \mu\text{mol dm}^{-3} \text{Pa}^{-1}$  and  $1.28 \times 10^{-5} \text{mmol dm}^{-3} \text{Pa}^{-1}$ , respectively). The rate of oxygenation ( $V_o$ ,  $\mu\text{mol m}^{-2} \text{s}^{-1}$ ) was assumed to be proportional to  $V_c$ :

$$V_o = V_c \phi \quad (S7.3)$$

where  $\phi$  is:

$$\phi = \frac{K_M^C R_{OC} O_2}{K_M^O C_C} \quad (S7.4)$$

$R_{OC}$  is the ratio between maximum rates of oxygenation and carboxylation; it was assumed to be constant.

### 2.1.2 Regulation of Rubisco activity

The values of  $f_{RB}$  were simulated dynamically assuming that Rubisco activation follows first-order kinetics with different rates of activation and deactivation. The rate constant of activation was assumed to be proportional to the amount of Rubisco activase (Mott & Woodrow, 2000) such that:

$$\frac{df_{RB}}{dt} = \begin{cases} (f_{RB}^{SS} - f_{RB})K_{RCA}RCA & \text{if } f_{RB}^{SS} > f_{RB} \\ (f_{RB}^{SS} - f_{RB})K_d^{RB} & \text{if } f_{RB}^{SS} \leq f_{RB} \end{cases} \quad (S7.5)$$

Here,  $f_{RB}^{SS}$  is the steady state value of  $f_{RB}$ ,  $K_{RCA}$  ( $\text{m}^2 \text{mg}^{-1} \text{s}^{-1}$ ) is a second order rate constant of Rubisco activation by Rubisco activase,  $RCA$  is the amount of Rubisco activase per unit of leaf area ( $\text{mg m}^{-2}$ ), and  $K_d^{RB}$  is the rate constant of Rubisco deactivation. The steady state value  $f_{RB}^{SS}$  is computed as follows:

$$f_{RB}^{SS} = \begin{cases} f_{RB,m} & \text{if } I_0 = 0 \\ f_{RB,nr}^{SS} & \text{if } f_{RB,nr}^{SS} < f_{RB,r}^{SS} \text{ and } I_0 > 0 \\ \min(f_{RB,r}^{SS}, f_{RB,M}) & \text{if } f_{RB,nr}^{SS} \geq f_{RB,r}^{SS} \text{ and } I_0 > 0 \end{cases} \quad (\text{S7.6})$$

where  $f_{RB,m}$  is the fraction of Rubisco that remains active in darkness and  $I_0$  is the irradiance incident on the leaf ( $\mu\text{mol m}^{-2} \text{s}^{-1}$ ).  $f_{RB,nr}^{SS}$  is the steady state value of  $f_{RB}$ , which is determined by the environmental conditions. It quantifies the reduction of Rubisco activity at low  $\text{CO}_2$  due to reduced carbamylation.  $f_{RB,r}^{SS}$  is the steady state value of  $f_{RB}$  when carboxylation is limited by NADPH production, triose phosphate utilisation or enzyme activity in the regeneration phase of the Calvin cycle. The maximum value of  $f_{RB}$  is limited by  $f_{RB,M}$ , which in turn is limited by the amount of Rubisco activase (Mate *et al.*, 1996, Mott & Woodrow, 2000):

$$f_{RB,M} = \frac{RCA}{RCA + K_A^{RCA}} \quad (\text{S7.7})$$

where  $K_A^{RCA}$  ( $\text{mg m}^{-2}$ ) is the amount of Rubisco activase at which maximum Rubisco activation is 50% of total Rubisco.  $f_{RB,r}^{SS}$  was calculated by inverting Equation S7.2 combined with Equation S7.1:

$$f_{RB,r}^{SS} = \frac{\min(V_{C,NADPH}, V_{C,R}, V_{C,TPU}) \left( C_C + K_M^C \left( 1 + \frac{O_2}{K_M^O} \right) \right)}{RB \cdot K_C \cdot C_C} \quad (\text{S7.8})$$

The value of  $f_{RB,nr}^{SS}$  was computed as:

$$f_{RB,nr}^{SS} = \frac{C_C}{C_C + K_a^C} \quad (\text{S7.9})$$

where  $K_a^C$  ( $\mu\text{mol mol}^{-1}$ ) is the half-saturation constant of Rubisco activation with respect to  $\text{CO}_2$ .

### 2.1.3 Effect of temperature on Rubisco

Leaf temperature ( $T_L$ , K) was assumed to increase the maximum rate of carboxylation as well as both Michaelis-Menten constants with respect to  $\text{CO}_2$  and  $\text{O}_2$ . This effect follows the Arrhenius equation as described by Walker *et al.* (2013):

$$V_{cmax} = V_{cmax,25} e^{\left( C^{Vcmax} - \frac{\Delta H_A^{Vcmax}}{RT_L} \right)} \quad (\text{S7.10})$$

$$K_M^C = 1 \text{Pa} \cdot e^{\left( C^{Kmc} - \frac{\Delta H_A^{Kmc}}{RT_L} \right)} \quad (\text{S7.11})$$

$$K_M^O = 1 \text{ kPa} \cdot e^{\left( c^{Kmo} - \frac{\Delta H_A^{Kmo}}{RT_L} \right)} \quad (\text{S7.12})$$

where  $c^{V_{cmax}}$ ,  $c^{K_{mc}}$  and  $c^{Kmo}$  are scaling constants,  $\Delta H_A^{V_{cmax}}$ ,  $\Delta H_A^{K_{mc}}$  and  $\Delta H_A^{Kmo}$  ( $\text{kJ mol}^{-1}$ ) are the activation energies of  $V_{cmax}$ ,  $K_M^C$  and  $K_M^O$ , respectively.  $V_{cmax,25}$  ( $\mu\text{mol m}^{-2} \text{ s}^{-1}$ ) is the value of  $V_{cmax}$  at 25 °C (298.15 K) and  $R$  is the universal gas constant ( $8.31 \text{ J mol}^{-1} \text{ K}^{-1}$ ). The scaling constants for  $K_M^C$  and  $K_M^O$  were chosen such that the exponent directly gave the values of the parameter (rather than relative values as in the case of Equation S7.10). However, since exponential functions are always dimensionless, they have to be multiplied by the correct units.

## 2.2 NADPH production

### 2.2.1 Potential rate of electron transport

In the original model by Farquhar et al. (1980), the potential rate of electron transport was calculated employing an empirical function of absorbed irradiance. The original equation has largely been substituted by the following expression (Von Caemmerer, 2000):

$$\theta J_2^{p2} - (I_2 + J_{2max})J_2^p + I_2 J_{2max} = 0 \quad (\text{S7.13})$$

where  $J_2^p$  ( $\mu\text{mol m}^{-2} \text{ s}^{-1}$ ) is the potential rate of electron transport through Photosystem II (PSII),  $I_2$  is the irradiance used for photochemistry ( $\mu\text{mol m}^{-2} \text{ s}^{-1}$ ),  $\theta$  is an empirical parameter that characterises the curvature of the hyperbola and  $J_{2max}$  ( $\mu\text{mol m}^{-2} \text{ s}^{-1}$ ) is the maximum rate of electron transport through PSII. Equation S7.10 was solved by taking the smaller root. This equation allows to take into account that (i) the rate of electron transport is proportional to absorbed irradiance at low light and that (ii) the electron transport rate asymptotically approaches a maximum value ( $J_{2max}$ ) at high light. Whereas the parameter  $\theta$  remains largely empirical, the initial slope can be interpreted in terms of a more mechanistic parameter as described by Yin and Struik (2009):

$$I_2 = I_0 \beta \sigma_2 \phi_{II}^p \quad (\text{S7.14})$$

where  $I_0$  ( $\mu\text{mol m}^{-2} \text{ s}^{-1}$ ) is the incident irradiance,  $\beta$  is the maximum leaf-level light absorbance by photosynthetic pigments,  $\sigma_2$  is the fraction of absorbed irradiance that is absorbed by pigments in the antennae of PSII and  $\phi_{II}^p$  is the maximum quantum yield of PSII.

The rate of electron transport *in vivo* is highly regulated in order to (i) couple the rate of NADPH and ATP production to the metabolic demand and (ii) to protect the protein complexes in the thylakoid from excessive energy that could result in photoinhibition (this type of protection is often called “photoprotection”). Still, exposure to high light intensities for prolonged periods of time results in photoinhibition. These different mechanisms can

affect steady-state photosynthesis (e.g., see Hikosaka *et al.*, 2004 for examples of the effect of photoinhibition) as well as photosynthesis during light transients (Zhu *et al.*, 2004; Armbruster *et al.*, 2014).

Excess energy may be dissipated as heat at the level of the antenna, to protect the reaction centre from excessive excitation. Under steady-state conditions, this form of non-photochemical quenching (NPQ) is assumed not to limit potential electron transport as the loss of quantum yield can be compensated by increasing the fraction of open reaction centres. However, during light transients when light decreases, the low quantum yield can be limiting to electron transport (Armbruster *et al.*, 2014). The description of our implementation of these processes is given in Section 2.2.2. The leaf absorbance in the photosynthetically active region decreases in high light, as chloroplasts move towards the anticlinal walls of the mesophyll cells (Haupt & Scheuerlein, 1990). We implemented this process, using an empirical approach described in Section 2.2.3. Finally, the equations to implement photoinhibition are described in Section 2.2.4. Section 2.2.5 describes how to calculate the maximum rate of carboxylation supported by potential production of NADPH, while Section 2.2.6 describes the equation to calculate the electron transport rate when metabolic demand is limiting. In Section 2.2.7, the equations used to calculate the different fluorescence coefficients from the simulations are provided. These equations do not affect the simulations but are required in order to compare simulations to experimental data obtained with fluorometers.

## 2.2.2 Dissipation of energy as heat

### 2.2.2.1 Teleonomic model of regulated heat dissipation

The mechanisms for dissipation of energy as heat were not simulated explicitly. Instead, we used a “teleonomic” approach whereby we calculated how strongly the quantum yield of PSII had to be reduced in order to achieve a particular degree of photoprotection. We assumed that photoprotection is achieved if, for the same rate of electron transport, the first stable electron acceptor (i.e.  $Q_A$ ) became more oxidised. This reduces the probability of acceptor-side photoinhibition (Tyystjärvi *et al.*, 2005).

As a proxy of oxidised  $Q_A$  we used the so-called qP parameter, calculated as

$$qP = \frac{\min(J_2^p, J_2^m)}{\phi_{II}^p I_2} \quad (S7.15)$$

where  $J_2^m$  ( $\mu\text{mol m}^{-2} \text{s}^{-1}$ ) is the rate of electron transport limited by metabolism (see Section 2.2.6 for details). Equation S7.15 does not imply that qP represents the oxidation state of  $Q_A$ , since energy transfer across antennae will break such an equality (Kramer *et al.*, 2004). However, qP is a monotonous function of  $Q_A$  oxidation state (i.e. as  $Q_A$  becomes more

oxidised, qP increases), it is equal to  $Q_A$  at the extremes (i.e. 0 and 1) and its usage does not require assuming a specific degree of connectivity among antennae of PSII units. We assume that, in the steady state, the increase in qP due to enhanced heat dissipation is proportional to the difference between current qP and a theoretical maximum value of 1:

$$qP^{SS} = qP + f_{qD}(1 - qP) \quad (S7.16)$$

where parameter  $f_{qD}$  is a measure of the overall photoprotective efficiency of the different mechanisms. The quantum yield of PSII, for the same rate of electron transport, but using  $qP^{SS}$  is simply:

$$\phi_{II0}^{SS} = \frac{\min(J_2^p, J_2^m)}{qP^{SS} I_2} \quad (S7.17)$$

Therefore, the reduction in quantum yield can be calculated as:

$$\phi_{qE}^{SS} = \min\left(\phi_{II}^d - \frac{\phi_{II}^{SS}}{(1-f_{II d})}, \phi_{qD,m}\right) \quad (S7.18)$$

where  $\phi_{II}^d$  is the quantum yield of PSII in the absence of photoinhibition and up-regulated heat dissipation,  $f_{II d}$  is the fraction of PSII units that are damaged (see Section 2.2.4), and  $\phi_{qD,m}$  is the maximum loss of PSII quantum yield that can be achieved by these mechanisms. The different mechanisms have been categorised as “fast” and “slow” mechanisms, depending on their kinetics of induction and relaxation. The fast mechanism is analogous to the well-known qE mechanism (Zaks *et al.*, 2012). The slow component corresponds to mechanisms with intermediate kinetics that are still unidentified, but are not associated with changes in absorbance. Such a mechanism was first postulated as a zeaxanthin-dependent qZ component (Nilkens *et al.*, 2010), but evidence from *Arabidopsis thaliana* mutants suggest that it is not dependent on zeaxanthin, although still affected by lumen pH (Dall’Osto *et al.*, 2014). Each group of mechanisms is assigned a fraction of total photoprotective efficiency:

$$f_{qD} = f_{qD}^s + f_{qD}^f \quad (S7.19)$$

where  $f_{qD}^s$  and  $f_{qD}^f$  are the photoprotective efficiencies of the slow and fast mechanisms of enhanced heat dissipation. The loss of quantum yield by the fast component at a given moment is calculated as:

$$\frac{d\phi_{qD}^f}{dt} = \begin{cases} \left(\phi_{qE}^{SS} \cdot \frac{f_{qD}^f}{f_{qD}} - \phi_{qD}^f\right) K_i^{qDf} & \text{if } \phi_{qE}^{SS} \frac{f_{qD}^f}{f_{qD}} > \phi_{qD}^f \\ \left(\phi_{qE}^{SS} \cdot \frac{f_{qD}^f}{f_{qD}} - \phi_{qD}^f\right) K_d^{qDf} & \text{if } \phi_{qE}^{SS} \frac{f_{qD}^f}{f_{qD}} \leq \phi_{qD}^f \end{cases} \quad (S7.20)$$

where  $K_i^{qDf}$  and  $K_d^{qDf}$  ( $s^{-1}$ ) are the rate constants of induction and relaxation. An analogous equation is used to simulate the loss of quantum yield for slow mechanisms:

$$\frac{d\phi_{qD}^s}{dt} = \begin{cases} \left( \phi_{qE}^{ss} \cdot \frac{f_{qD}^s}{f_{qD}} - \phi_{qD}^s \right) K_i^{qDs} & \text{if } \phi_{qE}^{ss} \frac{f_{qD}^s}{f_{qD}} > \phi_{qD}^s \\ \left( \phi_{qE}^{ss} \cdot \frac{f_{qD}^s}{f_{qD}} - \phi_{qD}^s \right) K_d^{qDs} & \text{if } \phi_{qE}^{ss} \frac{f_{qD}^s}{f_{qD}} \leq \phi_{qD}^s \end{cases} \quad (\text{S7.21})$$

where  $K_i^{qDs}$  and  $K_d^{qDs}$  ( $s^{-1}$ ) are the rate constants of induction and relaxation. The actual quantum yield of PSII, once heat dissipation is taken into account, becomes:

$$\phi_{II} = (\phi_{II}^d - \phi_{qD}^s - \phi_{qD}^f)(1 - f_{IIa}) \quad (\text{S7.22})$$

### 2.2.2.2 Transient limitations to photosynthesis

As described above, heat dissipation was assumed to be photoprotective and non-limiting to ETR under steady-state conditions. However, there is evidence (Armbruster *et al.*, 2014) that after irradiance decreases, these mechanisms can be transiently limiting as the losses in quantum yield can no longer be compensated by the redox state of the electron acceptor. We implemented this phenomenon by assuming that, whenever the actual quantum yield was higher than the one at steady-state, the potential rate of electron transport was reduced by a proportional amount:

$$J_2^p = \begin{cases} J_2^p & \text{if } \phi_{II}^{ss} > \phi_{II} \\ \frac{\phi_{II}}{\phi_{II}^{ss}} J_2^p & \text{if } \phi_{II}^{ss} \leq \phi_{II} \end{cases} \quad (\text{S7.23})$$

This equation does not imply that photosynthesis is always reduced whenever  $\phi_{II}^{ss} > \phi_{II}$ . This will only occur if the potential NADPH production limits photosynthesis (i.e. if  $V_{C,NADPH}$  is larger than other terms in Equation S7.1). Therefore, in ambient  $CO_2$  concentration, this limitation is only relevant when switching from high to low irradiances (e.g., during transient shading by clouds or after brief exposure to the sun through gaps in the canopy).

### 2.2.3 Chloroplast avoidance movement

Chloroplast avoidance movement is the mechanism by which chloroplasts respond to irradiance in the blue region of the spectrum by moving towards the anticlinal walls of the mesophyll cells (Haupt & Scheuerlein, 1990). This movement results in a net decrease in leaf-level light absorbance (Davis *et al.*, 2011). The decrease in light absorbance depends on the level of blue irradiance (Kasahara *et al.*, 2002); it has a photoprotective effect (Kasahara *et al.*, 2002; Davis & Hangarter, 2012) and therefore contributes to NPQ (Cazzaniga *et al.*, 2013; 'Dall'Osto *et al.*, 2014) derived from fluorometers (see Section 2.2.7).

Based on the light dependency reported by Kasahara *et al.* (2002) we approximated the effect of total irradiance on steady-state absorbance of photosynthetic pigments in the photosynthetically active region of the spectrum ( $\beta$ ) as follows:



$$\beta^{ss} = \max\left(\beta_0 - \beta_m \frac{I_0}{I_m^\beta}, \beta_m\right) \quad (\text{S7.24})$$

where  $\beta_0$  is the maximum value of  $\beta$  in darkness,  $\beta_m$  is the minimum value of  $\beta$ , at saturating irradiance  $I_m^\beta$  ( $\mu\text{mol m}^{-2} \text{s}^{-1}$ ). Changes in absorbance due to chloroplast movement were assumed to follow first-order kinetics:

$$\frac{d\beta}{dt} = \begin{cases} (\beta^{ss} - \beta)K_i^\beta & \text{if } \beta^{ss} > \beta \\ (\beta^{ss} - \beta)K_d^\beta & \text{if } \beta^{ss} \leq \beta \end{cases} \quad (\text{S7.25})$$

where  $K_i^\beta$  and  $K_d^\beta$  ( $\text{s}^{-1}$ ) are the apparent rate constants at which total leaf absorbance increases and decreases, respectively.

#### 2.2.4 Photoinhibition

In the process of photoinhibition, one has to distinguish between the processes that damage the reaction centres (photodamage) and the processes that contribute to their repair. There are several mechanisms that can contribute to photodamage of reaction centres (Tyystjärvi *et al.*, 2005) and several steps to their repair (Aro *et al.*, 1993). However, empirical evidence indicates that the rate of photodamage is proportional to incident irradiance (see Campbell & Tyystjärvi, 2012 for a review), although corrections due to changes in absorbance are required (Kasahara *et al.*, 2002; Davis & Hangarter, 2012). This proportionality allows defining a fixed quantum efficiency of photodamage ( $K_i^{qI}$ ,  $\text{m}^2 \mu\text{mol}^{-1}$ ). The repair of photodamaged reaction centres was assumed to follow first order kinetics ( $K_d^{qI}$ ,  $\text{s}^{-1}$ ), as proposed by Kok (1956). The fraction of reaction centres that are damaged at a given point in time was calculated as:

$$\frac{df_{II d}}{dt} = (1 - f_{II d})I_0\beta K_i^{qI} - f_{II d}K_d^{qI} \quad (\text{S7.26})$$

The quantum yield of a photodamaged PSII unit is, by definition, null. Also, we assumed that damaged PSII units remain highly quenched, with a constant fluorescence yield similar to the minimum fluorescence yield. From this, one can derive that the effective quantum yield at the population level ( $\phi_{II o}^p$ ) is proportional to the fraction of the population of PSII that remains functional:

$$\phi_{II}^p = \phi_{II}^d(1 - f_{II d}) \quad (\text{S7.27})$$

where  $\phi_{II}^d$  is the quantum yield of PSII in the absence of photoinhibition and up-regulated heat dissipation. The assumptions of our model of photoinhibition are analogous to the ones made by Hikosaka *et al.* (2004) when exploring the effects of photoinhibition on steady-state photosynthesis response curves.

### 2.2.5 Carboxylation limited by NADPH production

The rate of carboxylation limited by NADPH production ( $V_{C,NADPH}$ ,  $\mu\text{mol m}^{-2} \text{s}^{-1}$ ) was calculated as (modified from Yin & Struik, 2009)

$$V_{C,NADPH} = \frac{\min(J_2^p, J_2^{qD}) \left(1 - \frac{f_{pseudo}}{1 - f_{cyc}}\right)}{4(1 + \phi)} \quad (\text{S7.28})$$

where  $J_2^D$  ( $\mu\text{mol m}^{-2} \text{s}^{-1}$ ) is the potential rate of electron transport through PSII with possible limitations due to NPQ.  $f_{pseudo}$  and  $f_{cyc}$  are the fractions of electron transport through PSI that are allocated to pseudo-cyclic and cyclic electron transport, respectively.

### 2.2.6 Electron transport limited by metabolism

When the potential production of NADPH does not limit the flux of intermediates through the Calvin cycle, the electron transport chain needs down-regulation to meet NADPH consumption. Thus, the potential rate of electron transport limited by metabolism ( $J_2^m$ ,  $\mu\text{mol m}^{-2} \text{s}^{-1}$ ) can be calculated by inverting Eqn. S7.25 combined with Eqn. S7.1:

$$J_2^m = \frac{\min(V_{C,RB}, V_{C,R}, V_{C,TPU}) 4(1 + \phi)}{\left(1 - \frac{f_{pseudo}}{1 - f_{cyc}}\right)} \quad (\text{S7.29})$$

When  $V_{C,NADPH}$  is smaller than the other terms in Equation S7.1,  $J_2^m$  will simply be larger than  $J_2^p$  and no down-regulation of the electron transport chain takes place. No assumptions were made regarding the mechanism by which the electron transport chain is down-regulated, except that it must be sufficiently fast, such that it can be considered to be in quasi-steady state at the time scale of seconds.

### 2.2.7 Fluorescence coefficients

The actual rate of electron transport was calculated as:

$$J_2 = \min(J_2^p, J_2^{qD}, J_2^m) = \min(J_2^{qD}, J_2^m) \quad (\text{S7.30})$$

A simplification is achieved if  $J_2^{qD}$  is always equal or lower than  $J_2^p$ . The term  $J_2^{qD}$  includes the effects of chloroplast movement, photoinhibition and heat dissipation, whereas  $J_2^m$  reflects the fact that, even when the above-mentioned mechanisms are active, further down-regulation of the electron transport chain is required when metabolic demand is low (e.g., decrease of PQH<sub>2</sub> oxidation at cyt b<sub>6</sub>f due to acidification of the lumen).

In order to compare simulations with experimental data, it was necessary to compute the coefficients that are generally reported by fluorometers. Our calculations were based on the model of PSII fluorescence developed by Loriaux et al. (2013) which described maximum and minimum fluorescence yields, and we modified these equations to include explicit changes in absorbance, photoinhibition, and up-regulated heat dissipation. The maximum

quantum yield of PSII, in the absence of regulated heat dissipation and photoinhibition, was calculated as:

$$\phi_{II}^d = \frac{F_m}{F_m - F_o} \quad (S7.31)$$

where  $F_m$  and  $F_o$  are the maximum and minimum yields of fluorescence, respectively. The values of  $F_m$  and  $F_o$  can be calculated assuming a single-compartment model of energy transfer in quasi-steady state:

$$F_m = \frac{\beta_0 k_f}{k_f + k_D^0 + k_D^{red}} \quad (S7.32)$$

$$F_o = \frac{\beta_0 k_f}{k_f + k_D^0 + k_p} \quad (S7.33)$$

where  $k_f$  ( $s^{-1}$ ) is the rate of energy dissipation as fluorescence,  $k_D^0$  ( $s^{-1}$ ) is the basal rate of energy dissipation into heat in the antennae,  $k_p$  ( $s^{-1}$ ) is the rate constant of energy quenching by charge separation in the reaction centre, and  $k_D^{red}$  ( $s^{-1}$ ) is a rate constant representing additional losses of energy into heat in closed reactions due to charge recombination and other non-radiative forms of quenching. In light conditions, the maximum and minimum fluorescence yields of active (non-damaged) PSII units ( $F_m'$  and  $F_o'$ ) were calculated as:

$$F_{ma}' = \frac{\beta k_f}{k_f + k_D + k_D^{red}} \quad (S7.34)$$

$$F_{oa}' = \frac{\beta k_f}{k_f + k_D + k_p} \quad (S7.35)$$

where  $k_D$  ( $s^{-1}$ ) is the rate of energy dissipation into heat in the antennae in light. This rate constant was calculated from inverting Equation S7.28 applied to  $\phi_{II}^d - \phi_{qD}^s - \phi_{qD}^f$ :

$$k_D = \frac{k_p - k_D^{red}}{\phi_{II}^d - \phi_{qD}^s - \phi_{qD}^f} - k_f - k_p \quad (S7.36)$$

The maximum and minimum fluorescence of damaged PSII units were assumed to equal the fluorescence yield of open reaction centres:

$$F_{md}' = F_{oa}' \quad (S7.37)$$

$$F_{od}' = F_{oa}' \quad (S7.38)$$

These relationships appear contradictory at first sight, as damaged PSII units do not generate electron transport and one would thus expect them to behave as closed reaction centres. However, experimental results suggest that non-functional PSII units remain in a highly quenched state and thus their fluorescence yields are closer to  $F_{oa}'$  (Krause, 1988; Šetlík *et al.*, 1990). This high quenching has been confirmed by fluorescence lifetime measurements (Renger *et al.*, 1995; Gilmore *et al.*, 1996; Matsubara & Chow, 2004). The measured maximum and minimum fluorescence of the population of PSII units were then calculated as:

$$F'_m = (1 - f_{IIa})F'_{ma} + f_{IIa}F'_{md} = (1 - f_{IIa})F'_{ma} + f_{IIa}F'_{oa} \quad (\text{S7.39})$$

$$F'_o = (1 - f_{IIa})F'_{oa} + f_{IIa}F'_{md} = F'_{oa} \quad (\text{S7.40})$$

Thus, in the absence of photoinhibition, decreases in  $F'_m$  and  $F'_o$  are parallel, whereas photoinhibition only affects  $F'_m$ . Finally, the Stern-Volmer NPQ coefficient was defined as:

$$NPQ = \frac{F_m}{F_{m'}} - 1. \quad (\text{S7.41})$$

The contributions to NPQ of photoinhibition (qI), change in leaf-level light absorbance (qA), and fast and slow heat dissipation (qD<sub>f</sub> and qD<sub>s</sub>) were defined as follows:

$$qI = \frac{F_m}{(1 - f_{IIa})F_m + f_{IIa}F_o} - 1 \quad (\text{S7.42})$$

$$qD_s = (NPQ - qI - qA) \frac{\phi_{qD}^s}{\phi_{qD}^s + \phi_{qD}^f} \quad (\text{S7.43})$$

$$qD_f = (NPQ - qI - qA) \frac{\phi_{qD}^f}{\phi_{qD}^s + \phi_{qD}^f} \quad (\text{S7.44})$$

$$qA = NPQ - \left( \frac{F_m}{F_{m_a'}} \frac{\beta}{\beta_0} - 1 \right) \quad (\text{S7.45})$$

### 2.2.8 Effect of temperature on electron transport rates

Temperature effects on maximum ETR were calculated as in Bernacchi et al. (2003):

$$J_{max} = J_{max,25} \frac{e^{\left( cJ_{max} \frac{\Delta H_A^{J_{max}}}{RT_L} \right)}}{1 + e^{\left( \frac{T_L \Delta S^{J_{max}} - \Delta H_d^{J_{max}}}{RT_L} \right)}} \quad (\text{S7.46})$$

where  $J_{max,25}$  is the value of  $J_{max}$  at 25 °C (298.15 K),  $c^{J_{max}}$  is a scaling constant,  $\Delta H_A^{J_{max}}$  (kJ mol<sup>-1</sup>) is the activation energy of  $J_{max}$ ,  $\Delta S^{J_{max}}$  (J mol<sup>-1</sup> K<sup>-1</sup>) is an apparent entropy coefficient of  $J_{max}$  and  $\Delta H_d^{J_{max}}$  (kJ mol<sup>-1</sup>) is the deactivation energy of  $J_{max}$ .

### 2.3 Triose phosphate utilisation

The rate of carboxylation limited by triose phosphate utilisation was (Sharkey, 2015):

$$V_{C,TPU} = \frac{3TPU}{1 - \frac{(1+3\alpha)\phi}{2}} \quad (\text{S7.47})$$

where  $TPU$  (μmol m<sup>-2</sup> s<sup>-1</sup>) is the maximum rate of triose phosphate utilisation and  $\alpha$  is an empirical parameter that captures declines of TPU at high CO<sub>2</sub> concentrations. The exact mechanistic basis of this decrease is unclear and could be the result of several processes. Thus, current interpretations of this equation recommend the use of  $\alpha$  as an empirical parameter (Sharkey, 2015). Temperature effects on  $TPU$  were calculated as in Sharkey et al. (2007):

$$TPU = TPU_{25} \frac{e^{\left(\frac{c^{TPU} - \Delta H_A^{TPU}}{RT_L}\right)}}{1 + e^{\left(\frac{T_L \Delta S^{TPU} - \Delta H_d^{TPU}}{RT_L}\right)}} \quad (S7.48)$$

where  $TPU_{25}$  is the value of  $TPU$  at 25 °C (298.15 K),  $c^{TPU}$  is a scaling constant,  $\Delta H_A^{TPU}$  (kJ mol<sup>-1</sup>) is the activation energy of  $TPU$ ,  $\Delta S^{TPU}$  (J mol<sup>-1</sup> K<sup>-1</sup>) is an apparent entropy coefficient of  $TPU$  and  $\Delta H_d^{TPU}$  (kJ mol<sup>-1</sup>) is the deactivation energy of  $TPU$ .

## 2.4 Regeneration of RuBP

The rate of carboxylation limited by enzymes in the regeneration phases of the Calvin cycle was calculated analogous to the limitation by NADPH production:

$$V_{C,R} = \frac{f_R V_{rmax}}{1 + \phi} \quad (S7.49)$$

where  $f_R$  is the fraction of the limiting enzyme in the regeneration phase that is active, and  $V_{rmax}$  (μmol m<sup>-2</sup> s<sup>-1</sup>) is the maximum rate of RuBP regeneration limited by the kinetics of enzymes in the regeneration phase. In order to construct Equation S7.49, there is no need to assume a specific enzyme to be limiting in the regeneration phase, as long as it is regulated by irradiance. Most likely, the limiting step during transients is FBPase or phosphoribulokinase (Sassenrath-Cole & Pearcy, 1992; Sassenrath-Cole *et al.*, 1994). This step was assumed to be limiting only during transients, not in the steady state. Its effect on carboxylation is achieved due to transiently low concentrations of RuBP that kinetically limit the reaction of carboxylation. The steady-state fraction of the enzyme that is active increases with irradiance (Sassenrath-Cole & Pearcy, 1992; Sassenrath-Cole *et al.*, 1994):

$$f_R^{SS} = \min\left(1, \frac{I_0}{I_m^R}\right) \quad (S7.50)$$

where  $I_m^R$  (μmol m<sup>-2</sup> s<sup>-1</sup>) is the irradiance at which maximum activity is reached. The actual fraction of active enzyme changes following first order kinetics:

$$\frac{df_R}{dt} = \begin{cases} (f_R^{SS} - f_R)K_i^R & \text{if } f_R^{SS} > f_R \\ (f_R^{SS} - f_R)K_d^R & \text{if } f_R^{SS} \leq f_R \end{cases} \quad (S7.51)$$

where  $K_i^R$  and  $K_d^R$  (s<sup>-1</sup>) are the rate constants of enzyme activation and deactivation, respectively.

## 3 CO<sub>2</sub> diffusion

### 3.1 (Photo)respiration

The rate of mitochondrial respiration ( $R_d$ , μmol m<sup>-2</sup> s<sup>-1</sup>) was assumed to be constant and independent of light. Photorespiratory intermediates ( $PR$ , μmol m<sup>-2</sup>) are generated by oxygenation and are processed by the photorespiratory pathway assuming first order kinetics:

$$\frac{dPR}{dt} = V_C \phi - PR \cdot K_{PR} \quad (S7.52)$$

where  $K_{PR}$  ( $s^{-1}$ ) is the apparent rate constant at which photorespiration intermediates are consumed. This introduces a delay between the release of  $CO_2$  from glycine decarboxylase and oxygenation by Rubisco, which can transiently decrease the net exchange of  $CO_2$  when irradiance decreases, contributing to the post-illumination  $CO_2$  burst (Kaiser *et al.*, 2015).

### 3.2 $CO_2$ exchange

The net flux of  $CO_2$  into the chloroplast was calculated as the balance of carboxylation and  $CO_2$  released from mitochondrial respiration and photorespiration:

$$A = V_C - 0.5PR \cdot K_{PR} - R_d \quad (S7.53)$$

The chloroplast  $CO_2$  concentration was computed assuming a resistance-based approach:

$$\frac{dC_C}{dt} = \frac{[(C_i - C_C)g_m - A]T_{LR}}{V_r P} \quad (S7.54)$$

where  $g_m$  ( $mol\ m^{-2}\ s^{-1}$ ) is the bulk mesophyll conductance assumed to be fixed and independent of environmental conditions,  $C_i$  ( $\mu mol\ mol^{-1}$ ) is the  $CO_2$  molar fraction in the intercellular spaces, and  $P$  is air pressure (101 kPa).  $V_r$  is the leaf volume per unit of surface (i.e., equivalent to leaf width). A similar equation was used to calculate changes in  $C_i$ :

$$\frac{dC_i}{dt} = \frac{\left[ \frac{C_s - C_i}{1.6/g_{sw} + 1.37/g_{bw}} - (C_i - C_C)g_m \right] T_{LR}}{V_r P} \quad (S7.55)$$

where  $g_{sw}$  and  $g_{bw}$  are the stomatal and boundary layer conductances to fluxes of  $H_2O$  ( $mol\ m^{-2}\ s^{-1}$ ), respectively.

### 3.3 Effect of temperature on $g_m$

The sensitivity to temperature of  $g_m$  is calculated as described by Walker *et al.* (2013):

$$g_m = g_{m,25} \frac{e^{\left( c g_m \frac{\Delta H_A^{g_m}}{RT_L} \right)}}{1 + e^{\left( \frac{T_L \Delta S^{g_m} - \Delta H_d^{g_m}}{RT_L} \right)}} \quad (S7.56)$$

where  $g_{m,25}$  is the value of  $g_m$  at 25 °C (298.15 K),  $\Delta H_A^{g_m}$  ( $kJ\ mol^{-1}$ ) is the activation energy of  $g_m$ ,  $\Delta S^{g_m}$  ( $J\ mol^{-1}\ K^{-1}$ ) is an apparent entropy coefficient of  $g_m$  and  $\Delta H_d^{g_m}$  ( $kJ\ mol^{-1}$ ) is the deactivation energy of  $g_m$ .

## 4 Corrections due to open gas exchange system

The measurements of dynamic photosynthesis used in this study were performed with the LI6400 open gas exchange system (LI-COR Biosciences, Lincoln, Nebraska USA). This system encloses the leaf in a cuvette where air of known  $CO_2$  concentrations ( $C_r$ ,  $\mu mol\ mol^{-1}$ ) is introduced into the cuvette. The exchange of  $CO_2$  with the leaf alters this

concentration, the outflow concentration ( $C_s$ ,  $\mu\text{mol mol}^{-1}$ ) is measured by an infra-red gas analyzer (IRGA) and the difference between the two is used to calculate the rate of net  $\text{CO}_2$  exchange between the leaf and the air ( $Photo$ ,  $\mu\text{mol m}^{-2} \text{s}^{-1}$ ) as follows:

$$Photo = \frac{F_L C_R - (F_L + s_L E) C_S}{s_L} \quad (\text{S7.57})$$

where  $F_L$  ( $\mu\text{mol s}^{-1}$ ) is the air flow in the open gas exchange system,  $E$  ( $\text{mol m}^{-2} \text{s}^{-1}$ ) is the rate of transpiration and  $s_L$  ( $\text{m}^2$ ) is the surface of leaf exposed to the cuvette. Changes in  $C_s$  can be calculated to a first-order approximation as:

$$\frac{dC_s}{dt} = \frac{-(F_L + s_L E) C_S + F_L C_r + s_L A_n}{V_{ch} P} R T_a \quad (\text{S7.58})$$

where  $T_a$  (K) is the temperature of the sample air,  $R$  ( $\text{J mol}^{-1} \text{K}^{-1}$ ) is the universal gas constant,  $P$  (kPa) is air pressure and  $V_{ch}$  ( $\text{m}^3$ ) is the total mixing volume between the leaf surface and the IRGA sensors. Given a chamber volume of  $80 \text{ cm}^3$ , a temperature of  $25 \text{ }^\circ\text{C}$  and a flow of  $500 \mu\text{mol s}^{-1}$ , the time constant of the system associated with Equation S7.58 was  $6.53 \text{ s}$ .

## Supplementary Material 7.2

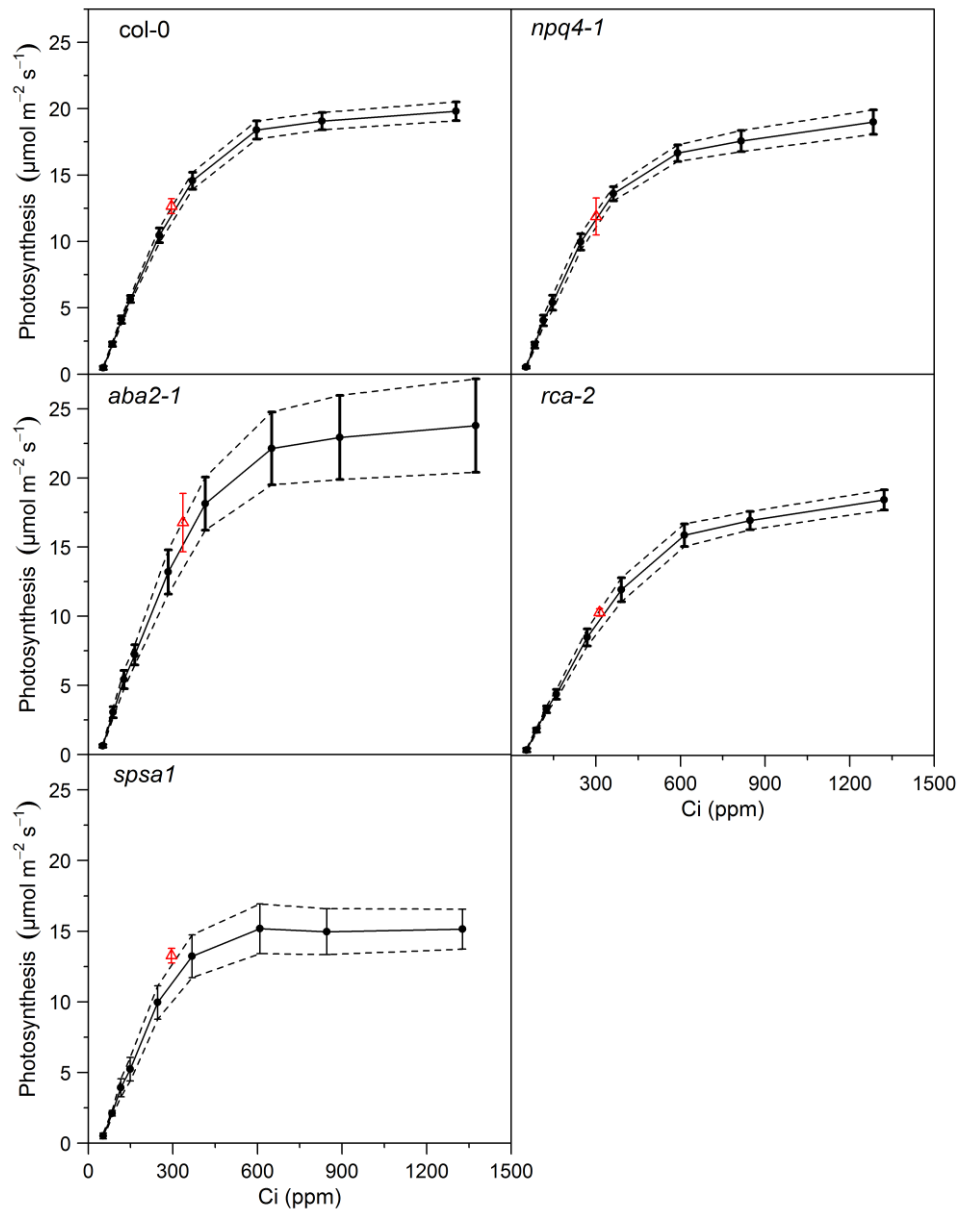


Fig. S7.1. Average CO<sub>2</sub> response curve (circles) and average photosynthesis at the end of the induction curve at  $1000 \mu\text{mol m}^{-2} \text{s}^{-1}$  (triangles). Data were derived from measurements. The averaging was performed over all replicates. The solid line represents the linear interpolation of the CO<sub>2</sub> response curve. All error bars represent 95% confidence intervals of the mean across replicates, and dashed lines represent their linear interpolation



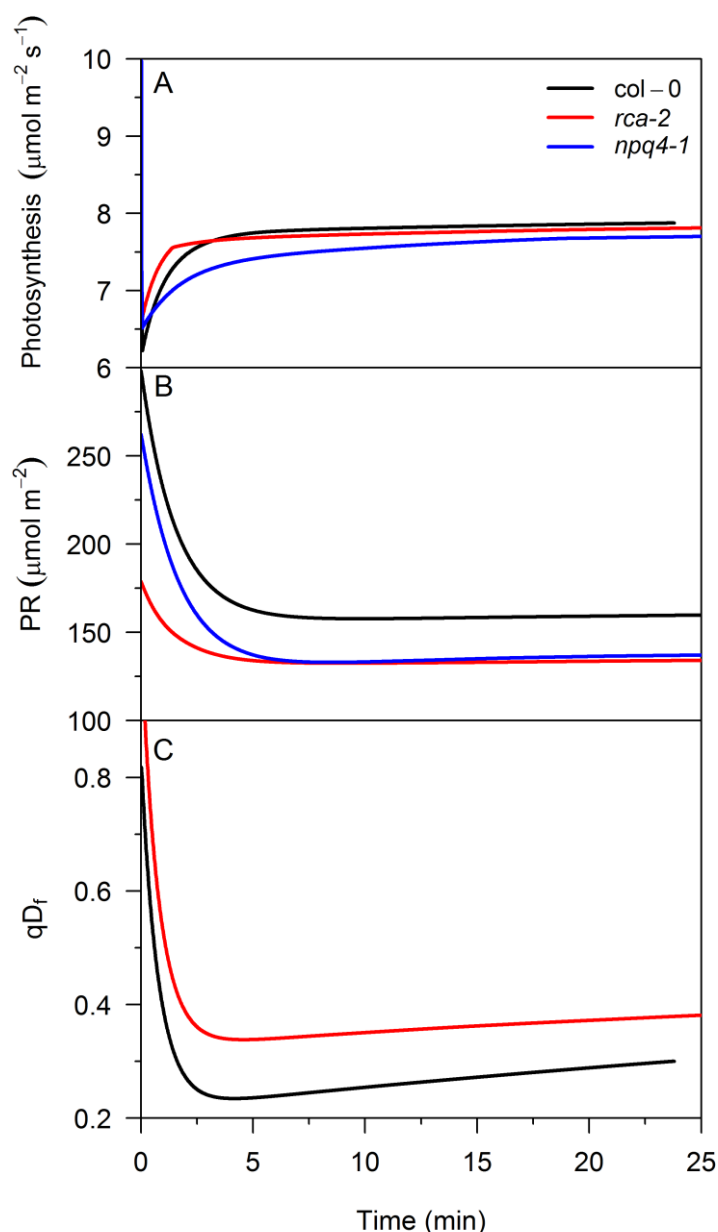


Fig. S7.2. Simulated photosynthesis (A), amount of photorespiration intermediates (B) and fast mechanism of heat dissipation (C) during a light transient where irradiance was decreased from 600 to 200  $\mu\text{mol m}^{-2} \text{s}^{-1}$

Table S7.1. Model parameters. When a parameter was not fitted to experimental data obtained from Kaiser et al. (Chapter 6), the source indicates the publications from where the parameters were taken or calculated. In some cases, the parameters were settings of the measurements (indicated as "known"). The fitted parameters refer to Col-0 (see Table S7.4 for the values associated to the mutants). All equations can be found in Supplementary Material 7.1. When a parameter appears in multiple equations, only the first equation is referenced

Parameter	Definition	Units	Value	Source	Equation
$c^{V_{cmax}}$	Scaling constant of the temperature response of $V_{cmax}$		16.6	Walker et al. (2013)	S7.10
$c^{K_{mc}}$	Scaling constant of the temperature response of $K_M^c$		23.2	Walker et al. (2013)	S7.11
$c^{K_{mo}}$	Scaling constant of the temperature response		14.7	Walker et al. (2013)	S7.12

	of $K_M^o$				
$c^{J_{max}}$	Scaling constant of the temperature response of $J_{max}$		17.7	Walker et al. (2013)	S7.46
$c^{TPU}$	Scaling constant of the temperature response of $TPU$		21.5	Sharkey et al. (2007)	S7.48
$c^{g_m}$	Scaling constant of the temperature response of $g_m$		3.0	Walker et al. (2013)	S7.56
$\Delta H_A^{V_{cmax}}$	Activation energy of $V_{cmax}$	$\text{kJ mol}^{-1}$	41.4	Walker et al. (2013)	S7.10
$\Delta H_A^{K_{Mc}^c}$	Activation energy of $K_M^c$	$\text{kJ mol}^{-1}$	49.7	Walker et al. (2013)	S7.11
$\Delta H_A^{K_{Mo}^o}$	Activation energy of $K_M^o$	$\text{kJ mol}^{-1}$	29.1	Walker et al. (2013)	S7.12
$\Delta H_A^{J_{max}}$	Activation energy of $J_{max}$	$\text{kJ mol}^{-1}$	43.9	Bernacchi et al (2003)	S7.46
$\Delta H_A^{TPU}$	Activation energy of $TPU$	$\text{kJ mol}^{-1}$	53.1	Sharkey et al (2007)	S7.48
$\Delta H_A^{g_m}$	Activation energy of $g_m$	$\text{kJ mol}^{-1}$	7.4	Walker et al. (2013)	S7.56
$\Delta S^{J_{max}}$	Entropy of $J_{max}$	$\text{kJ mol}^{-1} \text{K}^{-1}$	1.4	Bernacchi et al (2003)	S7.46
$\Delta S^{TPU}$	Entropy of $TPU$	$\text{kJ mol}^{-1} \text{K}^{-1}$	0.65	Sharkey et al (2007)	S7.48
$\Delta S^{g_m}$	Entropy of $g_m$	$\text{kJ mol}^{-1} \text{K}^{-1}$	1.4	Walker et al. (2013)	S7.56
$\Delta H_d^{J_{max}}$	Deactivation energy of $J_{max}$	$\text{kJ mol}^{-1}$	439.8	Bernacchi et al (2003)	S7.46
$\Delta H_d^{TPU}$	Deactivation energy of $TPU$	$\text{kJ mol}^{-1}$	201.8	Sharkey et al (2007)	S7.48
$\Delta H_d^{g_m}$	Deactivation energy of $g_m$	$\text{kJ mol}^{-1}$	434.0	Walker et al. (2013)	S7.56
$f_{cyc}$	Fraction of electron transport through PSI that goes into the cyclic pathway		0.05	Yin and Struik (2009)	S7.28
$F_L$	Air flow in the open gas exchange system	$\mu\text{mol s}^{-1}$	500	Known	S7.57
$f_{pseudo}$	Fraction of electron transport through PSI that goes into the pseudocyclic pathway		0.1	Yin and Struik (2009)	S7.28
$f_{qD}^f$	Photoprotective efficiency of the fast mechanism of enhanced heat dissipation		$1.93 \cdot 10^{-2}$	Fitted	S7.19
$f_{qD}^s$	Photoprotective efficiency of the slow mechanism of enhanced heat dissipation		$2.68 \cdot 10^{-2}$	Fitted	S7.19
$f_{RB,m}$	Fraction of Rubisco that remains active in darkness		$2.55 \cdot 10^{-1}$	Fitted	S7.6

$g_{bw}$	Boundary layer conductance to fluxes of water vapour	$\text{mol m}^{-2} \text{s}^{-1}$	9.29	Known	S7.55
$g_{m,25}$	Bulk mesophyll conductance at 25 °C	$\text{mol m}^{-2} \text{s}^{-1}$	0.2	Flexas et al. (2007)	S7.56
$I_m^R$	Irradiance at which maximum activity of enzymes in the regeneration phase of Calvin cycle is achieved	$\mu\text{mol m}^{-2} \text{s}^{-1}$	300	Sassenrath-Cole et al. (1994)	S7.50
$I_m^\beta$	Irradiance at which minimum leaf absorbance is achieved	$\mu\text{mol m}^{-2} \text{s}^{-1}$	500	Kasahara et al. (2002)	S7.24
$J_{max,25}$	Maximum rate of electron transport through PSII	$\mu\text{mol m}^{-2} \text{s}^{-1}$	119.17	Fitted	S7.13
$K_a^C$	Half-saturation constant of Rubisco activation with respect to $\text{CO}_2$	Pa	0.71	von Caemmerer and Edmonson (1986)	S7.9
$K_A^{RCA}$	Amount of Rubisco activase at which maximum Rubisco activation is 50% of total Rubisco	$\text{mg m}^{-2}$	12.3	Mott and Woodrow (2000)	S7.7
$K_C$	Rate constant of carboxylation	$\text{s}^{-1}$	4.4	Walker et al. (2013)	S7.2
$k_D^0$	Basal rate of energy dissipation as heat in LHCII	$\text{s}^{-1}$	$2.2 \cdot 10^9$	Loriaux et al. (2013)	S7.32
$K_d^{qDf}$	Rate constant of relaxation of the fast mechanism of enhanced heat dissipation	$\text{s}^{-1}$	$2.0 \cdot 10^{-2}$	Nilkens et al. (2010)	S7.20
$K_d^{qDs}$	Rate constant of relaxation of the slow mechanism of enhanced heat dissipation	$\text{s}^{-1}$	$1.1 \cdot 10^{-3}$	Nilkens et al. (2010)	S7.21
$K_d^{qI}$	Rate constant of protein D1 repair	$\text{s}^{-1}$	$1.3 \cdot 10^{-4}$	Kasahara et al. (2002)	S7.26
$K_d^{RB}$	Apparent rate constant of Rubisco deactivation	$\text{s}^{-1}$	$4.2 \cdot 10^{-4}$	Kirschbaum et al. (1998)	S7.5
$k_D^{red}$	Rate constant of other forms of non-radiative energy losses in closed PSII units	$\text{s}^{-1}$	$2.3 \cdot 10^8$	Loriaux et al. (2013)	S7.32
$K_d^\beta$	Rate constant of decrease in leaf absorbance	$\text{s}^{-1}$	$1.7 \cdot 10^{-3}$	Dall'Osto et al. (2014)	S7.25
$k_f$	Rate of energy dissipation as fluorescence in LHCII	$\text{s}^{-1}$	$5.6 \cdot 10^7$	Loriaux et al. (2013)	S7.32
$K_i^{qDf}$	Rate constant of induction of the fast	$\text{s}^{-1}$	$4.0 \cdot 10^{-2}$	Nilkens et al. (2010)	S7.20

	mechanism of enhanced heat dissipation				
$K_i^{qDs}$	Rate constant of induction of the slow mechanism of enhanced heat dissipation	$s^{-1}$	$1.7 \cdot 10^{-3}$	Nilkens et al. (2010)	S7.21
$K_i^{qI}$	Quantum efficiency of photodamage	$m^2 \mu mol^{-1}$	$7.4 \cdot 10^{-8}$	Kasahara et al. (2002)	S7.26
$K_i^R$	Rate constant of activation of enzymes in the regeneration phase of Calvin cycle	$s^{-1}$	$1.67 \cdot 10^{-3}$	Fitted	S7.51
$K_i^\beta$	Rate constant of increase in leaf absorbance	$s^{-1}$	$5.9 \cdot 10^{-4}$	Dall'Osto et al. (2014)	S7.25
$K_M^C$	Rubisco Michaelis-Menten constant with respect to $CO_2$	$\mu M$	8.9	Walker et al. (2013)	S7.2
$K_M^O$	Rubisco Michaelis-Menten constant with respect to $O_2$	mM	$2.6 \cdot 10^{-1}$	Walker et al. (2013)	S7.2
$k_p$	Rate constant of charge separation	$s^{-1}$	$2.6 \cdot 10^9$	Loriaux et al. (2013)	S7.33
$K_{PR}$	Apparent rate constant at which photorespiration intermediates are consumed	$s^{-1}$	0.01	Pearcy et al. (1997)	S7.52
$K_{RCA}$	Second order rate constant of Rubisco activation by Rubisco activase	$m^2 mg^{-1} s^{-1}$	$6.42 \cdot 10^{-5}$	Fitted	S7.5
$K_d^R$	Rate constant of deactivation of enzymes in the regeneration phase of Calvin cycle	$s^{-1}$	$3.0 \cdot 10^{-3}$	Kirschbaum et al. (1998)	S7.51
$O_2$	Oxygen molar fraction	$mmol mol^{-1}$	210	Known	S7.2
$P$	Air pressure	kPa	101	Known	S7.54
$\phi_{qDs,m}$	Maximum loss of PSII quantum yield that can be achieved by slow mechanism of heat dissipation		$4.31 \cdot 10^{-2}$	Fitted	S7.18
$\phi_{qDf,m}$	Maximum loss of PSII quantum yield that can be achieved by fast mechanism of heat dissipation		$1.77 \cdot 10^{-1}$	Fitted	S7.18
$R$	Universal gas constant	$J mol^{-1} K^{-1}$	8.31	NIST Physical Measurement Laboratory (2015)	S7.54
$RB$	Amount of Rubisco catalytic sites per unit	$\mu mol m^{-2}$	12.03	Fitted	S7.2

	of leaf area				
$RCA$	Amount of Rubisco activase per unit of leaf area	$\text{mg m}^{-2}$	124.4	Mott and Woodrow (2000); Carmo-Silva & Salvucci (2013)	S7.5
$R_{d,25}$	Rate of mitochondrial respiration	$\mu\text{mol m}^{-2} \text{s}^{-1}$	0.76	Fitted	S7.53
$R_{oc}$	Ratio between maximum rates of oxygenation and carboxylation		0.24	Walker et al. (2013)	S7.4
$s_L$	The surface of leaf exposed to the cuvette	$\text{cm}^2$	2	Li-Cor (2012)	S7.57
$TPU_{25}$	Maximum rate of triose phosphate utilization	$\mu\text{mol m}^{-2} \text{s}^{-1}$	10.0	Fitted	S7.47
$V_{ch}$	Total mixing volume between the leaf surface and the IRGA sensors	$\text{cm}^3$	80	LI-COR, Inc. (2012)	S7.58
$V_r$	Leaf volume per unit of surface	$\text{m}$	$1.5 \cdot 10^{-4}$	Weraduwage et al. (2015)	S7.54
$V_{rmax}$	Maximum rate of RuBP regeneration limited by the kinetics of enzymes in the regeneration phase	$\mu\text{mol m}^{-2} \text{s}^{-1}$	46.47	Assumed	S7.49
$\beta_0$	Maximum leaf absorbance by photosynthetic pigments		0.85	Davis et al. (2011)	S7.24
$\beta_m$	Minimum leaf absorbance		0.78	Davis et al. (2011)	S7.24
$\theta$	Empirical parameter that characterizes the curvature of the relationship between irradiance and potential electron transport		0.745	Fitted	S7.13
$\sigma_2$	Fraction of absorbed irradiance that is absorbed by pigments in LHCI		0.5	Yin and Struik (2009)	S7.14

Table S7.2. State variables of the model

Variable	Definition	Unit
$C_C$	$\text{CO}_2$ molar fraction inside the chloroplast	$\mu\text{mol mol}^{-1}$
$C_s$	$\text{CO}_2$ molar fraction in the sample air of the gas exchange system	$\mu\text{mol mol}^{-1}$
$f_{II d}$	Fraction of PSII units that are damaged	
$f_R$	Fraction of enzyme that potentially limits RuBP regeneration that is active	
$f_{RB}$	Fraction of Rubisco that is active	
$\phi_{qD}^f$	Loss of quantum yield of PSII due to fast mechanisms of heat dissipation	
$\phi_{qD}^s$	Loss of quantum yield of PSII due to slow mechanisms of heat dissipation	
$PR$	Amount of photorespiratory intermediates	$\mu\text{mol m}^{-2}$

Table S7.3. Dynamic inputs of the model

Variable	Definition	Unit
$g_{sw}$	Stomatal conductance to water vapour	$\text{mol m}^{-2} \text{s}^{-1}$
$I_0$	Irradiance incident on the leaf	$\mu\text{mol m}^{-2} \text{s}^{-1}$
$C_r$	CO <sub>2</sub> molar fraction in the reference air of the open gas exchange system	$\mu\text{mol mol}^{-1}$
$E$	Rate of transpiration	$\text{mol m}^{-2} \text{s}^{-1}$
$T_a$	Air temperature	K
$T_L$	Leaf temperature	K

Table S7.4. Parameters that differ with respect to wildtype for each mutant. All values were obtained by fitting to experimental data

Parameter	Mutant	Definition	Unit	Value
$g_m$	<i>aba2-1</i>	Bulk mesophyll conductance	$\text{mol m}^{-2} \text{s}^{-1}$	0.33
$J_{max,25}$	<i>aba2-1</i>	Maximum rate of electron transport through PSII	$\mu\text{mol m}^{-2} \text{s}^{-1}$	146.53
$\beta_m$	<i>aba2-1</i>	Minimum leaf-level light absorbance		0.85
$V_{max}$	<i>aba2-1</i>	Maximum rate of RuBP regeneration limited by the kinetics of enzymes in the regeneration phase	$\mu\text{mol m}^{-2} \text{s}^{-1}$	62.66
$RB$	<i>aba2-1</i>	Amount of Rubisco catalytic sites per unit of leaf area	$\mu\text{mol m}^{-2}$	12.68
$RCA$	<i>rca-2</i>	Amount of Rubisco activase per unit of leaf area	$\text{mg m}^{-2}$	25.52
$f_{qD}^f$	<i>npq4-1</i>	Photoprotective efficiency of the fast mechanism of enhanced heat dissipation		0
$f_{qD}^s$	<i>npq4-1</i>	Photoprotective efficiency of the slow mechanism of enhanced heat dissipation		$2.88 \cdot 10^{-2}$
$\phi_{qDs,m}$	<i>npq4-1</i>	Maximum loss of PSII quantum yield that can be achieved by slow mechanism of heat dissipation		$6.75 \cdot 10^{-2}$
$K_i^{qI}$	<i>npq4-1</i>	Quantum efficiency of photodamage	$\text{m}^2 \mu\text{mol}^{-1}$	$1.13 \cdot 10^{-7}$
$f_{qD}^s$	<i>npq4-1</i>	Photoprotective efficiency of the slow mechanism of enhanced heat dissipation		$3.10 \cdot 10^{-3}$
$TPU_{25}$	<i>spsa1</i>	Maximum rate of triose phosphate utilization	$\mu\text{mol m}^{-2} \text{s}^{-1}$	5.36

# **CHAPTER 8**

General discussion

Elias Kaiser

*“In any event, it is clear that much is to be learned concerning the dynamics of photosynthesis, and it is hoped that the considerations here set forth may be of value in this connection.”*

*Osterhout and Haas, 1918*

In this thesis, the control of dynamic photosynthesis (i.e. photosynthesis in fluctuating irradiance) by physiological processes and environmental factors has been addressed. Experiments were carried out using closely related genotypes of tomato (*Solanum lycopersicum* L.) and *Arabidopsis thaliana*, and varying irradiance regimes and several other environmental factors. The methodology involved literature review, gas exchange and chlorophyll fluorescence measurements, and mathematical modelling. The main findings are that a) CO<sub>2</sub> concentration ([CO<sub>2</sub>]) and air humidity strongly affect the rate of change of photosynthesis in fluctuating irradiance through a combination of diffusional and biochemical limitations; b) Rubisco activation kinetics are pivotal in controlling rates of photosynthesis increase after a stepwise increase in irradiance, and are further affected by background irradiance and [CO<sub>2</sub>]; c) stomatal conductance (g<sub>s</sub>) limits photosynthetic induction kinetics in *A. thaliana* but not in tomato in ambient conditions, and becomes a stronger limitation in low [CO<sub>2</sub>] or air humidity; and d) mesophyll conductance (g<sub>m</sub>), non-photochemical quenching (NPQ) and sucrose synthesis did not limit rates of dynamic photosynthesis under the conditions used.

### **Physiological limitations and their environmental modulation**

In this thesis, limitations due to Rubisco, g<sub>s</sub>, NPQ, sucrose synthesis and g<sub>m</sub> have been investigated. Furthermore, it was analysed how the environmental factors [CO<sub>2</sub>], leaf temperature, leaf-to-air vapour pressure deficit (VPD<sub>leaf-air</sub>) and blue irradiance impact on induction rates, and how they affect Rubisco activation and transient changes in g<sub>s</sub>, g<sub>m</sub> and NPQ.

#### *Rubisco activation*

The activation state of Rubisco generally has a similar shape to the irradiance response of net photosynthesis rates. Thus, in low irradiance, the activation state of Rubisco increases linearly with small increments in irradiance, and at higher irradiance it approaches saturation (Brooks & Portis, 1988; Lan *et al.*, 1992). Because of its low activation state in darkness or shade, Rubisco activity can quickly become limiting after an increase in irradiance, once sufficient pools of RuBP have been built up (Percy *et al.*, 1996). Activation of Rubisco requires, in sequence, the binding of a CO<sub>2</sub> molecule (carbamylation)



and of a  $Mg^{2+}$  molecule (reviewed in Tcherkez, 2013). After the subsequent addition of the substrate RuBP and enolization (which changes the structure of the enzymatic complex), another  $CO_2$  molecule can bind to the enzyme, which is then fixed (Tcherkez, 2013). If, however, RuBP binds to uncarbamylated catalytic sites of Rubisco, their activity is inhibited. The same is true for several other inhibitory compounds (Salvucci & Crafts-Brandner, 2004; Andralojc *et al.*, 2012). To remove these compounds from the active sites of Rubisco, the ATPase Rubisco activase (Rca) is necessary (Salvucci *et al.*, 1985). Its activity is generally irradiance-dependent (Lan *et al.*, 1992). However, between plant species, large differences in Rca regulation and isoforms exist (Carmo-Silva & Salvucci, 2013). In *A. thaliana*, there are two isoforms, the longer  $\alpha$ -isoform (46 kDa) and the shorter  $\beta$ -isoform (43 kDa; Salvucci *et al.*, 1987). While the activity of the  $\beta$ -isoform of Rca is not irradiance-dependent, the activity of the  $\alpha$ -isoform is strongly dependent on the ADP/ATP ratio and therefore on irradiance (Zhang & Portis, 1999; Zhang *et al.*, 2002). Furthermore, the  $\alpha$ -isoform controls the activity of the  $\beta$ -isoform (Zhang *et al.*, 2002). In transformants only containing the  $\beta$ -isoform (*rwt43*; Zhang *et al.*, 2002), Rubisco activation state is almost independent of irradiance (except in darkness, where Rubisco activation states of both Col-0 and *rwt43* were at ~50% of full activation; Carmo-Silva & Salvucci, 2013). It is therefore possible to use *rwt43* to determine how strongly inactive Rubisco controls rates of dynamic photosynthesis in shade-adapted leaves. Furthermore, the *rca-2* mutant was used, which has a decreased concentration of Rca (Shan *et al.*, 2011), to analyse how slower Rubisco activation affects dynamic photosynthesis.

The results (Chapter 6) show that the absence of the  $\alpha$ -isoform of Rca in *rwt43* increased the rates of Rubisco activation (lower apparent time constant of Rubisco activation,  $\tau_R$ ) after a stepwise irradiance increase in leaves adapted to shade (70 and 130  $\mu\text{mol m}^{-2} \text{s}^{-1}$ ), but not in dark-adapted leaves (Fig. 6.6B), thereby increasing rates of photosynthesis increases in shade-adapted leaves (Fig. S6.5 Table 6.2). A lower concentration of Rca in the *rca-2* mutant impacted heavily on rates of photosynthesis increase after an increase in irradiance, which was reflected in much higher  $\tau_R$  (Fig. 6.6A). The *rwt43* transformant did not show a larger lightfleck use efficiency than the wildtype, but the *rca-2* mutant did, most possibly due to higher relative post-irradiance carbon gain (Table 6.3), which was probably explained by larger RuBP pools resulting from a lower Rubisco activation state.

The rate of Rubisco activation was also affected by  $[CO_2]$ , air humidity and temperature. An increase in  $[CO_2]$  increased rates of Rubisco activation in tomato leaves (Chapters 3-5). While the positive effects of  $[CO_2]$  on Rubisco activation have been demonstrated before (Woodrow *et al.*, 1996), in this thesis it has been shown for the first time that elevated  $[CO_2]$  increases Rubisco activation irrespective of background irradiance (range: 0-200

$\mu\text{mol m}^{-2} \text{s}^{-1}$ ; Chapter 4). Detrimental effects of low air humidity on rates of Rubisco activation (Fig. 3.4C) are indirect and may be explained by a faster depletion of available  $\text{CO}_2$  (Fig. 3.5A), or a lower absolute  $\text{CO}_2$  concentration inside the chloroplast (Fig. 3.5B) during photosynthetic induction. Also, Rubisco activation showed a tendency to increase with leaf temperature (up to  $30.5^\circ\text{C}$ , Fig. 3.4B), confirming previous findings (Yamori *et al.*, 2012; Carmo-Silva & Salvucci, 2013).

### *Stomatal conductance*

Low stomatal conductance in dark- or shade-adapted leaves has often been shown to play a limiting role during photosynthetic induction, as stomata open rather slowly compared to the activation of RuBP regeneration and Rubisco (Tinoco-Ojanguren & Pearcy, 1992; Ooba & Takahashi, 2003; Vico *et al.*, 2011). Initial  $g_s$ , i.e.  $g_s$  in dark- or shade-adapted leaves before a stepwise increase in irradiance, can be a strong determinant for the rate of induction (Valladares *et al.*, 1997; Allen & Pearcy, 2000). How different the extent of this limitation can be between species has been shown in this thesis, where large differences in initial  $g_s$  had negligible (*Solanum lycopersicon* cv. Rheinlands Ruhm) or substantial (*A. thaliana*) effects. The abscisic acid (ABA) deficient *A. thaliana* mutant *aba2-1* exhibited  $\sim 2$ -4 times the initial  $g_s$  of its wildtype, Col-o, whose range in initial  $g_s$  values was  $0.08$ - $0.23 \text{ mol m}^{-2} \text{ s}^{-1}$ . This difference in initial  $g_s$  led to faster induction rates and a higher relative carbon gain during a series of lightflecks. In the ABA-deficient *flacca* mutant of tomato, which had  $\sim 4$ -5 times the initial  $g_s$  values of the wildtype ( $g_s$  range in wildtype:  $0.20$ - $0.25 \text{ mol m}^{-2} \text{ s}^{-1}$ ), induction was not faster than in the wildtype in ambient  $[\text{CO}_2]$ . Importantly, when comparing data from cv. Cappricia (Chapters 3 and 4) and cv. Rheinlands Ruhm wildtype (Chapter 5) leaves, initial  $g_s$ , final steady-state  $A_n$  and two indices of rates of photosynthetic induction ( $IS_{60}$  and  $t_{50}$ ) were not significantly different ( $P > 0.05$  in all cases) in the same environmental conditions ( $400 \text{ ppm } [\text{CO}_2]$ ,  $\sim 23^\circ\text{C}$  leaf temperature and  $\sim 0.8 \text{ kPa VPD}_{\text{leaf-air}}$ ). This suggests an absence of transient stomatal limitation in cv. Cappricia.

What could be the reason(s) for this interspecific difference in limitation of induction rates by stomata? To answer this question, data from single replicates of tomato and *A. thaliana*, pooled from Chapters 3-6 and obtained using identical environmental conditions ( $400 \text{ ppm } [\text{CO}_2]$ ,  $22^\circ\text{C}$  cuvette temperature and  $\sim 0.8 \text{ kPa VPD}_{\text{leaf-air}}$ ), were evaluated. The difference between maximum transient diffusional limitation and average, steady-state diffusional limitation ( $\Delta\text{DL}$ ; Fig. 8.1) was used as an index for the severity of stomatal limitation during photosynthetic induction. Furthermore, at the time of reaching maximum transient diffusional limitation ( $t_{\text{max}}$ ; Fig. 8.1), values of  $A_n$  and  $g_s$  were determin-

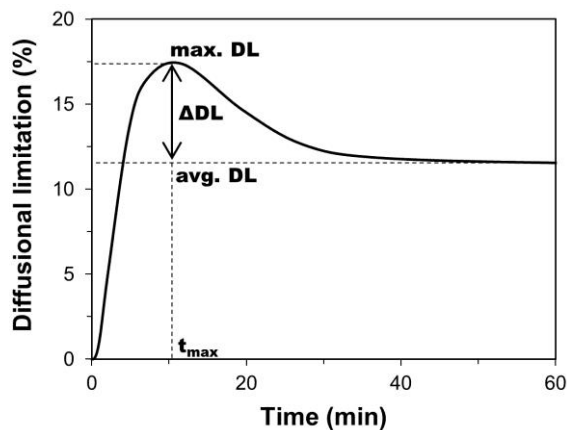


Fig. 8.1. Scheme describing how  $\Delta DL$  is calculated from time courses of DL.  $\Delta DL$  is the difference between average, steady-state diffusional limitation (avg. DL; %) and maximum DL (max. DL). At the time of reaching maximum DL ( $t_{max}$ ; minutes), transient net photosynthesis rate and stomatal conductance were determined. Furthermore, the difference between initial  $g_s$  ( $g_s$  at time = 0) and  $g_s$  at  $t_{max}$  was determined as stomatal opening until  $t_{max}$

ed. Also, the difference between  $g_s$  at  $t_{max}$  and initial  $g_s$ , named stomatal opening until  $t_{max}$ , was determined. The results of this analysis (Fig. 8.2) showed that  $\Delta DL$  decreased with increases in all three parameters, but was correlated most strongly with  $g_s$  at  $t_{max}$  ( $R^2 = 0.70$ ), less strongly with  $A_n$  at  $t_{max}$  ( $R^2 = 0.41$ ) and least strongly with stomatal opening until  $t_{max}$  ( $R^2 = 0.29$ ). Data from both species showed roughly similar functions of  $A_n$  and  $g_s$  at  $t_{max}$  with  $\Delta DL$  (Fig. 8.2A-B). Since  $A_n$  at  $t_{max}$  was almost identical with final, steady-state  $A_n$  ( $\sim 4\%$  difference;  $R^2 = 0.91$ ) and  $g_s$  at  $t_{max}$  was strongly dependent on initial  $g_s$  ( $\sim 20\%$  difference;  $R^2 = 0.97$ ), both final  $A_n$  and initial  $g_s$  had a strong effect on  $\Delta DL$  in both species. However, stomatal opening until the time of reaching maximum DL had no effect in tomato (i.e. no decrease in  $\Delta DL$  with increases in stomatal opening), but the response of stomatal opening until  $t_{max}$  to  $\Delta DL$  in *A. thaliana* could be approximated by a negative exponential relationship (Fig. 8.2C). Altogether, this analysis suggests that unlike tomato leaves, *A. thaliana* leaves had to rely more strongly on stomatal opening to alleviate stomatal limitation, and that in both genotypes, initial  $g_s$  and, to a lesser extent, final  $A_n$  affected transient stomatal limitation during photosynthetic induction. However, little is known about the extent of transient stomatal limitation in various (crop) plants, and this topic deserves further investigation.

### *Non-photochemical quenching*

Leaves use non-photochemical quenching (NPQ) to protect themselves from excess irradiance, by diverting a fraction of the energy captured in the light harvesting antennae away from linear electron transport, in the form of thermal dissipation (Jahns & Holzwarth, 2012; Ruban *et al.*, 2012). NPQ consists of several processes that are activated

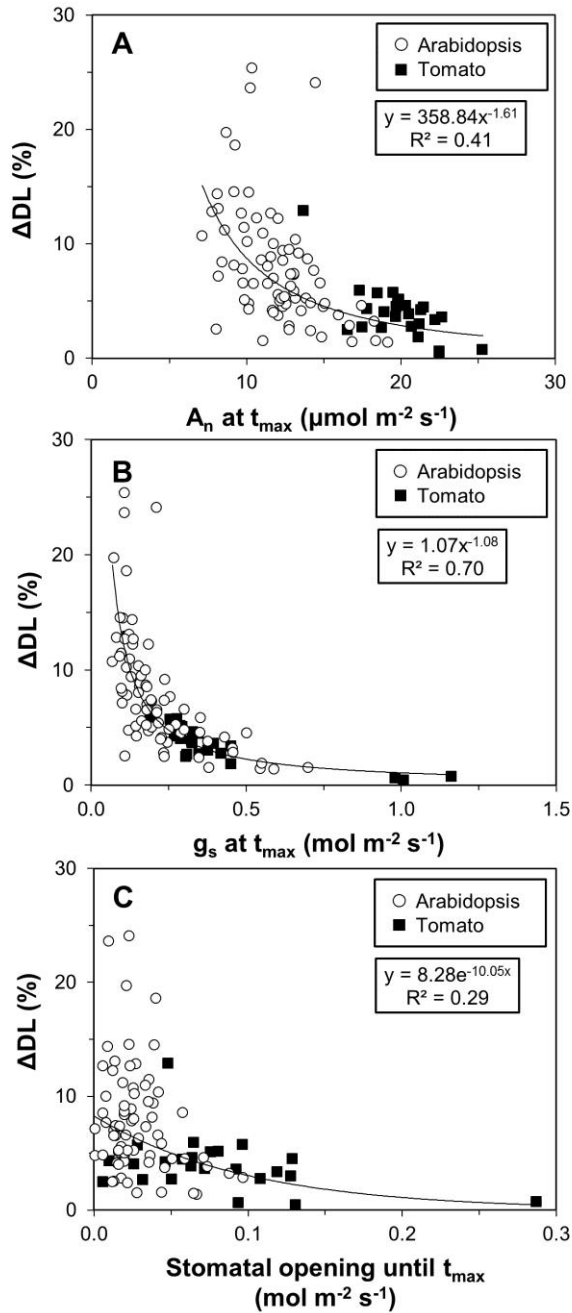


Fig. 8.2. Relationships of  $\Delta DL$  with A) net photosynthesis rate at  $t_{max}$  ( $A_{nr}$ ,  $\mu\text{mol m}^{-2} \text{s}^{-1}$ ); B) stomatal conductance at  $t_{max}$  ( $g_{sr}$ ,  $\text{mol m}^{-2} \text{s}^{-1}$ ); and C) stomatal opening until  $t_{max}$  ( $\text{mol m}^{-2} \text{s}^{-1}$ ) after stepwise increases in irradiance (for explanation see Fig. 8.1). Data represent single replicates of several *Arabidopsis thaliana* (circles;  $n = 75$ ) and tomato (squares;  $n = 25$ ) genotypes/cultivars, including Col-0, C24 and *aba2-1* in *A. thaliana* and cv. Cappricia, Rheinlands Ruhm wildtype and Rheinlands Ruhm *flacca*. Leaves were adapted to several background irradiances (0-200  $\mu\text{mol m}^{-2} \text{s}^{-1}$ ) and then exposed to near-saturating irradiance (600-1000  $\mu\text{mol m}^{-2} \text{s}^{-1}$  in *A. thaliana*, 1000  $\mu\text{mol m}^{-2} \text{s}^{-1}$  in tomato). Other conditions were: 70% relative humidity, 400 ppm leaf external  $\text{CO}_2$  concentration and 22 °C cuvette temperature

and deactivated on different time scales. The fastest and (in most situations) major part of NPQ is termed energy-dependent quenching (qE; Ruban *et al.*, 2012). qE has time constants of ~60 seconds for buildup (after an increase in irradiance) and ~30-50 seconds for relaxation (Nilkens *et al.*, 2010). After decreases in irradiance, net photosynthesis rates may get transiently limited by reduced electron transport rates (ETR), due to slowly relaxing thermal dissipation (Zhu *et al.*, 2004). This limitation has been estimated to decrease integrated carbon gain in fluctuating irradiance by ~17-32%, depending on temperature (Zhu *et al.*, 2004). In *A. thaliana* mutants lacking the thylakoid membrane K<sup>+</sup> efflux antiporter (*kea3*), a slower relaxation of NPQ after a stepwise decrease in irradiance slowed down assimilation rates (Armbruster *et al.*, 2014). In this thesis, two well-described low-NPQ mutants, *npq1-2* and *npq4-1* (Niyogi *et al.*, 1998; Li *et al.*, 2000) were used, to test the hypothesis that low NPQ increases rates of carbon gain (relative to the wildtype) after a decrease in irradiance. This was not the case (Figs. 6.10, S6.9E-F), even though in both mutants NPQ levels were reduced by ~50% compared to the wildtype, during photosynthetic induction (Fig. 6.5F). Thus, while relaxation kinetics of NPQ do have an effect on carbon gain (Armbruster *et al.*, 2014), the overall level of NPQ does not seem to. Rice transformants with constitutively high levels of NPQ showed slower increases of photosynthetic induction (Hubbart *et al.*, 2012). On the other hand, transformants with constitutively low NPQ did not show faster induction rates (Hubbart *et al.*, 2012). This suggests that photoprotection in wildtype rice plants was optimal with respect to ETR, since a decrease in photoprotection in the mutant did not increase ETR. From these results, it can be hypothesized that *npq1-2* and *npq4-1*, both having decreased NPQ, do not exhibit higher rates of photosynthetic induction, which was indeed the case (Fig. 6.3C).

### *Sucrose synthesis*

The triose phosphates formed in the Calvin cycle are exported to the cytosol in exchange for organic phosphate (P<sub>i</sub>), and then converted to sucrose (reviewed in Stitt *et al.*, 2010). If there is a mismatch between turnover rates in the Calvin cycle and the sucrose synthesis pathway, the Calvin cycle can either get source (RuBP) or sink (P<sub>i</sub>) limited (Stitt *et al.*, 2010). Major control over the sucrose synthesis pathway is exerted by sucrose phosphate synthase (SPS; Lunn & MacRae, 2003). Since the activation state of SPS is irradiance-dependent (reviewed in Huber & Huber, 1996; MacRae & Lunn, 2006), a mismatch between the Calvin cycle and sucrose synthesis can occur during photosynthetic induction. Especially after a stepwise irradiance increase in shade-adapted leaves exposed to elevated CO<sub>2</sub> concentrations, a transient ‘hiccup’ is visible (e.g. Tomimatsu & Tang, 2012), which has been explained by slowly activating SPS transiently limiting assimilation rates (Stitt &

Grosse, 1988). Furthermore, after a step decrease in irradiance, sucrose synthesis can transiently operate at higher rates than the Calvin Cycle, draining the Calvin cycle of intermediates (Prinsley *et al.*, 1986). It can therefore be hypothesized that a large decrease in SPS concentration slows down the increase in photosynthesis rates after a stepwise irradiance increase, while showing relatively larger carbon fixation after a stepwise decrease in irradiance.

These hypotheses were tested using the *A. thaliana* mutant *spsa1*, which has 20% of wildtype SPS activity (Sun *et al.*, 2011). Surprisingly, this large decrease in the capacity to form sucrose had almost no adverse effects on dynamic photosynthesis, although it significantly increased the time to reach 90% of full photosynthetic induction in dark-adapted leaves. However, the decrease in SPS did not affect rates of photosynthetic increase in shade-adapted leaves, lightfleck use efficiency or photosynthesis rates after a stepwise decrease in irradiance. Therefore, SPS in *A. thaliana* is highly unlikely to be a limiting factor in dynamic photosynthesis, at least not in ambient [CO<sub>2</sub>].

### *Mesophyll conductance*

Mesophyll conductance ( $g_m$ ) has been reported to vary with irradiance, CO<sub>2</sub> concentration and temperature (Flexas *et al.* 2007; 2008; von Caemmerer and Evans 2015). Therefore, it seemed plausible that it also changes during photosynthetic induction, and that these changes during induction could be further modulated by [CO<sub>2</sub>] and temperature. However, to my knowledge there has never been an attempt to measure  $g_m$  during photosynthetic induction. Therefore, the transient changes in  $g_m$  (Fig. 3.6A, C) during the first ~10 minutes could not be compared to previous data. However, there are two lines of evidence to suggest that  $g_m$  did not limit rates of photosynthetic induction: firstly, the relationship between ETR and gross photosynthesis rate was highly linear in the beginning of photosynthetic induction (Fig. 3.8), suggesting that in this phase no change in photorespiration occurred. If  $g_m$  had transiently limited photosynthesis rates more strongly in the beginning of induction than at steady-state, then it would be expected that photorespiration would increase (due to transiently low CO<sub>2</sub> in the chloroplast), thereby making the initial ETR/ $A_{gr}$  relationship nonlinear. Secondly, the sensitivity of  $g_m$  to errors in parameter estimations showed large changes in the range deemed unreliable (>50 dC<sub>d</sub>/dA<sub>gr</sub>; Harley *et al.*, 1992) within the first 10 minutes of photosynthetic induction (Fig. 3.6B, D), suggesting that the increase in  $g_m$  visible in the beginning of induction was a measurement artefact.

## Methodology

### *Assessing transient stomatal limitation after an increase in irradiance*

There are four methods to assess transient stomatal limitation after an increase in irradiance, each having its own drawbacks. These are a) dynamic  $A_n/C_i$  curves; b) correlation of initial  $g_s$  with the time to reach a percentage of final photosynthesis rates; c) stomatal limitation; and d) diffusional limitation.

The change of the relationship between net photosynthesis rates and leaf internal  $CO_2$  ( $C_i$ ) can be followed by constructing a 'dynamic  $A_n/C_i$ ' curve (Küppers & Schneider, 1993; Ögren & Sundin, 1996; Pearcy *et al.*, 1996). This analysis offers some insight as to which increments in photosynthesis have been caused by increases in  $g_s$ , as soon as  $A_n$  follows the steady-state  $A_n/C_i$  curve (Fig. 5.6). However, dynamic  $A_n/C_i$  curves give little insight into the percentage by which stomata limit overall induction rates, and no insight into the time course of this limitation. Also, it may be that they seemingly show stomatal limitation of induction rates without that actually being the case, as demonstrated in Chapter 5 (Figs. 5.6B).

Initial  $g_s$  mostly determines the limitation imposed by stomata, due to comparably slow stomatal opening (see above). In previous studies, a link between the time to reach 90% of full photosynthetic induction ( $t_{90}$ ) and initial  $g_s$  was shown (Valladares *et al.*, 1997; Allen & Pearcy, 2000a). The shape of this relationship was best described by two lines: one line with a negative slope in the region of low initial  $g_s$ , and a horizontal line at higher initial  $g_s$  (Fig. 6.7). This means that at a certain value of initial  $g_s$ ,  $t_{90}$  did not decrease any further, and that this value could be identified by the intersection of the two lines. This intersection therefore marks a threshold for the lowest value of initial  $g_s$  that is non-limiting for rates of photosynthetic induction. Using *A. thaliana* genotypes strongly differing in initial  $g_s$ , it was shown that the threshold between limiting and non-limiting  $g_s$  is remarkably stable across background irradiances and at different time points of increases in photosynthesis rates (Fig. 6.8). Altogether, this method offers insight into whether or not initial  $g_s$  is limiting, but cannot be used for determining the extent or the time course of this limitation.

Transient stomatal limitation can be calculated using the time courses of  $A_n$  and  $C_i$  during induction. Basically, transient  $A_n$  is recalculated using the  $C_i$  value reached at the end of photosynthetic induction, i.e. when  $g_s$  has reached a steady state due to stomatal opening (Tinoco-Ojanguren & Pearcy, 1993b; Allen & Pearcy, 2000b). This approach seemingly yields the percentage to which incompletely opened stomata are limiting during the time course of induction, the rest of the limitation being partitioned to inactive enzymes ('biochemical limitation'). However, there are three issues with this approach. Firstly, transient stomatal limitation is often calculated assuming a linear relationship between  $A_n$

and  $C_i$  from the  $\text{CO}_2$  compensation point to transient  $C_i$  (Woodrow & Mott, 1989; Tinoco-Ojanguren & Pearcy, 1993b). Indeed, the  $A_n/C_i$  relationship is approximately linear in the Rubisco-limited phase (Sharkey *et al.*, 2007), such that the assumption of linearity can be made if steady-state  $C_i$  is below  $\sim 350$  ppm (Ainsworth & Rogers, 2007), which was the case in most studies using this method. However, some studies using elevated  $[\text{CO}_2]$  (range: 700-1020 ppm) also used linear  $A_n/C_i$  relationships (Kořvancová *et al.*, 2009; Tomimatsu & Tang, 2012), and the values of transient stomatal limitation reported therein are most likely strong overestimations. If the steady-state  $A_n/C_i$  relationship is known, this issue can be resolved. The second issue is that stomatal limitation in the beginning of induction can transiently reach negative values (Allen & Pearcy, 2000b; Urban *et al.*, 2007), which can be explained by  $C_i$  being transiently larger than at steady-state after induction. Physiologically, a negative stomatal limitation is impossible, making the method less trustworthy. The third and most important issue is that because transient stomatal limitation approaches zero, the biological variation seemingly disappears towards the end of its time course, as the value in each replicate approaches zero, making a statistical comparison between transient and steady-state values of stomatal limitation impossible (Chapter 5).

The fourth method, diffusional limitation, is a solution to two of the issues that come with stomatal limitation. To my knowledge, this method has not been used in research on dynamic photosynthesis before. It is calculated similarly to transient stomatal limitation, however instead of using steady-state  $C_i$  to correct transient  $A_n$  for changes in  $C_i$ , leaf external  $[\text{CO}_2]$  is used as a reference. This means that diffusional limitation represents the totality of limitations to  $\text{CO}_2$  diffusion towards the site of carboxylation ( $g_s$  and  $g_m$ ), and the combination of their changes during photosynthetic induction. It does not drop below zero (e.g. Fig. 5.4). Also, since it does not approach a pre-defined value, the variance between samples does not diminish towards the end of its time course, allowing realistic statistical comparisons between diffusional limitation at steady-state and transient diffusional limitation (Fig. 5.4). One drawback of this method is that the values of diffusional limitation cannot be added up to the values of biochemical limitation. Another drawback is that between treatments, it is not easy to compare the extent of transient changes (e.g. Fig. 4.4) – this is much simpler using transient stomatal limitation. Thirdly, as mentioned already, diffusional limitation not only reflects the limitation by  $g_s$ , but also that by  $g_m$ . However, it is unlikely that  $g_m$  had any effect on rates of photosynthetic induction (see above). Regardless of the drawbacks, I consider this method most useful in estimating the limitations imposed by stomata, and have used it consistently throughout the thesis.



*The regular application of saturating flashes does not affect gas exchange rates during photosynthetic induction*

Next to information on gas exchange rates, information on electron transport can be very useful in interpreting processes underlying photosynthetic induction. Examples in this thesis are  $[\text{CO}_2]$  and leaf temperature effects on changes in photorespiration during photosynthetic induction (identified by correlating gross photosynthesis and ETR, Fig. 3.8), or mutations affecting Rubisco activase,  $g_s$  and NPQ, which feed back on electron transport and energy dissipation (Fig. 6.5). Several studies have used saturating flashes alone (Alter *et al.*, 2012; Carmo-Silva & Salvucci, 2013) or in conjunction with gas exchange data (Hubbart *et al.*, 2012; Yamori *et al.*, 2012; Armbruster *et al.*, 2014) to analyse transient rates of photosynthesis. However, to my knowledge, it has never been tested whether the regular application of saturating flashes affects the rates of photosynthesis or stomatal conductance change. Potentially, this could be the case, as each saturating flash transiently increases the leaf's temperature and therefore transpiration rate. Two data sets, which were derived from measurements of photosynthetic induction in 200, 400 and 800 ppm  $[\text{CO}_2]$  and from tomato leaves grown under identical growth conditions, were compared; in one data set (Chapter 3), no saturating flashes were applied while in the other (Chapter 4), saturating flashes were applied once every minute in the first ten minutes, and once every two minutes in the remaining 50 minutes of photosynthetic induction. This comparison showed that saturating flashes do not affect rates of photosynthetic induction or stomatal opening (Table S4.1).

*Multi-phase flashes to determine true  $F_m'$*

In order to determine the efficiency of electron transport through photosystem II ( $\Phi_{\text{PSII}}$ ) or NPQ, it is necessary to determine maximum chlorophyll fluorescence in dark-adapted leaves ( $F_m$ ) and in leaves exposed to irradiance ( $F_m'$ ). This is done using a short ( $\sim 1$  s) saturating flash that is several times the intensity of full sunlight (Ögren & Baker, 1985). The latter measurement is not trivial in leaves with intermediate to high photosynthetic capacity ('sun-type leaves'), as the complete reduction of the primary quinone acceptor in PSII and the plastoquinone pool (which are both necessary to obtain accurate  $F_m'$  values) cannot easily be accomplished, even with very high intensities of the saturating flash ( $\sim 10,000 \mu\text{mol m}^{-2} \text{s}^{-1}$ ; Earl & Ennahli, 2004). This causes an underestimation of  $\Phi_{\text{PSII}}$  (Earl & Ennahli, 2004; Loriaux *et al.*, 2013). Recently, a new method for the determination of  $F_m'$  in the LI-6400 (Li-Cor Biosciences, Lincoln, USA) has been described (Loriaux *et al.*, 2013). By the use of three sequential flashes with varying intensities and extrapolation of measured  $F_m'$  values to a 'true'  $F_m'$  value at theoretically infinite flash intensity, the

multi-phase flash technique (MPF) has been shown to yield more accurate determinations of  $F_m'$ , thereby strongly affecting estimations of  $\Phi_{PSII}$  and  $g_m$  (Loriaux *et al.*, 2013). In dark-adapted leaves, however, conventional saturating flashes are able to yield accurate  $F_m$ , so the use of MPF's is not necessary in this case (Loriaux *et al.*, 2013).

In this thesis, the MPF method has been used for the first time to determine  $\Phi_{PSII}$ , NPQ and  $g_m$  changes during photosynthetic induction. This was necessary in tomato leaves, since conventional flashes did not fully saturate  $F_m'$ , i.e.  $F_m'$  in light-adapted leaves increased with every increase in flash intensity within the range of flash intensities possible in the LI-6400. During photosynthetic induction in dark-adapted leaves, it was shown that within the first ten minutes, a progressive difference between  $F_m'$  determined by the conventional flash, and  $F_m'$  determined by the MPF, developed (Fig. S3.1). This difference was  $\sim 4\%$ , which would have resulted in large underestimations of  $\Phi_{PSII}$ , and unrealistic values of  $g_m$ , consistent with the findings of Loriaux *et al.* (2013).

In *A. thaliana* leaves, conventional flashes did saturate  $F_m'$ , making the use of the MPF method unnecessary. Considering that *A. thaliana* plants were grown under  $\sim 170 \mu\text{mol m}^{-2} \text{s}^{-1}$ , while tomato plants were grown under  $\sim 320 \mu\text{mol m}^{-2} \text{s}^{-1}$ , this may confirm that the plastoquinone pools of leaves grown in relatively low irradiance are more easily reduced. Loriaux *et al.* (2013) found a larger effect of using the MPF method (relative to the conventional method) in plants grown in greenhouses and fields than in climate-chamber grown plants. Since plants in climate chambers had experienced lower growth irradiance, they attributed this to higher capacities for ETR in field- and greenhouse-grown plants (Loriaux *et al.*, 2013).

### **Application of knowledge acquired in this thesis**

The knowledge acquired in this thesis may be applied in three ways: a) to identify targets for crop improvement, b) to improve the performance of models of dynamic photosynthesis and c) to construct tools for the exploration of new greenhouse lighting strategies.

#### *Identifying targets for crop improvement*

Several chapters in this thesis point to Rubisco activation state being the most limiting factor in dynamic photosynthesis. In Chapter 3, it was concluded that if Rubisco activation during photosynthetic induction was instantaneous, gains of 4-10% in photosynthesis rates (subject to  $[\text{CO}_2]$ , leaf temperature and air humidity) would be possible (Table 3.3). In Chapter 4, it was found that the apparent rate of Rubisco activation was similarly dependent on  $[\text{CO}_2]$  (range: 200-800 ppm) as it was on background irradiance

(range: 0-200  $\mu\text{mol m}^{-2} \text{s}^{-1}$ ; Fig. 4.5). This, together with the indirect modulation of Rubisco activation rates by air humidity (Fig. 3.4C), showcases the strong environmental dependency of Rubisco activation. Finally, in Chapter 6, it was shown that both the concentration and the regulation of Rubisco activase have strong effects on rates of photosynthetic induction, confirming earlier findings (e.g. Yamori *et al.*, 2012; Carmo-Silva & Salvucci, 2013). It seems, therefore, that enhancing Rubisco activation state in shade, or the rate of Rubisco activation after a stepwise increase in irradiance, is useful in increasing growth rates of plants in fluctuating irradiance (Carmo-Silva *et al.*, 2015).

However, a pressing question in this context is why an always-active activase (as in *rwt43*) reduces growth ( $\sim 41\%$  difference in constant growth irradiance between Col-o and *rwt43*; Carmo-Silva & Salvucci, 2013). Even in a growth environment with fluctuating irradiance ( $420/20 \mu\text{mol m}^{-2} \text{s}^{-1}$ ), Col-o accumulated  $\sim 11\%$  more dry mass than *rwt43* (Carmo-Silva & Salvucci, 2013). It could be that this apparent penalty of always-active Rubisco is caused by the fact that the direct progenitor of *rwt43* is *rca* (a mutant lacking Rubisco activase gene expression, whose progenitor is Col-o), not Col-o itself (Zhang *et al.*, 2002). However, it may also be that a) the maintenance of high Rubisco activity in the shade is too costly (Rubisco activase consuming ATP to keep Rubisco active; Zhang & Portis, 1999; Zhang *et al.*, 2002); b) always-active Rubisco introduces an imbalance in the Calvin cycle that causes futile cycling of intermediates in low irradiance, wasting energy (Zhang *et al.*, 2002); or c) wildtype Rubisco is protected better from degradation by proteases due to tight-binding inhibitors in low irradiance (Parry *et al.*, 2008), which may not be the case in *rwt43*. After all, it is remarkable that all genotypes examined so far show some kind of irradiance-dependent regulation of Rubisco activation state (discussed in Carmo-Silva & Salvucci, 2013), suggesting that keeping Rubisco active regardless of irradiance does not seem to confer an evolutionary advantage. It follows that if always-active Rubisco really conferred a disadvantage for plant growth (despite higher dynamic carbon gain after irradiance increases from shade, Chapter 6), then engineering crops analogous to *rwt43* is not a viable avenue for increasing crop yields.

Rubisco activase comprises  $\sim 5\%$  of soluble protein in plant leaves (He *et al.*, 1997). The optimum allocation of protein between Rubisco and Rca probably depends on the frequency of irradiance fluctuations a leaf is exposed to (Mott & Woodrow, 2000). A reduction of approximately 80% of Rca in the *A. thaliana* mutant *rca-2* (Chapter 7) strongly decreased rates of photosynthesis increases after stepwise increases in irradiance (Chapter 6), indicating the importance of Rubisco activase concentration for dynamic photosynthesis. Using gene transformation techniques, Rca concentrations were varied between 20 and 180% of wildtype levels in rice (Yamori *et al.*, 2012). In this study, higher

Rca concentration coincided with faster induction of photosynthesis, ETR and Rubisco activation (Yamori *et al.*, 2012). Also, after 20 selection cycles for agronomic improvement of maize, a 90% larger grain yield coincided with larger Rubisco activity, which was due to a higher amount of Rca, but not Rubisco (Martínez-Barajas *et al.*, 1997). Taken together, these results suggest that breeding for larger Rca contents could be useful in obtaining higher yields.

Stomatal conductance has been found to limit dynamic photosynthesis in *A. thaliana*, but not in tomato (in ambient conditions). Furthermore, the limitation due to stomata is reduced in elevated  $[\text{CO}_2]$  (and vice versa; Chapters 3-5) and increased in elevated  $\text{VPD}_{\text{leaf-air}}$  (Chapter 3). Generally, little knowledge on the extent of transient stomatal limitation, or the mechanistic reasons behind it, exists. Clearly, this topic requires more insight (Chapters 2, 5). In Chapter 6, it was proposed that screening (and breeding) for genotypes with constitutively high  $g_s$  is possible using thermography. Using the previously defined value of non-limiting initial  $g_s$  in shade or darkness (Fig. 6.8), transient stomatal limitation could effectively be overcome, however at the expense of water use efficiency.

In this thesis, it was also assessed whether NPQ, SPS or  $g_m$  limited the rates of dynamic photosynthesis. Under the conditions used for testing, this was not the case (Chapters 3, 5). Therefore, it seems unlikely that these processes are in need of improvement in order to increase crop yield in fluctuating irradiance.

### *Improving models of dynamic photosynthesis*

Data from the *A. thaliana* experiment (Chapter 6) were used to construct and calibrate a dynamic model of photosynthesis (Chapter 7). In this model, the behaviour of the wildtype, Col-0, and the effects of the mutations on the photosynthetic phenotypes of *aba2-1*, *rca-2*, *npq4-1* and *spsa1* were successfully reproduced (0.94-0.98 fraction of explained variance during model calibration; Fig. 7.2) by changing one (*rca-2*, *spsa1*) to five (*aba2-1*, *npq4-1*) parameters, respectively (Table S7.4). The model was further validated by comparing simulated and measured responses to lightfleck series, and a high fraction of total variation (0.86) was explained by the model (Fig. 7.5). A goal-seeking (or teleonomic) modelling approach was used to simulate dynamic regulation of Rubisco and NPQ regulation by assuming that the Calvin cycle and the electron transport chain are coupled in the steady state (Farquhar *et al.*, 1980). Such a model can reproduce the effects of irradiance and  $\text{CO}_2$  concentration with minimal parameterisation, making it easily applicable to different genotypes or growth conditions. Additionally, in the case of Rubisco regulation, this approach was considered to be superior to previously used steady-state irradiance response curves (Percy *et al.*, 1997; Kirschbaum *et al.*, 1998; Naumburg *et al.*,

2001), as it is more parsimonious and can additionally account for the effect of CO<sub>2</sub> concentration. In the case of NPQ, this approach was chosen mostly for practical reasons, as the exact mechanisms that determine NPQ are still under debate (Jahns & Holzwarth, 2012; Zaks *et al.*, 2013; Murchie & Harbinson, 2014).

This model is also the first to include dynamic changes in leaf-level NPQ, and the process was simulated accurately in all genotypes (0.86-0.98 fraction explained variance) except *rca2* (0.68; Fig. 7.3). The inclusion of NPQ enabled the model to explain the behaviour of *npq4-1* during photosynthetic induction by a combination of a complete lack of the fast component of heat dissipation (often termed qE; Li *et al.*, 2000), decreased contribution of chloroplast avoidance movement, and upregulation of photoinhibition and slow mechanisms of heat dissipation (Fig. 7.6). In *aba2-1*, a combination of decreased chloroplast avoidance movement (Rojas-Pierce *et al.*, 2014) and higher metabolic demand (due to higher C<sub>i</sub> caused by larger g<sub>s</sub>, and therefore higher photosynthetic quenching) explained lower rates of NPQ compared to Col-0 (Fig. 7.6). In the *rca-2* and *spsa1* mutants, the change in a single parameter value was sufficient to capture the effect of the mutation on leaf CO<sub>2</sub> exchange: in *rca-2*, the amount of Rca was 20% of wildtype levels, while in *spsa1*, the maximum rate of triose phosphate utilization was 50% of wildtype levels.

Work to extend the model is underway (Morales *et al.*, unpublished results) and aims to include a) the process of post-illumination CO<sub>2</sub> fixation; b) parameterisation using a different genotype (tomato); and c) effects of [CO<sub>2</sub>] on dynamic rates of photosynthesis (using data of Chapter 4; see below).

### *Towards exploring new greenhouse lighting strategies*

In order to explore new, dynamic lighting strategies in greenhouse horticulture, a tool needs to be developed that can simulate integrated crop photosynthesis to fluctuating irradiance, as affected by [CO<sub>2</sub>], temperature and air humidity. For this, the following steps are necessary: a) experimental analysis of the dynamic behaviour of leaf photosynthesis in fluctuating irradiance, and its control by [CO<sub>2</sub>], leaf temperature and air humidity; b) constructing and validating a leaf-level model that reproduces dynamics and c) scaling up to the canopy level.

Using the model described in Chapter 7, the framework laid out in the review (Fig. 2.2) and the data gathered on environmental control of dynamic photosynthesis (Chapters 3 and 4), significant steps towards modelling tomato leaf photosynthesis in fluctuating irradiance and as affected by several environmental factors, were made. However, several pieces of knowledge are still lacking in order to parameterize a complete model: a) leaf temperature effects on the gain and loss of photosynthetic induction, as affected by background

irradiance (similar to the work done on [CO<sub>2</sub>] effects, Chapter 3) and b) transient  $g_s$  as affected by air humidity. As for a), no such study exists, since temperature effects on photosynthetic induction have only been analysed using one background irradiance (Küppers and Schneider, 1993; Pepin and Livingston, 1997; Leakey *et al.*, 2003; Yamori *et al.*, 2012; Carmo-Silva and Salvucci, 2013; Chapter 3), and loss of induction has only been assessed in ten minutes of shade (Leakey *et al.*, 2003). Also, the response of photosynthesis to different temperatures depends on a plant's temperature acclimation (reviewed in Yamori *et al.*, 2014), further complicating the matter. Much more experimental research is necessary in this area.

As for air humidity effects on transient  $g_s$ , few data are available (though see Assmann & Grantz, 1990a, b; Tinoco-Ojanguren & Pearcy, 1993a; Chapter 3). Furthermore, a combination of several opening or closing stimuli does not produce a  $g_s$  change that is predictable, especially not across species: recently, Merilo *et al.* (2014) showed that stomata from different species showed similar opening responses when exposed to a single opening (increased irradiance or low [CO<sub>2</sub>]) or closing stimulus (reduced humidity, darkness or high [CO<sub>2</sub>]). However, when a combination of opening and closing stimuli was applied, the direction of the response ( $g_s$  increase or decrease) differed widely across species, and could not be predicted from single-stimulus responses (Merilo *et al.*, 2014). Considering these findings, it may be most useful to simulate transient  $g_s$  using empirical models (such as Violet-Chabrand *et al.*, 2013) that incorporate the steady-state effect of air humidity on  $g_s$ , but with time constants of  $g_s$  changes that are unaffected by air humidity.

Scaling up from the leaf to the canopy could be achieved by using functional-structural plant models (FSPM), which can include dynamic spatial and morphological information on plant growth and development (Vos *et al.*, 2010). A recently published static FSPM of tomato (Sarlikioti *et al.*, 2011) could be extended and used to simulate irradiance interception and growth. This FSPM includes a steady-state photosynthesis module (Farquhar *et al.*, 1980), which could be replaced by a dynamic photosynthesis module (described above). Depending on leaf age and exposure to shade, photosynthetic capacity and stomatal conductance may have to be adjusted. However, given that no principal difference in rates of photosynthetic induction between sun and shade leaves (Naumburg & Ellsworth, 2000; Urban *et al.*, 2007), or between leaf ages (Urban *et al.*, 2008) has been reported, no adjustment of time constants based on leaf position in the canopy seems necessary.

## Perspectives

### *Exploring sunflecks: towards flexible functional-structural plant models*

Research aiming at improving photosynthesis in fluctuating irradiance ought to focus on crops where such efforts are likely to yield the largest benefits. However, one of the big ‘unknowns’ in this field is the actual extent of fluctuating irradiance. The fraction of fluctuating irradiance at a given spot in a given canopy is affected by a plethora of factors, among them the direct/diffuse ratio of radiation, frequency of leaf movement and average background irradiance (Smith & Berry, 2013). Most efforts on quantifying fluctuating irradiance have focused on forest understory sites, leading to the rather broad conclusion that 20-80% of irradiance at the bottom of forests is received as sunflecks (Pearcy, 1990). Thus, few empirical studies on fluctuating irradiance in canopies exist (even less so in crops) and those that do are extremely site-specific (e.g. Pearcy *et al.*, 1990), making it difficult to draw general conclusions. Hypothetically, an environment where factors could be varied one by one would be an ideal setting to define the contribution of different factors to the extent of irradiance fluctuations.

A possible solution to this problem would be the study of sunflecks ‘in silico’, i.e. in 3D computer models of whole plants (FSPM, see above). Several recently developed FSPM already include leaf optical properties, such that irradiance absorption, reflection and transmittance are simulated; examples include wheat (Evers *et al.*, 2010), tomato (Sarlikioti *et al.*, 2011) and cucumber (Chen *et al.*, 2014). A property that current FSPM lack, however, is dynamic behaviour over short (seconds to minutes) time scales, such as organ movement in space. Especially in response to external forcing (wind), accurate simulation of plant movement is crucial for determining sunfleck dynamics. Movement in response to wind, and subsequent changes in irradiance interception, have been simulated in aspen (*Populus tremuloides*), and parameters were estimated using slow motion photography of leaves in a wind tunnel (Roden, 2003). Thus, it seems possible to implement leaf mechanical properties into FSPM, making these models ‘flexible’. The end product of such an effort could be predictions of dynamic irradiance environments as determined by cloudiness, wind, and canopy structure at any given location.

### *Data mining*

To date, there are hundreds of studies containing data on photosynthesis transients, mostly on photosynthetic induction. Of those, a subset (~80 studies) contains data that are a combination of transient photosynthesis rates,  $g_s$ , and/or  $C_i$ . From those data, indices like diffusional and biochemical limitation, and the apparent time constant of Rubisco activation, could be calculated. These data are therefore useful for question like: how strong

is overall diffusional limitation, and what factors (e.g. growth irradiance, measurement conditions) does it depend on? Are there interspecific differences in the rate of Rubisco activation? Can functional relationships between photosynthetic capacity, initial or maximum  $g_s$ , and rates of photosynthetic induction be identified? Data mining of those studies, using freely available digitizing software, can potentially provide answers to these questions.

### *'Looking into' dynamic photosynthesis: the use of mutants and transformants*

Point mutants or transformants with clearly defined changes relative to their progenitors can yield valuable insights about specific mechanisms and pathways (Stitt *et al.*, 2010). However, in previous research on mechanisms underlying dynamic photosynthesis, this has rarely been done (although see Hubbart *et al.*, 2012; Yamori *et al.*, 2012; Carmo-Silva & Salvucci, 2013; Armbruster *et al.*, 2014). Below, several areas are proposed in which mutants or genetic transformants can be of use.

In this thesis, the effects of a changed capacity for RuBP regeneration have not been addressed, mainly because the genetic material could not be obtained, even though it exists. However, from biochemical studies it is clear that the activation state of RuBP regeneration can be a strong limitation in naturally changing irradiance, especially in sunflecks that are separated by two minutes or less, as RuBP regeneration deactivates more quickly than does Rubisco (reviewed in Percy *et al.*, 1996). RuBP regeneration after irradiance increases is controlled by sedoheptulose-1,7-bisphosphatase (SBPase), fructose-1,6-bisphosphatase (FBPase) and phosphoribulokinase (PRK), as their activation state is irradiance-dependent (Percy *et al.*, 1996; Kaiser *et al.*, 2015). Plants with changed concentrations or properties of these enzymes could be used to elucidate their role in RuBP-regeneration limitation. Examples of such organisms are antisense potato plants with reduced levels of chloroplastic FBPase levels (Kossmann *et al.*, 1994), antisense tobacco plants with reduced SBPase concentrations (Harrison *et al.*, 1998), and tobacco plants with increased concentrations of chloroplastic FBPase, SBPase, or both (Lefebvre *et al.*, 2005; Simkin *et al.*, 2015). Since none of these organisms have been used to study photosynthesis in fluctuating irradiance, large steps in understanding the involvement of RuBP-regeneration limitation are yet to be made.

The *rwt43* transformant did not differ in behaviour compared to the wildtype in lightflecks of various amplitudes and duration (Chapter 6), although its rates of photosynthesis increase after an irradiance increase had been higher in shade-adapted leaves (Fig. S6.5A-B). This lack of a difference in lightflecks was most likely attributable to a narrow 'spacing' of lightflecks, the longest gap between lightflecks being 60 seconds. This leads to



an important question: at what duration in low irradiance, and what background irradiance, does the regulatory difference between wildtype and *rwt43* Rubisco activation state lead to an appreciable difference in photosynthesis rates once the leaf is re-illuminated? Perhaps exploration of various scenarios, using a well-parameterised mathematical model of both genotypes, would be the most useful strategy to answer that question.

Mutants that have similar photosynthetic capacity as their wildtype, but different  $g_s$ , can be used best to test hypotheses regarding stomatal limitation of dynamic photosynthesis. The tomato *flacca* mutant is an excellent example (Chapter 5). Other examples are *A. thaliana* epidermal patterning factor (EPF) mutants, of which overexpressors and knockout plants are available (Franks *et al.*, 2015). Both types of mutants have a similar steady-state  $CO_2$  response as the wildtype, but strongly different stomatal density and therefore  $g_s$  (Franks *et al.*, 2015). Using those mutants, the relationship between environmental factors like air humidity (or temperature) and stomatal effects in fluctuating irradiance could be analysed.



## REFERENCES

- Ainsworth EA, Rogers A. 2007. The response of photosynthesis and stomatal conductance to rising [CO<sub>2</sub>]: Mechanisms and environmental interactions. *Plant, Cell and Environment* 30: 258–270.
- Allen MT, Pearcy RW. 2000a. Stomatal behavior and photosynthetic performance under dynamic light regimes in a seasonally dry tropical rain forest. *Oecologia* 122: 470–478.
- Allen MT, Pearcy RW. 2000b. Stomatal versus biochemical limitations to dynamic photosynthetic performance in four tropical rainforest shrub species. *Oecologia* 122: 479–486.
- Alonso JM, Stepanova AN, Lisse TJ, Kim CJ, Chen H, Shinn P, Stevenson DK, Zimmerman J, Barajas P, Cheuk R, et al. 2003. Genome-wide insertional mutagenesis of *Arabidopsis thaliana*. *Science* 301: 653–657.
- Alter P, Dreissen A, Luo FL, Matsubara S. 2012. Acclimatory responses of *Arabidopsis* to fluctuating light environment: comparison of different sunfleck regimes and accessions. *Photosynthesis Research* 113: 221–37.
- Andralojc PJ, Madgwick PJ, Tao Y, Keys A, Ward JL, Beale MH, Loveland JE, Jackson PJ, Willis AC, Gutteridge S, et al. 2012. 2-Carboxy-D-arabinitol 1-phosphate (CA1P) phosphatase: evidence for a wider role in plant Rubisco regulation. *The Biochemical Journal* 442: 733–742.
- Arena C, Vitale L, De Santo AV. 2005. Photosynthetic response of *Quercus ilex* L. plants grown on compost and exposed to increasing photon flux densities and elevated CO<sub>2</sub>. *Photosynthetica* 43: 615–619.
- Armbruster U, Carrillo LR, Venema K, Pavlovic L, Schmidtman E, Kornfeld A, Jahns P, Berry JA, Kramer DM, Jonikas MC. 2014. Ion antiport accelerates photosynthetic acclimation in fluctuating light environments. *Nature Communications* 10.1038/ncomms6439
- Aro EM, Virgin I, Andersson B. 1993. Photoinhibition of Photosystem II. Inactivation, protein damage and turnover. *Biochimica et Biophysica Acta* 1143: 113–134.
- Assmann SM, Grantz DA. 1990a. Stomatal response to humidity in sugarcane and soybean: effect of vapour pressure difference on the kinetics of the blue light response. *Plant, Cell and Environment* 13: 163–169.
- Assmann SM, Grantz DA. 1990b. The magnitude of the stomatal response to blue light: modulation by atmospheric humidity. *Plant Physiology* 93: 701–709.
- Avron M, Gibbs M. 1974. Properties of phosphoribulokinase of whole chloroplasts. *Plant Physiology* 53: 136–139.
- Badger MR, Sharkey TD, von Caemmerer S. 1984. The relationship between steady-state gas exchange of bean leaves and the levels of carbon-reduction-cycle intermediates. *Planta* 160: 305–313.
- Baker NR, Harbinson J, Kramer DM. 2007. Determining the limitations and regulation of photosynthetic energy transduction in leaves. *Plant, Cell and Environment* 30: 1107–1125.
- Bernacchi CJ, Bagley JE, Serbin SP, Ruiz-Vera UM, Rosenthal DM, Vanlooche A. 2013. Modelling C<sub>3</sub> photosynthesis from the chloroplast to the ecosystem. *Plant, Cell and Environment* 36: 1641–1657.
- Bernacchi CJ, Pimentel C, Long SP. 2003. In vivo temperature response functions of parameters required to model RuBP-limited photosynthesis. *Plant, Cell and Environment* 26: 1419–1430.
- Bernacchi CJ, Portis AR, Nakano H, von Caemmerer S, Long SP. 2002. Temperature response of mesophyll conductance. Implications for the determination of Rubisco enzyme kinetics and for limitations to photosynthesis in vivo. *Plant Physiology* 130: 1992–1998.
- Bernacchi CJ, Singaas EL, Pimentel C, Portis AR, Long SP. 2001. Improved temperature response functions for models of Rubisco-limited photosynthesis. *Plant, Cell and Environment* 24: 253–259.

- Bilger W, Björkman O. 1991. Temperature dependence of violaxanthin de-epoxidation and non-photochemical fluorescence quenching in intact leaves of *Gossypium hirsutum* L. and *Malva parviflora* L. *Planta* 184: 226–234.
- Bradford KJ, Sharkey TD, Farquhar GD. 1983. Gas exchange, stomatal behavior, and  $\Delta^{13}\text{C}$  values of the *flacca* tomato mutant in relation to abscisic acid. *Plant Physiology* 72: 245–250.
- Brooks A, Portis AR. 1988. Protein-bound ribulose biphosphate correlates with deactivation of ribulose biphosphate carboxylase in leaves. *Plant Physiology* 87: 244–249.
- Brosché M, Merilo E, Mayer F, Pechter P, Puzõrjova I, Brader G, Kangasjärvi J, Kollist H. 2010. Natural variation in ozone sensitivity among *Arabidopsis thaliana* accessions and its relation to stomatal conductance. *Plant, Cell and Environment* 33: 914–925.
- Buckley TN. 2005. The control of stomata by water balance. *New Phytologist* 168: 275–92.
- Campbell DA, Tyystjärvi E. 2012. Parameterization of photosystem II photoinactivation and repair. *Biochimica et Biophysica Acta* 1817: 258–265.
- Cardon ZG, Mott KA, Berry JA. 1994. Dynamics of patchy stomatal movements, and their contribution to steady-state and oscillating stomatal conductance calculated using gas-exchange techniques. *Plant, Cell and Environment* 17: 995–1007.
- Carmo-Silva AE, Salvucci ME. 2011. The activity of Rubisco's molecular chaperone, Rubisco activase, in leaf extracts. *Photosynthesis Research* 108: 143–155.
- Carmo-Silva AE, Salvucci ME. 2013. The regulatory properties of Rubisco activase differ among species and affect photosynthetic induction during light transitions. *Plant Physiology* 161: 1645–1655.
- Carmo-Silva AE, Scales JC, Madgwick PJ, Parry MAJ. 2015. Optimizing Rubisco and its regulation for greater resource use efficiency. *Plant, Cell & Environment* 38: 1817–1832.
- Cazzaniga S, Dall'Osto L, Kong SG, Wada M, Bassi R. 2013. Interaction between avoidance of photon absorption, excess energy dissipation and zeaxanthin synthesis against photooxidative stress in *Arabidopsis*. *The Plant Journal* 76: 568–579.
- Champigny ML, Bismuth E. 1976. Role of photosynthetic electron transfer in light activation of Calvin cycle enzymes. *Physiologia Plantarum* 36: 95–100.
- Chazdon RL, Pearcy RW. 1986. Photosynthetic responses to light variation in rainforest species I. Induction under constant and fluctuating light conditions. *Oecologia* 69: 517–523.
- Chen TW, Henke M, de Visser PHB, Buck-Sorlin G, Wiechers D, Kahlen K, Stützel H. 2014. What is the most prominent factor limiting photosynthesis in different layers of a greenhouse cucumber canopy? *Annals of Botany* 114: 677–688.
- Clarke JE, Johnson GN. 2001. In vivo temperature dependence of cyclic and pseudocyclic electron transport in barley. *Planta* 212: 808–816.
- Cleveland WS, Grosse E, Shyu WM. 1992. Local regression models. In: Chambers JM, Hastie TJ, eds. *Statistical Models in S*. Wadsworth & Brooks/Cole
- Connolly D, Lund H, Mathiesen B V., Pican E, Leahy M. 2012. The technical and economic implications of integrating fluctuating renewable energy using energy storage. *Renewable Energy* 43: 47–60.
- Crews CE, Vines HM, Black CCJ. 1975. Postillumination burst of carbon dioxide in Crassulacean Acid Metabolism plants. *Plant Physiology* 55: 652–657.
- Cruz JA, Sacksteder CA, Kanazawa A, Kramer DM. 2001. Contribution of electric field ( $\Delta\psi$ ) to steady-state transthylakoid proton motive force (pmf) in vitro and in vivo. Control of pmf parsing into  $\Delta\psi$  and  $\Delta\text{pH}$  by ionic strength. *Biochemistry* 40: 1226–1237.
- D'Haese D, Vandermeiren K, Caubergs RJ, Guisez Y, De Temmerman L, Horemans N. 2004. Non-photochemical quenching kinetics during the dark to light transition in relation to the formation of antheraxanthin and zeaxanthin. *Journal of Theoretical Biology* 227: 175–186.
- Dall'Osto L, Cazzaniga S, Wada M, Bassi R. 2014. On the origin of a slowly reversible fluorescence decay component in the *Arabidopsis npq4* mutant. *Philosophical transactions of the Royal Society B* 369: 10.1098/rstb.2013.0221.

## References

- Damour G, Simonneau T, Cochard H, Urban L. 2010. An overview of models of stomatal conductance at the leaf level. *Plant, Cell and Environment* 33: 1419–1438.
- Dau H, Hansen UP. 1989. Studies on the adaptation of intact leaves to changing light intensities by a kinetic analysis of chlorophyll fluorescence and oxygen evolution as measured by the photoacoustic signal. *Photosynthesis Research* 20: 59–83.
- Davis PA, Caylor S, Whippo CW, Hangarter RP. 2011. Changes in leaf optical properties associated with light-dependent chloroplast movements. *Plant, Cell & Environment* 34: 2047–2059.
- Davis PA, Hangarter RP. 2012. Chloroplast movement provides photoprotection to plants by redistributing PSII damage within leaves. *Photosynthesis Research* 112: 153–161.
- Decker JP. 1955. A rapid, postillumination deceleration of respiration in green leaves. *Plant Physiology* 30: 82–84.
- Diaz-Espejo A, Nicolás E, Fernández JE. 2007. Seasonal evolution of diffusional limitations and photosynthetic capacity in olive under drought. *Plant, Cell and Environment* 30: 922–933.
- Downton WJS. 1970. Preferential C<sub>4</sub>-dicarboxylic acid synthesis, the postillumination CO<sub>2</sub> burst, carboxyl transfer step, and grana configurations in plants with C<sub>4</sub>-photosynthesis. *Canadian Journal of Botany* 48: 1795–1800.
- Drake PL, Froend RH, Franks PJ. 2013. Smaller, faster stomata: scaling of stomatal size, rate of response, and stomatal conductance. *Journal of Experimental Botany* 64: 495–505.
- Earl HJ, Ennahli S. 2004. Estimating photosynthetic electron transport via chlorophyll fluorometry without Photosystem II light saturation. *Photosynthesis Research* 82: 177–186.
- Eckardt NA, Portis ARJ. 1997. Heat denaturation profiles of ribulose-1,5-bisphosphate carboxylase/oxygenase (Rubisco) and Rubisco activase and the inability of Rubisco activase to restore activity of heat-denatured Rubisco. *Plant Physiology* 113: 243–248.
- Eckstein J, Beyschlag W, Mott KA, Ryel RJ. 1996. Changes in photon flux can induce stomatal patchiness. *Plant, Cell and Environment* 19: 1066–1074.
- Ethier GJ, Livingston NJ. 2004. On the need to incorporate sensitivity to CO<sub>2</sub> transfer conductance into the Farquhar-von Caemmerer-Berry leaf photosynthesis model. *Plant, Cell and Environment* 27: 137–153.
- Evans JR, von Caemmerer S. 2013. Temperature response of carbon isotope discrimination and mesophyll conductance in tobacco. *Plant, Cell and Environment* 36: 745–756.
- Evers JB, Vos J, Yin X, Romero P, van der Putten PEL, Struik PC. 2010. Simulation of wheat growth and development based on organ-level photosynthesis and assimilate allocation. *Journal of Experimental Botany* 61: 2203–2216.
- Farquhar GD. 1979. Models describing the kinetics of ribulose biphosphate carboxylase-oxygenase. *Archives of Biochemistry and Biophysics* 193: 456–468.
- Farquhar GD, von Caemmerer S, Berry JA. 1980. A biochemical model of photosynthetic CO<sub>2</sub> assimilation in leaves of C<sub>3</sub> species. *Planta* 149: 78–90.
- Farquhar GD, Sharkey TD. 1982. Stomatal conductance and photosynthesis. *Annual Review of Plant Physiology* 33: 317–345.
- Fay PA, Knapp AK. 1993. Photosynthetic and stomatal responses of *Avena sativa* (Poaceae) to a variable light environment. *American Journal of Botany* 80: 1369–1373.
- Feller U, Crafts-Brandner SJ, Salvucci ME. 1998. Moderately high temperatures inhibit ribulose-1,5-bisphosphate carboxylase/oxygenase (Rubisco) activase-mediated activation of Rubisco. *Plant Physiology* 116: 539–546.
- Flexas J, Barbour MM, Brendel O, Cabrera HM, Carriquí M, Díaz-Espejo A, Douthe C, Dreyer E, Ferrio JP, Gago J, et al. 2012. Mesophyll diffusion conductance to CO<sub>2</sub>: An unappreciated central player in photosynthesis. *Plant Science* 193–194: 70–84.
- Flexas J, Diaz-Espejo A, Galmés J, Kaldenhoff R, Medrano H, Ribas-Carbo M. 2007a. Rapid variations of mesophyll conductance in response to changes in CO<sub>2</sub> concentration around leaves. *Plant, Cell and Environment* 30: 1284–1298.

- Flexas J, Medrano H. 2002. Drought-inhibition of photosynthesis in C<sub>3</sub> plants: Stomatal and non-stomatal limitations revisited. *Annals of Botany* 89: 183–189.
- Flexas J, Niinemets U, Gallé A, Barbour MM, Centritto M, Diaz-Espejo A, Douthe C, Galmés J, Ribas-Carbo M, Rodriguez PL, et al. 2013a. Diffusional conductances to CO<sub>2</sub> as a target for increasing photosynthesis and photosynthetic water-use efficiency. *Photosynthesis Research* 117: 45–59
- Flexas J, Ortuño MF, Ribas-Carbo M, Diaz-Espejo A, Flórez-Sarasa ID, Medrano H. 2007b. Mesophyll conductance to CO<sub>2</sub> in *Arabidopsis thaliana*. *New Phytologist* 175: 501–511.
- Flexas J, Ribas-Carbo M, Bota J, Galmés J, Henkle M, Martínez-Cañellas S, Medrano H. 2006. Decreased Rubisco activity during water stress is not induced by decreased relative water content but related to conditions of low stomatal conductance and chloroplast CO<sub>2</sub> concentration. *New Phytologist* 172: 73–82.
- Flexas J, Ribas-Carbo M, Diaz-Espejo A, Galmés J, Medrano H. 2008. Mesophyll conductance to CO<sub>2</sub>: current knowledge and future prospects. *Plant, Cell and Environment* 31: 602–621.
- Flexas J, Scoffoni C, Gago J, Sack L. 2013b. Leaf mesophyll conductance and leaf hydraulic conductance: an introduction to their measurement and coordination. *Journal of Experimental Botany* 64: 3965–3981.
- Foyer CH, Bloom AJ, Queval G, Noctor G. 2009. Photorespiratory metabolism: genes, mutants, energetics, and redox signaling. *Annual Review of Plant Biology* 60: 455–484.
- Foyer CH, Neukermans J, Queval G, Noctor G, Harbinson J. 2012. Photosynthetic control of electron transport and the regulation of gene expression. *Journal of Experimental Botany* 63: 1637–1661.
- Franks PJ, Doheny-Adams TW, Britton-Harper ZJ, Gray JE. 2015. Increasing water-use efficiency directly through genetic manipulation of stomatal density. *New Phytologist* 207: 188–195.
- Gardemann A, Schimkat D, Heldt HW. 1986. Control of CO<sub>2</sub> fixation. Regulation of stromal fructose-1,6-bisphosphatase in spinach by pH and Mg<sup>2+</sup> concentration. *Planta* 168: 536–545.
- Genty B, Briantais JM, Baker NR. 1989. The relationship between the quantum yield of photosynthetic electron transport and quenching of chlorophyll fluorescence. *Biochimica et Biophysica Acta* 990: 87–92.
- Gibeaut DM, Hulett J, Cramer GR, Seemann JR. 1997. Maximal biomass of *Arabidopsis thaliana* using a simple, low-maintenance hydroponic method and favorable environmental conditions. *Plant Physiology* 115: 317–319.
- Gilmore AM, Björkman O. 1995. Temperature-sensitive coupling and uncoupling of ATPase-mediated, nonradiative energy dissipation: Similarities between chloroplasts and leaves. *Planta* 197: 646–654.
- Gilmore AM, Hazlett TL, Debrunner PG, Govindjee. 1996. Comparative time-resolved photosystem II chlorophyll a fluorescence analyses reveal distinctive differences between photoinhibitory reaction center damage and xanthophyll cycle-dependent energy dissipation. *Photochemistry and Photobiology* 64: 552–563.
- Godfray HCJ, Beddington JR, Crute IR, Haddad L, Lawrence D, Muir JF, Pretty J, Robinson S, Thomas SM, Toulmin C. 2010. Food security: The challenge of feeding 9 billion people. *Science* 327: 812–818.
- Goral TK, Johnson MP, Duffy CDP, Brain APR, Ruban AV, Mullineaux CW. 2012. Light-harvesting antenna composition controls the macrostructure and dynamics of thylakoid membranes in *Arabidopsis*. *The Plant Journal* 69: 289–301.
- Grassi G, Magnani F. 2005. Stomatal, mesophyll conductance and biochemical limitations to photosynthesis as affected by drought and leaf ontogeny in ash and oak trees. *Plant, Cell and Environment* 28: 834–849.
- Griffiths H, Helliker BR. 2013. Mesophyll conductance: internal insights of leaf carbon exchange. *Plant, Cell and Environment* 36: 733–735.

## References

- Gu L, Sun Y. 2014. Artefactual responses of mesophyll conductance to CO<sub>2</sub> and irradiance estimated with the variable *J* and online isotope discrimination methods. *Plant, Cell & Environment* 37: 1231–1249.
- Gutteridge S, Parry MAJ, Burton S, Keys AJ, Mudd A, Feeney J, Servaites JC, Pierce J. 1986. A nocturnal inhibitor of carboxylation in leaves. *Nature* 324: 274–276.
- Harley PC, Loreto F, Di Marco G, Sharkey TD. 1992. Theoretical considerations when estimating the mesophyll conductance to CO<sub>2</sub> flux by analysis of the response of photosynthesis to CO<sub>2</sub>. *Plant Physiology* 98: 1429–1436.
- Harrison EP, Willingham NM, Lloyd JC, Raines CA. 1998. Reduced sedoheptulose-1,7-bisphosphatase levels in transgenic tobacco lead to decreased photosynthetic capacity and altered carbohydrate accumulation. *Planta* 204: 27–36.
- Haupt W, Scheuerlein R. 1990. Chloroplast movement. *Plant, Cell and Environment* 13: 595–614.
- He Z, von Caemmerer S, Hudson GS, Price GD, Badger MR, Andrews TJ. 1997. Ribulose-1,5-bisphosphate carboxylase/oxygenase activase deficiency delays senescence of ribulose-1,5-bisphosphate carboxylase/oxygenase but progressively impairs its catalysis during tobacco leaf development. *Plant Physiology* 115: 1569–1580.
- Heuvelink E, Bakker MJ, Hogendonk L, Janse J, Kaarsemaker R, Maaswinkel R. 2006. Horticultural lighting in the Netherlands: New developments. *Acta Horticulturae* 711: 25–33.
- Hikosaka K, Kato MC, Hirose T. 2004. Photosynthetic rates and partitioning of absorbed light energy in photoinhibited leaves. *Physiologia Plantarum* 121: 699–708.
- Hills A, Chen ZH, Amtmann A, Blatt MR, Lew VL. 2012. OnGuard, a computational platform for quantitative kinetic modeling of guard cell physiology. *Plant Physiology* 159: 1026–1042.
- Hindmarsh AC, Brown PN, Grant KE, Lee SL, Serban R, Shumaker DE, Woodward CS. 2005. SUNDIALS: Suite of nonlinear and differential/algebraic equation solvers. *ACM Transactions on Mathematical Software* 31: 363–396.
- Holišová P, Zitová M, Klem K, Urban O. 2012. Effect of elevated carbon dioxide concentration on carbon assimilation under fluctuating light. *Journal of Environmental Quality* 41: 1931–1938.
- Howard TP, Lloyd JC, Raines CA. 2011. Inter-species variation in the oligomeric states of the higher plant Calvin cycle enzymes glyceraldehyde-3-phosphate dehydrogenase and phosphoribulokinase. *Journal of Experimental Botany* 62: 3799–3805.
- Howard TP, Metodiev M, Lloyd JC, Raines CA. 2008. Thioredoxin-mediated reversible dissociation of a stromal multiprotein complex in response to changes in light availability. *PNAS*, 105: 4056–4061.
- Hubbart S, Ajigboye OO, Horton P, Murchie EH. 2012. The photoprotective protein PsbS exerts control over CO<sub>2</sub> assimilation rate in fluctuating light in rice. *The Plant Journal* 71: 402–412.
- Huber SC, Huber JL. 1996. Role and regulation of sucrose-phosphate synthase in higher plants. *Annual Review of Plant Physiology and Plant Molecular Biology* 47: 431–444.
- Huisman R, Mahieu R. 2003. Regime jumps in electricity prices. *Energy Economics* 25: 425–434.
- Ikeuchi M, Uebayashi N, Sato F, Endo T. 2014. Physiological functions of PsbS-dependent and PsbS-independent NPQ under naturally fluctuating light conditions. *Plant and Cell Physiology* 55: 1286–1295.
- IPCC. Stocker TF, et al, eds. 2013. *Climate change 2013: the physical science basis. Contribution of Working Group I to the Fifth Assessment Report of the Intergovernmental Panel on Climate Change*. Cambridge, UK & New York, NY, USA: Cambridge University Press
- Ishijima S, Uchibori A, Takagi H, Maki R, Ohnishi M. 2003. Light-induced increase in free Mg<sup>2+</sup> concentration in spinach chloroplasts: Measurement of free Mg<sup>2+</sup> by using a fluorescent probe and necessity of stromal alkalization. *Archives of Biochemistry and Biophysics* 412: 126–132.

- Jackson RB, Woodrow IE, Mott KA. 1991. Nonsteady-state photosynthesis following an increase in photon flux density (PFD): Effects of magnitude and duration of initial PFD. *Plant Physiology* 95: 498–503.
- Jahns P, Holzwarth AR. 2012. The role of the xanthophyll cycle and of lutein in photoprotection of photosystem II. *Biochimica et Biophysica Acta* 1817: 182–193.
- Johnson MP, Goral TK, Duffy CDP, Brain APR, Mullineaux CW, Ruban A V. 2011. Photoprotective energy dissipation involves the reorganization of Photosystem II light-harvesting complexes in the grana membranes of spinach chloroplasts. *The Plant Cell* 23: 1468–1479.
- Kaiser H, Kappen L. 2000. In situ observation of stomatal movements and gas exchange of *Aegopodium podagraria* L. in the understorey. *Journal of Experimental Botany* 51: 1741–1749.
- Kaiser H, Kappen L. 2001. Stomatal oscillations at small apertures: indications for a fundamental insufficiency of stomatal feedback-control inherent in the stomatal turgor mechanism. *Journal of Experimental Botany* 52: 1303–1313.
- Kaiser E, Morales A, Harbinson J, Kromdijk J, Heuvelink E, Marcelis LFM. 2015. Dynamic photosynthesis in different environmental conditions. *Journal of Experimental Botany* 66: 2415–2426.
- Kaiser H, Paoletti E. 2014. Dynamic stomatal changes. In: Tausz M, Grulke N, eds. *Trees in a Changing Environment*. Dordrecht, NL: Springer, 61–82.
- Kasahara M, Kagawa T, Oikawa K, Suetsugu N, Miyao M, Wada M. 2002. Chloroplast avoidance movement reduces photodamage in plants. *Nature* 420: 829–832.
- Kirschbaum MUF, Küppers M, Schneider H, Giersch C, Noe S. 1998. Modelling photosynthesis in fluctuating light with inclusion of stomatal conductance, biochemical activation and pools of key photosynthetic intermediates. *Planta* 204: 16–26.
- Kirschbaum MUF, Ohlemacher C, Küppers M. 2004. Loss of quantum yield in extremely low light. *Planta* 218: 1046–1053.
- Kirschbaum MUF, Oja V, Laisk A. 2005. The quantum yield of CO<sub>2</sub> fixation is reduced for several minutes after prior exposure to darkness. Exploration of the underlying causes. *Plant Biology* 7: 58–66.
- Kirschbaum MUF, Percy RW. 1988. Gas exchange analysis of the fast phase of photosynthetic induction in *Alocasia macrorrhiza*. *Plant Physiology* 87: 818–821.
- Kjaer KH, Ottosen CO, Jørgensen BN. 2011. Cost-efficient light control for production of two campanula species. *Scientia Horticulturae* 129: 825–831.
- Knapp AK. 1992. Leaf gas exchange in *Quercus macrocarpa* (Fagaceae): Rapid stomatal responses to variability in sunlight in a tree growth form. *American Journal of Botany* 79: 599–604.
- Kobza J, Edwards GE. 1987. The photosynthetic induction response in wheat leaves: net CO<sub>2</sub> uptake, enzyme activation, and leaf metabolites. *Planta* 171: 549–559.
- Kok B. 1956. On the inhibition of photosynthesis by intense light. *Biochimica et Biophysica Acta* 21: 234–244.
- Kono M, Terashima I. 2014. Long-term and short-term responses of the photosynthetic electron transport to fluctuating light. *Journal of Photochemistry and Photobiology. B: Biology* 137: 89–99.
- Kossmann J, Sonnewald U, Willmitzer L. 1994. Reduction of the chloroplastic fructose-1,6-bisphosphatase in transgenic potato plants impairs photosynthesis and plant growth. *The Plant Journal* 6: 637–650.
- Košvancová M, Urban O, Šprtová M, Hrstka M, Kalina J, Tomášková I, Špunda V, Marek M V. 2009. Photosynthetic induction in broadleaved *Fagus sylvatica* and coniferous *Picea abies* cultivated under ambient and elevated CO<sub>2</sub> concentrations. *Plant Science* 177: 123–130.
- Košvancová-Zitová M, Urban O, Navrátil M, Špunda V, Robson TM, Marek M V. 2009. Blue radiation stimulates photosynthetic induction in *Fagus sylvatica* L. *Photosynthetica* 47: 388–398.



## References

- Krah NM, Logan BA. 2010. Loss of psbS expression reduces vegetative growth, reproductive output, and light-limited, but not light-saturated, photosynthesis in *Arabidopsis thaliana* (Brassicaceae) grown in temperate light environments. *American Journal of Botany* 97: 644–649.
- Kramer DM, Evans JR. 2011. The importance of energy balance in improving photosynthetic productivity. *Plant Physiology* 155: 70–78.
- Kramer DM, Johnson G, Kiirats O, Edwards GE. 2004. New fluorescence parameters for the determination of Q<sub>A</sub> redox state and excitation energy fluxes. *Photosynthesis Research* 79: 209–218.
- Krause GH. 1988. Photoinhibition of photosynthesis. An evaluation of damaging and protective mechanisms. *Physiologia Plantarum* 74: 566–574.
- Külheim C, Agren J, Jansson S. 2002. Rapid regulation of light harvesting and plant fitness in the field. *Science* 297: 91–93.
- Küppers M, Pfiz M. 2009. Role of photosynthetic induction for daily and annual carbon gains of leaves and plant canopies. In: Laisk A, Nedbal L, Govindjee, eds. *Photosynthesis in silico: Understanding Complexity from Molecules to Ecosystems*. Dordrecht, NL: Springer, 417–440.
- Küppers M, Schneider H. 1993. Leaf gas exchange of beech (*Fagus sylvatica* L.) seedlings in lightflecks: effects of fleck length and leaf temperature in leaves grown in deep and partial shade. *Trees* 7: 160–168.
- Laing WA, Stitt M, Heldt HW. 1981. Control of CO<sub>2</sub> fixation. Changes in the activity of ribulosephosphate kinase and fructose- and sedoheptulose-bisphosphatase in chloroplasts. *Biochimica et Biophysica Acta* 637: 348–359.
- Laisk A, Eichelmann H, Oja V. 2006. C<sub>3</sub> photosynthesis in silico. *Photosynthesis Research* 90: 45–66.
- Laisk A, Kiirats O, Oja V. 1984. Assimilatory power (postillumination CO<sub>2</sub> uptake) in leaves. *Plant Physiology* 76: 723–729.
- Lan Y, Woodrow I. E, Mott KA. 1992. Light-dependent changes in ribulose bisphosphate carboxylase activase activity in leaves. *Plant Physiology* 99: 304–309.
- Lawson T, Blatt MR. 2014. Stomatal size, speed, and responsiveness impact on photosynthesis and water use efficiency. *Plant Physiology* 164: 1556–1570.
- Lawson T, Davey PA, Yates SA, Bechtold U, Baeshen M, Baeshen N, Mutwakil MZ, Sabir J, Baker NR, Mullineaux PM. 2014a. C<sub>3</sub> photosynthesis in the desert plant *Rhazya stricta* is fully functional at high temperatures and light intensities. *New Phytologist* 201: 862–873.
- Lawson T, Simkin AJ, Kelly G, Granot D. 2014b. Mesophyll photosynthesis and guard cell metabolism impacts on stomatal behaviour. *New Phytologist* 203: 1064–1081.
- Leakey ADB, Press MC, Scholes JD. 2003. High-temperature inhibition of photosynthesis is greater under sunflecks than uniform irradiance in a tropical rain forest tree seedling. *Plant, Cell and Environment* 26: 1681–1690.
- Leakey ADB, Press MC, Scholes JD, Watling JR. 2002. Relative enhancement of photosynthesis and growth at elevated CO<sub>2</sub> is greater under sunflecks than uniform irradiance in a tropical rain forest tree seedling. *Plant, Cell and Environment* 25: 1701–1714.
- Lefebvre S, Lawson T, Zakhleniuk OV, Lloyd JC, Raines CA. 2005. Increased sedoheptulose-1,7-bisphosphatase activity in transgenic tobacco plants stimulates photosynthesis and growth from an early stage in development. *Plant Physiology* 138: 451–460.
- Leon-Kloosterziel K, Alvarez Gil M, Ruijs GJ, Jacobsen SH, Zeevaart JAD, Koornneef M. 1996. Isolation and characterisation of abscisic acid-deficient *Arabidopsis* mutants at two new loci. *The Plant Journal* 10: 655–661.
- Li XP, Björkman O, Shih C, Grossman AR, Rosenquist M, Jansson S, Niyogi KK. 2000. A pigment-binding protein essential for regulation of photosynthetic light harvesting. *Nature* 403: 391–395.

- Li XP, Gilmore AM, Caffarri S, Bassi R, Golan T, Kramer D, Niyogi KK. 2004. Regulation of photosynthetic light harvesting involves intrathylakoid lumen pH sensing by the PsbS protein. *The Journal of Biological Chemistry* 279: 22866–22874.
- LI-COR Biosciences. 2012. *Using the LI-6400 / LI-6400XT Portable Photosynthesis System. Version 6.* LI-COR Biosciences, Lincoln, Nebraska, USA
- Long SP, Ainsworth EA, Rogers A, Ort DR. 2004. Rising atmospheric carbon dioxide: plants FACE the future. *Annual Review of Plant Biology* 55: 591–628.
- Long SP, Bernacchi CJ. 2003. Gas exchange measurements, what can they tell us about the underlying limitations to photosynthesis? Procedures and sources of error. *Journal of Experimental Botany* 54: 2393–2401.
- Long SP, Zhu XG, Naidu SL, Ort DR. 2006. Can improvement in photosynthesis increase crop yields? *Plant, Cell and Environment* 29: 315–330.
- Loriaux SD, Avenson TJ, Welles JM, McDermitt DK, Eckles RD, Riensche B, Genty B. 2013. Closing in on maximum yield of chlorophyll fluorescence using a single multiphase flash of sub-saturating intensity. *Plant, Cell & Environment* 36: 1755–1570.
- Lunn JE, MacRae E. 2003. New complexities in the synthesis of sucrose. *Current Opinion in Plant Biology* 6: 208–214.
- MacRae E, Lunn J. 2006. Control of sucrose biosynthesis. In: Plaxton WC, McManus MT, eds. *Control of primary metabolism in plants.* Oxford: Blackwell Publishing Ltd, 234–250.
- Marcelis LFM, Maas FM, Heuvelink E. 2002. The latest developments in the lighting technologies in Dutch horticulture. *Acta Horticulturae* 580: 35–42.
- Martínez-Barajas E, Galán-Molina J, Sánchez de Jiménez E. 1997. Regulation of Rubisco activity during grain-fill in maize: possible role of Rubisco activase. *The Journal of Agricultural Science* 128: 155–161.
- Mate CJ, von Caemmerer S, Evans JR, Hudson GS, Andrews TJ. 1996. The relationship between CO<sub>2</sub>-assimilation rate, Rubisco carbamylation and Rubisco activase content in activase-deficient transgenic tobacco suggests a simple model of activase action. *Planta* 198: 604–613.
- Mate CJ, Hudson GS, von Caemmerer S, Evans JR, Andrews TJ. 1993. Reduction of ribulose biphosphate carboxylase activase levels in tobacco (*Nicotiana tabacum*) by antisense RNA reduces ribulose biphosphate carboxylase carbamylation and impairs photosynthesis. *Plant Physiology* 102: 1119–1128.
- Matsubara S, Chow WS. 2004. Populations of photoinactivated Photosystem II reaction centers characterized by chlorophyll a fluorescence lifetime in vivo. *PNAS* 101: 18234–18239.
- McAusland L, Davey PA, Kanwal N, Baker NR, Lawson T. 2013. A novel system for spatial and temporal imaging of intrinsic plant water use efficiency. *Journal of Experimental Botany* 64: 4993–5007.
- McNevin D, von Caemmerer S, Farquhar G. 2006. Determining Rubisco activation kinetics and other rate and equilibrium constants by simultaneous multiple non-linear regression of a kinetic model. *Journal of Experimental Botany* 57: 3883–3900.
- Merilo E, Jõesaar I, Brosché M, Kollist H. 2014. To open or to close: species-specific stomatal responses to simultaneously applied opposing environmental factors. *New Phytologist* 202: 499–508.
- Mizokami Y, Noguchi K, Kojima M, Sakakibara H, Terashima I. 2015. Mesophyll conductance decreases in the wild type but not in an ABA-deficient mutant (*aba1*) of *Nicotiana plumbaginifolia* under drought conditions. *Plant, Cell & Environment* 38: 388–398.
- Monteith JL. 1995. A reinterpretation of stomatal responses to humidity. *Plant, Cell and Environment* 18: 357–364.
- Moore BD, Kobza J, Seemann JR. 1991. Measurement of 2-carboxyarabinitol 1-phosphate in plant leaves by isotope dilution. *Plant Physiology* 96: 208–213.

## References

- Mott KA, Woodrow IE. 1993. Effects of O<sub>2</sub> and CO<sub>2</sub> on nonsteady-state photosynthesis. Further evidence for ribulose-1,5-bisphosphate carboxylase/oxygenase limitation. *Plant Physiology* 102: 859–866.
- Mott KA, Woodrow IE. 2000. Modelling the role of Rubisco activase in limiting non-steady-state photosynthesis. *Journal of Experimental Botany* 51: 399–406.
- Murchie EH, Chen Y, Hubbart S, Peng S, Horton P. 1999. Interactions between senescence and leaf orientation determine in situ patterns of photosynthesis and photoinhibition in field-grown rice. *Plant Physiology* 119: 553–564.
- Murchie EH, Harbinson J. 2014. Non-photochemical fluorescence quenching across scales: from chloroplasts to plants to communities. In: Demmig-Adams B, Garab G, Adams W, Govindjee, eds. *Non-photochemical Quenching and Energy Dissipation in Plants, Algae and Cyanobacteria*. Dordrecht, NL: Springer, 553–582.
- Murchie EH, Niyogi KK. 2011. Manipulation of photoprotection to improve plant photosynthesis. *Plant Physiology* 155: 86–92.
- Naumburg E, Ellsworth DS. 2000. Photosynthetic sunfleck utilization potential of understory saplings growing under elevated CO<sub>2</sub> in FACE. *Oecologia* 122: 163–174.
- Naumburg E, Ellsworth DS. 2002. Short-term light and leaf photosynthetic dynamics affect estimates of daily understory photosynthesis in four tree species. *Tree Physiology* 22: 393–401.
- Naumburg E, Ellsworth DS, Katul GG. 2001. Modeling dynamic understory photosynthesis of contrasting species in ambient and elevated carbon dioxide. *Oecologia* 126: 487–499.
- Niinemets U. 2007. Photosynthesis and resource distribution through plant canopies. *Plant, Cell & Environment* 30: 1052–1071.
- Nilkens M, Kress E, Lambrev P, Miloslavina Y, Müller M, Holzwarth AR, Jahns P. 2010. Identification of a slowly inducible zeaxanthin-dependent component of non-photochemical quenching of chlorophyll fluorescence generated under steady-state conditions in *Arabidopsis*. *Biochimica et Biophysica Acta* 1797: 466–475.
- NIST (2015) *NIST standard reference on constants, units and uncertainty*. NIST physical measurement laboratory. <http://physics.nist.gov/cuu/Constants/index.html>. Accessed 26 September 2015.
- Niyogi KK, Grossman AR, Björkman O. 1998. *Arabidopsis* mutants define a central role for the xanthophyll cycle in the regulation of photosynthetic energy conversion. *The Plant Cell* 10: 1121–1134.
- Noe SM, Giersch C. 2004. A simple dynamic model of photosynthesis in oak leaves: coupling leaf conductance and photosynthetic carbon fixation by a variable intracellular CO<sub>2</sub> pool. *Functional Plant Biology* 31: 1195–1204.
- Ögren E, Baker NR. 1985. Evaluation of a technique for the measurement of chlorophyll fluorescence from leaves exposed to continuous white light. *Plant, Cell and Environment* 8: 539–547.
- Ögren E, Sundin U. 1996. Photosynthetic responses to variable light: a comparison of species from contrasting habitats. *Oecologia* 106: 18–27.
- Ooba M, Takahashi H. 2003. Effect of asymmetric stomatal response on gas-exchange dynamics. *Ecological Modelling* 164: 65–82.
- Ort DR, Merchant SS, Alric J, Barkan A, Blankenship RE, Bock R, Croce R, Hanson MR, Hibberd JM, Long SP, et al. 2015. Redesigning photosynthesis to sustainably meet global food and bioenergy demand. *PNAS* 112: 8529–8536.
- Osmond CB, Oja V, Laik A. 1988. Regulation of carboxylation and photosynthetic oscillations during sun-shade acclimation in *Helianthus annuus* measured with a rapid-response gas exchange system. *Australian Journal of Plant Physiology* 15: 239–251.
- Osterhout WJV, Haas ARC. 1918. Dynamical aspects of photosynthesis. *PNAS* 4: 85–91.

- Oxborough K, Baker NR. 1997. Resolving chlorophyll a fluorescence images of photosynthetic efficiency into photochemical and non-photochemical components – calculation of  $qP$  and  $F_v'/F_m'$  without measuring  $F_o'$ . *Photosynthesis Research* 54: 135–142.
- Ozturk I, Holst N, Ottosen CO. 2012. Simulation of leaf photosynthesis of  $C_3$  plants under fluctuating light and different temperatures. *Acta Physiologiae Plantarum* 34: 2319–2329.
- Parry MAJ, Andralojc PJ, Scales JC, Salvucci ME, Carmo-Silva AE, Alonso H, Whitney SM. 2013. Rubisco activity and regulation as targets for crop improvement. *Journal of Experimental Botany* 63: 717–730.
- Parry MAJ, Keys AJ, Madgwick PJ, Carmo-Silva AE, Andralojc PJ. 2008. Rubisco regulation: a role for inhibitors. *Journal of Experimental Botany* 59: 1569–80.
- Peak D, Mott KA. 2011. A new, vapour-phase mechanism for stomatal responses to humidity and temperature. *Plant, Cell and Environment* 34: 162–178.
- Pearcy RW. 1990. Sunflecks and photosynthesis in plant canopies. *Annual Review of Plant Physiology* 41: 421–453.
- Pearcy RW, Gross LJ, He D. 1997. An improved dynamic model of photosynthesis for estimation of carbon gain in sunfleck light regimes. *Plant, Cell and Environment* 20: 411–424.
- Pearcy RW, Krall JP, Sassenrath-Cole GF. 1996. Photosynthesis in fluctuating light environments. In: Baker NR, ed. *Photosynthesis and the Environment*. Dordrecht, NL: Kluwer Academic Publishers 321–346.
- Pearcy RW, Roden JS, Gamon JA. 1990. Sunfleck dynamics in relation to canopy structure in a soybean (*Glycine max* (L.) Merr.) canopy. *Agricultural and Forest Meteorology* 52: 359–372.
- Pearcy RW, Way DA. 2012. Two decades of sunfleck research: looking back to move forward. *Tree Physiology* 32: 1059–1061.
- Peguero-Pina JJ, Gil-Pelegrín E, Morales F. 2013. Three pools of zeaxanthin in *Quercus coccifera* leaves during light transitions with different roles in rapidly reversible photoprotective energy dissipation and photoprotection. *Journal of Experimental Botany* 64: 1649–1661.
- Pepin S, Livingston NJ. 1997. Rates of stomatal opening in conifer seedlings in relation to air temperature and daily carbon gain. *Plant, Cell and Environment* 20: 1462–1472.
- Peressotti A, Marchiol L, Zerbi G. 2001. Photosynthetic photon flux density and sunfleck regime within canopies of wheat, sunflower and maize in different wind conditions. *Italian Journal of Agronomy* 4: 87–92.
- Peterson RB. 1983. Estimation of photorespiration based on the initial rate of postillumination  $CO_2$  release II. Effects of  $O_2$ ,  $CO_2$ , and temperature. *Plant Physiology* 73: 983–988.
- Pons TL, Pearcy RW, Seemann JR. 1992. Photosynthesis in flashing light in soybean leaves grown in different conditions. I. Photosynthetic induction state and regulation of ribulose-1,5-bisphosphate carboxylase activity. *Plant, Cell and Environment* 15: 569–576.
- Pons TL, Pearcy RW. 1992. Photosynthesis in flashing light in soybean leaves grown in different conditions. II. Lightfleck utilization efficiency. *Plant, Cell and Environment* 15: 577–584.
- Pons TL, Welschen RAM. 2002. Overestimation of respiration rates in commercially available clamp-on leaf chambers. Complications with measurement of net photosynthesis. *Plant, Cell and Environment* 25: 1367–1372.
- Portis ARJ. 2003. Rubisco activase - Rubisco's catalytic chaperone. *Photosynthesis Research* 75: 11–27.
- Portis ARJ, Salvucci ME, Ogren WL. 1986. Activation of ribulosebisphosphate carboxylase/oxygenase at physiological  $CO_2$  and ribulosebisphosphate concentrations by Rubisco activase. *Plant Physiology* 82: 967–971.
- Powell MJD. 2009. The BOBYQA algorithm for bound constrained optimization without derivatives. *Department of Applied Mathematics and Theoretical Physics, Centre for Mathematical Sciences*: 1–39.

## References

- Prinsley RT, Hunt S, Smith AM, Leegood RC. 1986. The influence of a decrease in irradiance on photosynthetic carbon assimilation in leaves of *Spinacia oleracea* L. *Planta* 167: 414–420.
- Prinsley RT, Leegood RC. 1986. Factors affecting photosynthetic induction in spinach leaves. *Biochimica et Biophysica Acta* 849: 244–253.
- Raines CA, Lloyd JC, Dyer TA. 1999. New insights into the structure and function of sedoheptulose-1,7-bisphosphatase; an important but neglected Calvin cycle enzyme. *Journal of Experimental Botany* 50: 1–8.
- Rawsthorne S, Hylton CM. 1991. The relationship between the post-illumination CO<sub>2</sub> burst and glycine metabolism in leaves of C<sub>3</sub> and C<sub>3</sub>-C<sub>4</sub> intermediate species of *Moricandia*. *Planta* 186: 122–126.
- Rees D, Young A, Noctor G, Britton G, Horton P. 1989. Enhancement of the ΔpH-dependent dissipation of excitation energy in spinach chloroplasts by light-activation: correlation with the synthesis of zeaxanthin. *FEBS Letters* 256: 85–90.
- Renger G, Eckert HJ, Bergmann A, Bernarding J, Liu B, Napiwotzki A, Reifarh F, Eichler HJ. 1995. Fluorescence and spectroscopic studies of exciton trapping and electron transfer in Photosystem II of higher plants. *Australian Journal of Plant Physiology* 22: 167–181.
- Riikonen J, Holopainen T, Oksanen E, Vapaavuori E. 2005. Leaf photosynthetic characteristics of silver birch during three years of exposure to elevated concentrations of CO<sub>2</sub> and O<sub>3</sub> in the field. *Tree Physiology* 25: 621–632.
- Roden JS. 2003. Modeling the light interception and carbon gain of individual fluttering aspen (*Populus tremuloides* Michx) leaves. *Trees* 17: 117–126.
- Roden JS, Pearcy RW. 1993. Photosynthetic gas exchange response of poplars to steady-state and dynamic light environments. *Oecologia* 93: 208–214.
- Rojas-Pierce M, Whippo CW, Davis PA, Hangarter RP, Springer PS. 2014. PLASTID MOVEMENT IMPAIRED1 mediates ABA sensitivity during germination and implicates ABA in light-mediated chloroplast movements. *Plant Physiology and Biochemistry* 83: 185–193.
- van Rooijen R, Aarts MGM, Harbinson J. 2015. Natural genetic variation for acclimation of photosynthetic light use efficiency to growth irradiance in *Arabidopsis thaliana*. *Plant Physiology* 167: pp.114.252239.
- Ruban AV, Johnson MP, Duffy CDP. 2012. The photoprotective molecular switch in the Photosystem II antenna. *Biochimica et Biophysica Acta* 1817: 167–181.
- Ruelland E, Miginiac-Maslow M. 1999. Regulation of chloroplast enzyme activities by thioredoxins: activation or relief from inhibition? *Trends in Plant Science* 4: 136–141.
- Ruuska S, Andrews TJ, Badger MR, Hudson GS, Laisk A, Price GD, von Caemmerer S. 1998. The interplay between limiting processes in C<sub>3</sub> photosynthesis studied by rapid-response gas exchange using transgenic tobacco impaired in photosynthesis. *Australian Journal of Plant Physiology* 25: 859–870.
- Salvucci ME, Crafts-Brandner SJ. 2004. Inhibition of photosynthesis by heat stress: the activation state of Rubisco as a limiting factor in photosynthesis. *Physiologia Plantarum* 120: 179–186.
- Salvucci ME, Portis ARJ, Ogren WL. 1985. A soluble chloroplast protein catalyzes ribulosebisphosphate carboxylase/oxygenase activation in vivo. *Photosynthesis Research* 7: 193–201.
- Salvucci ME, Werneke JM, Ogren WL, Portis AR. 1987. Purification and species distribution of Rubisco activase. *Plant Physiology* 84: 930–936.
- Sarlikioti V, de Visser PHB, Marcelis LFM. 2011. Exploring the spatial distribution of light interception and photosynthesis of canopies by means of a functional-structural plant model. *Annals of Botany* 107: 875–883.
- Sassenrath-Cole GF, Pearcy RW. 1992. The role of ribulose-1,5-bisphosphate regeneration in the induction requirement of photosynthetic CO<sub>2</sub> exchange under transient light conditions. *Plant Physiology* 99: 227–234.

- Sassenrath-Cole GF, Pearcy RW. 1994. Regulation of photosynthetic induction state by the magnitude and duration of low light exposure. *Plant Physiology* 105: 1115–1123.
- Sassenrath-Cole GF, Pearcy RW, Steinmaus S. 1994. The role of enzyme activation state in limiting carbon assimilation under variable light conditions. *Photosynthesis Research* 41: 295–302.
- Scales JC, Parry MAJ, Salvucci ME. 2014. A non-radioactive method for measuring Rubisco activase activity in the presence of variable ATP:ADP ratios, including modifications for measuring the activity and activation state of Rubisco. *Photosynthesis Research* 119: 355–365.
- Scheibe R. 2004. Malate valves to balance cellular energy supply. *Physiologia Plantarum* 120: 21–26.
- Schimkat D, Heineke D, Heldt HW. 1990. Regulation of sedoheptulose-1,7-bisphosphatase by sedoheptulose-7-phosphate and glycerate, and of fructose-1,6-bisphosphatase by glycerate in spinach chloroplasts. *Planta* 181: 97–103.
- Scholl RL, May ST, Ware DH. 2000. Seed and molecular resources for Arabidopsis. *Plant Physiology* 124: 1477–1480.
- Schymanski SJ, Or D, Zwieniecki M. 2013. Stomatal control and leaf thermal and hydraulic capacitances under rapid environmental fluctuations. *PLoS One* 8: e54231.
- Seemann JR, Kirschbaum MUF, Sharkey TD, Pearcy RW. 1988. Regulation of ribulose-1,5-bisphosphate carboxylase activity in *Alocasia macrorrhiza* in response to step changes in irradiance. *Plant Physiology* 88: 148–152.
- Seemann JR, Kobza J, Moore BD. 1990. Metabolism of 2-carboxyarabinitol 1-phosphate and regulation of ribulose-1,5-bisphosphate carboxylase activity. *Photosynthesis Research* 23: 119–130.
- Šetlík I, Allakhverdiev SI, Nedbal L, Šetlíková E, Klimov V V. 1990. Three types of Photosystem II photoinactivation. 1. Damaging processes on the acceptor side. *Photosynthesis Research* 23: 39–48.
- Shan X, Wang J, Chua L, Jiang D, Peng W, Xie D. 2011. The role of *Arabidopsis* Rubisco activase in jasmonate-induced leaf senescence. *Plant Physiology* 155: 751–764.
- Sharkey TD. 1985a. Photosynthesis in intact leaves of C<sub>3</sub> plants: Physics, physiology and rate limitations. *The Botanical Review* 51: 53–105.
- Sharkey TD. 1985b. O<sub>2</sub>-insensitive photosynthesis in C<sub>3</sub> plants. Its occurrence and a possible explanation. *Plant Physiology* 78: 71–75.
- Sharkey TD. 1989. Evaluating the role of Rubisco regulation in photosynthesis of C<sub>3</sub> plants. *Philosophical Transactions of the Royal Society B* 323: 435–448.
- Sharkey TD. 2015. Commentary: What gas exchange data can tell us about photosynthesis. *Plant, Cell and Environment*. 10.1111/pce.12641
- Sharkey TD, Bernacchi CJ, Farquhar GD, Singsaas EL. 2007. Fitting photosynthetic carbon dioxide response curves for C<sub>3</sub> leaves. *Plant, Cell and Environment* 30: 1035–1040.
- Sharkey TD, Seemann JR, Pearcy RW. 1986. Contribution of metabolites of photosynthesis to postillumination CO<sub>2</sub> assimilation in response to lightflecks. *Plant Physiology* 82: 1063–1068.
- Shikanai T. 2014. Central role of cyclic electron transport around Photosystem I in the regulation of photosynthesis. *Current Opinion in Biotechnology* 26: 25–30.
- Shimazaki K, Doi M, Assmann SM, Kinoshita T. 2007. Light regulation of stomatal movement. *Annual Review of Plant Biology* 58: 219–247.
- Simkin AJ, McAusland L, Headland LR, Lawson T, Raines CA. 2015. Multigene manipulation of photosynthetic carbon assimilation increases CO<sub>2</sub> fixation and biomass yield in tobacco. *Journal of Experimental Botany* 66: 4075–4090.
- Smith WK, Berry ZC. 2013. Sunflecks? *Tree Physiology* 33: 233–237.
- Stegemann J, Timm H-C, Küppers M. 1999. Simulation of photosynthetic plasticity in response to highly fluctuating light: an empirical model integrating dynamic photosynthetic induction and capacity. *Trees* 14: 145–160.

## References

- Stitt M, Grosse H. 1988. Interactions between sucrose synthesis and CO<sub>2</sub> fixation I. Secondary kinetics during photosynthetic induction are related to a delayed activation of sucrose synthesis. *Journal of Plant Physiology* 133: 129–137.
- Stitt M, Lunn J, Usadel B. 2010. Arabidopsis and primary photosynthetic metabolism - more than the icing on the cake. *The Plant Journal* 61: 1067–1091.
- Stitt M, Wirtz W, Heldt HW. 1980. Metabolite levels during induction in the chloroplast and extrachloroplast compartments of spinach protoplasts. *Biochimica et Biophysica Acta* 593: 85–102.
- Sun J, Edwards GE, Okita TW. 1999. Feedback inhibition of photosynthesis in rice measured by O<sub>2</sub> dependent transients. *Photosynthesis Research* 59: 187–200.
- Sun J, Zhang J, Larue CT, Huber SC. 2011. Decrease in leaf sucrose synthesis leads to increased leaf starch turnover and decreased RuBP regeneration-limited photosynthesis but not Rubisco-limited photosynthesis in *Arabidopsis* null mutants of SPSA1. *Plant, Cell and Environment* 34: 592–604.
- Suorsa M, Järvi S, Grieco M, Nurmi M, Pietrzykowska M, Rantala M, Kangasjärvi S, Paakkarinen V, Tikkanen M, Jansson S, et al. 2012. PROTON GRADIENT REGULATION5 is essential for proper acclimation of *Arabidopsis* Photosystem I to naturally and artificially fluctuating light conditions. *The Plant Cell* 24: 2934–2948.
- Tal M, Nevo Y. 1973. Abnormal stomatal behavior and root resistance, and hormonal imbalance in three wilted mutants of tomato. *Biochemical Genetics* 8: 291–300.
- Tausz M, Warren CR, Adams MA. 2005. Dynamic light use and protection from excess light in upper canopy and coppice leaves of *Nothofagus cunninghamii* in an old growth, cool temperate rainforest in Victoria, Australia. *New Phytologist* 165: 143–156.
- Tazoe Y, von Caemmerer S, Estavillo GM, Evans JR. 2011. Using tunable diode laser spectroscopy to measure carbon isotope discrimination and mesophyll conductance to CO<sub>2</sub> diffusion dynamically at different CO<sub>2</sub> concentrations. *Plant, Cell and Environment* 34: 580–591.
- Tcherkez G. 2013. Modelling the reaction mechanism of ribulose-1,5-bisphosphate carboxylase/oxygenase and consequences for kinetic parameters. *Plant, Cell and Environment* 36: 1586–1596.
- Tholen D, Boom C, Noguchi K, Ueda S, Katase T, Terashima I. 2008. The chloroplast avoidance response decreases internal conductance to CO<sub>2</sub> diffusion in *Arabidopsis thaliana* leaves. *Plant, Cell and Environment* 31: 1688–1700.
- Tholen D, Ethier G, Genty B, Pepin S, Zhu XG. 2012. Variable mesophyll conductance revisited: theoretical background and experimental implications. *Plant, Cell and Environment* 35: 2087–2103.
- Tikkanen M, Grieco M, Nurmi M, Rantala M, Suorsa M, Aro EM. 2012. Regulation of the photosynthetic apparatus under fluctuating growth light. *Philosophical Transactions of the Royal Society of London B* 367: 3486–3493.
- Tilman D, Balzer C, Hill J, Befort BL. 2011. Global food demand and the sustainable intensification of agriculture. *PNAS* 108: 20260–20264.
- Timm HC, Küppers M, Stegemann J. 2004. Non-destructive analysis of architectural expansion and assimilate allocation in different tropical tree saplings: consequences of using steady-state and dynamic photosynthesis models. *Ecotropica* 10: 101–121.
- Tinoco-Ojanguren C, Pearcy RW. 1992. Dynamic stomatal behavior and its role in carbon gain during lightflecks of a gap phase and an understory *Piper* species acclimated to high and low light. *Oecologia* 92: 222–228.
- Tinoco-Ojanguren C, Pearcy RW. 1993a. Stomatal dynamics and its importance to carbon gain in two rainforest *Piper* species. I. VPD effects on the transient stomatal response to lightflecks. *Oecologia* 94: 388–394.

- Tinoco-Ojanguren C, Pearcy RW. 1993b. Stomatal dynamics and its importance to carbon gain in two rainforest *Piper* species. II. Stomatal versus biochemical limitations during photosynthetic induction. *Oecologia* 94: 395–402.
- Tomimatsu H, Iio A, Adachi M, Saw L-G, Fletcher C, Tang Y. 2014. High CO<sub>2</sub> concentration increases relative leaf carbon gain under dynamic light in *Dipterocarpus sublamellatus* seedlings in a tropical rain forest, Malaysia. *Tree Physiology* 34: 944–954.
- Tomimatsu H, Tang Y. 2012. Elevated CO<sub>2</sub> differentially affects photosynthetic induction response in two *Populus* species with different stomatal behavior. *Oecologia* 169: 869–78.
- Tyystjärvi E, Hakala M, Sarvikas P. 2005. Mathematical modelling of the light response curve of photoinhibition of Photosystem II. *Photosynthesis Research* 84: 21–27.
- Urban O, Košvancová M, Marek M V., Lichtenthaler HK. 2007. Induction of photosynthesis and importance of limitations during the induction phase in sun and shade leaves of five ecologically contrasting tree species from the temperate zone. *Tree Physiology*: 1207–1215.
- Urban O, Šprtová M, Košvancová M, Lichtenthaler HK, Marek M V. 2008. Comparison of photosynthetic induction and transient limitations during the induction phase in young and mature leaves from three poplar clones. *Tree Physiology* 28: 1189–1197.
- Valladares F, Allen MT, Pearcy RW. 1997. Photosynthetic responses to dynamic light under field conditions in six tropical rainforest shrubs occurring along a light gradient. *Oecologia* 111: 505–514.
- Vialet-Chabrand S, Dreyer E, Brendel O. 2013. Performance of a new dynamic model for predicting diurnal time courses of stomatal conductance at the leaf level. *Plant, Cell and Environment* 36: 1529–1546.
- Vico G, Manzoni S, Palmroth S, Katul G. 2011. Effects of stomatal delays on the economics of leaf gas exchange under intermittent light regimes. *New Phytologist* 192: 640–652.
- Vines HM, Tu ZP, Armitage AM, Chen SS, Black CCJ. 1983. Environmental responses of the post-lower illumination CO<sub>2</sub> burst as related to leaf photorespiration. *Plant Physiology* 73: 25–30.
- von Caemmerer S. 2000. *Biochemical Models of Leaf Photosynthesis*. Collingwood, Australia: CSIRO Publishing
- von Caemmerer S. 2013. Steady-state models of photosynthesis. *Plant, Cell and Environment* 36: 1617–1630.
- von Caemmerer S, Edmondson DL. 1986. Relationship between steady-state gas exchange, in vivo ribulose biphosphate carboxylase activity and some carbon reduction cycle intermediates in *Raphanus sativus*. *Australian Journal of Plant Physiology* 13: 669–688.
- von Caemmerer S, Evans JR. 2015. Temperature responses of mesophyll conductance differ greatly between species. *Plant, Cell & Environment* 38: 629–637.
- Vos J, Evers JB, Buck-Sorlin GH, Andrieu B, Chelle M, de Visser PHB. 2010. Functional-structural plant modelling: a new versatile tool in crop science. *Journal of Experimental Botany* 61: 2101–2115.
- Walker B, Ariza LS, Kaines S, Badger MB, Cousins AB. 2013. Temperature response of *in vivo* Rubisco kinetics and mesophyll conductance in *Arabidopsis thaliana*: comparisons to *Nicotiana tabacum*. *Plant, Cell & Environment* 36: 2108–2119.
- Walters RG, Horton P. 1991. Resolution of components of non-photochemical chlorophyll fluorescence quenching in barley leaves. *Photosynthesis Research* 27: 121–133.
- Wang ZY, Snyder GW, Esau BD, Portis AR, Ogren WL. 1992. Species-dependent variation in the interaction of substrate-bound ribulose-1,5-bisphosphate carboxylase/oxygenase (Rubisco) and rubisco activase. *Plant Physiology* 100: 1858–1862.
- Way DA, Pearcy RW. 2012. Sunflecks in trees and forests: from photosynthetic physiology to global change biology. *Tree Physiology* 32: 1066–1081.
- Wedel N, Soll J, Paap BK. 1997. CP12 provides a new mode of light regulation of Calvin cycle activity in higher plants. *PNAS* 94: 10479–10484.



## References

- Willmer C, Fricker M. 1996. *Stomata*, 2<sup>nd</sup> ed. London, UK: Chapman & Hall
- Woodrow IE, Kelly ME, Mott KA. 1996. Limitation of the rate of ribulosebiphosphate carboxylase activation by carbamylation and ribulosebiphosphate carboxylase activase activity: development and tests of a mechanistic model. *Australian Journal of Plant Physiology* 23: 141–149.
- Woodrow IE, Mott KA. 1989. Rate limitation of non-steady-state photosynthesis by ribulose-1,5-bisphosphate carboxylase in spinach. *Australian Journal of Plant Physiology* 16: 487–500.
- Yamori W, Hikosaka K, Way DA. 2014. Temperature response of photosynthesis in C<sub>3</sub>, C<sub>4</sub>, and CAM plants: temperature acclimation and temperature adaptation. *Photosynthesis Research* 119: 101–117.
- Yamori W, Masumoto C, Fukayama H, Makino A. 2012. Rubisco activase is a key regulator of non-steady-state photosynthesis at any leaf temperature and, to a lesser extent, of steady-state photosynthesis at high temperature. *The Plant Journal* 71: 871–880.
- Yamori W, Suzuki K, Noguchi K, Nakai M, Terashima I. 2006. Effects of Rubisco kinetics and Rubisco activation state on the temperature dependence of the photosynthetic rate in spinach leaves from contrasting growth temperatures. *Plant, Cell and Environment* 29: 1659–1670.
- Yin X, Harbinson J, Struik PC. 2006. Mathematical review of literature to assess alternative electron transports and interphotosystem excitation partitioning of steady-state C<sub>3</sub> photosynthesis under limiting light. *Plant, Cell & Environment* 29: 1771–1782.
- Yin X, Struik PC. 2009. C<sub>3</sub> and C<sub>4</sub> photosynthesis models: An overview from the perspective of crop modelling. *NJAS-Wageningen Journal of Life Sciences* 57: 27–38.
- Yin X, Struik PC, Romero P, Harbinson J, Evers JB, Van Der Putten PEL, Vos J. 2009. Using combined measurements of gas exchange and chlorophyll fluorescence to estimate parameters of a biochemical C<sub>3</sub> photosynthesis model: a critical appraisal and a new integrated approach applied to leaves in a wheat (*Triticum aestivum*) canopy. *Plant, Cell & Environment* 32: 448–464.
- Zaks J, Amarnath K, Kramer DM, Niyogi KK, Fleming GR. 2012. A kinetic model of rapidly reversible nonphotochemical quenching. *PNAS* 109: 15757–15762.
- Zaks J, Amarnath K, Sylak-Glassman EJ, Fleming GR. 2013. Models and measurements of energy-dependent quenching. *Photosynthesis Research* 116: 389–409
- Zhang SB, Guan ZJ, Chang W, Hu H, Yin Q, Cao K-F. 2011. Slow photosynthetic induction and low photosynthesis in *Paphiopedilum armeniacum* are related to its lack of guard cell chloroplast and peculiar stomatal anatomy. *Physiologia Plantarum* 142: 118–27.
- Zhang N, Kallis RP, Ewy RG, Portis AR. 2002. Light modulation of Rubisco in *Arabidopsis* requires a capacity for redox regulation of the larger Rubisco activase isoform. *PNAS* 99: 3330–3334.
- Zhang N, Portis AR. 1999. Mechanism of light regulation of Rubisco: A specific role for the larger Rubisco activase isoform involving reductive activation by thioredoxin-f. *PNAS* 96: 9438–9443.
- Zhu XG, Long SP, Ort DR. 2010. Improving photosynthetic efficiency for greater yield. *Annual Review of Plant Biology* 61: 235–261.
- Zhu XG, Ort DR, Whitmarsh J, Long SP. 2004. The slow reversibility of Photosystem II thermal energy dissipation on transfer from high to low light may cause large losses in carbon gain by crop canopies: a theoretical analysis. *Journal of Experimental Botany* 55: 1167–1175.
- Zhu XG, Wang Y, Ort DR, Long SP. 2013. e-photosynthesis: a comprehensive dynamic mechanistic model of C<sub>3</sub> photosynthesis: from light capture to sucrose synthesis. *Plant, Cell and Environment* 36: 1711–1727.
- Zipperlen S, Press M. 1997. Photosynthetic induction and stomatal oscillations in relation to the light environment of two dipterocarp rain forest tree species. *Journal of Ecology* 85: 491–503.



## SUMMARY

Irradiance is the main driver of photosynthesis. In natural conditions, irradiance incident on a leaf often fluctuates, due to the movement of leaves, clouds and the sun. These fluctuations force photosynthesis to respond dynamically, however with delays that are subject to rate constants of underlying processes, such as regulation of electron transport, activation states of enzymes in the Calvin cycle, and stomatal conductance ( $g_s$ ). For example, in leaves adapted to low irradiance that are suddenly exposed to high irradiance, photosynthesis increases slowly (within tens of minutes); this process is called photosynthetic induction. Photosynthesis in fluctuating irradiance (dynamic photosynthesis) is limited by several physiological processes, and is further modulated by environmental factors other than irradiance, such as CO<sub>2</sub> concentration, air humidity and temperature. Studying dynamic photosynthesis and its environmental and physiological control can help to identify targets for improvements of crop growth, improve the accuracy of mathematical models of photosynthesis, and explore new, dynamic lighting strategies in greenhouses.

In this thesis, the limitations acting on dynamic photosynthesis are explored by reviewing the literature, by experimenting with a suite of environmental factors (CO<sub>2</sub> concentration, temperature, air humidity, irradiance intensity and spectrum), genetic diversity in the form of mutants, genetic transformants and ecotypes, and by mathematical modelling. Several genotypes of tomato (*Solanum lycopersicum*) and the model plant *Arabidopsis thaliana*, all grown in climate chambers, were used in the experiments. The main findings of the thesis are that a) CO<sub>2</sub> concentration and air humidity strongly affect the rate of change of dynamic photosynthesis through a combination of diffusional and biochemical limitations; b) Rubisco activation kinetics are pivotal in controlling rates of photosynthesis increase after a stepwise increase in irradiance, and are further affected by CO<sub>2</sub> concentration; c)  $g_s$  limits photosynthetic induction kinetics in *A. thaliana* but not in tomato in ambient conditions, and becomes a stronger limitation in low CO<sub>2</sub> concentration or air humidity; and d) mesophyll conductance, non-photochemical quenching (NPQ) and sucrose synthesis do not limit dynamic photosynthesis under the conditions used.

In Chapter 1, the rationale for the research conducted is described, by introducing the concept of fluctuating irradiance and its effects on photosynthesis rates. The chapter discusses how dynamic photosynthesis is measured and described, and provides a range of possible applications of the insights gained by the research conducted in this dissertation.

In **Chapter 2**, the current literature is reviewed and a mechanistic framework is built to explore the effects that the environmental factors CO<sub>2</sub> concentration, temperature and air humidity have on rates of dynamic photosynthesis. Across data from literature, higher CO<sub>2</sub> concentration and temperature speed up photosynthetic induction and slow down its loss, thereby facilitating higher rates of dynamic photosynthesis. Major knowledge gaps exist regarding the loss of photosynthetic induction in low irradiance, dynamic changes in mesophyll conductance, and the extent of limitations imposed by  $g_s$  across species and environmental conditions.

**Chapter 3** is an experimental exploration of the effects of CO<sub>2</sub> concentration, leaf temperature, air humidity and percentage of blue irradiance on rates of photosynthetic induction in dark-adapted tomato leaves. Rubisco activation, changes in stomatal and mesophyll conductance, diffusional and biochemical limitations, efficiency of electron transport through photosystem II, NPQ and transient water use efficiency, were examined to give a comprehensive overview of the environmental modulation of dynamic photosynthesis. Unlike the percentage of blue irradiance, increases in CO<sub>2</sub> concentration, leaf temperature and air humidity all positively affected the rates of photosynthetic induction, and these effects were explained by changes in diffusional and biochemical limitations. Maximising the rates of Rubisco activation would increase CO<sub>2</sub> assimilation by 6-10%, while maximising the rates of stomatal opening would increase assimilation by at most 1-2%, at the same time negatively affecting intrinsic water use efficiency.

In **Chapter 4** it is explored whether the effects of CO<sub>2</sub> concentration on dynamic photosynthesis are similar across various irradiance environments. Gain and loss of photosynthetic induction in several low irradiance treatments, as well as sinusoidal changes in irradiance, were studied using tomato leaves. Elevated CO<sub>2</sub> concentration (800 ppm) enhanced the rate of photosynthetic induction by 4-12% (compared to 400 ppm) and decreased the loss of photosynthetic induction by 21-25%. Elevated CO<sub>2</sub> concentration enhanced rates of dynamic photosynthesis regardless of initial photosynthetic induction state to a similar extent. Therefore, rising global CO<sub>2</sub> concentration will benefit integrated assimilation throughout whole canopies, where different leaf layers experience widely differing irradiance regimes.

In **Chapter 5** it is tested whether stomatal limitation exists during photosynthetic induction in tomato leaves. The abscisic acid-deficient *flacca* mutant and its wildtype were exposed to various CO<sub>2</sub> concentrations to change the diffusion gradient. Despite  $g_s$  being much larger in *flacca*, photosynthetic induction proceeded with the same speed in both genotypes in ambient CO<sub>2</sub> concentration. This suggested that stomata did not limit photosynthetic

induction in the wildtype. Using these findings, several indices of stomatal limitations were compared. Diffusional limitation, a new index, was found to be the most useful.

In Chapter 6, an exploration of some physiological limitations underlying dynamic photosynthesis is undertaken. Several mutants, transformants and ecotypes of *A. thaliana*, affecting rates of Rubisco activation,  $g_s$ , NPQ and sucrose metabolism, were used. Next to a characterisation of their steady-state responses to CO<sub>2</sub> concentrations and irradiance, leaves were exposed to stepwise increases and decreases in irradiance (using several intensities) and to lightflecks of several amplitudes and frequencies. Rubisco activase isoform and concentration, as well as various levels of  $g_s$ , strongly affected rates of dynamic photosynthesis, while this was not the case with low NPQ or sucrose phosphate synthase concentration. This suggests Rubisco activase and  $g_s$  as targets for improvement of photosynthesis in fluctuating irradiance.

Chapter 7 is a modelling exercise of dynamic photosynthesis, based on data obtained from measurements on mutants of *A. thaliana* (Chapter 6). This includes a goal-seeking model that allows reproducing the regulation of Rubisco by irradiance and CO<sub>2</sub> concentration. The model also includes a full description of leaf-level NPQ, incorporates mesophyll conductance and accounts for the fundamental physics of delays introduced by open gas exchange systems on CO<sub>2</sub> measurements. Different data sets for model calibration and validation were used. It was found that the model accurately predicted the effects of the mutants, suggesting that the assumptions of the model were sound and represented the underlying mechanisms correctly.

In Chapter 8, the findings in this thesis are synthesized. The insights gained throughout this dissertation are related to existing literature to give a comprehensive overview of the state of knowledge about the limitations of dynamic photosynthesis. The methodology of assessing transient stomatal limitations, and some aspects of using chlorophyll fluorescence measurements during photosynthetic induction, are discussed. Finally, possible applications and ideas for future research on photosynthesis in fluctuating irradiance are discussed.



# SAMENVATTING

Licht is de voornaamste aanjager van de fotosynthese. Onder natuurlijke omstandigheden fluctueert de lichtintensiteit op de bladeren sterk, vanwege de beweging van de bladeren, de wolken en de zon. Deze fluctuaties dwingen de fotosynthese om dynamisch te reageren, maar dit gebeurt met vertragingen die afhankelijk zijn van snelheidsconstanten van onderliggende processen, zoals regulatie van elektronentransport, activeringstoestanden van enzymen in de Calvin cyclus, en stomataire geleidbaarheid ( $g_s$ ). In bladeren, die aan lage lichtintensiteit aangepast zijn en die opeens aan een hogere lichtintensiteit bloot gesteld worden, stijgt de fotosynthese langzaam (gedurende enkele tientallen minuten); dit verloop heet inductie van fotosynthese. Fotosynthese onder fluctuerend licht (dynamische fotosynthese) wordt beperkt door meerdere fysiologische processen, en wordt verder beïnvloed door omgevingsfactoren, zoals  $CO_2$ -concentratie, luchtvochtigheid en temperatuur. Het onderzoeken van dynamische fotosynthese en de invloed van omgevings- en fysiologische factoren daarop kan helpen doelen voor de verbetering van gewasgroei te identificeren, de nauwkeurigheid van mathematische fotosynthesemodellen te verbeteren, en nieuwe dynamische belichtingsstrategieën in kassen te ontwikkelen.

In dit proefschrift zijn factoren die invloed hebben op dynamische fotosynthese geanalyseerd door literatuuronderzoek, door het experimenteren met meerdere omgevingsfactoren ( $CO_2$ -concentratie, temperatuur, luchtvochtigheid, lichtintensiteit en -spectrum), en nauw verwante genotypen, en door mathematische modellering. Meerdere genotypen van tomaat (*Solanum lycopersicum*) en de modelplant *Arabidopsis thaliana*, geteeld in klimaatcellen, werden in de proeven gebruikt. De voornaamste resultaten van het onderzoek zijn dat a)  $CO_2$ -concentratie en luchtvochtigheid de snelheid van de verandering van fotosynthese beïnvloeden door effecten op diffusie- en biochemische reactiesnelheden; b) de activeringskinetica van Rubisco cruciaal is in het bepalen van de snelheid van fotosyntheseverhoging na een stapsgewijze verhoging in lichtintensiteit, en dat de activeringskinetica van Rubisco verder worden beïnvloed door  $CO_2$ -concentratie; c)  $g_s$  de inductie van fotosynthese onder normale omstandigheden in *Arabidopsis* beperkt, maar niet in tomaat, en dat die beperkingen sterker zijn in lage  $CO_2$ -concentraties of lage luchtvochtigheid; en d) mesofylgeleidbaarheid, non-photochemical quenching (NPQ) en de synthese van sucrose niet beperkend zijn voor dynamische fotosynthese onder de gebruikte condities.

In Hoofdstuk 1 wordt de aanleiding voor het onderzoek in dit proefschrift beschreven, door het introduceren van het concept van fluctuerende lichtintensiteiten en hun effecten

op de snelheid van fotosynthese. Er wordt besproken hoe dynamische fotosynthese wordt gemeten en hoe de inzichten die door het onderzoek zijn verkregen kunnen worden toegepast.

In Hoofdstuk 2 wordt een overzicht van de literatuur gegeven en een mechanistisch raamwerk gepresenteerd, om de effecten van de omgevingsfactoren CO<sub>2</sub>-concentratie, temperatuur en luchtvochtigheid op de snelheid van dynamische fotosynthese te bepalen. Uit de literatuurgegevens blijkt dat hogere CO<sub>2</sub>-concentraties en temperaturen de inductie van fotosynthese versnellen (bij een toename van lichtintensiteit) en het verlies vertragen (bij een afname van lichtintensiteit). Hierdoor kunnen hogere temperaturen en CO<sub>2</sub>-concentraties een hogere snelheid van dynamische fotosynthese mogelijk maken. Grote hiaten in de kennis zijn er met betrekking tot het verlies van de inductie van fotosynthese bij lage lichtintensiteiten, dynamische veranderingen van mesofylgeleidbaarheid en de mate van stomataire beperkingen bij de verschillende plantensoorten en omgevingsfactoren.

Hoofdstuk 3 is een experimentele exploratie van de effecten van CO<sub>2</sub>-concentratie, bladtemperatuur, luchtvochtigheid en het percentage blauw licht op de snelheid van de inductie van fotosynthese in donker-aangepaste tomatenbladeren. De activering van Rubisco, veranderingen in stomataire- en mesofylgeleidbaarheid, diffusie- en biochemische reactiesnelheden, efficiency van elektronentransport door fotosysteem II, NPQ en kortstondig waterverbruiks-efficiency werden onderzocht om een uitgebreid overzicht van de invloed op dynamische fotosynthese door omgevingsfactoren te verkrijgen. Anders dan het percentage blauw licht (geen effect), hadden verhogingen van CO<sub>2</sub>-concentratie, bladtemperatuur en luchtvochtigheid elk een positieve invloed op de inductie van fotosynthese, en deze effecten werden veroorzaakt door veranderingen in diffusie- en biochemische reactiesnelheden. Het maximaliseren van de snelheid van Rubisco activatie zou de fotosynthese met 6-10% verhogen, terwijl het maximaliseren van de snelheid van stomataire opening de CO<sub>2</sub> assimilatie met op zijn hoogst 1-2% zou verhogen, maar dit zou tegelijkertijd de waterverbruiks-efficiency negatief beïnvloeden.

In Hoofdstuk 4 wordt onderzocht of de effecten van CO<sub>2</sub>-concentratie op dynamische fotosynthese gelijk zijn bij diverse lichtintensiteiten. De toe- en afname van fotosynthese-inductie bij verschillende behandelingen met lage lichtintensiteit, en de reactie op sinusvormige veranderingen van lichtintensiteit werden gemeten in tomatenbladeren. Als de CO<sub>2</sub>-concentratie van 400 naar 800 ppm werd verhoogd dan nam de snelheid van de inductie van fotosynthese met 4-12% toe en verminderde het verlies van de inductie van fotosynthese met 21-25%. Een verhoging van de CO<sub>2</sub>-concentratie doet de snelheid van de dynamische fotosynthese toenemen, welke toename niet afhangt van de aanvangsstatus van



inductie. Daarom zal ook in een gewassituatie waarbij verschillende bladeren zeer verschillende lichtintensiteiten ervaren, de stijgende wereldwijde CO<sub>2</sub>-concentratie de CO<sub>2</sub> assimilatie verhogen.

In Hoofdstuk 5 wordt onderzocht, of tijdens de inductie van fotosynthese in tomatenbladeren stomataire beperking optreedt. De *flacca* mutant zonder abscisinezuur en zijn wildvorm werden bloot gesteld aan meerdere CO<sub>2</sub>-concentraties om de diffusiegradiënt te veranderen. Ondanks het feit dat in *flacca* g<sub>s</sub> veel hoger was dan in het wildtype, was de snelheid van de inductie van fotosynthese gelijk in beide genotypen bij een CO<sub>2</sub> concentratie van 400 ppm. Dit suggereert dat huidmondjes de inductie van fotosynthese in het wildtype niet beperkten. Met behulp van deze bevindingen werden meerdere indices van stomataire beperking vergeleken. Difusionele beperking, een nieuw index, wordt als de meest nuttige geïdentificeerd.

In Hoofdstuk 6 wordt een analyse gemaakt van sommige fysiologische beperkingen die ten grondslag liggen aan dynamische fotosynthese. Meerdere mutanten, genetisch gemodificeerde planten en ecotypen van *Arabidopsis*, die de snelheid van Rubisco activering, g<sub>s</sub>, NPQ of het metabolisme van sucrose beïnvloedden, werden gebruikt. Niet alleen zijn de effecten van CO<sub>2</sub>-concentratie en lichtintensiteit op fotosynthese in een stabiele toestand gemeten, maar is fotosynthese ook gemeten onder invloed van stapsgewijze verhogingen en verlagingen in lichtintensiteit (met gebruik van meerdere lichtintensiteiten). Tevens zijn deze metingen uitgevoerd tijdens lichtvlekken met meerdere amplitudes en frequenties. De isovorm en concentratie van Rubisco activase, evenals g<sub>s</sub>, hadden sterke invloed op de snelheid van dynamische fotosynthese, terwijl dit niet het geval was voor NPQ of de concentratie van sucrose fosfaat synthase. Dit suggereert Rubisco activase en g<sub>s</sub> als doelen voor de verbetering van fotosynthese bij fluctuerende lichtintensiteiten.

Hoofdstuk 7 is een mathematische modellering van dynamische fotosynthese, gebaseerd op de gegevens van metingen aan mutanten van *Arabidopsis* (Hoofdstuk 6). Dit omvat een doelzoekend model dat de regulatie van Rubisco door lichtintensiteit en CO<sub>2</sub>-concentratie simuleert. Het model omvat zowel een volledige beschrijving van NPQ op bladniveau, als mesofylgeleidbaarheid en neemt de onderliggende fysica van vertragingen van CO<sub>2</sub>-metingen door open gaswisselingssystemen voor zijn rekening. Verschillende datasets werden voor de calibratie en de validatie van het model gebruikt. Het model bleek de effecten van de mutanten nauwkeurig te voorspellen, en dit suggereert dat de aannames van het model solide waren en de onderliggende mechanismen correct weergaven.

In Hoofdstuk 8 worden de resultaten van dit proefschrift samengevat. De inzichten, verkregen in deze dissertatie, worden in verband gebracht met bestaande literatuur om een

uitgebreid overzicht van de kennis van de beperkingen van dynamische fotosynthese te geven. De methodologie voor het inschatten van stomataire beperkingen en sommige aspecten van het gebruik van chlorofylfluorescentiemetingen tijdens de inductie van fotosynthese worden besproken. Tenslotte worden mogelijke toepassingen en ideeën voor toekomstige onderzoek op dynamische fotosynthese onder fluctuerende lichtintensiteiten gepresenteerd.

# ACKNOWLEDGEMENTS

To do science, we stand on the shoulders of giants. However, in order not to slip and stumble, standing on the shoulders of giants requires a good balance. In the last four years, many people have provided that balance for me, and I thank every one of them.

Firstly, I want to thank my supervisors Leo Marcelis, Ep Heuvelink and Jeremy Harbinson. I thank you all for your guidance, encouragement and criticism, and I admire your hard work. Leo, you are an outstanding example of someone who loves their job and manages to transform that enthusiasm into great results. You will forever be a role model regarding constant effort and fresh ideas. Ep, thank you for always being there whenever I needed advice, and for the occasional ‘clap on the back’. Jeremy, thank you for many fresh ideas and for staying as critical as you are – this has pushed the quality of my research. I also want to thank Wanne Kromdijk for being my supervisor in the beginning of this project, and for staying on ‘from afar’ after starting a new job in Illinois.

A very special thank you goes to Alejandro Morales. Without your input, this thesis would look completely different, and this is reflected in the many (co-) authorships throughout the dissertation. I am always amazed at your wealth of knowledge of (dynamic) photosynthesis and mathematical modelling, and have cherished this collaboration very much. I also want to thank Dianfan Zhou, for the hard work both during the M.Sc. thesis and the internship in Jülich on my topic – I highly appreciate your enthusiasm! Furthermore, I want to thank Zhihan Li for doing his B.Sc. thesis with me.

I highly appreciate my paranymphs Aaron and Faline. Aaron, you are both a role model of a researcher and a very good friend, and I hope you’ll stay a bit longer in Antwerpen – it is always a pleasure to visit Halloumi, Mozzarella, Ilane and yourself. Faline, it has been lots of fun to be your ‘desk neighbour’, and you’ve experienced (and tolerated) both my best and worst moods (grumpy me!). It will be fun to finally see how well you’ll do on that stage trying not to look stupid for 1 hour.

All of my fellow (current and past) Ph.D. candidate colleagues: Andreas, Tao, Nikos, Pavlos, Alejandro, Maarten, Yongran, Xixi, Ningyi, Rachel, Roxanne, Arian, René, Priscila, Anna, Okello, Geert, Pádraic, Sasan, Craig, Graham and Jonathan – thank you all for making our shared office a lively and pleasant (yet often enough calm) place to work in. Doing a Ph.D. is often tough, but talking about it with your fellow sufferers can indeed make it easier. Andreas, thank you and Niovi so much for your hospitality (Souvlakia x Sheftalia + sunshine = awesome). Tao a.k.a. Mr. President: I admire your attitude never to

get stuck, and I still need to visit your family in Beijing. Nikos: always good talking to you, I'm looking forward to many more years of that! Pavlos, you're the nicest bully I know. Maarten: ...wat een grote dankzegging!! Alejandro Bustamante, you make the group a livelier bunch simply by being yourself. Yongran: awesome food, thanks again!

I thank all the remaining colleagues from the Horticulture and Product Physiology chair group for making my time as a M.Sc. and P.hD. student a highly stimulating and pleasant experience, for great lunch sessions, and for providing lots of useful feedback during research seminars: Wim, Aina, Julian, Rob, Sander, Haris (let's play ball!), Menno, Maarten (thanks for saving me several times when I had severe and/or acute Li-Cor problems), Arjen, Joke, Dalia, Ernst, Uulke and Pauline. I have the feeling that this group is still growing, both in numbers and in character. It is a nice thought that although I'm leaving H&PP, I am only a few steps away and that we will hopefully collaborate a lot in the future. I also want to thank my new colleagues from the business unit WUR Greenhouse Horticulture for the warm welcome, especially Eric, Tom, Chantal, Anja, Esther and Cecilia. I am convinced that I have found a great new team to work in!

To the people in the Forschungszentrum Jülich who made me feel welcome (especially Shizue Matsubara, Hendrik Poorter, Marcel and Trang) and who provided me with all the necessities: thank you very much! The time in Jülich has been a very stimulating time full of important lessons for me. I also want to thank Prof. Christine Foyer (University of Leeds) for the hospitality and the detailed explanations of measuring leaf biochemistry during my stay in her lab. Chris Tebarts is thanked for highly competent technical assistance with the climate chamber. I thank Geurt Versteeg for help with any issues regarding plant irrigation.

To all the people I've met in Wageningen that have become great friends and that have made (and continue to make) living in this great little diverse town an amazing experience: thanks to you, this has been quite a ride! All the guys from Sphinx – playing Basketball with all of you has regularly saved me from loneliness during my Ph.D., and I'm especially happy that I met Martin, Kevin, Maciek (best flatmate ever!), Stefan, Thijs and Patricia in that way. All the other really important people: Ichsani & Tom, Wanka & Blair, Larissa, the Creative Garden Community. Everyone who made my M.Sc. days perfect, and especially Maja, Devika, Triantafyllos & Toon (Berlin!!). To Sissy, for 5 great years, and for being there for me for most of my Ph.D. To Michael, for being the most patient friend I could wish for.

## Acknowledgements

To Lim: 사랑해!

To my parents, who have provided me with constant love, support, a beautiful home and the education that has been the foundation of everything: I cannot thank you enough, but I hope you make you proud with what I do. To my sisters and brother, and the families that accompany them: Sarah, Moritz, Felix & Lukas; Hannes, Merle, Nora, Jakob & X; Lene, Kai, Emilia, Mattis & Paula – always a pleasure to spend time with all of you, it's high time you come and visit me in Wageningen!

If I forgot anyone who thinks they should be mentioned: you're probably right, and I'm sorry if that's the case.



# **ABOUT THE AUTHOR**





## **CURRICULUM VITAE**

Elias Kaiser was born on March 8, 1984 in Filderstadt, Germany. After graduating from school in 2004, he did voluntary work with mentally disabled adults for one year in Stirling, Scotland (UK). In 2006, Elias started studying horticultural sciences at the Leibniz University of Hanover (Germany) and obtained a B.Sc. degree in 2009. This was followed by a double-degree M.Sc. study of plant sciences at Wageningen University and the Leibniz University of Hanover (degree obtained in August 2011). From December 1, 2011 until November 30, 2015, Elias has been employed at Wageningen University as a Ph.D. student. This dissertation is a result of that work. In January 2016, Elias has started to work as a full-time researcher at Wageningen UR Greenhouse Horticulture.

## **LIST OF PUBLICATIONS**

E. Kaiser, A. Morales, J. Harbinson, J. Kromdijk, E. Heuvelink, L.F.M. Marcelis. 2015. Dynamic photosynthesis in different environmental conditions. *Journal of Experimental Botany* 2015, 66 (9), pp. 2415-2426

T. Li, J. Kromdijk, E. Heuvelink, F. Van Noort, E. Kaiser, L.F.M. Marcelis. 2016. Effects of diffuse light on radiation use efficiency depend on the response of stomatal conductance to dynamic light intensity. *Frontiers in Plant Science*, DOI: 10.3389/fpls.2016.00056

## **PE&RC Training and Education Statement**

With the training and education activities listed below the PhD candidate has complied with the requirements set by the C.T. de Wit Graduate School for Production Ecology and Resource Conservation (PE&RC) which comprises of a minimum total of 32 ECTS (= 22 weeks of activities)



### **Review of literature (6 ECTS)**

- Dynamic photosynthesis in different environmental conditions (2014)

### **Writing of project proposal (4.5 ECTS)**

- Dynamic transitions of leaf photosynthesis in response to changes in light intensity (2012)

### **Post-graduate courses (6.4 ECTS)**

- Linear models; PE&RC (2012)
- Applied methods in crop physiology; Univ. Aarhus, Denmark (2012)

### **Laboratory training and working visits (3.9 ECTS)**

- Enzyme activity assays; Plant Physiology group, Leeds University, UK (2013)
- Plant acclimation under lightflecks 1<sup>st</sup> experiment; Biosphere II, Forschungszentrum Juelich, GE (2014)
- Plant acclimation under lightflecks 2<sup>nd</sup> experiment; Forschungszentrum Juelich, GE (2015)

### **Invited review of (unpublished) journal manuscript (2 ECTS)**

- ACTA Horticulturae: photosynthesis (2012, 2014)

### **Competence strengthening / skills courses (2.55 ECTS)**

- Competence assessment (2012)
- EndNote; WUR Library (2012)
- Li-Cor User's course; Li-Cor, Hannover, Germany (2012)
- Techniques of writing and presenting a scientific paper (2013)
- How to write a world-class paper (2013)

### **PE&RC Annual meetings, seminars and the PE&RC weekend (1.2 ECTS)**

- PE&RC Day (2012, 2014)
- PE&RC Weekend; last year's programme (2014)

### **Discussion groups / local seminars / other scientific meetings (6 ECTS)**

- Frontier Literature of Plant Physiology (FLOP) (2011-2015)

### **International symposia, workshops and conferences (7.2 ECTS)**

- 7<sup>th</sup> International symposium on light; Wageningen (2012)
- Photosynthesis: from science to industry; Noordwijkerhout (2012)
- Meeting of the society of experimental biology; Manchester (2014)
- The photosynthetic phenome; Wageningen (2014)

### **Lecturing / supervision of practical's / tutorials (1.8 ECTS)**

- Concepts in environmental plant physiology (2013, 2014)
- Research methods in crop science (2014)

### **Supervision of 2 MSc students**

- Alternative methods of measuring stomatal conductance in transients
- Loss of photosynthetic induction as affected by CO<sub>2</sub>, temperature and light intensities



This work was carried out within the research programme of BioSolarCells, co-financed by the Dutch Ministry of Economic Affairs, and was additionally supported financially by Powerhouse.

## **COLOPHON**

Cover and layout design: Elias Kaiser

Cover photo: Taiga | Shutterstock.com

Printed by: Uitgeverij Boxpress | [proefschriftmaken.nl](http://proefschriftmaken.nl)